UC San Diego
UC San Diego Electronic Theses and Dissertations

Title

Petrogenesis of intraplate lavas from isolated volcanoes in the Pacific : implications for the origin of the enriched mantle source of OIB

Permalink

https://escholarship.org/uc/item/1211q6h4

Author

Tian, Liyan

Publication Date

2011

Peer reviewed|Thesis/dissertation

eScholarship.org

Powered by the California Digital Library
University of California

UNIVERSITY OF CALIFORNIA, SAN DIEGO

Petrogenesis of Intraplate Lavas from Isolated Volcanoes in the Pacific: Implications for the Origin of the Enriched Mantle Source of OIB

A dissertation submitted in partial satisfaction of the requirements for the degree of

Doctor of Philosophy

in

Earth Sciences

by

Liyan Tian

Committee in charge:

Professor Paterno Castillo, Chair
Professor David Hilton
Professor James Hawkins
Professor Mark Thiemens
Professor Peter Lonsdale

2011

Copyright

Liyan Tian, 2011

All rights reserved.

The Dissertation of Liyan Tian is approved, and it is acceptable in quality and form for publication on microfilm and electronically:

Chair

University of California, San Diego

2011

This dissertation is dedicated to my parents, You Tian and Xiufen Jiang,

who taught me to value education.

TABLE OF CONTENTS

SIGNATURE PAGE……………………………………………………………….iii
DEDICATION……………………………………………………………………...iv
TABLE OF CONTENTS………………………………………………………...v
LIST OF FIGURES…………………………………………………………….vii
LIST OF TABLES……………………………………………………………..viii
ACKNOWLEDGEMENTS……………………………………………………..ix
VITA AND PUBLICATIONS…………………………………………………..xii
ABSTRACT……………………………………………………………………….xv

CHAPTER 1: Introduction…………………………………………………………1
1.1. Scientific background and objectives of this dissertation………………………...1
1.2. Contents of the dissertation…………………………………………………4
1.2.1. Chapter 2……………………………………………………………………..4
1.2.2. Chapter 3 and 4…………………………………………………………………6
1.2.3. Chapter 5……………………………………………………………………..7
1.3. Conclusions……………………………………………………………………8
References…………………………………………………………………………12

CHAPTER 2: Major and trace element and Sr-Nd isotope signatures of the northern Lau Basin lavas: implications for the composition and dynamics of the back-arc basin mantle………………………………………………………………………...15
Abstract…………………………………………………………………………15
2.1. Introduction…………………………………………………………………...16
2.2. Geological setting and sample analyzed……………………………………...18
2.3. Analytical methods………………………………………………………….....20
2.4. Results…………………………………………………………………………...21
2.5. Discussion……………………………………………………………………23
2.5.1. Geochemical variations of the NLB lavas……………………………………23
2.5.2. Nature of the NLB mantle……………………………………………………27
2.5.2.1. The nature of composition of subduction components……………………...28
2.5.2.2. Water and extent of melting………………………………………………33
2.5.2.3. Influence of OIB mantle components……………………………………….36
2.5.3. Tectonic implications…………………………………………………………39
2.6. Conclusions……………………………………………………………………...42
Acknowledgements……………………………………………………………….43
Appendix……………………………………………………………………………..66
References…………………………………………………………………………78

CHAPTER 3: Petrology and Sr-Nd-Pb-He isotope geochemistry of post-spreading lavas on fossil spreading axes off Baja California Sur, Mexico……………………...88
Abstract…………………………………………………………………………88
3.1. Introduction……………………………………………………………………...89

3.2. Geological setting and sample description……………………………………91
3.3. Analytical methods………………………………………………………………95
3.4. Results………………………………………………………………………...98
3.5. Discussion……………………………………………………………………...102
3.5.1. Geochemical variations of post-spreading lavas on fossil spreading axes off Baja California Sur……………………………………………………………………102
3.5.2. Comparison with post-spreading lavas on other fossil spreading axes in the eastern Pacific……………………………………………………………………104
3.5.3. Petrogenesis of post-spreading lavas on fossil spreading axes………………107
3.5.4. Nature of the mantle source……………………………………………….109
3.6. Summary and conclusions…………………………………………………...113
Acknowledgements…………………………………………………………………114
References…………………………………………………………………………..140

CHPATER 4: Geochemistry of post-spreading lavas from fossil Mathematician and Galapagos spreading axes, revisited……………………………………………..149
Abstract……………………………………………………………………………..149
4.1. Introduction……………………………………………………………………… 150
4.2. Geological setting and previous work……………………………………… 152
4.3. Samples and analytical methods…………………………………………….154
4.4. Results……………………………………………………………………………155
4.4.1. Mathematician Ridge area………………………………………………...155
4.4.2. Galapagos Rise area………………………………………………………….157
4.5. Discussion……………………………………………………………………...159
4.5.1. Formation of magmas at the fossil spreading axes…………………………..159
4.5.2. Nature of the mantle source………………………………………………….161
4.6. Conclusions……………………………………………………………………….165
References…………………………………………………………………………..194

CHAPTER 5: A geochemical comparison of alkalic lavas in the Trans-Mexican volcanic belt, Baja California and intraplate volcanoes in the eastern Pacific……..200
Abstract……………………………………………………………………………..200
5.1. Introduction……………………………………………………………………….201
5.2. Geological setting and samples investigated…………………………………...203
5.3. Chemical and Sr and Nd isotopic compositions of alkalic lavas from TMVB...204
5.4. Discussion……………………………………………………………………...207
5.4.1. Hypotheses to explain the alkaline magmatism in the TMVB………………207
5.4.2. Are the alkalic lavas from TMVB the same lavas as those in peninsular Baja California and eastern Pacific?...210
5.5. Conclusions……………………………………………………………………….212
References…………………………………………………………………………..221

LIST OF FIGURES

Figure 1.1. Primitive mantle-normalized trace element concentration diagrams…....10
Figure 1.2. $^{87}Sr/^{86}Sr$ versus $^{143}Nd/^{144}Nd$ diagram..11

Figure 2.1. Schematic tectonic map of the Lau Basin………………………………44
Figure 2.2. Silica versus total alkalis diagram..45
Figure 2.3. MgO versus major elements oxides diagrams………………………...46
Figure 2.4. Normal-MORB normalized trace element concentration diagrams.…....47
Figure 2.5. $^{87}Sr/^{86}Sr$ versus $^{143}Nd/^{144}Nd$ plot ……………………………..…........48
Figure 2.6. $(La/Sm)_N$ versus (a) Ba/Nb and (b) Nb/Yb ratios………………………49
Figure 2.7. (a) Nb/Yb versus Ba/Yb, (b) Ba/Th versus Th/Nb, (c) Ba/Th versus $^{87}Sr/^{86}Sr$, and (d) Th/Nb versus $^{143}Nd/^{144}Nd$ ratios………………………………..50
Figure 2.8. Plots of $^{87}Sr/^{86}Sr$ versus $^{143}Nd/^{144}Nd$ ratios showing the influence of subduction and OIB components to the NLB mantle…………………………......52
Figure 2.9. C^0_{H2O} versus F……………………………………………………....54
Figure 2.10. (a) Ti_8 and (b) Na_8 versus Fe_8, and (c) Ti_8 and (d) Na_8 versus H_8, and (e) Fe_8 versus H_8……………………………………………………………………55
Figure 2.11. Plots of $^3He/^4He$ versus (a) $^{87}Sr/^{86}Sr$ and (b) $^{143}Nd/^{144}Nd$ ratios……….57

Figure 3.1. Simplified map showing the study area………………………………...115
Figure 3.2. Silica versus total alkalis diagram……………………………………...117
Figure 3.3. MgO versus major elements oxides diagrams…………………………118
Figure 3.4. Primitive mantle-normalized trace element concentration diagrams…..119
Figure 3.5. Sr-Nd-Pb isotopic compositions………………………………………..120
Figure 3.6. $^3He/^4He$ ratios and ^4He abundances……………………………………122
Figure 3.7. MgO versus trace elements diagrams…………………………………..123
Figure 3.8. Plots of Zr versus Ba, La versus Sm, Zr versus Nb and Ta....................124
Figure 3.9. Plots of (a) Rb/Sr versus $^{87}Sr/^{86}Sr$ and (b) La/Sm versus $^{143}Nd/^{144}Nd$....125

Figure 4.1. Simplified map showing the study area..167
Figure 4.2. Silica versus total alkalis diagram……………………………………...168
Figure 4.3. MgO versus major elements oxides diagrams…………………………169
Figure 4.4. Primitive mantle-normalized trace element concentration diagrams......172
Figure 4.5. Sr-Nd-Pb isotopic compositions………………………………………..174
Figure 4.6. Plots of (a) Nb versus Zr and (b) La versus Sm………………………...176
Figure 4.7. Plots of Nb/Zr and Sr-Nd-Pb isotopic ratios versus La/Sm………….....178
Figure 4.8. Plots of (a) Rb/Sr versus $^{87}Sr/^{86}Sr$ and (b) La/Sm versus $^{143}Nd/^{144}Nd$…180

Figure 5.1. Simplified map of the Trans-Mexican Volcanic Belt (TMVB)………...213
Figure 5.2. Silica versus total alkalis diagram……………………………………...215
Figure 5.3. Primitive mantle-normalized trace element concentration diagrams…..216
Figure 5.4. $^{87}Sr/^{86}Sr$ versus $^{143}Nd/^{144}Nd$ plot..218
Figure 5.5. Plots of (a) La versus Sm and (b) Zr versus Nb………………………..219

LIST OF TABLES

Table 2.1. Dredge locations……………………………………………………….58
Table 2.2. Trace element and Sr-Nd isotope compositions………………………….59
Table 2.3. End-member compositions for the mixing calculations………………….65
Table 2.A1. Major element compositions…………………………………………....67

Table 3.1. Dredge locations……………………………………………………...127
Table 3.2. Major and trace element compositions………………………………….128
Table 3.3. Sr-Nd-Pb compositions………………………………………………….137
Table 3.4. Helium isotope compositions……………………………………………139

Table 4.1. Dredge locations…………………………………………………………182
Table 4.2. Major and trace element compositions…………………………………..183
Table 4.3. Sr-Nd-Pb isotope compositions………………………………………….192

ACKNOWLEDGEMENTS

Writing a Ph.D. dissertation has taken a lot of hard work on my part, but could not have been accomplished without substantial help and input from a number of people.

First and foremost, I would like to express my deepest gratitude to my research advisor, Professor Paterno Castillo, for his never-ending support, both financially and emotionally, ingenious guidance and cordial encouragement throughout my Ph.D. education at Scripps. Professor Castillo has guided me through the steps of research - from sample analysis to writing up the results as scientific publications; in addition, he is full of ideas, and lots of these ideas are incorporated into the chapters of this dissertation.

Never can I thank enough the other members of my committee: Professors David Hilton, James Hawkins and Peter Lonsdale. They were always prompt to answer my questions on volatile and noble gas geochemistry, petrology and tectonics. They also helped me define what topics might make a good dissertation and provided me with important suggestions on completing the essential components of the dissertation. Professor Mark Thiemens of the Chemistry and Biochemistry department and Dean of the Division of Physical Sciences is thanked for kindly serving on my committee despite his busy schedule.

Very special thanks go to the people in Isotope Geology and Geochronology Lab: Chris MacIsaac for his help in the laboratory, from running column chemistry to loading samples, Professor Gunter Lugmair and Dr. Alex Shukolyukov for their help

in using the mass spectrometer, and labmates Natalie Juda and Xijun Liu for their help on chemistry work.

Many special thanks also go to Bruce Deck and Sean Duncan in the SIO Analytical Facility for their assistance on using the instruments to finish most of my analyses.

Furthermore, I would like to thank my co-authors in the two papers in this dissertation - Dr. Doshik Hahm and Professors Barry Hanan and Aaron Pietruszka, for their help and important comments that have helped me produce much better manuscripts.

I would never have completed my Ph.D. degree without the constant and friendly support from the staff of the SIO Graduate office and GRD office and financial support from the National Science Foundation, Sobrato Fellowship and SIO Graduate Department.

Other people that have made my Ph.D. time more enjoyable at Scripps are my fellow graduate students. Thanks for their companionships through these years and help both on my study and daily life.

Besides friends and colleagues, I owe much to my wonderful family in China. They have let me choose my own path in life and have always encouraged my decision to seek higher education. Without their continuous support, I could not imagine I can go through these years and complete my Ph.D. study.

Chapter 2, in full, was submitted to *Journal of Geophysical Research - Solid Earth* by L. Tian, P. R. Castillo, D. R. Hilton, J. W. Hawkins, B. B. Hanan, and A. J.

Pietruszka (2011JB008475). The dissertation author was the primary investigator and author of this paper. The co-authors directed, supervised and contributed to the research.

Chapter 3, in full, is a reprint of the material as it appears in *Geochemistry, Geophysics, Geosystems*, 2011, by L. Tian, P. R. Castillo, P. F. Lonsdale, D. Hahm, and D. R. Hilton (doi: 10.1029/2010GC003319). The dissertation author was the primary investigator and author of this paper. The co-authors directed, supervised and contributed to the research.

VITA

2011	Doctor of Philosophy in Earth Sciences, Scripps Institution of Oceanography, University of California, San Diego
2007	Master of Science in Earth Sciences, Scripps Institution of Oceanography, University of California, San Diego
2010-2011	Teaching Assistant, Scripps Institution of Oceanography, University of California, San Diego
2005-2011	Research Assistant, Scripps Institution of Oceanography, University of California, San Diego
2003	Master of Science in Marine Geology, College of Marine Geosciences, Ocean University of China
2000-2003	Research Assistant, College of Marine Geosciences, Ocean University of China
2000-2002	Teaching Assistant, College of Marine Geosciences, Ocean University of China
2000	Bachelor of Science in Marine Geology, College of Marine Geosciences, Ocean University of China

PUBLICATIONS

Tian, L., P. R. Castillo, P. F. Lonsdale, D. Hahm, and D. R. Hilton (2011), Petrology and Sr-Nd-Pb-He isotope geochemistry of post-spreading lavas on fossil spreading axes off Baja California Sur, Mexico, *Geochemistry, Geophysics, Geosystems*, *12*(2), Q0AC10.

Tian, L., P. R. Castillo, J. W. Hawkins, D. R. Hilton, B. B. Hanan, and A. J. Pietruszka (2008), Major and trace element and Sr-Nd isotope signatures of lavas from the Central Lau Basin: Implications for the nature and influence of subduction components in the back-arc mantle, *Journal of Volcanology and Geothermal Research*, *178*, 657-670.

Tian, L., X. Shi, H. Lu, G. Zhao and G. Wang (2006), Reconstructed millennial scale climatic changes in the tropical sea area, *Marine Geology & Quaternary Geology*, *26*(5), 77-84 (in Chinese with English abstract).

Tian, L., G. Zhao, G. Zhao, X. Shi, and H. Lv (2005), Geochemistry of basaltic lavas from the Mariana Trough: Evidence for influence of subduction component on the generation of backarc basin magmas, *International Geology Review, 47*(4), 371-386.

Tian, L., and J. Lin (2004), Chinese translation of the InterRidge Next Decade Initiative Science Plan (2004-2013), *Marine Geology Letters, 20*, 10-15.

Zhao, G., J. Peng, L. Tian, Z. Han, and S. Yang (2004), Geochemistry of ferromanganese and the tracing of paleocean environment, *Periodical of Ocean University of China*, *34*(5), 886-892 (in Chinese with English abstract).

Tian, L., G. Zhao, Z. Chen, Y. Wang, and S. Wu (2003), Preliminary investigation of the petrology and geochemistry of basalts from hydrothermal regions, Mariana Trough, *Journal of Ocean University of Qingdao*, *33*(3), 405-412 (in Chinese with English abstract).

MANUSCRIPT IN REVISION/UNDER REVIEW

Tian, L., P. R. Castillo, D. R. Hilton, J. W. Hawkins, B. B. Hanan, and A. J. Pietruszka, Major and trace element and Sr-Nd isotope signatures of the northern Lau Basin lavas: implications for the composition and dynamics of the back-arc basin mantle, *Journal of Geophysical Research - Solid Earth*, in revision.

Zhao, G., W. Luo, L. Tian, D. Li, C. Xu and Y. He, Influence of subduction components on magma genesis in back-arc basins: a comparison between Mariana Trough and Okinawa Trough, J*ournal of Asian Earth Sciences*, under review.

ABSTRACTS

Tian, L., P. R. Castillo, and D. R. Hilton (2010), Geochemistry of post-spreading lavas from fossil Mathematician and Galapagos spreading axes, revisited, *Eos Trans. AGU Abstract*, V11A-2242.

Tian, L., P. R. Castillo, and P. F. Lonsdale (2008), Petrology and geochemistry of abandoned spreading center lavas off Baja California: Implications for intraplate magmatism in eastern Pacific, *Eos Trans. AGU Abstract*, V43B-2158.

Hanan, B., T. Rooney, A. Pietruszka, L. Tian, D. Hahm, P. Castillo, D. Hilton, and J. Hawkins (2008), Hf and Pb isotope constraints on the source origin of Northern Lau Basin Back-Arc Basin Basalts, *Geochimica et Cosmochimica Acta*, *72*(12), A347.

Tian, L., P. R. Castillo, D. R. Hilton, and J. W. Hawkins (2007), Major and trace element and Sr-Nd-He isotope signature of the mantle beneath Central Lau Basin, *International Conference on Evolution, Transfer and Release of Magmas and Volcanic Gases Abstracts*, 39.

ABSTRACT OF THE DISSERTATION

Petrogenesis of Intraplate Lavas from Isolated Volcanoes in the Pacific: Implications for the Origin of the Enriched Mantle Source of OIB

by

Liyan Tian

Doctor of Philosophy in Earth Sciences

University of California, San Diego, 2011

Professor Paterno Castillo, Chair

Years of studies show that most of the ocean island basalts (OIB) that comprise the bulk of prominent linear volcanic chains are geochemically different from mid-ocean ridge basalts (MORB). However, the cause of the geochemical differences between OIB and MORB as well as the origin of geochemical enrichment and heterogeneity in OIB are highly controversial. Volcanic glasses and lavas with OIB-like composition from isolated intraplate volcanoes in the northern Lau Basin in the southwestern Pacific and from abandoned spreading centers in the eastern Pacific were investigated for their petrology and geochemistry to indirectly evaluate the man-

tle source and origin of the enriched geochemical signature of OIB that form prominent linear volcanic chains.

The study of the OIB-like lavas from isolated intraplate volcanoes in the Pacific suggests that (1) the mantle source of the OIB-like lavas is the compositionally heterogeneous upper mantle; (2) in the northern Lau Basin, the heterogeneity was created by the introduction into a pre-existing Indian Ocean-type suboceanic mantle of subduction components from the Tonga Trench and later by OIB components from the nearby Samoan mantle plume; (3) in the eastern Pacific, the geochemically enriched, OIB-like compositional signature of post-spreading lavas on fossil spreading axes were produced by low degrees of partial melting of the compositionally heterogeneous Pacific suboceanic mantle; and (4) OIB comprising prominent linear volcanic chains could not have been formed through the same mechanism of partial melting of random, enriched heterogeneities in the upper mantle; instead they appear to be coming from distinct, relatively large reservoirs that reside deeper in the mantle.

CHAPTER 1

Introduction

1.1. Scientific background and objectives of this dissertation

It is widely accepted that most of the magmatic activities responsible for the construction of the oceanic crust take place along mid-ocean ridges. Along mid-ocean ridges, mid ocean ridge basalts (MORB) are produced through adiabatic decompression partial melting of the upper mantle upwelling from below. As a whole, MORB show relatively small geochemical variations, low abundances of highly incompatible trace elements and low radiogenic Sr and Pb, but high radiogenic Nd isotopic ratios. However, intraplate magmatism, represented by volcanoes that form prominent linear island and seamount chains as well as those that occur individually or form less conspicuous aseismic ridges in a variety of tectonic settings, is also a significant source of crustal materials. Years of studies show that most of the ocean island basalts (OIB) that comprise the bulk of prominent linear volcanic chains are geochemically different from MORB. In particular, the former is more enriched in highly incompatible trace elements and more radiogenic and heterogeneous in terms of long-lived radiogenic isotopes than the latter (Figs. 1.1 and 1.2).

The cause of the geochemical differences between OIB and MORB as well as the origin of geochemical enrichment and heterogeneity in OIB are highly controversial. One proposal is the plume model, which claims the OIB comprising prominent linear volcanic chains are formed by the interaction of relatively fixed mantle plumes with moving lithospheric plates [*Morgan*, 1971]. The mantle plumes originate from deep in the mantle, perhaps at the 660-km mantle discontinuity or even at the core-mantle boundary. The enriched mantle components in the plume source of OIB are believed to originate through recycling of crustal materials (e.g., subducted oceanic crust or sediments, detached continental lithosphere, continental crust, and metasomatized mantle/lithosphere) in the mantle [e.g., *Zindler and Hart*, 1986; *Plank and Langmui*r, 1998; *Class and le Roex*, 2006; *Jackson et al.*, 2007; *Pilet et al.*, 2008]. In contrast, MORB are assumed to sample a relatively geochemically depleted and homogeneous upper mantle above the 660-km discontinuity left behind by the extraction of continental material in the early Earth [e.g., *Jacobsen and Wasserburg*, 1979; *Galer and O'Nions*, 1985; *Hawkesworth and Kemp*, 2006].

Many studies have shown that a large number of intraplate volcanoes forming isolated or short chains of seamounts on the flanks of the East Pacific Rise erupt tholeiitic to alkalic lavas with enriched-MORB-like or even OIB-like geochemical signatures [e.g., *Batiza and Vanko*, 1984; *Zindler et al.*, 1984; *Niu and Batiza*, 1997; *Niu et al.*, 2002]. Moreover, the geochemically depleted mantle source of MORB (DMM) is actually compositionally heterogeneous and is the source of these riseflank volcanoes. The enriched-MORB and OIB-like geochemical signatures observed in riseflank seamount lavas can be explained through smaller degrees and volumes of partial melting of the DMM. Relatively small extents of partial melting tend to favor the more easily meltable, enriched heterogeneities embedded in the depleted source of normal-MORB. In addition, the relatively small volumes of melt produced bypass the mixing and homogenizing processes occurring directly underneath active spreading centers [e.g., *Batiza and Vanko*, 1984; *Zindler et al.*, 1984; *Castillo and Batiza*, 1989; *Niu et al.*, 2002].

A major alternative hypothesis to the plume model is called the SUMA (Statistical Upper Mantle Assemblage or Sampling Upon Melting and Averaging) model [*Meibom and Anderson*, 2003]. The SUMA model proposes a mechanism to produce OIB comprising prominent linear volcanic chains that is analogous to the aforementioned mechanism for generating lavas comprising riseflank seamounts (i.e., through low degree of partial melting of the compositionally heterogeneous upper mantle). The SUMA model claims that: 1) the upper mantle is a heterogeneous assemblage of depleted residues and enriched, subducted oceanic crust, lithosphere and sediments; 2) the heterogeneities are statistical in nature, and have wide ranges in shape, size, and origin; and 3) the geochemical compositions of both OIB and MORB are the outcome of homogenization and sampling by variable degrees of partial melting of the statistically distributed, small to moderately sized mantle heterogeneities. In contrast to the plume model, the SUMA model does not call for the existence of a distinct, deeper, plume source for OIB since both OIB and MORB share a common heterogeneous upper mantle source. In other words, all intraplate lavas are formed by random sampling of dispersed and variably enriched heterogeneities from the same, statistically heterogeneous upper mantle.

In this dissertation, I did a detailed petrologic and geochemical investigation of lavas from isolated intraplate volcanoes in the Pacific to indirectly evaluate the mantle source and origin of the enriched geochemical signature of OIB that form prominent linear volcanic chains. This approach stems from the facts that the geochemical composition of lavas from isolated intraplate volcanoes (e.g., riseflank seamounts) overlaps with those of OIB that form prominent linear volcanic chains [e.g., *Graham et al.*, 1988; *Castillo and Batiza*, 1989; *Hahm et al.*, 2009]. Moreover, both lavas are proposed to have been formed through the same mechanism. Through the study of OIB-like lavas from isolated intraplate volcanoes in the Pacific, I tried to determine whether both OIB-like lavas in isolated intraplate volcanoes and OIB in prominent linear volcanic chains indeed originate from the same upper mantle source through partial melting of randomly dispersed, variably enriched heterogeneities.

Samples analyzed in this study include volcanic lavas and glasses from isolated volcanoes in the northern Lau Basin (NLB) in the southwestern Pacific and from abandoned spreading centers in the eastern Pacific. These were analyzed for their petrology, major and trace element chemistry and Sr, Nd and Pb isotopic ratios. Some of the NLB samples have been analyzed for their volatile and He isotopic contents [*Hahm et al.*, in revision] and the He isotopic composition of some of the samples from fossil spreading centers off Baja California Sur (Mexico) have also been analyzed for their He isotopic composition; these analyses are also included in this investigation.

1.2. Contents of the dissertation

The rest of the dissertation includes the following chapters:

1.2.1. Chapter 2

This chapter presents the petrology and major element, trace element, and Sr-Nd isotope geochemistry of lavas from two intraplate volcanoes (Rochambeau Bank –

RB and Niuafo’ou Island - NF) as well as from the three-limbed ridge system (Mangatolu Triple Junction - MTJ) and a volcanic ridge along a transform fault (Peggy Ridge - PR) within NLB in the southwestern Pacific. Results of the study show that some lavas from the two intraplate volcanoes (RB and NF) and PR are enriched in incompatible trace elements and Sr-Nd isotopes compared to normal-MORB; they are compositionally similar to OIB that comprise some of the nearby Samoan Islands, which are proposed to have been formed by a mantle plume. There are also lavas from MTJ and RB which are enriched in large ion lithophile elements, but depleted in high field strength elements compared to normal-MORB; these are typical characteristics of island arc lavas. In general, results indicate that the ambient mantle beneath NLB is similar to that beneath the Indian Ocean, but this had been modified by subduction and, later, by OIB mantle components. The subduction components are composed mainly of fluid, dehydrated from subducted oceanic crust, and a minor sediment contribution. The fluid component is best represented in the depleted RB samples, and the sediment component is best shown in MTJ samples. MTJ lavas show the most significant subduction signature and represent the highest degree of H_2O-fluxed melting of the underlying mantle in NLB. More important, the geochemically enriched signature of PR, NF and enriched RB lavas are caused by at least two OIB end-components, most likely derived from enriched Samoan mantle plume materials leaking into NLB. The PR and NF regions experience a Samoan plume far field influence or post-erosional type of magmatism whereas the RR-RB region receives the greatest, although still variable, influence from the mantle source of Samoan shield magmatism.

1.2.2. Chapters 3 and 4

Chapters 3 and 4 present results of systematic petrologic and major element, trace element, and Sr-Nd-Pb isotope geochemical investigations of post-spreading lavas on fossil spreading axes off Baja California Sur (Mexico), Mathematician Ridge and Galapagos Rise. The geochemistry of these post-spreading lavas from fossil spreading axes are combined with those from seamount volcanoes on the East Pacific Rise flanks in order to evaluate the generation of lavas that form isolated intraplate volcanoes and the nature of the suboceanic mantle in the eastern Pacific. Results show that the majority of lavas from these fossil spreading centers are alkalic, and the rest are tholeiitic to transitional in composition. The alkalic lavas have OIB-like geochemical signatures, and the tholeiitic to transitional ones are similar to enriched-MORB. Moreover, the geochemistry of fossil spreading center lavas overlaps with that of riseflank seamounts and the geochemically depleted end-member of OIB from major linear volcanic chains in the Pacific, such as Hawaii and Galapagos, and collectively defines a compositional continuum ranging from MORB-like to OIB-like. Similar to those for riseflank seamounts [e.g., *Batiza and Vanko*, 1984; *Zindler et al.*, 1984; *Castillo and Batiza*, 1989; *Niu et al.*, 2002], results of this study suggest that the compositional spectrum of the fossil spreading center lavas is due to different degrees of partial melting of the compositionally heterogeneous suboceanic mantle in the eastern Pacific. A large degree of partial melting of this heterogeneous mantle during vigorous mantle upwelling at an active spreading center produces normal-MORB melts whereas a lesser degree of partial melting during weak mantle upwelling following cessation of spreading produces OIB-like melts. Results also suggest that these OIB-like melts originate from a mantle source different from those of the OIB comprising the major linear volcanic chains in the Pacific.

1.2.3. Chapter 5

The final chapter of this dissertation is an exploratory comparison of the trace element and Sr-Nd isotope geochemistry among alkalic, OIB-like lavas from the Trans-Mexican Volcanic Belt (TMVB), peninsular Baja California and intraplate volcanoes in the eastern Pacific. Such a comparison can provide constraints on the compositions of their respective magma sources and is necessary in order to better understand the true mechanism for generating OIB-like alkalic lavas in a convergent margin environment. Results show that a few of the alkalic lavas from TMVB have similar trace element and isotopic compositions as the OIB-like alkalic lavas from peninsular Baja California and eastern Pacific, suggesting that they might all have come from a similar, initial source - the compositionally heterogeneous Pacific asthenosphere. However, the majority of TMVB alkalic lavas are compositionally more heterogeneous, more so than the less-alkalic Nb-enriched basalts variety of the OIB-like lavas in peninsular Baja California. These Nb-enriched basalts represent OIB-like alkalic lavas that had been contaminated by other mantle components and/or crustal materials in peninsular Baja California. Thus, more detailed studies are needed in order to understand the true mechanism(s) for the formation of OIB-like alkalic lavas along TMVB.

1.3. Conclusions

My comprehensive petrologic and geochemical investigation of volcanic glasses and lavas with OIB-like composition from isolated intraplate volcanoes in the Pacific generates the following conclusions.

1) The mantle source of the OIB-like lavas is the compositionally heterogeneous upper mantle.

2) In NLB, the heterogeneity was created by the introduction into a pre-existing Indian Ocean-type suboceanic mantle of subduction components from the Tonga Trench and later by OIB components from the nearby Samoan mantle plume. The geochemically enriched signature of lavas in the two intraplate volcanoes comes from at least two end-components in the Samoan mantle plume.

3) In the eastern Pacific, the heterogeneous suboceanic mantle provides the source for both Pacific normal-MORB melts at active spreading centers and OIB-like melts at fossil spreading centers. The geochemically enriched, OIB-like compositional signature of intraplate lavas that do not form prominent linear volcanic chains is produced by smaller degrees of partial melting of the compositionally heterogeneous Pacific suboceanic mantle.

4) Finally, although the mechanism for generating OIB-like lavas found in the isolated intraplate volcanoes in the eastern Pacific is similar to that for generating OIB that form prominent linear volcanic chains as claimed by the SUMA model, the detailed petrology and geochemistry of the two lava suites are different. For example, the geochemistry of lavas in the isolated volcanoes in the eastern Pacific is much less variable than that of lavas in the prominent linear volcanic chains and does not seem

to approach the extreme compositions of the proposed end-components of the mantle sources of OIB. Moreover, none of the intraplate lavas has high $^3He/^4He$ ratios (> 8 ± 1 R_A), a distinctive feature of OIB in prominent volcanic chains. Finally, results indicate that geochemically enriched lavas coming directly from the upper mantle through low degrees of partial melting are much less voluminous than OIB that form prominent volcanic chains. All these evidences clearly suggest that true OIB could not have been formed through partial melting of random, enriched heterogeneities in the upper mantle. Ocean island basalts comprising prominent linear volcanic chains appear to be coming from distinct, relatively large reservoirs that reside deeper in the mantle, consistent with the some of the predictions of the plume model.

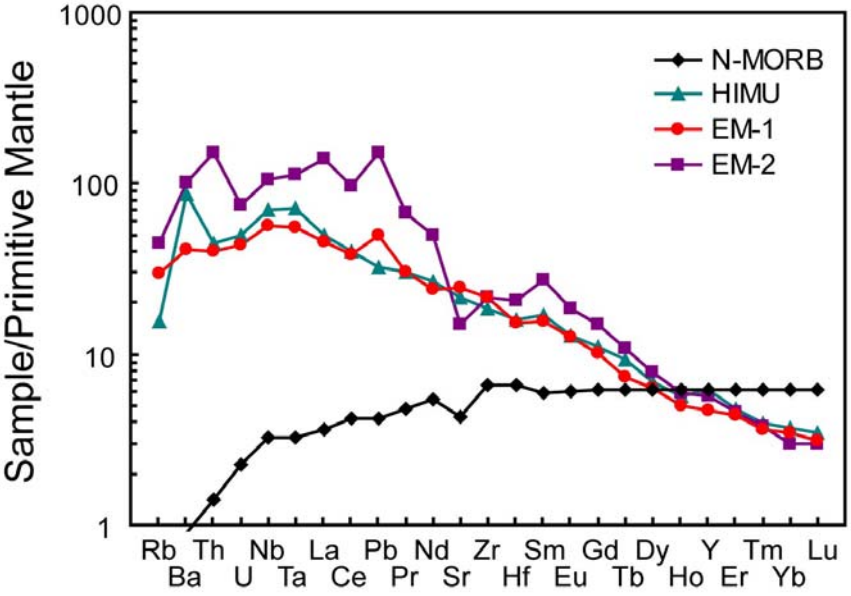

Figure 1.1. Primitive mantle-normalized trace element concentration diagram for average MORB [*Sun and McDonough*, 1989] and representative samples of high-μ(HIMU) [*Woodhead*, 1996], enriched mantle (EM)-1 [*Eisele et al.*, 2002], and EM-2 [*Jackson et al.*, 2007] OIB end-components. Normalizing values are from *Sun and McDonough* [1989].

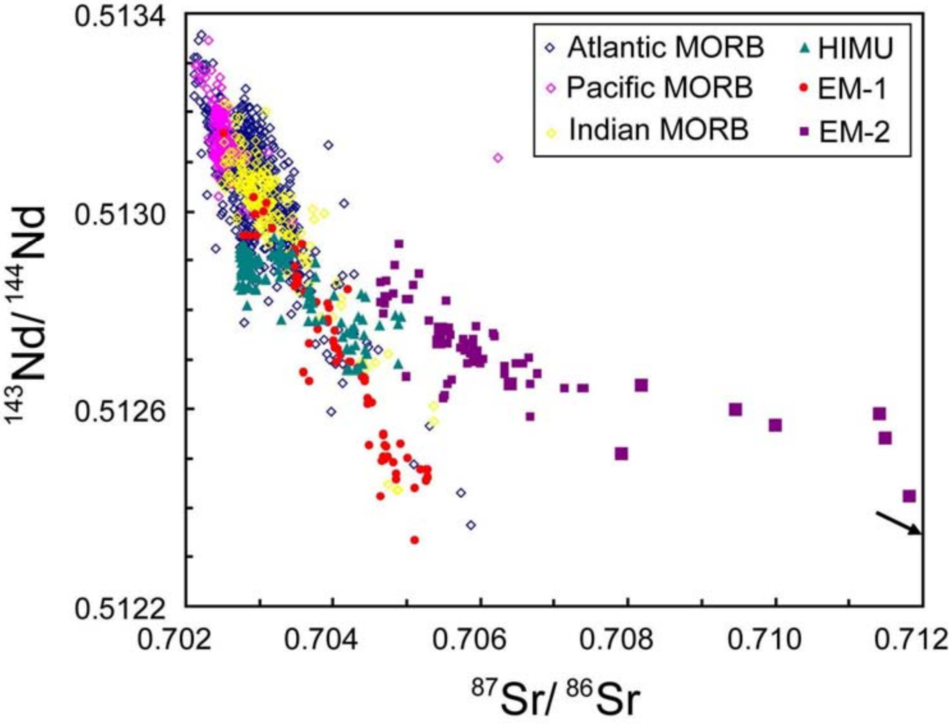

Figure 1.2. ^{87}Sr/^{86}Sr versus ^{143}Nd/^{144}Nd diagram for representative OIB end-components. Data are from the compilation by *Stracke et al.* [2003].

References

Batiza, R., and D. Vanko (1984), Petrology of Young Pacific Seamounts, *J. Geophys. Res.*, *89*(B13), 11235-11260.

Castillo, P. R. and R. Batiza (1989), Strontium, neodymium and lead isotope constraints on near-ridge seamount production beneath the South Atlantic, *Nature*, *342*, 262–265.

Class, C. and A. P. le Roex (2006), Continental material in the shallow oceanic mantle: How does it get there? *Geology*, *34*, 129–132.

Eisele, J., M. Sharma, S. J. G. Galer, J. Blichert-toft, C. W. Devey, and A. W. Hofmann (2002), The role of sediment recycling in EM-1 inferred from Os, Pb, Hf, Nd, Sr isotope and trace element systematics of he Pitcairn hotspot, *Earth Planet. Sci. Lett.*, *196*, 197-212.

Galer, S. J. G. and R. K. O'Nions (1985), Residence time of thorium, uranium and lead in the mantle with implications for mantle convection, *Nature*, *316*,778–782.

Graham, D. W., A. Zindler, M. D. Kurz, W. J. Jenkins, and R. Batiza (1988), He, Pb, Sr and Nd isotope constraints on magma genesis and mantle heterogeneity beneath young Pacific seamounts, *Contrib. Mineral. Petrol.*, *99*(4), 446–463.

Hahm, D., P. R. Castillo and D. R. Hilton (2009), A deep mantle source for high ^{3}He/^{4}He ocean island basalts (OIB) inferred from Pacific near-ridge seamount lavas, *Geophys. Res. Lett.*, *36*, L20316.

Hahm, D., D. R. Hilton, P. R. Castillo, J. W. Hawkins, B. B. Hanan and E. H. Hauri, An overview of the volatile systematics of the Lau Basin - resolving the effects of source variation, magmatic degassing and crustal contamination, *Geochim. Cosmochim. Acta.*, in revision.

Hawkesworth, C. J. and A. I. S. Kemp (2006), Evolution of the continental crust, *Nature*, *443*(7113), 811–817.

Jacobsen, S. B. and G. J. Wasserburg (1979), Mean age of mantle and crustal reservoirs, *J. Geophys. Res.*, *84*, 7,411–7,427.

Jackson, M. G., S. R. Hart, A. A. P. Koppers, H. Staudigel, J. Konter, J. Blusztajn, M. Kurz, and J. A. Russell (2007), The return of subducted continental crust in Samoan lavas, *Nature*, *448*, 684-687.

Meibom, A. and D. L. Anderson (2003), The Statistical Upper Mantle Assemblage, *Earth Planet. Sci. Lett.*, *217*, 123-139.

Morgan, W. J. (1971), Convection plumes in the lower mantle, *Nature*, *230*, 42–43.

Niu, Y. and R. Batiza (1997), Trace element evidence from seamounts for the recycled oceanic crust in the eastern Pacific mantle, *Earth Planet. Sci. Lett.*, *148*, 471-483.

Niu, Y., M. Regelous, I. J. Wendt, R. Batiza, and M. J. O'Hara (2002), Geochemistry of near-EPR seamounts: importance of source vs. process and the origin of enriched mantle component, *Earth Planet. Sci. Lett.*, *199*(3-4), 327-345.

Pilet, S., M. B. Baker, and E. M. Stolper (2008), Metasomatized lithosphere and the origin of alkaline lavas, *Science*, *320*, 916–919.

Plank, T. and C.H. Langmuir (1998), The geochemical composition of subducting sediment and its consequences for the crust and mantle, *Chem. Geol.*, *145*, 325-394.

Stracke, A., M. Bizimis, and V. J. M. Salters (2003), Recycling oceanic crust: quantitative constrains, *Geochem. Geophys. Geosyst.*, *4*(3), 8003.

Sun, S.-S. and W. F. McDonough (1989), Chemical and isotopic systematics of oceanic basalts: Implications for mantle composition and processes, in: Saunders, A. D. and M. K. Norry (ed.) Magmatism in the Ocean Basins, *Geol. Soc. Spec. Publ.*, *42*, 313–345.

Woodhead, J. (1996), Extreme HIMU in an oceanic setting: the geochemistry of Mangaia Island (Polynesia), and temporal evolution of the Cook-Austral hotspot, *J. Volcanol. Geotherm. Res.*, *72*, 1-19.

Zindler, A., H. Staudigel, and R. Batiza (1984), Isotope and trace element geochemistry of young Pacific seamounts: implications for the scale of upper mantle heterogeneity, *Earth Planet. Sci. Lett.*, *70*(2), 175-195.

Zindler, A. and S. Hart (1986), Chemical geodynamics, *Annu. Rev.Earth Pl. Sc.*, *14*, 493–571.

CHAPTER 2

Major and trace element and Sr-Nd isotope signatures of the northern Lau Basin lavas: Implications for the composition and dynamics of the back-arc basin mantle

Abstract

We present new major element, trace element and Sr-Nd isotope analyses of volcanic glasses from Mangatolu Triple Junction (MTJ), Peggy Ridge (PR), Rochambeau Bank (RB), and Niuafo’ou Island (NF) within the northern Lau Basin (NLB). The lavas from MTJ range from tholeiitic basalts to basaltic andesites and andesites: such a lava series can be ascribed to fractional crystallization. Lavas from NF, RB and PR are mainly tholeiitic basalts save for two transitional basalts from RB. The ambient mantle beneath NLB is a pre-existing Indian mid-ocean basalt (MORB)-like mantle modified by subduction and then ocean island basalt (OIB) components. The subduction components are composed mainly of fluid, dehydrated from subducted oceanic crust, with a minor sediment contribution. The fluid component is best represented in the depleted RB samples, which show enrichment in large ion lithophile elements but depletion in high field strength elements; the sediment component is best shown in MTJ samples. MTJ lavas show the most significant subduction signature and represent the highest degree of H_2O-fluxed melting of the underlying mantle in NLB. The geochemically enriched signature of PR, NF and enriched RB lavas are caused by at least two OIB end-components, most likely derived from enriched Samoan mantle plume materials leaking into NLB. The PR and NF regions experience a Samoan plume far field influence or post-erosional type of magmatism whereas the RR-RB region receives the greatest, although still variable, influence from the mantle source of Samoan shield magmatism.

Key words: Lau Basin; geochemistry; back-arc basin basalts; subduction component; OIB component; tectonics

2.1. Introduction

The Lau Basin, located behind Tonga Arc in the SW Pacific, is an active back-arc basin that has been opening over the last 6 Ma [*Hawkins*, 1995; Fig. 2.1]. As is typical of back-arc basins elsewhere, the formation of oceanic crust along spreading centers in the central and southern parts of the Lau Basin is similar to the generation of mid-ocean ridge basalt (MORB) although it is also influenced by subduction processes [e.g. *Volpe et al.*, 1988; *Sunkel*, 1990; *Loock et al.*, 1990; *Falloon et al.*, 1992; *Hawkins and Allan*, 1994]. The subduction signature in basin crust (e.g., enrichment in large ion lithophile elements (LILE) and depletion in high field strength elements (HFSE)) increases with proximity to the arc [e.g. *Pearce et al.*, 1995; *Peate et al.*, 2001; *Tian et al.*, 2008; *Escrig et al.*, 2009]. Compared to the narrower central and southern parts of the basin, however, the northern Lau Basin (NLB) has a more complex tectonic setting. In addition to MORB-like and arc-like lavas, ocean island basalt (OIB)-like lavas are erupted in the NLB [e.g. *Reay et al.*, 1974; *Ewart*, 1976; *Volpe et al.*, 1988; *Hawkins*, 1995]. The presence of OIB-like lavas is supported by the presence of anomalously high $^3He/^4He$ ratios (up to 28 R_A, where R_A= $^3He/^4He$ of air; MORB= 8 ± 1 R_A) in NLB basalts [e.g., *Poreda*, 1985; *Poreda and Craig*, 1992; *Lupton et al.*, 2009; *Hahm et al.*, in revision]. One possibility is that the OIB-like geochemical signature comes from Samoan mantle plume material that has mixed with the mantle beneath the NLB [e.g. *Volpe et al.*, 1988; *Poreda and Craig*, 1992; *Turner and Hawkesworth*, 1998; *Falloon et al.*, 2007; *Regelous et al.*, 2008]. In this scenario, the tearing of the subducted Pacific plate at the northern terminus of the Tonga subduction zone may have allowed the southward infiltration of Samoan plume material into the extending NLB [e.g., *Turner and Hawkesworth*, 1998; *Falloon et al.*, 2007; *Regelous et al.*, 2008]. An alternative view is that the OIB-like geochemical signature, including the high $^3He/^4He$ ratios, in some of the NLB lavas, relates to the southward propagation of the undegassed South Pacific Isotopic and Thermal Anomaly (SOPITA) [*Pearce et al.*, 2007].

The Lau Basin, therefore, offers an excellent opportunity to investigate important geologic processes related to the petrogenesis of back-arc basin lavas, the composition of the mantle source of these lavas, and the dynamics of the mantle beneath a back-arc basin. In this respect, the present work is the third in a series of our collective efforts to better understand these processes in the Lau Basin through investigations of the petrology and geochemistry of its lavas. The first paper, by *Tian et al.* [2008], investigated the major and trace element and Sr-Nd isotope signatures of lavas from the spreading centers in the central Lau Basin in order to constrain the nature and influence of subduction components in the underlying mantle. The second paper, by *Hahm et al.* [in revision], presents an overview of the volatile systematics of the Lau Basin in order to resolve the effects of volatile source variation, magmatic degassing and crustal contamination throughout the entire Lau Basin. In this contribution, we report the major and trace element and Sr-Nd isotopic ratios of volcanic glasses in lavas from the Mangatolu Triple Junction, Peggy Ridge, Rochambeau Bank, and Niuafo'ou Island in NLB. These data are combined with unpublished He isotope and volatile data [*Hahm et al.*, in revision] for the same sample set in order to describe in more detail the geochemical characteristics of the NLB lavas and thereby better constrain the nature and dynamics of the mantle beneath NLB.

2.2. Geological setting and sample analyzed

The Tonga-Kermadec subduction system, which extends for 2550 km between Tonga and New Zealand in the southwest Pacific, is an intraoceanic convergent plate margin formed as a result of subduction of the Pacific plate beneath the Indo-Australian plate. The Lau back-arc basin (Fig. 2.1) is a triangular-shaped area of seafloor located between ~15°-25°S and 174°-179°W and separates the 1100 km long active Tonga Ridge to the east from the Lau Ridge (remnant arc) to the west [*Hawkins*, 1995]. Basin depths are predominantly between 2000 and 3000 m except for the region proximal to Niuafo'ou Island.

The Lau Basin contains a number of rifts and spreading centers. In the south lies the Eastern Lau Spreading Center (ELSC), which terminates at the Valu Fa Ridge (VFR) - its southernmost propagating tip. At about 19º22´S, the northern end of the ELSC overlaps with the southern end of the Central Lau Spreading Center (CLSC) in an area called the Relay Zone (RZ; also known as Intermediate Lau Spreading Center). In the northwestern part of the basin, the Peggy Ridge (PR), a NW-SE trending volcanic ridge along a transform fault, links the northern end of the CLSC to the Lau Extensional Transform Zone (LETZ). Extending northeast from the PR is a short ridge segment called the Northwestern Lau Spreading Center (NWLSC). In the northeastern part of the basin lies the Fonualei Rift and Spreading Center (FRSC; or FSC in *Keller et al.*, 2008): extending north of the FRSC is a three-limbed ridge system called the Mangatolu Triple Junction (MTJ; also known as King's Triple Junction). Further to the northeast lies the Northeastern Lau Spreading Center (NELSC). The only subaerial active volcano, Niuafo'ou Island (NF), lies to the west of the western arm of the MTJ. To the west of NF, a series of rifts, uplifted and extended blocks and individual volcanic centers form the Rochambeau Rifts (RR) between 14.6ºS and 15.5ºS [*Lupton et al.*, 2009]. The RR terminate northwards in a series of faults adjacent to the westward-striking extension of the Tonga trench [*Lupton et al.*, 2009]. Based upon seismic evidence, the Pacific Plate is tearing in the vicinity of RR [*Millen and Hamburger*, 1998]. Along the east-southeastern margin of RR lies the Rochambeau Bank (RB), a northwest trending elongated seamount that sits atop a broad shoal area about 2000 m deep and rising to nearly 1500 m above it [*Parson and Tiffin*, 1993; *Hawkins*, 1995].

Glass samples analyzed in this study come from ridge-axis and off-axis volcanic lavas dredged from NLB during the Scripps Institution of Oceanography (SIO) 7-TOW expedition in 1970 [*Hawkins*, 1976], PAPATUA (PPTU) expedition, Leg 4 in 1985-1986 [*Hawkins*, 1988], ROUNDABOUT (RNDB) expedition, Leg 15 in 1989 [*Hawkins*, 1989] and MAGELLAN expedition (MGLN), Leg 8 in 2006 [*Hahm et al.*, in revision]. Samples were collected from 13 dredge sites in MTJ, 2 sites from the submarine part of NF, 10 sites in RB, and 3 sites in PR (Table 2.1).

2.3. Analytical methods

Samples for geochemical analysis were selected based on location and apparent freshness. Fresh glasses were separated from the rinds of specimens and then crushed into centimeter-sized chips. Major element oxides of 116 glass samples were analyzed by electron microprobe at the Smithsonian Institution in Washington, D.C. The method, accuracy, precision, and standards used in the microprobe laboratory are similar to those described by *Melson et al.* [2002].

Trace element analyses were performed on 37 representative samples analyzed for major elements. Concentrations of rare earth elements (REE) and other trace elements (Rb, Sr, Y, Ba, Pb, Th, Zr, Nb, and Hf) were determined using a Finnigan Element 2 high resolution inductively-coupled plasma mass spectrometry (ICP-MS) at the SIO Analytical Facility following the method of *Janney and Castillo* [1996] with some modifications. Prior to ICP analysis, the glass chips were ultrasonically washed twice in deionized water for 30 minutes, and hand-picked under a binocular microscope. The selected chips were further ultrasonically washed in quartz-distilled water; for each sample, about 25 mg of clean glass chips were digested with an ultrapure 2:1 concentrated HF: HNO3 solution in a Teflon beaker, and then the mixture was placed on a hot plate (~ 60℃) and dried under a heat lamp. About 2 ml of ultrapure 12 N HNO_3 was twice added to the digested sample and evaporated to dryness. After dryness, the digested sample was diluted 4000-fold with 2% HNO_3 solution containing 1 ppb Indium as an internal standard. The instrument drift was corrected by measuring well-analyzed international rock standards as unknowns within the run. Concentrations of compatible elements Cr and Ni were determined by inductively coupled plasma-optical emission spectrometry (ICP-OES) on a Perkin Elmer Optima 3000DV, also at the SIO Analytical Facility, also following the method cited above.

Strontium and Nd isotopic ratios of a subset of 30 samples were then measured on a Micromass Sector 54 multicollector thermal ionization mass spectrometer (TIMS) at SIO following the method described in *Solidum* [2002]. For the isotopic analysis, glass chips were rinsed with 0.75 N HCl for about 10 minutes to remove possible contamination by seawater. Rare earth elements and Sr were separated on cation ion exchange resin using HCl as the eluent, and Nd was separated from other REE using MCI GEL CK08P cation exchange resin in alpha hydroxyisobutyric acid (α-HIBA) medium.

Details of the analytical accuracy and precision of the trace element and Sr and Nd isotope analyses are described in footnotes to Table 2.2.

2.4. Results

Major element data for the NLB samples are given in Table 2.A1. The glass compositions are plotted in a total alkali versus silica plot (TAS; Fig. 2.2), and suggest that NF, RB and PR samples are tholeiitic basalts, save for two transitional basalt samples from RB, whereas samples from MTJ include tholeiitic basalts, basaltic andesites and andesites. The tholeiitic basalts from NF, RB and PR range from relatively primitive (MgO as high as 9.7 wt%; Mg# (100 Mg/(Mg+ Fe^{2+}))= 70.6) to moderately fractionated (MgO down to 5.3 wt%; Mg# = 46.5). Lavas from MTJ, which is geographically closer to Tonga Arc, show larger variations, ranging from relatively primitive (MgO up to 8.2 wt%; Mg# = 68.2) to highly fractionated (MgO down to 1.4 wt%; Mg# = 22.2). Altogether, the samples define clear fractionation trends (Fig. 2.3). SiO_2, Na_2O, and K_2O increase whereas Al_2O_3 and CaO decrease with decreasing MgO. The major element trends of lavas from NLB are parallel to the fractionation trends for lavas from the CLSC [*Tian et al.*, 2008]. In detail, however, the MTJ and RB lavas are displaced towards the field of the Tonga arc lavas [*Turner et al.*, 1997; *Ewart et al.*, 1998] in terms of Al_2O_3 and K_2O versus MgO.

Trace element data of the NLB samples analyzed are given in Table 2.2. The NLB lavas show depleted to slightly enriched light-REE (LREE) concentration patterns relative to average normal- (N-) MORB (Fig. 2.4). The MTJ lavas display the widest range of concentrations and, in addition, develop negative Sr and Eu anomalies with increasing fractionation. Among the basaltic samples, samples from RB generally show more LREE-enriched patterns compared to those from the other three regions (i.e., MTJ, PR and NF); MGLN8-11-8, one of the two transitional basalts (the other is MGLN8-11-7), displays the most LREE enriched pattern. In terms of total incompatible trace element concentrations, NLB basalts are generally enriched in large ion lithophile elements (LILE; e.g., Rb, Ba and Sr) relative to N-MORB. However, they show variable high field strength element (HFSE; e.g., Nb and Zr) concentrations. Basaltic samples from MTJ are all depleted in HFSE. Three out of the four basalts from PR (i.e. PPTU4-19-1, PPTU4-20-2 and PPTU4-20-5) have slightly positive HFSE anomalies whereas sample PPTU4-21-2 does not show an obvious anomaly. Basalts from RB can also be divided into two groups; one displays HFSE depletion (henceforth referred to as depleted RB) whereas the other displays HFSE enrichment (henceforth referred to as enriched RB). The same is true for NF samples: two out of five samples have HFSE depletion (i.e. PPTU4-6-1 and PPTU4-6-3), and the remaining three have HFSE enrichment (i.e. PPTU4-11-1, PPTU4-11-2 and PPTU4-11-11).

The Sr and Nd isotopic compositions of representative NLB samples are also given in Table 2.2. The NLB lavas show large variations in $^{87}Sr/^{86}Sr$ (0.70321~0.70467) and $^{143}Nd/^{144}Nd$ (0.51277~0.51310). Two samples from PR (PPTU4-19-1 and PPTU4-21-2) and the depleted RB samples (except MGLN8-14-2) plot within the field of CLSC lavas, which overlaps with the Indian-MORB field (Fig. 2.5). On the other hand, samples from NF and MTJ and enriched RB samples as well as PR sample PPTU4-20-5 have higher $^{87}Sr/^{86}Sr$ and low $^{143}Nd/^{144}Nd$ values, plotting toward/within the Cook-Austral OIB field. The transitional basalt MGLN8-11-8 from RB plots within the Samoa OIB field and has the highest $^{87}Sr/^{86}Sr$ value.

2.5. Discussion

2.5.1. Geochemical variations of the NLB lavas

The volcanic lavas from NLB display two types of compositional variation: (1) variations in major and trace element contents from tholeiitic basalts to andesites (e.g., MTJ lavas) that can be ascribed to fractional crystallization of lavas from a common mantle source, and (2) intra- and inter-regional geochemical variations due to a compositionally heterogeneous mantle source. Such compositional heterogeneity of the mantle source of NLB lavas is a result of the complex tectonic history of the Lau Basin, geochemical enrichment of the mantle by the nearby subduction process, which also affects the degree of partial melting of the mantle, and the introduction of enriched OIB mantle components into the subduction influenced mantle.

The broad linear correlations between MgO and other major element oxides exhibited by the MTJ lavas are consistent with differentiation trends through fractional crystallization (Fig. 2.3). The same can be said for their subparallel incompatible trace element concentration patterns (Fig. 2.4). Specifically, the concentrations of incompatible elements such as Rb, Ba, Th, REE, and HFSE generally increase from primitive basalts to differentiated andesites (not shown). Interestingly, samples recovered from the northern arm of MTJ are mostly basaltic andesites and andesites whereas samples from the southern and western arms are comparatively more primitive basalts (Fig. 2.2), i.e., there is a general trend of increasing degree of fractionation toward the north within MTJ. The wide range in Sr and Nd isotopic ratios of undifferentiated MTJ samples (Fig. 2.5; Table 2.2) and large variation in highly/moderately incompatible trace element ratios (e.g., La/Sm, Nb/Zr and Ba/Zr ratios) of MTJ lavas overall, however, indicate that the lavas originate from a compositionally heterogeneous mantle source and then experienced similar fractional crystallization histories.

Although there are two distinct trace element patterns (i.e. both HFSE depletion and enrichment) for samples from NF (Fig. 2.4), their limited range of Sr and Nd isotope ratios (Fig. 2.5 and Table 2.2) indicates that NF lavas come from a common, homogeneous mantle source. Thus, NF lavas may still be related through complex fractional crystallization of cogenetic lavas or by different degrees of partial melting of a common source (see below).

As mentioned previously, samples from PR, RB and NF are more primitive than those from MTJ. These samples also display fractionation trends of increasing SiO_2, TiO_2, Na_2O, and K_2O with decreasing MgO (Fig. 2.3). However, most of the other compositional variations can be ascribed to mantle source heterogeneities. For example, among the RB samples, the depleted RB samples are depleted to slightly enriched in LREE, depleted in HFSE (Nb and Zr), and slightly enriched in LILE relative to N-MORB (Rb, Ba and Sr); thus, their mantle source bears the imprint of subduction components. In comparison, the enriched RB samples are enriched in LREE, LILE and HFSE; thus, their mantle source may have been influenced by a mantle source (or sources) similar to those of enriched OIB. The Sr and Nd isotopic compositions of RB basalts also display a bimodal distribution; depleted RB samples overlap with lavas from CLSC, with $^{87}Sr/^{86}Sr \leq 0.7036$ and $^{143}Nd/^{144}Nd \geq 0.51296$, and enriched RB samples extend to an enriched mantle component, with $^{87}Sr/^{86}Sr \geq 0.7039$ and $^{143}Nd/^{144}Nd \leq 0.51285$ (Fig. 2.5). The exception is sample MGLN8-14-2, which is a depleted RB sample in terms of trace elements, but has an isotopic composition within the range of the enriched RB samples.

The PR samples that display two different incompatible trace element patterns (Fig. 2.4) span a wide range of isotopic composition: two samples (i.e. PPTU4-19-1 and PPTU4-21-2) fall within the CLSC field and one sample (i.e. PPTU4-20-5) has a more enriched composition. These observations indicate mantle source heterogeneity.

Volpe et al. [1988] proposed that there is a systematic geographic distribution of the isotopic composition of Lau Basin lavas. They divided Lau Basin basalts into two types: type Ⅰ basalts ($^{87}Sr/^{86}Sr \leq 0.7037$, $^{143}Nd/^{144}Nd \geq 0.51297$), and these occur along and to the south of PR, and type Ⅱ basalts with more enriched isotopic compositions ($^{87}Sr/^{86}Sr \geq 0.7038$, $^{143}Nd/^{144}Nd \leq 0.51288$) and these occur north of PR. However, although our new data indeed show that two PR samples (PPTU4-19-1 and PPTU4-21-2) can be classified as type Ⅰ basalts and enriched RB, NF and MTJ samples (to the north) as type Ⅱ basalts, one PR sample (PPTU4-20-5) is type II and all depleted RB samples (save for MGLN8-14-2) are type I. Moreover, lavas from Futuna Island and Manatu Seamount [*Jackson et al.*, 2010] that are located north of PR but to the northwest of RB have $^{143}Nd/^{144}Nd \leq 0.512975$, which is within the range of CLSC values (Fig. 2.5). Therefore, our data suggest that there is no systematic geographic distribution of the isotopic compositions of NLB lavas. Instead, it appears that the mantle beneath NLB is variably heterogeneous in composition.

Another important feature of the Lau Basin lavas that is borne out by our new data is the lack of obvious correlation between trace element contents and isotope ratios, indicating that a part of the compositional variability of the mantle beneath NLB has a fairly recent origin, specifically through a mantle enrichment/metasomatism process by subduction and, later, by pollution with OIB mantle components. This process will be discussed in more detail below.

2.5.2. Nature of the NLB mantle

Previous studies based on the geochemistry of lavas from the Lau Basin crust [e.g., *Ewart et al.*, 1994; *Hergt and Farley*, 1994; *Hergt and Hawkesworth*, 1994; *Ewart et al.*, 1998] and the active Lau spreading centers [e.g., *Falloon et al.*, 1992; *Peate et al.*, 2001; *Hergt and Woodhead*, 2007; *Tian et al.*, 2008; *Escrig et al.*, 2009] have clearly shown that an initially Pacific MORB-like mantle beneath the Lau Basin has been replaced by a southward-migrating Indian MORB-like mantle. As indicated above, NLB samples with relatively low $^{87}Sr/^{86}Sr$ and high $^{143}Nd/^{144}Nd$ values plot within the CLSC field, which overlaps the Indian MORB field (Fig. 2.5). Thus the current mantle beneath the NLB may have already been completely replaced with Indian-MORB mantle, consistent with previous results [e.g., *Falloon et al.*, 1992; *Peate et al.*, 2001; *Hergt and Woodhead*, 2007; *Tian et al.*, 2008; *Escrig et al.*, 2009]. Compared to Indian MORB, however, both the CLSC and most depleted NLB samples generally have higher $^{87}Sr/^{86}Sr$ for given $^{143}Nd/^{144}Nd$ values (Fig. 2.5) and elevated LILE concentrations relative to N-MORB (Fig. 2.4), indicating the influence of slab-derived components. On the other hand, the Sr and Nd isotopic ratios of MTJ, NF, enriched RB and one PR samples (PPTU4-21-2) are trending away from the field of Indian MORB and toward an enriched component (Fig. 2.5); the presence of OIB components in the Lau Basin mantle has been proposed previously for the enriched component [e.g., *Volpe et al.*, 1988; *Turner and Hawkesworth*, 1998; *Falloon et al.*, 2007; *Regelous* et al., 2008].

To a first order, the influence of both subduction and OIB components on a pre-existing Indian MORB-like mantle is illustrated by data trends of the NLB samples in the Ba/Nb vs. $(La/Sm)_N$ diagram (Fig. 2.6a). Barium, together with other mobile components, is mobilized by fluids from the subducted slab, but this is not the case for HFSE such as Nb, and thus the subduction-influenced samples have high Ba/Nb ratios and only moderate $(La/Sm)_N$ ratios. On the other hand, the OIB component-influenced basalts have elevated $(La/Sm)_N$ ratios and a narrow range of Ba/Nb ratios. These two enrichment trends are also shown in the Nb/Yb vs. $(La/Sm)_N$ diagram (Fig. 2.6b). In general, PR, enriched RB and NF lavas plot along the OIB trend, but the rest of the NLB samples plot between the OIB and subduction enrichment trends.

2.5.2.1. The nature and composition of subduction components

One of the key features of back-arc basin lava composition is its more variable but generally higher contents of fluid-mobile elements, notably water and LILE, relative to N-MORB. Among NLB lavas, samples from MTJ have the highest H_2O contents (0.9~1.9 wt%; *Hahm et al.*, in revision) and these are higher than those of N-MORB (0.17~0.6 wt%; *Jambon and Zimmermann*, 1990). *Nilsson* [1993] compared the andesites from MTJ and VF and proposed that they have similar major element contents and followed similar fractionation paths from similar parental magmas. It has been suggested that the VF marks the tip of the propagating rift system that opened the Lau Basin [*Parson et al.*, 1992], and that rift propagation can prolong the fractionation history of the erupted lavas [*Sinton et al.*, 1983]. Thus, the occurrence of differentiated andesites in the northern arm of MTJ may be ascribed to crystal fractionation associated with rift propagation rather than due to the influence of subduction components. It is important to note, however, that the andesitic samples from the northern arm of MTJ do not show systematically higher H_2O contents than the basaltic samples from the western and southern arms [*Hahm et al.*, in revision] and, thus, H_2O enrichment in MTJ lavas is inconsistent with a crystal fractionation origin, but instead is due to addition of subduction components.

The addition of subduction components to a mantle source can be assessed by comparing trace element abundances in lavas to a reference composition. Here we use the Indian MORB as the reference back-arc mantle and the behavior of Ba/Yb for a given Nb/Yb ratio as a tracer for the origin of subduction components in the NLB mantle (Fig. 2.7a). Ytterbium is refractory and also fluid-immobile in the subduction environment and thus is used as a normalizing factor for both Ba and Nb to reduce the effect of crystal fractionation and phenocryst accumulation on the Ba/Nb ratio [*Pearce et al.*, 2005; *Pearce and Stern*, 2006]. In the plot, NLB samples show a wide scatter with most of the samples plotting either inside or slightly above the Indian-MORB array toward higher Ba/Nb values (i.e., toward subduction components; also see Fig. 2.6a). Those that plot above the array are from MTJ and FRSC [*Keller et al.*, 2008], and hence these data suggest that the influence of subduction components is stronger in lavas erupted from locations near the Tonga arc. However, depleted RB samples and some samples from NF, Futuna Island and Manatu Seamount [*Jackson et al.*, 2010] are also influenced by subduction components and these indicate that the influence of subduction components is actually widespread, though somewhat sporadic, in the NLB mantle.

Another key question regarding the nature of subduction components is whether they are transported from the subducted slab into the mantle wedge through bulk material transfer or through fluids (i.e., aqueous fluid and/or melt). The combination of our new trace element and isotopic data set with published data from Tonga Arc can provide some insight into this question. The elemental ratios involving three incompatible elements Ba, Th and Nb are instructive because they have similar behavior during partial melting and fractional crystallization processes, but are decoupled during subduction process [e.g., *Pearce et al.*, 2005; *Pearce and Stern*, 2006]. High Ba/Th ratio could come from low temperature aqueous fluid released from either dehydration of altered oceanic crust or dewatering of sediments. On the other hand, high Th/Nb ratios could come from bulk addition or partial melt of sediments. In NLB, the subduction-influenced samples which plot above Indian MORB array in Figure 2.7a (i.e., FRSC, MTJ, depleted RB, and some NF, Futuna Island and Manatu Seamount samples) trend from slightly ~right of Indian MORB toward Tonga Arc in the Ba/Th versus Th/Nb plot (Fig. 2.7b). Such a trend indicates that the subduction components that influenced the compositions of NLB lavas represent a mixture of materials transported by both aqueous fluid and bulk or partial melt of sediments. In detail, the aqueous fluid component is dominant in the depleted RB and several MTJ samples with higher Ba/Th ratios whereas the sediment component is dominant in most of the MTJ samples with higher Th/Nb ratios.

To further constrain the nature of subduction components in NLB lavas, we use $^{87}Sr/^{86}Sr$ ratios because these are not fractionated during dehydration or partial melting of the slab and mantle. For clarity, we only plot the Futuna Island, Manatu Seamount and our depleted RB and MTJ samples which are clearly enriched by subduction components (Figs. 2.6, 2.7a and 2.7b) and depleted in HFSE (Fig. 2.4). Except for RB sample MGLN8-14-2, the depleted RB samples have low $^{87}Sr/^{86}Sr$ values and display a roughly positive relationship between Ba/Th and $^{87}Sr/^{86}Sr$; this is consistent with an aqueous fluid component (Fig. 2.7c). Based on the composition of Tonga arc lavas, which naturally are influenced most by subduction components, the estimated $^{87}Sr/^{86}Sr$ ratio of the fluid end-member is ~0.70425; this is within the range of altered MORB value (0.7029~0.7068) [e.g., *Staudigel et al.*, 1995; *Hauff et al.*, 2003]. Therefore, the aqueous fluid must have been derived mainly from the subducted altered oceanic crust. Several samples from Futuna Island, Manatu Seamount, and MTJ - especially the differentiated basaltic andesites and andesites (with x's in Figs. 2.5 and 2.7), and the depleted RB sample MGLN8-14-2 have moderate Ba/Th but higher $^{87}Sr/^{86}Sr$ values relative to Indian MORB; these could be due to a sediment contribution as also indicated in Figure 2.7b. It is noteworthy that based on volatile data, *Hahm et al.* [in revision] proposed that the differentiated MTJ samples may be contaminated by crustal materials.

The geochemistry of Th and Nb with $^{143}Nd/^{144}Nd$ ratios can be used to constrain sediment contributions to the genesis of NLB lavas. Since Th, Nb and Nd are generally thought to be fluid-immobile or, at least less fluid-mobile compared to LILE, their concentrations in back-arc basin lavas are controlled by their background mantle abundances plus inputs from bulk sediment or sediment melt. In a Th/Nb versus $^{143}Nd/^{144}Nd$ plot (Fig. 2.7d), MTJ samples and the depleted RB sample MGLN8-14-2 plot relatively close to the sediment field with higher Th/Nb and lower $^{143}Nd/^{144}Nd$ values relative to Indian MORB, again suggesting that their subduction component signature may have been mainly controlled by sediment addition. As a whole, however, the amount of sediment contribution in MTJ samples and the depleted RB sample MGLN8-14-2 is lower compared to that in Tonga arc lavas (Figs. 2.7b and d), indicating that sediment contributions to MTJ and depleted RB lavas, and to NLB lavas in general, is relatively small. This makes it difficult to unequivocally distinguish and/or separate sediment melt from bulk sediment contribution in NLB lavas. Results of many studies on Tonga arc lavas, on the other hand, have shown that the sediment contribution takes place through a melt [e.g., *Turner and Hawkesworth,* 1997; *Turner et al.*, 1997; *Ewart et al.*, 1998]. Thus, we assume here that sediment contribution is also in the form of a melt in NLB lavas.

Figure 2.8a presents our attempt to model the influence of the subduction components on Indian MORB-like mantle (M - Table 2.3) beneath NLB using Sr and Nd isotopes. It should be noted that in this simple exercise, we are mainly interested in the addition of the subduction components to the pre-existing depleted NLB mantle (Fig. 2.8a); the influence of enriched components in the ambient NLB mantle will be discussed later (Fig. 2.8b). We contend that the fluid component from altered oceanic crust (AF) has $^{87}Sr/^{86}Sr$ ~ 0.70425 and $^{143}Nd/^{144}Nd$ ~ 0.513002. Our model results show that even the least subduction-influenced depleted RB samples, represented by MGLN8-9-9 and MGLN8-10-2, have already been affected by a small amount of aqueous fluid (< 2%). The remaining depleted RB and MTJ samples appear to have been variably influenced by a mixture of aqueous fluid (≤ 7%) and a small amount (≤ 1.5%) of sediment melt (SM; 5% partial melts of Tonga pelagic sediment).

2.5.2.2. Water and extent of melting

As discussed above, the mantle beneath NLB has been influenced by subduction components, which mainly consist of aqueous fluids derived from altered oceanic crust. The dissolved H_2O contents in NLB samples are quite variable [*Langmuir et al.*, 2006; *Hahm et al.*, in revision], ranging from MORB-like water contents (0.17~0.6 wt%; *Jambon and Zimmermann*, 1990) in most PR and NF samples, to intermediate (0.5~1.0 wt%) in RB samples, to the highest values (up to 1.9 wt%) in MTJ samples. *Stolper and Newman* [1994] proposed that fluxing of the mantle by H_2O-rich fluids places an important control on the extents of mantle melting beneath back-arc basins and the resultant compositions of erupted lavas, and this notion is consistent with results of later studies [e.g., *Taylor and Martinez*, 2003; *Kelley et al.*, 2006; *Langmuir et al.*, 2006; *Tian et al.*, 2008; *Bézos et al.*, 2009].

The heavy REE Yb is chosen here to calculate the extent of melting (F) for each of our sample suites (MgO ≥ 5.8 wt%) because it is insensitive to addition of hydrous components and prior source depletion. Results show that melt fraction F positively correlates with calculated water content in the mantle source (C^o_{H2O}) for MTJ, RB and NF sample suites (Fig. 2.9), indicating that extent of melting increases with water content, as in other BABB [e.g., *Taylor and Martinez*, 2003; *Kelley et al.*, 2006; *Langmuir et al.*, 2006; *Tian et al.*, 2008; *Bézos et al.*, 2009]. On the other hand, melt fraction F of three PR samples show negative correlations with C^o_{H2O} as N-MORB [e.g., *Detrick et al.*, 2002; *Asimow et al.*, 2004; *Cushman et al.*, 2004], indicating that the melting process involved in their generation occurred under almost anhydrous conditions, consistent with their low water contents. In detail, PR and NF samples with ≤ 0.04 wt% C^o_{H2O} show ~1.0-9.2% extents of partial melting, overlapping with CLSC samples [*Hahm et al.*, in revision]; MTJ samples which have a significant range of C^o_{H2O} contents (0.03~0.32 wt%) vary from 6.6 to 17.4% extents of melting; depleted and enriched RB samples show large variations in C^o_{H2O} contents (0.02~0.16%) and extents of melting (1.8~17.4%). Finally, FRSC samples show a large extent of melting (>12.8%) and higher C^o_{H2O} content (>0.16wt %), consistent with the location of FRSC closer to the Tonga Arc than MTJ, PR, RB and NF. It should be noted that the melt fraction F values we calculated here are based on a constant MORB source (DMM) composition [*Salters and Stracke*, 2004] although the mantle beneath the NLB is heterogeneous; however, *Kelley et al.* [2006] showed that the melt fraction F values for MTJ samples calculated from constant and variable mantle sources are very similar.

Fractionation-corrected major element concentrations (e.g., Na_2O, FeO and TiO_2 etc.) can also be used to constrain variations in the degree of mantle melting [e.g., *Klein and Langmuir*, 1987; *Taylor and Martinez*, 2003; *Kelley et al.*, 2006; *Langmuir et al.*, 2006] or alternatively, degree of mantle source fertility or depletion [*Niu and O'Hara*, 2008]. For example, it is widely accepted that the global MORB trend of decreasing wt% Na_2O corrected for fractionation to 8 wt% MgO (Na_8) with increasing Fe_8 is due to an increase in the degree of melting induced by an increase in mantle potential temperature [*Klein and Langmuir*, 1987; *Langmuir et al.*, 1992]. However, basalts generated in subduction zones typically have higher H_2O contents and oxygen fugacities (fO_2; e.g. *Carmichael*, 1991), and thus back-arc basin lavas show greater compositional variation and more scattered major elements trends compared to

MORB [e.g. *Taylor and Martinez*, 2003; *Kelley et al.*, 2006; *Langmuir et al.*, 2006]. To further investigate the relationship between partial melting and water content of the NLB mantle, the FeO_t, Na_2O, TiO_2 contents of samples analyzed with ≥ 5.8 wt% MgO were corrected to 8 wt% MgO using the equations of *Taylor and Martinez* [2003]. Although this particular calculation does not take into account the effects of water on the liquid line of descent (cf., *Kelley et al.* [2006] and *Langmuir et al.* [2006]), which may make differences to absolute values, the overall correlations among major elements and water contents are not affected (Figs. 2.10a-b). Positive linear trends exist between Fe_8 and Ti_8 (or Na_8) for samples from MTJ and NF and similar, although more scattered, trends also exist for the majority of RB samples. In contrast, roughly negative trends exist for samples from PR. The positive correlations between Fe_8 and Ti_8 (or Na_8) for MTJ samples, at least, are matched by negative correlations of these parameters with fractionation-corrected H_2O concentration (H_8) (Figs. 2.10c-e), and these are consistent with the global systematics of BABB [*Taylor and Martinez*, 2003; *Kelley et al.*, 2006; *Langmuir et al.*, 2006]. These relationships further indicate that addition of H_2O increases the degree of melting by lowering the mantle solidus beneath MTJ.

In summary, the addition of subduction components not only modifies the composition, through addition of volatiles and fluid-mobile trace elements, but also positively affects the degree of partial melting of the Lau Basin mantle. The mantle source of all NLB lavas, save for those that are geochemically enriched, has been variably affected by subduction components, and lavas that contain the highest signature of subduction components appear to have been produced by the highest degree of partial melting of the underlying mantle.

2.5.2.3. Influence of OIB mantle components

In addition to the influence of subduction components, OIB component(s) must have been involved to explain the geochemically enriched trace element and isotope signature of some NLB lavas. For example, geochemically enriched OIB typically have high concentrations of HFSE such as Nb, and therefore have high Nb/Yb ratios (e.g., shield and post-erosional lavas from Samoa have Nb/Yb ratios ranging from 14.1 to 31.4), whereas typical arc lavas have low Nb/Yb ratios (e.g., Nb/Yb < 0.44 for central Tonga arc lavas) (Fig. 2.6b). Our basaltic samples from NF, PR and RB have Nb/Yb values > 0.76, much higher than the average of 0.52 in DMM [*Salters and Stracke*, 2004], and the enriched RB lavas in particular have values >3. Similarly, REEs are thought to be less affected by subduction-derived materials though LREEs are enriched in subducted sediment [*Plank and Langmuir*, 1998], and $(La/Sm)_N$ ratios in the basaltic samples from NLB range up to 1.86, higher than the range of N-MORB (e.g., 5% to 20% melting of a depleted mantle [DMM; *Salters and Stracke*, 2004] can only produce a $(La/Sm)_N$ range of 0.61 to 0.84). Moreover, the high Nb/Yb ratios of enriched RB samples are accompanied by high La/Sm values (>1) (Fig. 2.6b), which clearly represents a signature of geochemically enriched lavas. *Wendt et al.* [1997] and *Ewart et al.* [1998] attributed this enriched feature of NLB lavas to the presence of a Samoan plume component in their mantle source. Alternatively, *Pearce et al.* [2007] proposed on the basis of Nd and Hf isotopic variations that the heterogeneous mantle beneath the Lau Basin contains easily fusible "plums" of enriched material that were formed by several mantle plumes, including Samoa. These plums are progressively extracted by melting during the southward migration of the mantle, producing enriched lavas [*Pearce et al.,* 2007].

The presence of geochemically enriched or OIB components in the mantle source of NLB lavas can be also observed in the radiogenic nature of their Sr and Nd isotopes (Fig. 2.8b). The enriched RB lavas as well as those from NF and one PR sample PPTU4-20-5 that are enriched in incompatible trace elements, including HFSE, also have lower Nd isotopic ratios than central Tonga arc lavas derived from a mantle metasomatized by subduction components [e.g., *Turner et al.*, 1997; *Ewart et al.*, 1998]. Perhaps the most significant indication of an OIB mantle component beneath NLB is the presence of high $^{3}He/^{4}He$ ratios (> MORB value; Fig. 2.11) in PR and RB lavas; this has been interpreted as due to the incursion of Samoan mantle plume into NLB [e.g., *Poreda*, 1985; *Poreda and Craig*, 1992; *Lupton et al.*, 2009; *Hahm et al.*, in revision].

We now illustrate the nature and contribution of the OIB mantle source components in the ambient NLB mantle in Figure 2.8b, similar to the previously described contribution of subduction components to the pre-existing mantle illustrated in Figure 2.8a. For OIB end-member, we chose (1) mantle source of OIB that is similar in composition to that feeding the shield magmatic phase of the Samoan mantle plume on Upolu Island (O1) [*Workman et al.*, 2004], and (2) the mantle source of OIB that is similar in composition to that of Uo Mamae Seamount lavas (O2), which contributes to post-erosional magmatism on Savai'i and Upolu Islands [*Pearce et al.*, 2007]. Although the origin of O2 component is only based on the isotopic compositions of post-erosional lavas from Savai'i and Upolu Islands, we find it necessary in order to explain the variable isotopic signatures of enriched NLB lavas [see also *Falloon et al.*, 2007; *Regelous et al.*, 2008]. For the ambient mantle, we noted earlier that the mantle source of all NLB lavas, save for the geochemically enriched ones, had been variably affected by subduction components. For example, although CLSC lavas have the most depleted isotopic signature in the Lau Basin, generally they have higher ^{87}Sr/^{86}Sr for given ^{143}Nd/^{144}Nd ratios than Indian MORB (Fig. 2.5) and some of them, including the depleted NLB lavas (Fig. 2.4), have negative Nb anomalies [e.g., *Pearce et al.*, 1995; *Peate et al.*, 2001; *Tian et al.*, 2008]. Thus, the Lau Basin mantle already bears the signature of subduction components, such as the isotopic ratios of fluid mobile elements Sr. Consequently, we pick a possible mantle source from the fairly uniform CLSC lavas instead of an Indian MORB mantle as the ambient Lau Basin mantle (L) in the model.

The mixing model illustrates that the isotopic signature of the enriched NLB lavas is due to the presence of OIB mantle components in their source. For examples, PR lava PPTU4-19-1 plots within the CLSC field, indicating the presence of only a minor amount of OIB mantle components in its mantle source whereas two PR samples PPTU4-20-5 and PPTU4-21-2 can be produced by the addition of O2 (≤ 10%) into the ambient Lau mantle. The majority of NF (including those from *Regelous et al.* [2008]) and enriched RB samples can be produced by mixing L with a variable mixture of O1 and O2. Particularly, NF samples can be explained by mixing L with O2-dominated (≥ 50%) O1-O2 mixture. The model also implies that the variable though relatively high ^{3}He/^{4}He ratios of enriched RB lavas (Fig. 2.11) are due to mixing of these OIB mantle components with ambient NLB mantle. This is because adding OIB components to such a heterogeneous mantle source would give variable geochemical signals, particularly those involving volatiles as exemplified by e.g., variable CO_2/Nb ratios [*Hahm et al.*, in revision].

In summary, combined trace element and Sr, Nd and He isotope data suggest that the geochemically enriched signature of some NLB lavas comes from two enriched OIB mantle end-member components [see also, *Falloon et al.*, 2007; *Regelous et al.*, 2008]. Through modeling, we are able to show that the OIB end-member components, especially when combined with geographic considerations, most probably come from the Samoan mantle plume [e.g., *Turner and Hawkesworth*, 1998; *Falloon et al.*, 2007; *Regelous et al.*, 2008]. The geochemical signature of these components is not readily apparent in NLB lavas unless they make up a substantial part of the source because they mix with ambient mantle that is compositionally heterogeneous due to prior metasomatism by subduction components.

2.5.3. Tectonic implications

Our results, in concert with several other studies [e.g., *Turner and Hawkesworth*, 1998; *Falloon et al.*, 2007; *Regelous et al.*, 2008], favor the idea that the Samoan mantle plume is mainly responsible for the enriched signature of some lavas from NLB. However, the question of how this material gets into NLB is an enigma. One idea, first proposed by *Natland* [1980] in order to accommodate the geometry of the plate boundaries along the northern margin of the Lau Basin, is that there is a tear in the Pacific plate. The idea that the Samoan mantle plume flowed southward into the basin through such a slab tear at the northern margin of Lau Basin was developed further based on geochemical grounds [e.g., *Turner and Hawkesworth*, 1998; *Falloon et al.*, 2007; *Regelous et al.*, 2008] and appears to be consistent with some seismological data [*Millen and Hamburger*, 1998]. An alternative explanation is that the aforementioned Indian mantle domain, which contains Samoan plume in addition to other OIB source materials, is the western edge of the much larger thermal and isotopic anomalous region in the south Pacific [*Pearce et al.*, 2007]. Portions of this isotopically heterogeneous mantle domain entered the southwestern Pacific arc-backarc region < 12 Ma, following the detachment of the Pacific plate barrier to its westward flow. In this scenario, the Indian mantle domain entered the Lau Basin from the northwest, through the North Fiji Basin and into NW Lau Basin (Fig. 2.1).

More detailed geophysical and geochemical data are needed in order to determine the exact tectonic mechanism on how Samoan mantle plume or OIB mantle source materials entered the Lau Basin. However, our new data and model illustrations combined with previous results indicate a quasi-systematic geographic distribution of Samoan plume influence. That is, the RR-RB region receives the greatest influence of the source of Samoan magmatism, particularly the high ^{3}He/^{4}He ratio in NLB (see also, *Lupton et al.* [2009]). Ibn comparison, the PR and NF regions are less influenced by plume material. We propose, therefore, that if the Samoan plume is indeed coming through a tear in the slab, then the tear is centered near the northern end of the NWLSC, along RR (Fig. 2.1), consistent with geophysical results [*Millen and Hamburger*, 1998]. We further argue that the geochemical signature of the Samoan mantle plume would only be variably exhibited by the lavas even in this region because the plume materials mix with a subduction metasomatized mantle and, hence, is compositionally heterogeneous [see also *Jackson et al.*, 2010]. The plume materials propagate outward from this region and further lose their geochemical coherence, as evidenced by the geochemical signature of lavas from NF, the middle of PR and perhaps the North Fiji Basin [e.g., *Gill*, 1984; *Sinton et al.*, 1991; *Eissen et al.*, 1994; *Nohara et al.*, 1994; *Lagabrielle et al.*, 1997]. For example, lavas from the PR and NF on average have lower ^{3}He/^{4}He ratios than RR and RB lavas (Fig. 2.11) [e.g., *Poreda*, 1985; *Poreda and Craig*, 1992; *Lupton et al.*, 2009; *Hahm et al.*, in revision]. This is because the noble gas signature can be diluted by both pre-eruptive degassing and addition of ambient, heterogeneous mantle materials [e.g., *Hilton et al.*, 1993]. We also argue that the sphere of plume influence is asymmetric, affecting larger area in the west (North Fiji Basin) than in the east (NF and RB) due to the presence of subducted Pacific slab in the east.

In nearby Samoa, *Poreda and Farley* [1992] reported ^{3}He/^{4}He ratio of ~11R$_A$ in xenoliths brought up by post-erosional Savai'i lavas (13.7R$_A$ by *Workman et al.*, 2004); this is lower than those of Samoan shield lavas [*Workman et al.*, 2004]. Although the xenoliths are not petrogenetically related to their post-erosional hosts, their He isotopic signature indicates that the post-erosional source has relatively lower ^{3}He/^{4}He values compared to the shield source (see also *Wright and White* [1986]). If this is true, and if post-erosional magmas in ocean islands are low-degree melting of the enriched, but plum-free (eclogite or pyroxenite that has a solidus temperature lower than the more refractory peridotite "pudding") peridotite in the melting tail of a plume [*White and Morgan*, 2004], then another way of interpreting the geochemical signature of the PR and NF regions is that they are experiencing the far field influence of the plume inflow - they have the geochemical features of post-erosional lavas with lower $^3He/^4He$ ratios. Either way, with increasing distance from the main inflow, plume characteristics (the noble gas signature in particular,) become diluted by e.g., degassing, mixing and addition of subduction components as well as crustal contamination by back-arc crust immediately prior to eruption [e.g., *Hahm et al.,* in revision], generating relatively lower $^3He/^4He$ lavas.

2.6. Conclusions

Our new major, trace element and isotope analyses of lavas from NLB, combined with other published and unpublished data, bring new constraints on the heterogeneity of the underlying mantle, origins of the subduction and OIB mantle components, and hydrous melting in this back-arc basin.

Lavas from MTJ range from tholeiitic basalts, basaltic andesites to andesites, which can be generally ascribed to fractional crystallization. Lavas from NF, RB and PR are mainly tholeiitic basalts. Samples from RB can be divided into two groups in terms of their trace element geochemistry. One is a depleted group, showing BABB characteristics (i.e., MORB-like with slight subduction component signature), and the other is more geochemically enriched, indicating the influence of OIB mantle source components. Samples from NF also display two patterns in terms of HFSE depletion and enrichment.

Within NLB, MTJ lavas show the most significant subduction compositional signature and represent the highest degree of H_2O-fluxed melting of the underlying mantle. Trace element and isotope data and modeling indicate that the subduction components are mainly composed of a fluid component derived from subducted oceanic crust with minor sediment contributions. The fluid component is best represented in the depleted RB samples whereas the sediment component is clearest in the MTJ samples.

The geochemically enriched signature of some of NLB lavas comes from at least two end-member components in the enriched Samoan mantle plume materials. The entrance of Samoan mantle plume materials into NLB is centered along the RR, and then the materials propagate and spread outward. The PR and NF regions represent the far field influence and/or post-erosional type of Samoan plume magmatism whereas RR-RB region receives the greatest, but still variable, influence from the source of Samoan magmatism.

Acknowledgements

We are grateful to T. O’Hearn and W. Melson at the National Museum of Natural History of the Smithsonian Institution for analyzing the major elements of the samples, and G. Lugmair and C. MacIsaac at SIO for their assistance with the TIMS analyses. This work is funded by NSF Grant OCE 0453608 to D.H. and P.C. and OCE 0453138 to B.H. and A.P.

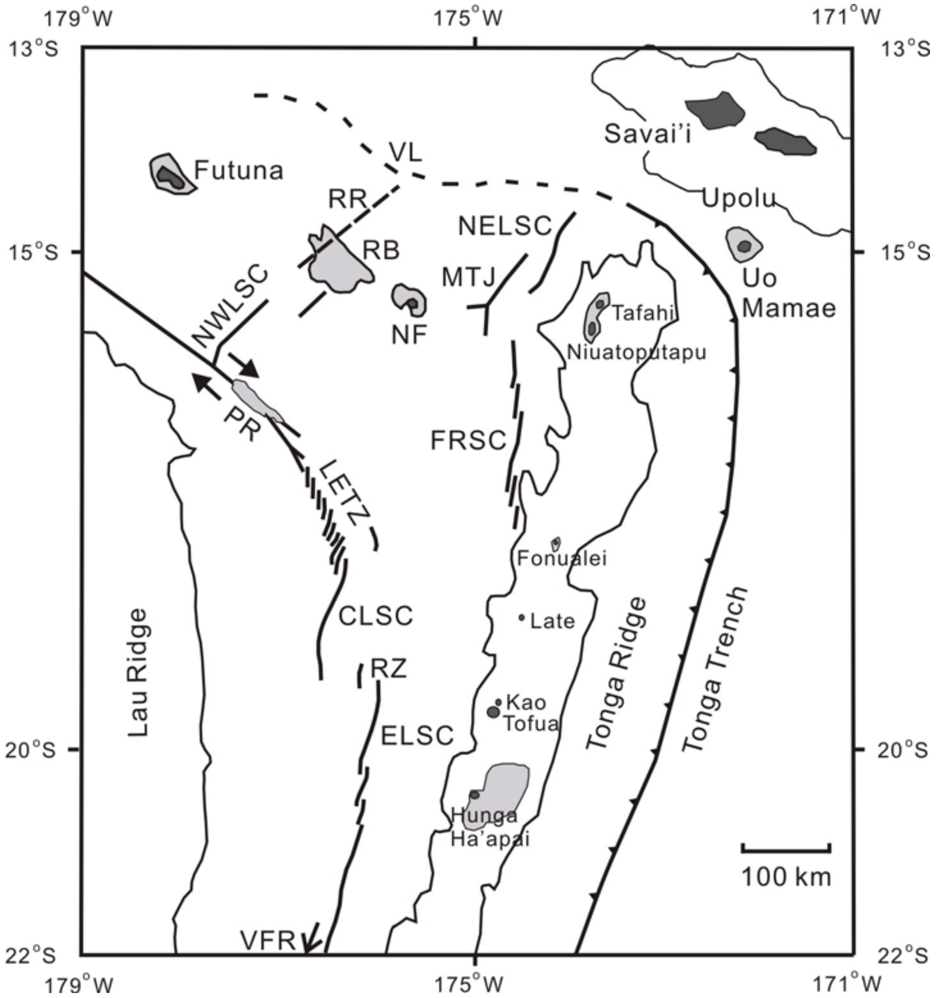
179°W
175°W
171°W
13°S
15°S
20°S
22°S
Savai'i
Upolu
VL
Futuna
RR
RB
NELSC
MTJ
NWLSC
NF
Uo Mamae
Tafahi
Niuatoputapu
PR
FRSC
LETZ
Fonualei
CLSC
Late
RZ
Kao
Tofua
ELSC
Lau Ridge
Tonga Ridge
Tonga Trench
Hunga Ha'apai
100 km
VFR

Figure 2.1. Schematic tectonic map of the Lau Basin (after *Regelous et al.* [2008]). Locations of main tectonic features are from *Zellmer and Taylor* [2001] except for the Rochambeau Rifts, which are inferred from *Lupton et al.* [2009]. Abbreviations: CLSC - Central Lau Spreading Center; RZ - Relay Zone; ELSC - Eastern Lau Spreading Center; VF - Valu Fa Ridge; LETZ - Lau Extensional Transform Zone; PR - Peggy Ridge; RR - Rochambeau Rifts; NWLSC - Northwestern Lau Spreading Center; FRSC - Fonualei Rift and Spreading Center; MTJ - Mangatolu triple junction; NELSC - Northeastern Lau Spreading Center; NF - Niuafo'ou; RB- Rochambeau Bank; VL - Vitiaz Lineament.

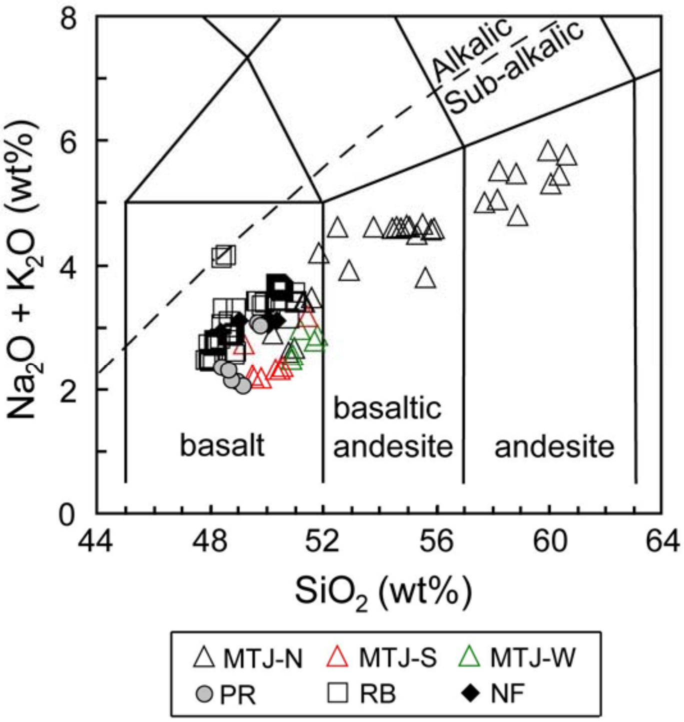

Figure 2.2. Silica (SiO_2) versus total alkalis ($Na_2O + K_2O$) diagram for glasses from lavas from the northern Lau Basin (NLB) (after *Le Bas et al.*, 1986). The lava samples are from the following locations: MTJ-N, northern arm of Mangatolu Triple Junction; MTJ-S, southern arm of Mangatolu Triple Junction; MTJ-W, western arm of Mangatolu Triple Junction; PR, Peggy Ridge; RB, Rochambeau Bank; NF, Niuafo’ou Island.

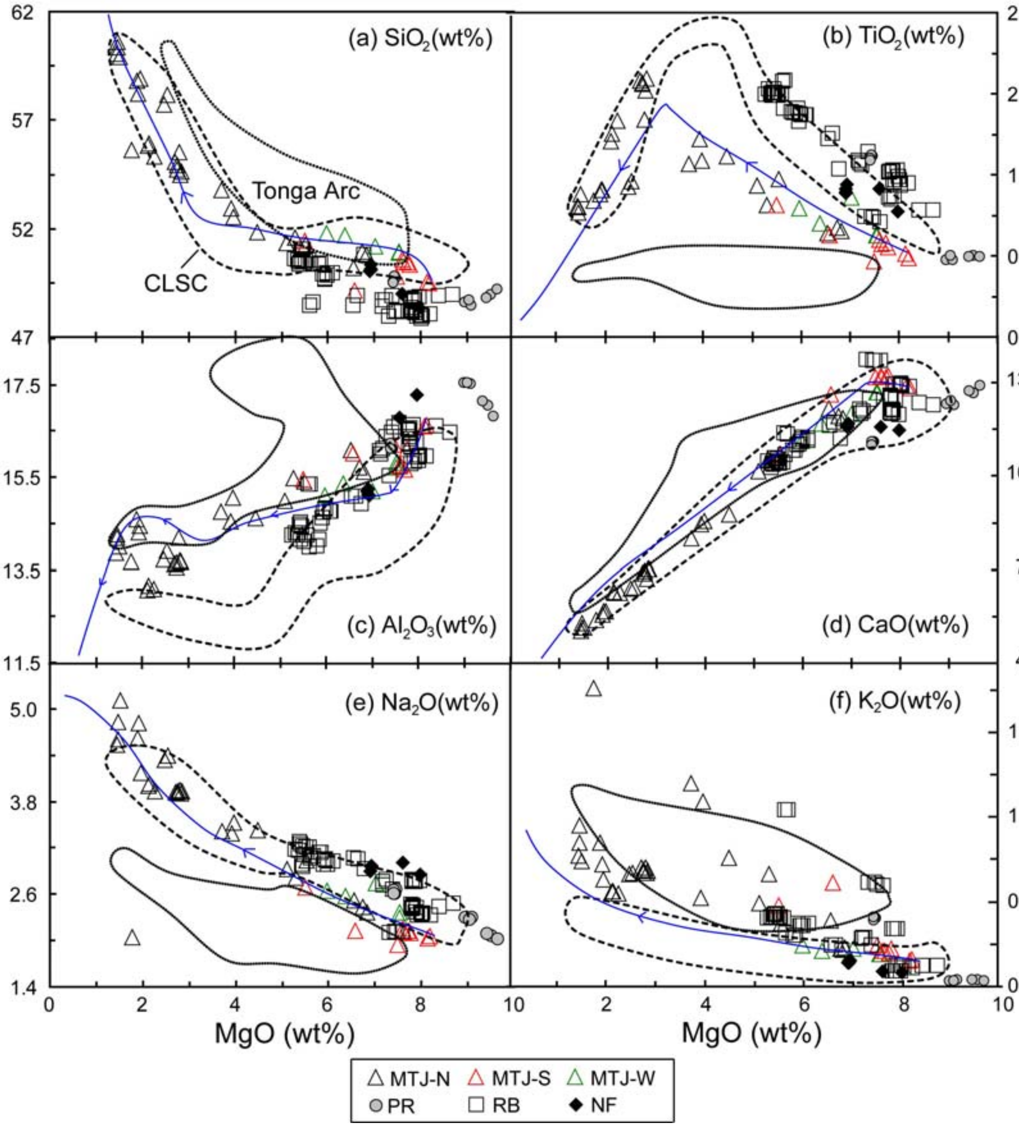

Figure 2.3. MgO versus SiO$_2$, TiO$_2$, Al$_2$O$_3$, CaO, Na$_2$O, and K$_2$O diagrams for NLB lavas. Fields shown are for Central Lau Spreading Center (CLSC, *Tian et al.* [2008] and references therein; dashed lines) and Tonga Arc [*Turner et al.*, 1997; *Ewart et al.* [1998]; dotted lines]. Liquid lines of descend (blue lines) were calculated using the PELE software [*Boudreau*, 1999]. The primitive basalt RNDB15-44-2 was used as the parental melt. Data symbols are as in Figure 2.2.

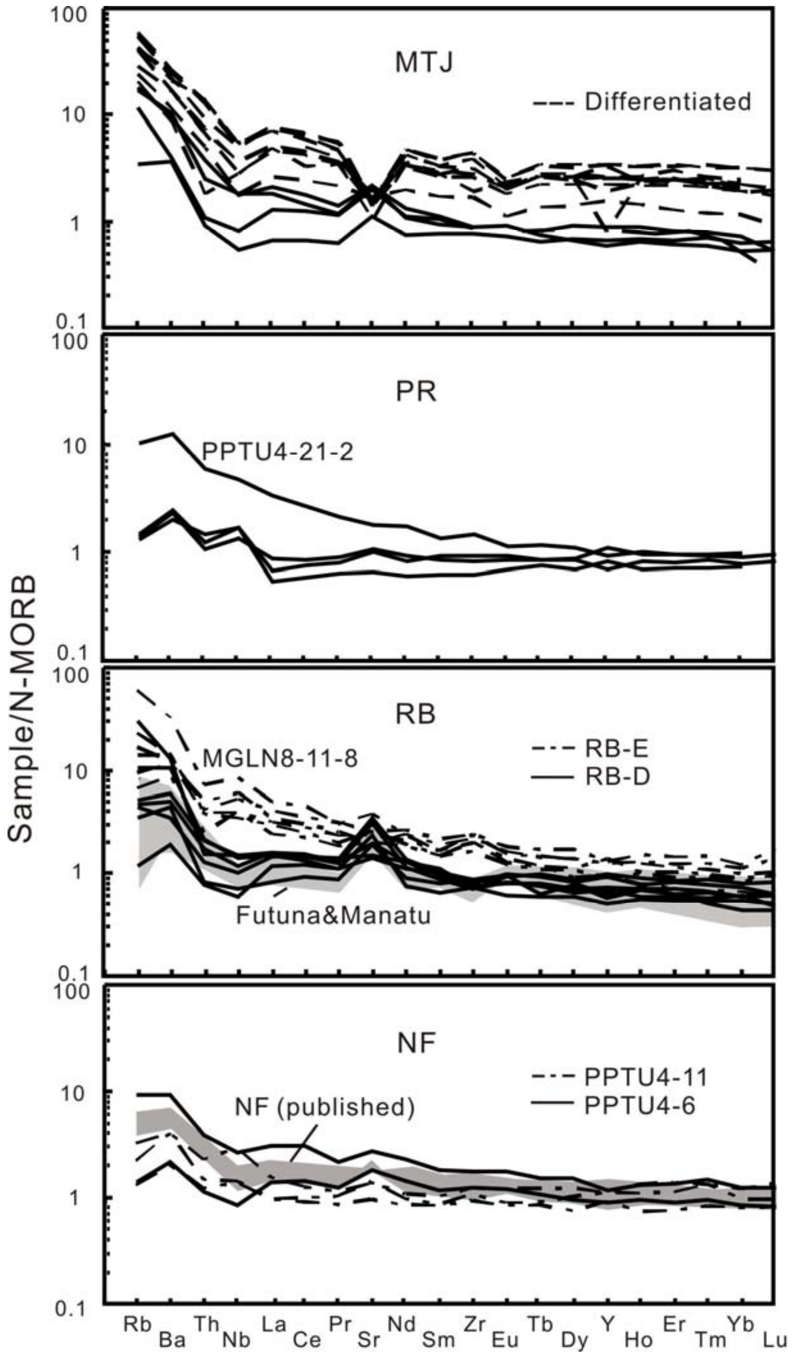

Figure 2.4. Normal-MORB normalized [*Sun and McDonough*, 1989] incompatible trace element concentrations of MTJ, PR, RB, and NF lavas. The two groups from RB are called enriched (in HFSE) RB (RB-E) and depleted (in HFSE) RB (RB-D). Reference fields shown are for Futuna Island and Manatu Seamount [*Jackson et al.*, 2010] and NF [*Regelous et al.*, 2008].

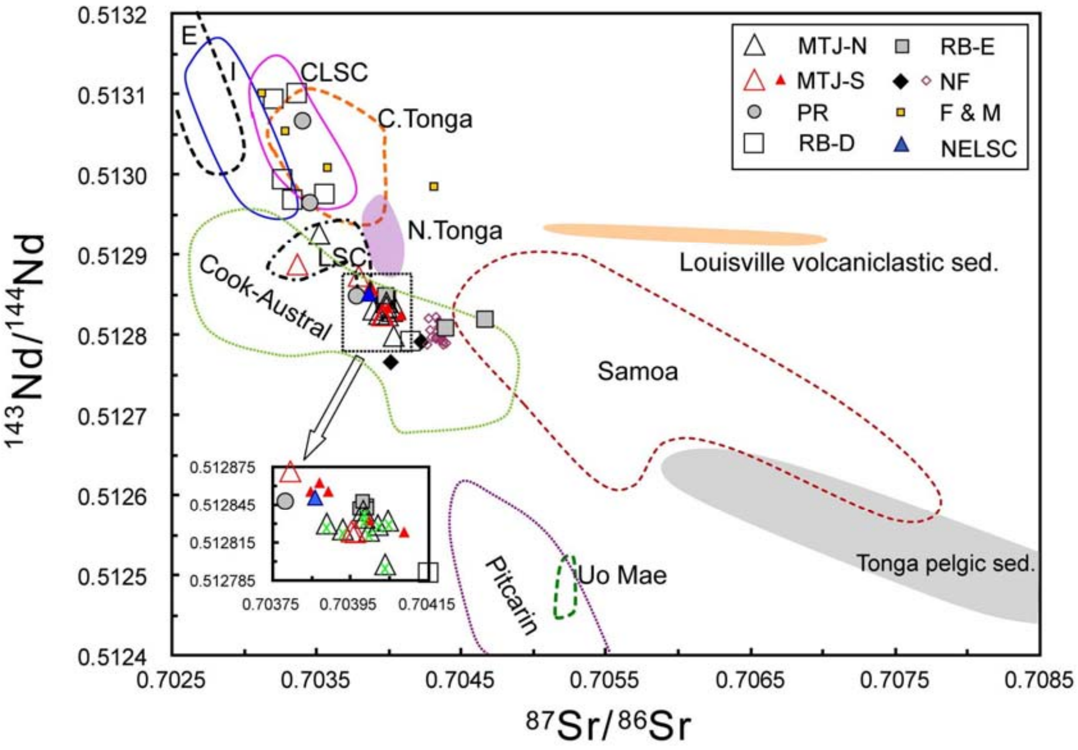

Figure 2.5. $^{87}Sr/^{86}Sr$ versus $^{143}Nd/^{144}Nd$ plot of MTJ (northern and southern arms = MTJ-N and MTJ-S, respectively), PR, RB (depleted RB: RB-D, and enriched RB: RB-E), and NF lavas. Basaltic andesites and andesites from MTJ (triangle) are designated by green x's in the inset graph. Additional data for MTJ (small solid triangle), NF (open purple diamond) and northeast Lau spreading center (NELSC; solid blue triangle) are from *Regelous et al.* [2008] and data for Futuna Island and Manatu seamount (F&M; small solid square) are from *Jackson et al.* [2010]. Fields shown are for EPR MORB (E) and Indian MORB (I) (compiled by *Stracke et al.* [2003]), CLSC (*Tian et al.* [2008] and references therein), Tonga Arc (central: Fonualei, Late, Kao, Tofua, and Hunga Ha'apai; northern: Tafahi and Niuatoputapu; *Turner et al.*, 1997; *Ewart et al.*, 1998), Louisville Seamount Chain (LSC; *Cheng et al.*, 1987), Cook-Austral and Pitcarin Islands [*Stracke et al.*, 2003], Uo Mae Seamount [*Pearce et al.*, 2007], Samoan Islands [*Workman et al.*, 2004], Tonga pelagic sediments, and Louisville volcaniclastic sediments [*Turner et al.*, 1997; *Ewart et al.*, 1998].

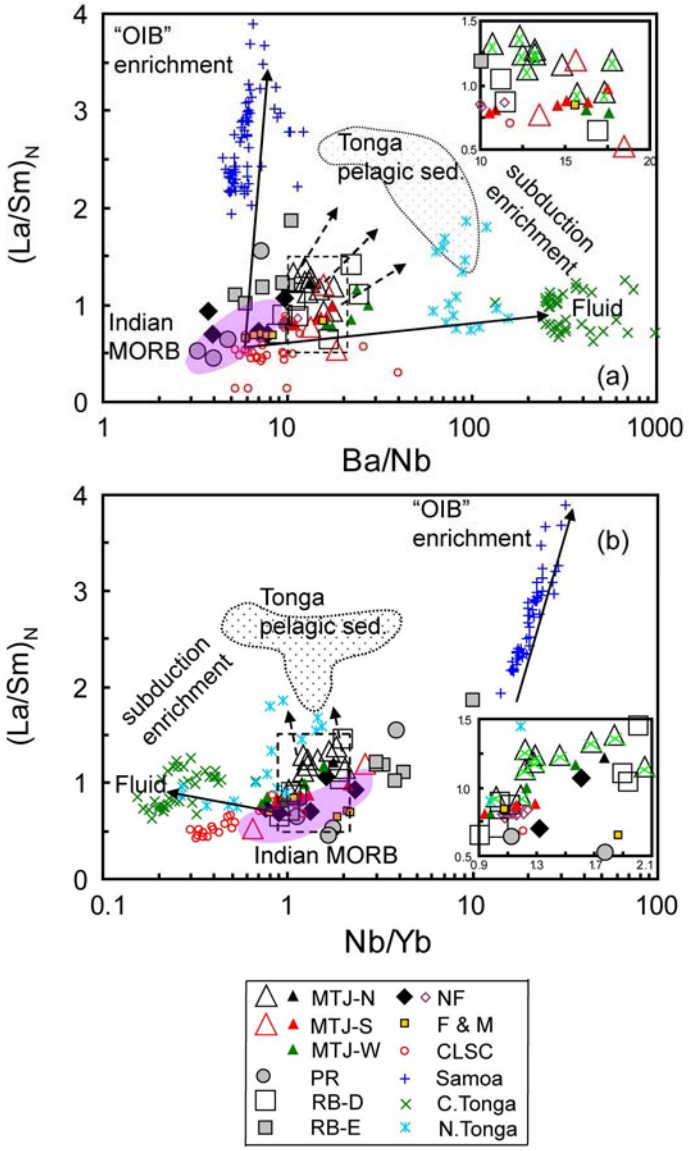

Figure 2.6. (a) (La/Sm)$_N$ versus Ba/Nb ratios and (b) (La/Sm)$_N$ versus Nb/Yb ratios of MTJ, PR, RB, and NF lavas. The subduction components have high Ba/Nb, low Nb/Yb and moderate (La/Sm)$_N$ values: sediment has higher (La/Sm)$_N$ values than fluid due to LREE enrichment in sediment. The OIB component has low Ba/Th, high Nb/Yb and high (La/Sm)$_N$ values. Reference data shown are from MTJ (compiled by *Langmuir et al.* [2006]), NF [*Regelous et al.*, 2008], CLSC (*Tian et al.* [2008] and references therein), Futuna Island and Manatu seamount (F&M; *Jackson et al.* [2010]), Samoa Islands [*Workman et al.*, 2004], and Tonga Arc (central and northern arcs; *Turner et al.*, 1997; *Ewart et al.*, 1998); data symbols are as in Figure 2.5. Reference fields are for Indian MORB and Tonga pelagic sediments, and data sources are as in Figure 2.5.

Figure 2.7. (a) Nb/Yb versus Ba/Yb ratios of MTJ, PR, RB, and NF lavas. Subduction-influenced lavas trend away from the Indian MORB field toward higher Ba/Nb ratios (subduction enrichment). (b) Ba/Th versus Th/Nb ratios of MTJ, PR, RB, and NF lavas. Solid lines with arrows indicate element enrichments - interpreted to have been caused by addition of aqueous fluid (i.e., increasing Ba/Th at a constant and low Th/Yb ratio) and sediment (i.e., increasing Th/Nb at a constant and low Ba/Th ratio) from the subducted slab. (c) Ba/Th versus ^{87}Sr/^{86}Sr ratios of MTJ and depleted RB (RB-D) samples. The arrows point toward the proposed end-member compositions of fluids dehydrated from the subducted altered oceanic crust and sediment. (d) Th/Nb versus ^{143}Nd/^{144}Nd ratios of MTJ and RB-D samples. The higher Th/Nb at a constant ^{143}Nd/^{144}Nd value of the samples relative to Indian MORB represents addition of bulk sediment or sediment melt. Fields shown are for Indian MORB, central and northern Tonga Arc and Tonga pelagic sediment. Reference data shown include MTJ, NF, Futuna Island and Manatu seamount, CLSC, and Fonualei Rift and Spreading Center (FRSC, *Keller et al.*, 2008). Data symbols and sources are as in Figures 2.5 and 2.6.

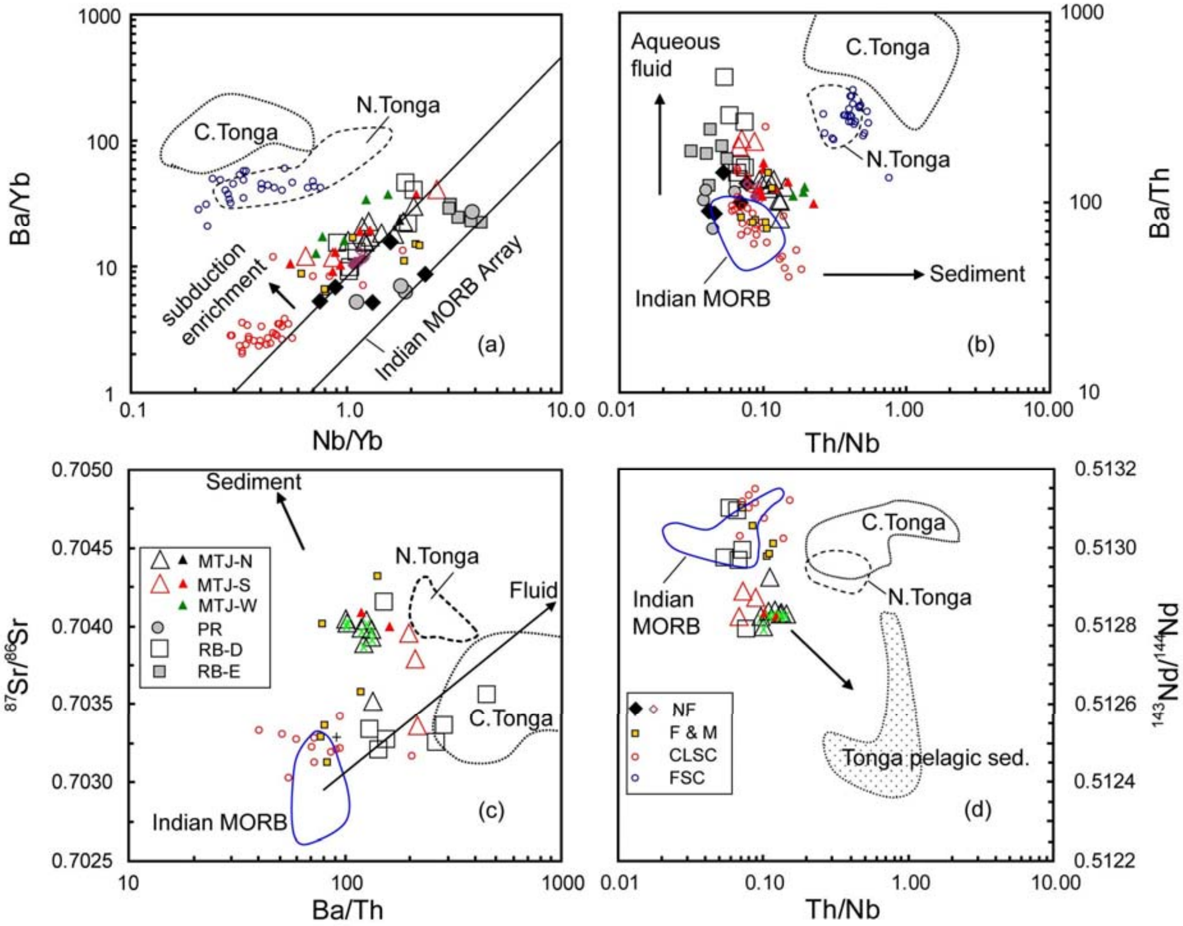

Ba/Yb
1000
100
10
1
0.1
1.0
10.0
Nb/Yb
C.Tonga
N.Tonga
subduction enrichment
Indian MORB Array
(a)
Aqueous fluid
C.Tonga
N.Tonga
Indian MORB
Sediment
(b)
Ba/Th
1000
100
10
0.01
0.10
1.00
10.00
Th/Nb
$^{87}Sr/^{86}Sr$
0.7050
0.7045
0.7040
0.7035
0.7030
0.7025
Sediment
N.Tonga
Fluid
C.Tonga
Indian MORB
(c)
MTJ-N
MTJ-S
MTJ-W
PR
RB-D
RB-E
10
100
1000
Ba/Th
Indian MORB
C.Tonga
N.Tonga
Tonga pelagic sed.
(d)
NF
F & M
CLSC
FSC
$^{143}Nd/^{144}Nd$
0.5132
0.5130
0.5128
0.5126
0.5124
0.5122
0.01
0.10
1.00
10.00
Th/Nb

Figure 2.8. (a) Plots of $^{87}Sr/^{86}Sr$ versus $^{143}Nd/^{144}Nd$ ratios of MTJ and depleted RB (RB-D) lavas showing the influence of subduction components to the NLB mantle. Hexagons represent proposed end-member compositions: pre-existing Indian MORB mantle (M), fluids dehydrated from altered oceanic crust (AF) and sediment melt (SM). End-member compositions are given in Table 2.3. Tick marks on the mixing curves (red and green solid lines) indicate the fraction of added aqueous fluid or sediment melt. Mixings between aqueous fluid and different percentages of 5% partial melts of Tonga pelagic sediment (0.25%, 0.5%, 0.75%, 1% and 1.5%) are also shown as thin black lines. (b) Plots of $^{87}Sr/^{86}Sr$ versus $^{143}Nd/^{144}Nd$ of enriched RB (RB-E), NF and PR lavas showing the influence of OIB components to the NLB mantle. The proposed end-members are ambient Lau Basin mantle (L), an OIB mantle source compositionally similar to that feeding shield magmatism on Upolu Island (O1), and an OIB mantle source similar to that contributing to post-erosional magmatism on Savai'i and Upolu Islands (O2). Tick marks on the mixing curves (red and green solid lines) indicate the fraction of added OIB components. Mixings between O1 and O2 are also shown as thin black lines. Fields shown are for EPR MORB, Indian MORB, CLSC, central and northern Tonga Arc, Uo Mae Seamount, and Upolu Shield Volcano. Data symbols and sources are as in Figure 2.5.

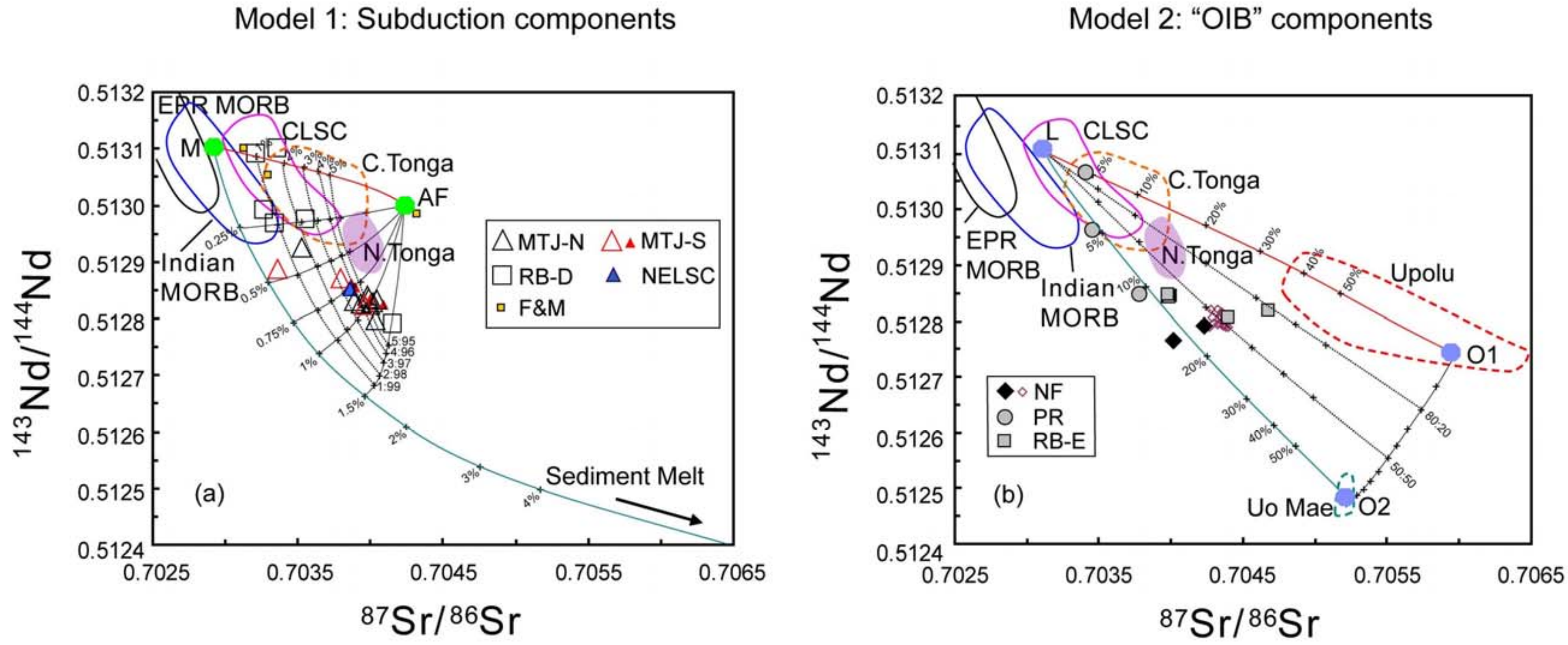

Model 1: Subduction components

Model 2: “OIB” components

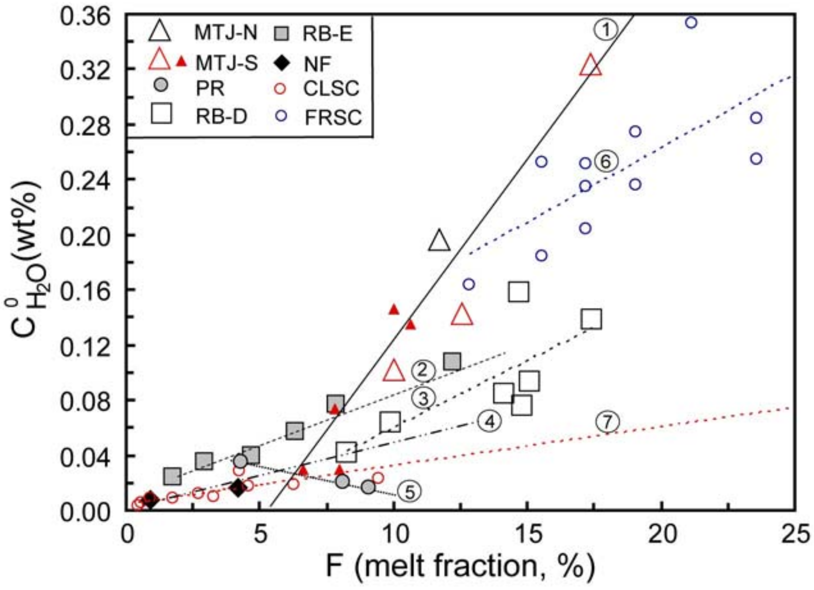

Figure 2.9. C^0_{H2O} (H_2O concentration of the mantle source) versus F (mantle melt fraction) of MTJ, PR, RB, and NF basalts (MgO ≥ 5.8 wt %). The various lines are linear regressions through different data sets: MTJ = 1, enriched RB (RB-E) = 2, depleted RB (RB-D) = 3, NF = 4, PR = 5, FRSC = 6, and CLSC = 7 lavas. The value of melt fraction F is calculated based on batch melting equation: $F= [(C^0_{Yb}/\ C^l_{Yb}) - D_{Yb}]/(1 - D_{Yb})$, where $C^0_{Yb} = 0.401$ ppm [*Salters and Stracke*, 2004], $D_{Yb} = 0.095$ [*Kelley et al.*, 2006], and C^l_{Yb} is the measured concentration of Yb. The output of F is then used to calculate C^0_{H2O} based on batch melting equation: $C^0_{H2O} = C^l_{H2O}\,[F\ (1- D_{H2O}) + D_{H2O}]$, where $D_{H2O} = 0.012$ [*Stolper and Newman*, 1994], and C^l_{H2O} is the measured concentration of H_2O. H_2O concentrations of Lau Basin samples are from the compilation of *Langmuir et al.* [2006] and *Hahm et al.* [in revision]. Other data sources are as in Figure 2.6.

Figure 2.10. (a) Ti_8 and (b) Na_8 versus Fe_8, of basaltic lavas and (c) Ti_8 and (d) Na_8 versus H_8, and (e) Fe_8 versus H_8 of representative basalts from MTJ, PR, RB, and NF. All basalts ($MgO \geq 5.8$ wt%) are corrected for fractional crystallization to $MgO = 8$ wt% (after *Taylor and Martinez*, 2003). Both depleted and enriched RB samples show positive correlations between water content of the mantle source and degree of melting (Fig. 2.9) and, thus, they are grouped together as RB. In order to remove inter-laboratory analytical bias, the major element compositions from the literature were first normalized to the electron microprobe analysis of the Smithsonian Institution of Washington using the correction factor in *Langmuir et al.* [2006]. Data sources are as in Figure 2.6.

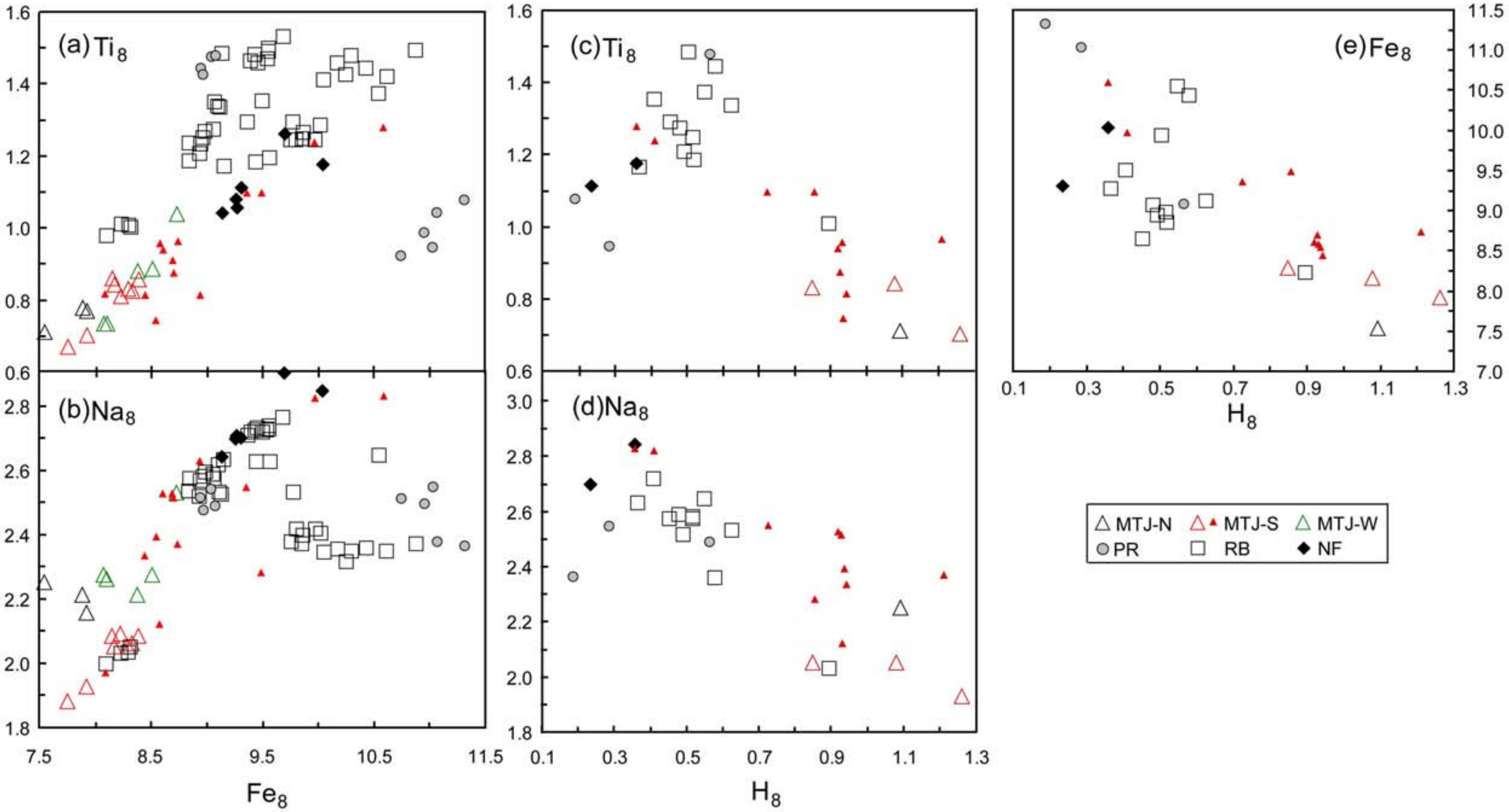
(a) Ti8
(b)Na8
(c)Ti8
(d)Na8
(e)Fe8
Fe8
H8
H8
1.6
1.4
1.2
1.0
0.8
0.6
2.8
2.6
2.4
2.2
2.0
1.8
3.0
11.5
11.0
10.5
10.0
9.5
9.0
8.5
8.0
7.5
7.0
7.5
8.5
9.5
10.5
11.5
0.1
0.3
0.5
0.7
0.9
1.1
1.3
MTJ-N
MTJ-S
MTJ-W
PR
RB
NF

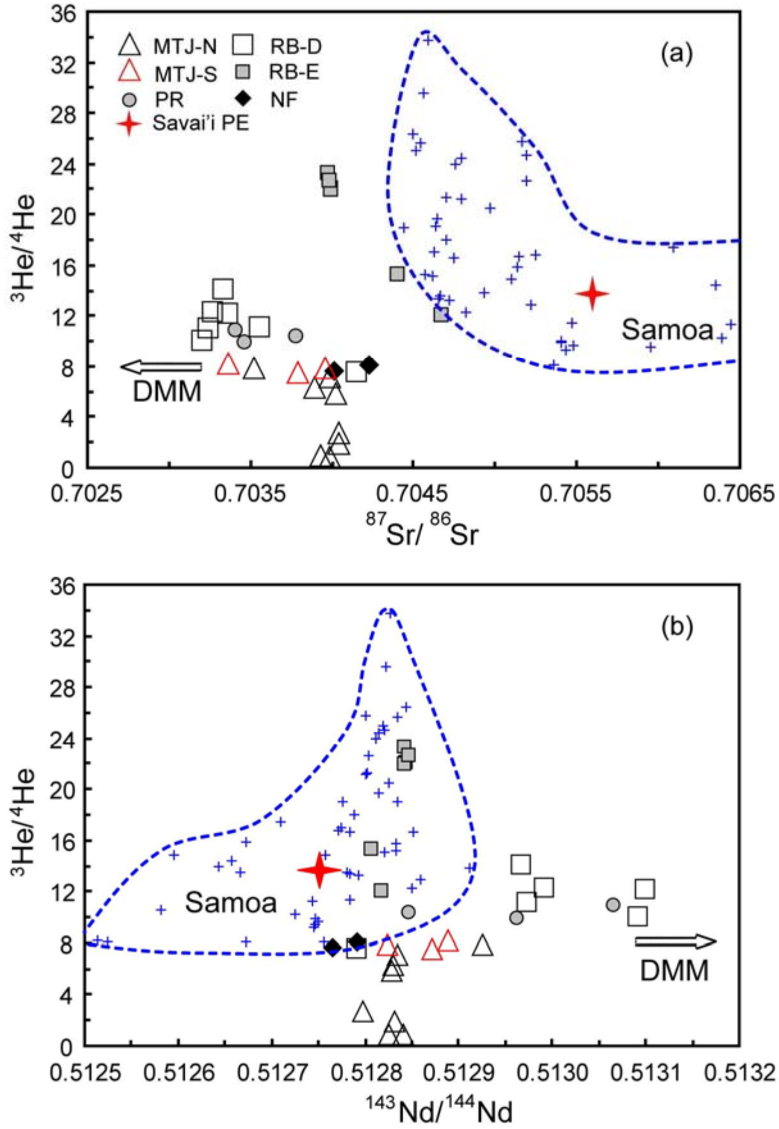

Figure 2.11. Plots of ^{3}He/^{4}He versus (a) ^{87}Sr/^{86}Sr and (b) ^{143}Nd/^{144}Nd ratios of MTJ, PR, RB, and NF lavas. Enriched RB (RB-E) samples with high ^{3}He/^{4}He values have relatively higher ^{87}Sr/^{86}Sr and lower ^{143}Nd/^{144}Nd values relative to other samples from NLB. Samoa Islands (including the Savai'i post-erosional xenolith) data are from *Workman et al.* [2004].

Table 2.1. Dredge locations for lavas from the northern Lau Basin

Location	Cruise	Dredge Station	Lat. (S)	Long.(W)	Depth (m)
MTJ-N	PPTU4	3	15°23.2'	174°40.7'	2172-2098
	PPTU4	9	15°24.6'	174°41.4'	2120-2058
	RNDB15	17	15°32.6'	174°47.1'	2294-2214
	RNDB15	20	15°26.4'	174°41.1'	2168-2165
	RNDB15	21	15°22.5'	174°33.6'	2197-2151
	RNDB15	22	15°20.5'	174°36.7'	2150-2130
	RNDB15	45	15°36.7'	174°48.5'	2238-2188
	RNDB15	46	15°29.5'	174°44.3'	2168-2052
	RNDB15	47	15°18.2'	174°26.2'	2225-1684
MTJ-W	RNDB15	24	15°37.5'	174°53.0'	2366-2310
MTJ-S	PPTU4	4	15°47.8'	174°34.7'	2166-1945
	RNDB15	19	15°41.3'	174°48.3'	2362-2335
	RNDB15	44	15°51.7'	174°51.1'	2574-2554
NF	PPTU4	6	15°19.9'	175°20.5'	1630
	PPTU4	11	15°28.6'	175°34.0'	1839-1541
RB	PPTU4	23	15°12.3'	176°37.8'	1870-1627
	PPTU4	24	15°25.6'	176°15.8'	2257-1758
	MGLN8	7	15°13.0'	176°16.0'	1716
	MGLN8	8	15°26.0'	176°16.0'	2255
	MGLN8	9	15°14.0'	176°35.0'	1746
	MGLN8	10	15°10.0'	176°27.0'	1742
	MGLN8	11	14°56'	176°47.0'	1303
	MGLN8	12	14°49'	176°47.0'	1601
	MGLN8	14	15°02'	175°59.0'	1720
	7 TOW	106	15°09.9'	176º 37.7'	1400-1250
PR	PPTU4	19	16°10.0'	177°21.6'	2725-2202
	PPTU4	20	16°20.2'	177°29.7'	1621-1002
	PPTU4	21	16°17.7'	177°52.7'	2865-1604

Table 2.2. Trace element and Sr-Nd isotope compositions for glassy rinds of epresentative lava samples from the northern Lau Basin.

Group	MTJ-N	MTJ-N	MTJ-N	MTJ-N	MTJ-N	MTJ-N	MTJ-N	MTJ-N	MTJ-N	MTJ-N
Cruise	PPTU4	PPTU4	PPTU4	PPTU4	RNDB15	RNDB15	RNDB15	RNDB15	RNDB15	RNDB15
Sample ID	3-1	3-3	9-1	9-3	17-2	20-1	20-7	21-3	22-1	45-2
Rock Type[a]	BA	BA	An	BA	An	An	An	BA	An	BA
Cr[b]	1	6	11	13	36	4	6	1	3	8
Ni	5	30	12	6	12	6	9	5	11	14
Rb	16.09	11.59	30.75	24.52	23.58	33.19	31.53	23.22	22.59	13.63
Sr	148	92	143	133	142	139	126	162	124	154
Y	71.1		92.5	73.1	53.0	97.0	95.9	62.4	72.2	43.5
Zr	206.5	141.9	287.3	232.1		327.2	332.6	193.6	236.0	124.4
Nb	6.71		11.45	12.62	8.85	12.51	11.75	8.56	8.32	4.17
Ba	105.6	55.8	141.2	134.6	156.8	165.2	155.6	107.1	106.6	72.3
La	11.52	12.30	18.90	17.88	14.08	19.87	19.65	13.12	12.84	6.61
Ce	31.89	24.80	47.61	44.51	37.86	49.55	50.73	32.68	33.82	18.42
Pr	4.54	4.54	6.19	6.12	5.20	7.42	7.14	4.76	4.80	2.83
Nd	24.69	25.11	30.77	30.94	26.47	35.13	34.76	23.99	24.78	14.48
Sm	7.94	7.36	8.84	8.69	7.64	10.34	9.90	6.84	7.35	4.53
Eu	2.10		2.17	2.05	1.97	2.52	2.60	1.84	2.03	1.14
Tb	1.78	1.79	1.78	1.89		2.32	2.23	1.50	1.75	0.91
Dy	11.97	11.69	12.09	12.83	11.45	15.74	14.65	10.12	11.24	6.41
Ho	2.53	2.52	2.42	2.69	2.30	3.35	3.30	2.18	2.49	1.46
Er	7.33	7.55	7.18	8.95	7.20	10.20	9.76	6.50	7.26	3.79
Tm	1.11	1.00	1.04	1.20	1.16	1.47	1.55	0.95	1.04	0.55
Yb	6.59	5.75	6.24	7.52	6.91	9.72	9.63	5.86	6.83	3.51
Lu	2.13	0.90	1.79			1.36	1.41	0.80	0.92	0.42
Hf	5.13	3.79	7.63	6.44	5.20	8.67	8.61	5.21	6.23	3.28
Pb	2.36	1.55	2.22	2.14		2.21	2.90	1.90	1.94	1.41
Th	0.80	0.22	1.13	1.64		1.61	1.54	0.81	0.90	0.60
^{87}Sr/^{86}Sr[c]	0.703982		0.704037		0.703996	0.704019	0.704045		0.703986	0.703889
2σ	0.000010		0.000010		0.000009	0.000008	0.000010		0.000009	0.000011
^{143}Nd/^{144}Nd	0.512840		0.512798		0.512824	0.512829	0.512832		0.512835	0.512830
2σ	0.000008		0.000010		0.000008	0.000007	0.000008		0.000008	0.000007

Table 2.2. Trace element and Sr-Nd isotope compositions (continued)

Location	MTJ-N	MTJ-S	MTJ-S	MTJ-S	MTJ-S	NF	NF	NF	NF	NF
Cruise	RNDB15	PPTU4	RNDB15	RNDB15	RNDB15	PPTU4	PPTU4	PPTU4	PPTU4	PPTU4
Sample ID	47-8	4-1	19-1	19-4	44-2	6-1	6-3	11-1	11-2	11-11
Rock Type[a]	ThB	ThB	ThB	ThB	ThB	ThB	ThB	ThB	ThB	ThB
Cr[b]	139	382	363	322	353	274	268	287	294	283
Ni	60	105	97	77	102	146	70	50	57	52
Rb	10.18	9.45	6.47	3.57	1.94	0.79	5.42	1.87	1.28	0.75
Sr	196	196	179		101	169	254	125	129	88
Y	23.6	16.5	24.8	4.8	18.1	25.1	33.5	31.4	31.7	25.9
Zr	65.8	64.3	63.0		55.4	92.4	133.4	92.8	80.4	70.5
Nb	4.10	4.19	1.88		1.25	2.01	6.25	7.00	3.39	3.29
Ba	60.6	65.4	25.3	18.9	23.1	14.0	60.1	26.2	26.1	13.0
La	5.27	4.51	3.24	0.58	1.64	3.57	7.92	3.95	2.48	2.44
Ce	13.24	10.82	9.22	1.54	4.89	10.94	23.38	9.62	7.59	6.95
Pr	1.84	1.54	1.50	0.25	0.82	1.64	2.92	1.54	1.39	1.16
Nd	9.55	7.96	8.11	1.40	5.39	10.49	16.90	8.03	7.29	6.35
Sm	2.95	2.43	2.73	0.49	2.01	3.14	4.80	2.73	2.31	2.24
Eu		0.93			0.74	1.26	1.83	1.25	0.92	0.87
Tb	0.53	0.50	0.55		0.43	0.72	1.03	0.83	0.62	0.58
Dy	3.79	3.00	4.09	0.86	3.06	4.45	7.13	5.72	4.72	3.46
Ho	0.83	0.64	0.88	0.22	0.69	0.98	1.36	1.37	1.13	0.76
Er	2.28	1.79	2.39	0.67	1.98	2.73	4.04	4.17	3.44	2.28
Tm	0.37	0.27	0.36	0.11	0.32	0.44	0.69	0.62	0.62	0.39
Yb	2.00	1.59	2.16	0.80	1.92	2.65	3.88	3.02	3.79	2.49
Lu	0.19	0.24	0.24		0.29	0.38	0.58	0.44	0.63	0.38
Hf	1.76	1.77	1.75		1.51	2.40	3.74	2.21	2.16	1.95
Pb	0.82	0.57	0.74		0.27	0.87	1.00	0.48	0.5	0.34
Th	0.45	0.30	0.13		0.11	0.14	0.48	0.28	0.18	0.15
^{87}Sr/^{86}Sr[c]	0.703523	0.703362	0.703955	0.703963	0.703793		0.704012	0.704229		
2σ	0.000010	0.000010	0.000009	0.000010	0.000009		0.000010	0.000011		
^{143}Nd/^{144}Nd	0.512925	0.512888	0.512824	0.512824	0.512872		0.512765	0.512791		
2σ	0.000008	0.000010	0.000011	0.000007	0.000007		0.000007	0.000010		

Table 2.2. Trace element and Sr-Nd isotope compositions (continued)

Group	RB-D	RB-D	RB-D	RB-D	RB-D	RB-D	RB-D	RB-E	RB-E	RB-E
Cruise	PPTU4	PPTU4	MGLN8	MGLN8	MGLN8	MGLN8	7-TOW	PPTU4	PPTU4	PPTU4
Sample ID	23-2	23-3	9-9	10-2	12-1	14-2	106-1	24-1	24-2	24-3
Rock Type[a]	ThB	ThB	ThB	ThB	ThB	ThB	ThB	ThB	ThB	ThB
Cr[b]	252	232	355	306	246	326	255	119	237	134
Ni	164	70	459	110	113	372	122	51	76	66
Rb	0.63	2.84	1.92	2.41	17.20	2.63	5.81	5.28	3.71	7.79
Sr	123	130	165	311	276	173	208	171	179	224
Y	15.4	16.9	19.5	25.2	18.4	26.2	13.5	34.2	24.7	35.3
Zr	62.9	53.2	61.3	56.2	49.5	49.8	52.3	158.7	117.6	175.1
Nb	1.33	3.35	1.60	2.27	3.34	2.65	3.20	14.00	9.20	12.00
Ba	11.8	37.6	27.0	21.4	81.7	30.6	65.2	73.0	54.6	87.9
La	2.81	3.88	1.99	3.54	3.79	3.85	3.65	8.41	5.94	10.14
Ce	8.71	10.63	6.67	10.99	10.55	11.31	9.59	22.22	16.48	25.87
Pr	1.41	1.81	1.12	1.76	1.61	1.65	1.42	3.29	2.39	4.07
Nd	7.83	9.12	6.28	9.80	8.02	9.17	5.27	17.14	13.11	18.94
Sm	2.58	2.41	2.00	2.56	2.22	2.86	1.62	4.90	3.79	5.56
Eu	0.95	0.79	0.78	0.96	0.81	0.90	0.59	1.63	1.21	1.80
Tb	0.41		0.51	0.60	0.49	0.64	0.38	0.94	0.71	1.11
Dy	3.34	3.46	3.04	3.61	2.80	3.87	2.55	6.11	4.73	7.60
Ho	0.67	0.72	0.68	0.76	0.58	0.88	0.54	1.26	0.97	1.50
Er	1.76	1.81	2.00	2.38	1.66	2.41	1.54	3.57	2.60	4.20
Tm	0.22	0.28	0.29	0.34	0.25	0.39	0.24	0.55	0.41	0.65
Yb	1.28	1.73	1.75	2.17	1.76	2.36	1.59	3.30	2.41	3.61
Lu	0.19	0.28	0.26	0.27	0.21	0.36	0.22	0.61	0.43	0.77
Hf	1.73	1.48	1.66	1.56	1.37	1.37		3.60	2.60	3.87
Pb	0.97	0.74	0.44	0.39	0.51	0.70		1.33	0.85	1.28
Th	0.09	0.24	0.09	0.15	0.18	0.20	0.25	0.59	0.29	0.49
^{87}Sr/^{86}Sr[c]	0.703338	0.703270	0.703364	0.703210	0.703558	0.704150	0.703260	0.703994	0.703976	0.703992
2σ	0.000009	0.000009	0.000012	0.000010	0.000010	0.000010	0.000011	0.000009	0.000010	0.000010
^{143}Nd/^{144}Nd	0.512967	0.512992	0.513100	0.513092	0.512974	0.512791		0.512844	0.512842	0.512842
2σ	0.000010	0.000011	0.000014	0.000008	0.000007	0.000007		0.000007	0.000008	0.000008

Table 2.2. Trace element and Sr-Nd isotope compositions (continued)

Group	RB-E	RB-E	RB-E	PR	PR	PR	PR		
Cruise	MGLN8	MGLN8	MGLN8	PPTU4	PPTU4	PPTU4	PPTU4		
Sample ID	7-25	8-3	11-8	19-1	20-2	20-5	21-2	BHVO-1	
Rock Type[a]	ThB	ThB	TrB	ThB	ThB	ThB	ThB	measured	recommended
Cr[b]	124	114	101.6	396	321	397	298	292	289
Ni	51	52	46	326	199	300	257	121	121
Rb	12.80	9.39	34.45	0.73	0.77	0.84	5.95	10.29	11
Sr	212	224	336	59	95	91	161	383	403
Y		37.5	25.7	23.0	31.1	19.5	26.3	25.5	27.6
Zr	172.2	146.0	144.8	46.0	60.9	69.6	108.2	175.9	179
Nb	8.90	7.95	19.68	4.00	3.15	4.00	11.52	17.43	19
Ba	90.1	75.3	206.9	13.0	15.0	16.0	83.6	133.0	139
La	7.79	7.23	12.26	1.33	2.21	1.70	8.63	15.4	15.8
Ce	20.69	18.29	33.53	4.43	6.47	5.67	20.67	37.4	39
Pr	3.05	2.57	3.90	0.83	1.21	1.06	2.84	5.4	5.7
Nd	14.93	13.76	16.94	4.38	6.70	6.05	12.75	24.1	25.2
Sm	4.25	3.85	4.25	1.63	2.24	2.42	3.60	5.95	6.2
Eu	1.51	1.26	1.38	0.70	0.88	0.94	1.16	2.15	2.06
Tb	0.96	0.75	0.77	0.50	0.58	0.57	0.78	1.03	0.96
Dy	6.07	5.00	4.03	3.15	4.04	3.92	4.98	5.20	5.2
Ho	1.23	1.00	0.78	0.71	0.96	0.82	1.02	0.94	0.99
Er	3.27	2.98	2.02	2.12	2.81	2.42	2.85	2.3	2.4
Tm	0.48	0.43	0.30	0.33	0.42	0.38	0.44	0.34	0.33
Yb	2.92	2.63	1.95	2.25	2.79	2.40	2.99	1.98	2.02
Lu	0.45	0.42	0.25		0.43	0.37		0.275	0.291
Hf	4.28	3.61	3.55	1.31		1.85	3.05	4.58	4.38
Pb	0.80	0.44	0.95	0.23	0.37	0.35	0.96	2.47	2.6
Th	0.46	0.45	0.86	0.18	0.13	0.15	0.74	0.98	1.08
^{87}Sr/^{86}Sr[c]	0.704399	0.703981	0.704673	0.703407		0.703785	0.703462		
2σ	0.000009	0.000009	0.000009	0.000011		0.000011	0.000009		
^{143}Nd/^{144}Nd	0.512807	0.512847	0.512818	0.513066		0.512847	0.512963		
2σ	0.000008	0.000007	0.000007	0.000008		0.000006	0.000011		

Table 2.2. Trace element and Sr-Nd isotope compositions (continued)

[a] ThB = Tholeiitic Basalt; TrB = Transitional Basalt; BA = Basaltic Andesite; An = Andesite.

[b] Concentrations in ppm. Each sample was analyzed in duplicates and reproducibility was better than 10% (2σ) based on repeated analyses of BHVO-1 as unknowns. The accuracy of BHVO-1 is within 10% of the suggested values (n = 33; *Govindaraju*, 1994), but generally better than 5% for rare earth elements (REEs).

[c] Strontium isotopic ratios were measured through dynamic multi-collection and fractionation corrected to ^{86}Sr/^{88}Sr = 0.1194. Repeated measurements of NBS 987 yielded ^{87}Sr/^{86}Sr = 0.710259 ± 0.000017 (n = 19); 2σ indicates in-run precisions. Neodymium isotopic ratios were measured in oxide form through dynamic multi-collection and fractionation corrected to ^{146}NdO/^{144}NdO = 0.72225 (^{146}Nd/^{144}Nd = 0.7219). Repeated measurements of the La Jolla Nd standard yielded ^{143}Nd/^{144}Nd = 0.511859 ± 0.000008 (n = 11). All Sr and Nd isotopic data are reported relative to NBS 987 (^{87}Sr/^{86}Sr = 0.71025) and La Jolla Nd standard (^{143}Nd/^{144}Nd = 0.51185). Total procedural blanks are negligible: < 35 picograms (pg) for Sr and < 10 pg for Nd.

Table 2.3. End-member compositions for the mixing calculations discussed in the text

	Indian MORB mantle[a]	AOC Fluid[b]	Sediment Melt[c]	Ambient Lau Basin mantle[d]	Upolu Shield[e]	Uo Mamae PE[f]
	M	AF	SM	L	O1	O2
$^{87}Sr/^{86}Sr$	0.702900	0.704250	0.708819	0.703100	0.705953	0.705221
$^{143}Nd/^{144}Nd$	0.513101	0.513002	0.512373	0.513101	0.512746	0.512487
Sr (ppm)	20	583	251	211	543	959
Nd (ppm)	1.6	27.9	143.4	14.2	32.8	79.4

[a] Hypothetical composition is based on Indian MORB data compiled by *Stracke et al.* [2003].

[b] Altered oceanic crust (AOC) fluid; trace element composition is adopted from *Falloon et al.* [2007]; Sr and Nd isotopic composition is after *Staudigel et al.* [1995].

[c] Calculated trace element composition of sediment melt assuming 5% melting of sediment, and using experimentally determined sediment/melt partition coefficients at 2 GPa and 900℃ from *Johnson and Plank* [1999] ($D_{Sr} = 1.23$ and $D_{Nd} = 1.46$); trace element and isotopic compositions of sediment are from DSDP Site 204 sediment (5-5) [*Ewart et al.*, 1998].

[d] The end-member composition is from CLSC lava compositions [*Tian et al.*, 2008].

[e] The end-member composition of Upolu shield lava is from *Workman et al.* [2004].

[f] The end-member composition of Uo Mamae post-erosional (PE) lava is from *Pearce et al.* [2007].

Appendix

The provided table includes major element oxides data of 116 glass samples from the northern Lau Basin, which were analyzed by electron microprobe at the Smithsonian Institution in Washington, D.C.

Table 2.A1. Major element compositions for glassy rinds of lavas dredged from the northern Lau Basin

Location	MTJ-N	MTJ-N	MTJ-N	MTJ-N	MTJ-N	MTJ-N	MTJ-N	MTJ-N	MTJ-N	MTJ-N	MTJ-N	MTJ-N
Voyage	PPTU4	PPTU4	PPTU4	PPTU4	PPTU4	PPTU4	RNDB15	RNDB15	RNDB15	RNDB15	RNDB15	RNDB15
Sample	3-1	3-2	3-3	9-1	9-2	9-3	17-1	17-2	17-3	17-4	20-1	20-2
SiO_2[a]	55.9	55.84	55.33	58.9	58.23	55.61	51.59	58.82	51.29	53.77	60.04	60.37
TiO_2	1.85	1.79	1.97	1.37	1.37	1.28	1.24	1.33	1.46	1.59	1.23	1.22
Al_2O_3	13.16	13.07	13.1	14.45	14.3	13.67	15.47	14.6	15.42	14.76	13.87	14.19
FeO_t[b]	13.49	13.47	13.85	10.1	10.16	9.12	10.52	10.36	9.97	10.92	10.59	10.14
MnO	0.28	0.27	0.28	0.2	0.21	0.17	0.21	0.25	0.21	0.26	0.22	0.24
MgO	2.14	2.12	2.25	1.95	1.92	1.76	5.29	1.89	5.53	3.71	1.44	1.46
CaO	6.26	6.3	6.27	5.67	5.68	5.39	10.52	5.57	10.72	7.99	5.04	5.27
Na_2O	4.03	4.01	3.94	4.17	4.81	2.05	2.82	4.62	3.04	3.41	4.54	4.61
K_2O	0.56	0.56	0.55	0.63	0.72	1.76	0.66	0.85	0.37	1.2	0.77	0.85
P_2O_5	0.39	0.36	0.33	0.37	0.37	0.36	0.25	0.39	0.18	0.34	0.36	0.37
Total	98.07	97.8	97.88	97.81	97.77	91.18	98.56	98.68	98.19	97.96	98.09	98.72
Mg#[c]	25.0	24.8	25.4	28.8	28.4	28.8	51.3	27.7	53.8	41.6	22.2	23.2

Table 2.A1. Major element compositions (continued)

Location	MTJ-N	MTJ-N	MTJ-N	MTJ-N	MTJ-N	MTJ-N	MTJ-N	MTJ-N	MTJ-N	MTJ-N	MTJ-N	MTJ-N
Voyage	RNDB15	RNDB15	RNDB15	RNDB15	RNDB15	RNDB15	RNDB15	RNDB15	RNDB15	RNDB15	RNDB15	RNDB15
Sample	20-3	20-6	20-7	21-1	21-3	21-4	21-6	21-7	22-1	22-2	45-1	45-2
SiO_2[a]	55.52	59.93	60.59	54.61	54.94	55.05	54.46	54.72	57.69	58.14	50.78	52.92
TiO_2	1.98	1.33	1.17	2.33	2.29	2.31	2.23	2.28	1.4	1.44	1.01	1.81
Al_2O_3	14.2	14.01	14.26	13.67	13.57	13.64	13.7	13.65	13.72	13.92	15.63	14.54
FeO_t[b]	12.63	10.05	9.84	13.06	12.86	13.13	13.02	12.92	11.12	11.36	9.07	11.52
MnO	0.28	0.23	0.26	0.26	0.26	0.26	0.25	0.27	0.23	0.21	0.19	0.23
MgO	2.8	1.51	1.46	2.84	2.76	2.71	2.83	2.75	2.47	2.54	6.82	3.92
CaO	6.71	5.15	5.13	7.01	6.88	6.9	7.02	6.94	6.39	6.42	11.86	8.46
Na_2O	3.95	5.11	4.83	3.93	3.94	3.92	3.91	3.91	4.34	4.39	2.36	3.39
K_2O	0.7	0.74	0.95	0.68	0.69	0.7	0.67	0.67	0.66	0.67	0.23	0.52
P_2O_5	0.28	0.36	0.36	0.31	0.33	0.32	0.32	0.31	0.24	0.25	0.11	0.22
Total	99.05	98.4	98.85	98.71	98.52	98.94	98.41	98.4	98.25	99.35	98.06	97.53
Mg#[c]	31.7	24.0	23.7	31.3	31.0	30.2	31.3	30.9	31.8	31.9	61.2	41.6

Table 2.A1. Major element compositions (continued)

Location	MTJ-N	MTJ-N	MTJ-N	MTJ-N	MTJ-N	MTJ-W	MTJ-W	MTJ-W	MTJ-W	MTJ-W	MTJ-S	MTJ-S
Voyage	RNDB15	RNDB15	RNDB15	RNDB15	RNDB15	RNDB15	RNDB15	RNDB15	RNDB15	RNDB15	PPTU4	RNDB15
Sample	45-3	46-1	46-2	46-3	47-8	24-1	24-2	24-3	24-4	24-6	4-1	19-1
SiO_2[a]	50.95	52.51	51.35	51.83	50.21	51.8	51.68	50.93	50.87	51.18	49.16	50.48
TiO_2	1.04	1.62	1.41	1.66	1	1.21	1.08	0.98	0.98	1.3	0.98	0.9
Al_2O_3	15.71	15.05	14.98	14.62	16.08	15.1	15.36	15.81	15.71	15.2	16.03	15.76
FeO_t[b]	9.1	10.53	10.9	11.56	8.83	10.18	9.73	9.03	8.9	9.9	9.31	8.69
MnO	0.17	0.21	0.21	0.24	0.18	0.21	0.18	0.18	0.18	0.19	0.18	0.18
MgO	6.74	3.97	5.1	4.48	6.54	5.97	6.37	7.54	7.52	7.01	6.58	7.63
CaO	11.93	8.56	10.16	8.78	12.17	11.12	11.68	12.68	12.68	12	12.62	13.18
Na_2O	2.44	3.53	2.92	3.43	2.52	2.64	2.58	2.36	2.3	2.75	2.13	2.11
K_2O	0.22	1.09	0.49	0.76	0.39	0.24	0.21	0.19	0.19	0.22	0.61	0.21
P_2O_5	0.11	0.34	0.2	0.27	0.13	0.11	0.1	0.11	0.11	0.13	0.17	0.1
Total	98.41	97.4	97.73	97.62	98.04	98.59	98.96	99.79	99.45	99.88	97.77	99.24
Mg#[c]	60.8	44.2	49.5	44.8	60.8	55.2	57.9	63.7	63.9	59.8	59.7	64.8

Table 2.A1. Major element compositions (continued)

Location	MTJ-S	MTJ-S	MTJ-S	MTJ-S	MTJ-S	MTJ-S	MTJ-S	NF	NF	NF	NF	NF
Voyage	RNDB15	RNDB15	RNDB15	RNDB15	RNDB15	RNDB15	RNDB15	PPTU4	PPTU4	PPTU4	PPTU4	PPTU4
Sample	19-2	19-3	19-4	19-11	44-1	44-2	44-3	6-1	6-3	11-1	11-2	11-8
SiO_2[a]	51.45	50.46	50.57	50.33	49.5	49.53	49.81	49.01	48.36	50.12	50.07	50.35
TiO_2	1.24	0.91	0.94	0.87	0.78	0.82	0.75	1.38	1.18	1.42	1.35	1.38
Al_2O_3	15.46	15.67	15.73	16.11	16.63	16.61	16.2	16.78	17.29	15.1	15.24	15.13
FeO_t[b]	10.64	8.69	8.56	8.59	8.02	8.03	8.23	10.28	10.07	10.73	10.69	10.68
MnO	0.24	0.18	0.2	0.19	0.17	0.16	0.16	0.2	0.17	0.2	0.23	0.21
MgO	5.5	7.72	7.6	7.76	8.19	8.13	7.49	7.59	7.98	6.93	6.92	6.92
CaO	10.68	13.19	13.21	13.21	12.83	12.89	13.19	11.57	11.49	11.67	11.6	11.61
Na_2O	2.69	2.13	2.15	2.1	2.06	2.03	1.95	3.01	2.85	2.96	2.97	2.96
K_2O	0.48	0.2	0.21	0.22	0.16	0.15	0.24	0.09	0.08	0.15	0.15	0.14
P_2O_5	0.17	0.08	0.09	0.08	0.08	0.08	0.1	0.1	0.07	0.1	0.1	0.1
Total	98.54	99.23	99.26	99.45	98.42	98.43	98.12	99.99	99.53	99.39	99.33	99.48
Mg#[c]	52.0	65.1	65.1	65.5	68.2	68.0	65.6	60.8	62.4	57.5	57.6	57.6

Table 2.A1. Major element compositions (continued)

Location	NF	RB	RB	RB	RB	RB	RB	RB	RB	RB	RB	RB
Voyage	PPTU4	PPTU4	PPTU4	PPTU4	PPTU4	PPTU4	PPTU4	MGLN8	MGLN8	MGLN8	MGLN8	MGLN8
Sample	11-11	23-1	23-2	23-3	24-1	24-2	24-3	7-2	7-3	7-4	7-6	7-9
SiO_2[a]	50.04	48.46	48.91	48.88	49.64	49.69	49.87	50.61	50.35	50.43	51.02	51.02
TiO_2	1.34	1.81	1.85	1.7	2.07	1.96	2.03	2.19	2.2	2.18	2.24	2.21
Al_2O_3	15.2	15.08	15.08	15.53	14.61	14.74	14.5	14.25	14.23	14.29	14.51	14.43
FeO_t[b]	10.55	11.3	11.36	9.93	11.53	11.33	11.54	12.75	12.42	12.49	12.65	12.94
MnO	0.2	0.21	0.21	0.19	0.21	0.21	0.2	0.23	0.25	0.23	0.24	0.24
MgO	6.9	6.56	6.65	7.38	5.94	5.95	5.89	5.28	5.38	5.4	5.46	5.48
CaO	11.59	11.62	11.71	12.45	11.04	11.08	11	10.46	10.4	10.36	10.46	10.52
Na_2O	2.9	3.06	3.05	2.66	3.05	3.04	2.98	3.18	3.28	3.25	2.96	3.11
K_2O	0.14	0.24	0.24	0.24	0.36	0.36	0.37	0.4	0.4	0.42	0.42	0.43
P_2O_5	0.1	0.17	0.16	0.16	0.2	0.18	0.2	0.21	0.19	0.18	0.2	0.19
Total	98.96	98.53	99.22	99.11	98.65	98.55	98.59	99.57	99.1	99.23	100.17	100.58
Mg#[c]	57.8	54.9	55.1	60.9	51.9	52.4	51.7	46.5	47.6	47.6	47.5	47.0

Table 2.A1. Major element compositions (continued)

Location **Voyage** **Sample**	RB MGLN8 7-17	RB MGLN8 7-19	RB MGLN8 7-23	RB MGLN8 7-24	RB MGLN8 7-25	RB MGLN8 7-26	RB MGLN8 7-28	RB MGLN8 8-1	RB MGLN8 8-2	RB MGLN8 8-3	RB MGLN8 8-4	RB MGLN8 8-5
SiO_2[a]	50.52	51.05	50.54	50.5	50.47	50.48	50.8	49.85	50.35	49.93	49.93	50.41
TiO_2	2.24	2.21	2.2	2.2	2.18	2.2	1.55	2.02	2.07	2.01	2.01	2.03
Al_2O_3	14.29	14.47	14.24	14.11	14.1	14.15	14.91	14.82	13.99	14.76	14.76	14.15
FeO_t[b]	12.68	12.99	12.36	12.58	12.53	12.7	10.73	11.27	12.68	11.45	11.36	12.56
MnO	0.24	0.25	0.23	0.22	0.25	0.23	0.21	0.22	0.24	0.24	0.21	0.24
MgO	5.35	5.43	5.6	5.52	5.53	5.45	6.78	5.99	5.65	6.11	6.1	5.85
CaO	10.25	10.56	10.44	10.42	10.41	10.41	11.18	11.17	10.67	11.14	11.18	10.8
Na_2O	3.16	2.98	3.2	3.21	3.21	3.22	2.92	2.98	3.1	3.02	3.03	3.13
K_2O	0.41	0.43	0.4	0.41	0.41	0.41	0.21	0.36	0.31	0.37	0.37	0.3
P_2O_5	0.2	0.19	0.2	0.19	0.2	0.19	0.13	0.19	0.17	0.19	0.21	0.18
Total	99.34	100.57	99.42	99.36	99.3	99.44	99.42	98.88	99.25	99.22	99.16	99.67
Mg#[c]	46.9	46.7	48.7	47.9	48.1	47.4	57.0	52.7	48.3	52.8	53.0	49.4

Table 2.A1. Major element compositions (continued)

Location	RB	RB	RB	RB	RB	RB	RB	RB	RB	RB	RB	RB
Voyage	MGLN8	MGLN8	MGLN8	MGLN8	MGLN8	MGLN8	MGLN8	MGLN8	MGLN8	MGLN8	MGLN8	MGLN8
Sample	8-6	8-7	9-1	9-2	9-3	9-4	9-5	9-6	9-7	9-8	9-9	10-1
SiO_2[a]	50.36	49.93	48.8	48.71	48.84	48.68	48.72	48.89	48.63	48.67	48.95	47.94
TiO_2	2.04	2.01	1.54	1.53	1.54	1.53	1.52	1.19	1.52	1.53	1.19	1.45
Al_2O_3	14.01	14.79	16.32	16.17	16.25	16.14	16.22	16.6	16.2	16.22	16.47	15.83
FeO_t[b]	12.44	11.42	9.74	9.64	9.73	9.74	9.73	9.2	9.64	9.81	9.4	10.38
MnO	0.24	0.23	0.19	0.17	0.2	0.2	0.2	0.2	0.19	0.18	0.18	0.21
MgO	5.8	6	7.87	7.85	7.97	7.87	7.8	8.4	7.82	7.81	8.7	7.92
CaO	10.81	11.23	12.09	12.12	11.97	12.04	12.04	12.34	12	12.02	12.26	12.92
Na_2O	3.14	3.02	2.76	2.76	2.77	2.77	2.78	2.44	2.76	2.77	2.48	2.33
K_2O	0.3	0.36	0.09	0.09	0.09	0.09	0.09	0.12	0.09	0.09	0.12	0.12
P_2O_5	0.17	0.18	0.12	0.13	0.12	0.12	0.12	0.1	0.12	0.13	0.1	0.1
Total	99.31	99.18	99.52	99.17	99.49	99.18	99.22	99.48	98.97	99.23	99.85	99.2
Mg#[c]	49.4	52.4	62.9	63.1	63.2	62.9	62.7	65.7	63.0	62.5	66.0	61.5

Table 2.A1. Major element compositions (continued)

Location	RB	RB	RB	RB	RB	RB	RB	RB	RB	RB	RB	RB
Voyage	MGLN8	MGLN8	MGLN8	MGLN8	MGLN8	MGLN8	MGLN8	MGLN8	MGLN8	MGLN8	MGLN8	MGLN8
Sample	10-2	10-3	10-4	10-5	10-6	10-7	11-1	11-2	11-3	11-4	11-5	11-6
SiO_2[a]	47.97	48.02	48.03	48.09	47.85	47.98	48.25	48.36	48.27	48.17	48.16	48.2
TiO_2	1.43	1.48	1.43	1.45	1.41	1.45	1.3	1.3	1.31	1.31	1.29	1.3
Al_2O_3	15.96	15.92	15.95	15.78	15.86	15.93	16.55	16.54	16.62	16.36	16.56	16.5
FeO_t[b]	10.37	10.32	10.54	10.25	10.57	10.15	10.06	10.11	10.16	10.12	10.23	10.15
MnO	0.22	0.18	0.18	0.2	0.18	0.22	0.2	0.18	0.19	0.19	0.18	0.19
MgO	8.04	7.99	8.2	7.87	8.03	8.02	7.79	7.79	7.91	7.83	7.83	7.8
CaO	12.9	12.93	12.86	12.92	12.96	12.95	12.5	12.58	12.44	12.55	12.51	12.52
Na_2O	2.35	2.35	2.33	2.37	2.34	2.35	2.42	2.46	2.42	2.43	2.45	2.41
K_2O	0.11	0.12	0.11	0.12	0.12	0.12	0.34	0.34	0.34	0.34	0.34	0.34
P_2O_5	0.11	0.1	0.12	0.12	0.12	0.1	0.11	0.11	0.11	0.12	0.1	0.11
Total	99.46	99.41	99.75	99.17	99.43	99.27	99.52	99.77	99.77	99.42	99.65	99.52
Mg#[c]	61.9	61.9	62.0	61.7	61.4	62.4	61.9	61.8	62.0	61.9	61.6	61.7

Table 2.A1. Major element compositions (continued)

Location	RB	RB	RB	RB	RB	RB	RB	RB	RB	RB	PR	PR
Voyage	MGLN8	MGLN8	MGLN8	MGLN8	MGLN8	MGLN8	MGLN8	7-TOW	7-TOW	7-TOW	PPTU4	PPTU4
Sample	11-7	11-8	12-1	12-2	12-3	12-4	14-2*	106-1	106-2	106-4	19-1	19-2
SiO_2[a]	48.43	48.57	48.19	48.16	47.94	48.16		48.67	48.4	48.67	48.96	49.19
TiO_2	2.3	2.31	1.13	1.14	1.14	1.09	*1.15*	1.6	1.62	1.58	0.8	0.79
Al_2O_3	15.35	15.33	16.57	16.47	16.38	16.68	*14.89*	16	16.07	16.12	17.06	16.81
FeO_t[b]	11.2	11.34	8.78	8.9	8.81	8.74	*9.79*	10.15	10.11	10.06	8.54	8.41
MnO	0.19	0.18	0.17	0.18	0.18	0.18	*0.17*	0.21	0.19	0.19	0.19	0.16
MgO	5.62	5.68	7.48	7.44	7.31	7.61	*13.78*	7.19	7.18	7.25	9.52	9.65
CaO	11.36	11.34	13.7	13.69	13.74	13.69	*9.85*	12	12.12	12.08	12.64	12.9
Na_2O	3.07	3.1	2.11	2.12	2.1	2.11		2.71	2.76	2.79	2.06	2.02
K_2O	1.04	1.04	0.6	0.61	0.61	0.59	*0.17*	0.29	0.28	0.29	0.04	0.03
P_2O_5	0.24	0.23	0.16	0.16	0.16	0.13		0.15	0.16	0.15	0.03	0.05
Total	98.82	99.12	98.87	98.85	98.36	98.97		98.95	98.88	99.16	99.85	100.02
Mg#[c]	51.3	51.2	64.1	63.7	63.5	64.6	*74.7*	59.8	59.8	60.2	70.0	70.6

Table 2.A1. Major element compositions (continued)

Location	PR	PR	PR	PR	PR	PR	PR	PR
Voyage	PPTU4	PPTU4	PPTU4	PPTU4	PPTU4	PPTU4	PPTU4	PPTU4
Sample	19-3	20-2	20-5	20-6	21-1	21-2	21-3	21-4
SiO_2[a]	48.77	48.58	48.44	48.68	49.67	49.78	49.56	49.5
TiO_2	0.79	0.76	0.76	0.8	1.66	1.67	1.64	1.62
Al_2O_3	17.14	17.54	17.52	17.55	16.12	16.12	16.24	16.12
FeO_t[b]	8.56	9.13	9.1	9.15	9.72	9.79	9.66	9.69
MnO	0.17	0.18	0.2	0.16	0.18	0.17	0.19	0.19
MgO	9.42	8.96	9.1	9.04	7.46	7.44	7.42	7.42
CaO	12.71	12.32	12.27	12.41	11.08	11.11	11.09	10.99
Na_2O	2.09	2.3	2.3	2.27	2.66	2.61	2.64	2.6
K_2O	0.04	0.03	0.04	0.03	0.4	0.41	0.39	0.41
P_2O_5	0.05	0.05	0.04	0.04	0.21	0.21	0.21	0.2
Total	99.74	99.84	99.77	100.12	99.16	99.31	99.04	98.74
Mg#[c]	69.8	67.3	67.7	67.4	61.7	61.4	61.7	61.6

[a] Concentrations in wt%.

[b] FeO_t is total Fe expressed as Fe^{2+}.

[c] Mg# = 100 Mg/(Mg+ Fe^{2+}) assuming Fe_2O_3/FeO=0.15.

* The major element composition of MGLN8-14-2 was measured by ICP-OES at SIO Analytical Facility.

References

Asimow, P. D., J. E. Dixon, and C. H. Langmuir (2004), A hydrous melting and fractionation model for mid-ocean ridge basalts: Application to the Mid-Atlantic Ridge near the Azores, *Geochem. Geophys. Geosyst.*, 5, Q01E16, doi:10.1029/2003GC000568.

Boudreau, A. (1999), PELE - a version of the MELTS software program for the PC platform, *Comput. Geosci.*, 25, 201-203, doi:10.1016/S0098-3004(98)00117-4.

Bézos, A., S. Escrig, C. H. Langmuir, P. J. Michael, and P. D. Asimow (2009), Origins of chemical diversity of back-arc basin basalts: a segment-scale study of the Eastern Lau Spreading Center, *J. Geophys. Res.*, 114, B06212, doi:10.1029/2008JB005924.

Carmichael, I. S. E. (1991), The redox state of basic and silicic magmas: a reflection of their source regions?, *Contrib. Mineral Petrol.*, 106, 129-141, doi:10.1007/BF00306429.

Cheng, Q., K. H. Park, J. D. Macdougall, A. Zindler, G. W. Lugmuir, H. Staudigel, J. Hawkins, and P. Lonsdale (1987), Isotopic evidence for a hotspot origin of the Louisville Seamount Chain, in: Keating, B. H. (ed.) *Seamounts, islands, and atolls*, American Geophysical Union, Washington DC, 283–296.

Cushman, B., J. Sinton, G. Ito, and J. Eaby Dixon (2004), Glass compositions, plume-ridge interaction, and hydrous melting along the Galápagos Spreading Center, 90.5°W to 98°W, *Geochem. Geophys. Geosyst.*, 5, Q08E17, doi:10.1029/2004GC000709.

Detrick, R. S., J. M. Sinton, G. Ito, J. P. Canales, M. Behn, T. Blacic, B. Cushman, J. E. Dixon, D. W. Graham, and J. J. Mahoney (2002), Correlated geophysical, geochemical, and volcanological manifestations of plume-ridge interaction along the Galápagos Spreading Center, *Geochem. Geophys. Geosyst.*, 3(10), 8501, doi:10.1029/2002GC000350.

Escrig, S., A. Bézos, S. L. Goldstein, C. H. Langmuir, and P. J. Michael (2009), Mantle source variations beneath the Eastern Lau Spreading Center and the nature of subduction components in the Lau basin–Tonga arc system, *Geochem. Geophys. Geosyst.*, Q04014, doi:10.1029/2008GC002281.

Eissen, J. P., M. Nohara, and J. Cotten (1994), North-Fiji Basin basalts and their magma sources. I: Incompatible elements constraints, *Mar. Geol.*, 116, 163–178, doi:10.1016/0025-3227(94)90174-0.

Ewart, A. (1976), A petrological study of the younger Tongan andesites and dacites, and the olivine tholeiites of Niuafo'ou island, S.W. Pacific, *Contrib. Mineral Petrol.*, 58, 1-21, doi: 10.1007/BF00384740.

Ewart, A., J. M. Hergt, and J. W. Hawkins (1994), Major element, trace element, and isotope (Pb, Sr, and Nd) geochemistry of site 839 basalts and basaltic andesites: Implications for arc volcanism, in: Hawkins, J. W., Parson, L. M., Allan, J. F. et al. (ed.) *Proceedings of the Ocean Drilling Program, Scientific Results, 135*, College Station, TX: Ocean Drilling Program, 519–531, doi:10.2973/odp.proc.sr.135.161.1994,

Ewart, A., K.D. Collerson, M. Regelous, J. I.Wendt, Y. Niu (1998), Geochemical evolution within the Tonga-Kermadec-Lau arc back-arc systems: the role of varying mantle wedge composition in space and time, *J. Petrolog.*, 39, 331-368, doi:10.1093/petroj/39.3.331.

Escrig, S., A. Bézos, S. L. Goldstein, C. H. Langmuir, and P. J. Michael (2009), Mantle source variations beneath the Eastern Lau Spreading Center and the nature of subduction components in the Lau basin-Tonga arc system, *Geochem. Geophys. Geosyst.*, 10, Q04014, doi:10.1029/2008GC002281.

Falloon, T. J., A. Malahoff, L. P. Zonenshain, and Y. Bogdanov (1992), Petrology and geochemistry of back-arc basin basalts from Lau Basin spreading ridges at 15º, 18º, 19ºS, *Mineral Petrol.*, 47, 1-35.

Falloon, T. J., L. V. Danyushevsky, T. J. Crawford, R. Mass, J. W. Woodhead, S. M. Eggins, S. H. Bloomer, D. J. Wright, S. K. Zlobin, and A. R. Stacey (2007), Multiple mantle plume components involved in the petrogenesis of subduction - related lavas from the northern termination of the Tonga Arc and northern Lau Basin: Evidence from the geochemistry of arc and backarc submarine volcanics, *Geochem. Geophys. Geosyst.*, 8, Q09003, doi:10.1029/2007GC001619.

Gill, J. B. (1984), Sr-Pb-Nd isotopic evidence that both MORB and OIB sources contribute to oceanic island arc magmas in Fiji, *Earth Planet. Sci. Lett.*, 68, 443–458, doi:10.1016/0012-821X(84)90129-8.

Govindaraju, K. (1994), Compilation of working values and samples description for 383 geostandards. *Geostandard Newsletter* 18, 1-158.

Hahm, D., D. R. Hilton, P. R. Castillo, J. W. Hawkins, B. B. Hanan and E. H. Hauri, An overview of the volatile systematics of the Lau Basin – resolving the effects of source variation, magmatic degassing and crustal contamination, *Geochim. Cosmochim. Acta*., in revision.

Hawkins, J. W. (1976), Petrology and geochemistry of basaltic rocks of the Lau Basin, *Earth Planet. Sci. Lett.*, 28, 283-297, doi:10.1016/0012-821X(76)90190-4.

Hawkins, J. W. (1988), Cruise Report - PAPATUA expedition, Leg 04, *R/V Thomas Washington SIO Reference Series,* 88-14.

Hawkins, J. W. (1989), Cruise Report - ROUNDABOUT expedition, Leg 14, 15, *R/V Thomas Washington SIO Reference Series,* 89-13.

Hawkins, J.W. (1995), The geology of the Lau Basin. In: Taylor, B. (ed.) *Backarc basins: Tectonics and Magmatism*, New York: Plenum, 63-138.

Hawkins, J.W., and J. F. Allan (1994), Petrologic evolution of the Lau Basin, Sites 834-839, in: Hawkins, J. W. , L. M. Parson, and J. F. Allan et al, *Proceedings of the Ocean Drilling Program, Scientific Results*, *135*, College Station, TX: Ocean Drilling Program, 427-470, doi:10.2973/odp.proc.sr.135.136.1994.

Hauff, F., K. Hoernle, and A. Schmidt (2003), Sr-Nd-Pb composition of Mesozoic Pacific oceanic crust (Site 1149 and 801, ODP Leg 185): Implications for alteration of ocean crust and the input into the Izu-Bonin-Mariana subduction system, *Geochem. Geophys. Geosyst.*, 4, 8913, doi:10.1029/2002GC000421.

Hergt, J. M., and K. N. Farley (1994), Major element, trace element, and isotope (Pb, Sr, and Nd) variations in Site 834 basalts: Implications for the initiation of backarc opening, in: Hawkins, J. W., Parson, L. M., Allan, J. F. et al. (ed.) *Proceedings of the Ocean Drilling Program, Scientific Results*, *135*, College Station, TX: Ocean Drilling Program, 471–485, doi:10.2973/odp.proc.sr.135.144.1994.

Hergt, J. M., and C. J. Hawkesworth (1994), The Pb, Sr, and Nd isotopic evolution of the Lau Basin: implications for mantle dynamics during the back-arc opening, in: Hawkins, J. W., Parson, L. M., Allan, J. F. et al. (ed.) *Proceedings of the Ocean Drilling Program, Scientific Results, 135*, College Station, TX: Ocean Drilling Program,, 505-517, doi:10.2973/odp.proc.sr.135.142.1994.

Hergt, J. M., and J. D. Woodhead (2007), A critical evaluation of recent models for Lau-Tonga arc-backarc basin magmatic evolution, *Chem. Geol.*, 245, 9–44, doi:10.1016/j.chemgeo.2007.07.022.

Hilton, D. R., K. Hammerschmidt, G. Loock, and H. Frierichsen (1993), Helium and argon isotope systematics of the central Lau Basin and Valu Fa Ridge: Evidence of crust/mantle interactions in a back-arc basin, *Geochim. Cosmochim. Acta*, 57, 2819–2841, doi:10.1016/0016-7037(93)90392-A.

Jackson, M. G., S. R. Hart, J. G. konter, A. A. P. Koppers, H. Staudigel, M. D. Kurz, J. Blusztajn, and J. M. Sinton (2010), Samoan hot spot track on a “hot spot highway”: Implications for mantle plumes and a deep Samoan mantle source, *Geochem. Geophys. Geosyst.*, 11, Q12009, doi:10.1029/2010GC003232.

Jambon, A., and J. L. Zimmermann (1990), Water in oceanic basalts: evidence for dehydration of recycled crust, *Earth Planet. Sci. Lett.*, 101, 323–331, doi:10.1016/0012-821X(90)90163-R.

Janney, P. E., and P. R. Castillo (1996), Basalts from the Central Pacific Basin: evidence for the origin of Cretaceous igneous complexes in the Jurassic western Pacific, *J. Geophys. Res.*, 101(B2), 2875-2893, doi:10.1029/95JB03119.

Johnson, M. C., and T. Plank (1999), Dehydration and melting experiments constrain the fate of subducted sediments, *Geochem. Geophys. Geosyst.*, 1(12), 1007, doi:10.1029/1999GC000014.

Keller, N. S., R. J. Arculus, J. Hermann, and S. Richards (2008), Submarine back-arc lava with arc signature: Fonualei Spreading Center, northest Lau Basin, Tonga, *J. Geophys. Res.*, 113, B08S07, doi: 10.1029/2007IB005451.

Kelly, K. A., T. Plank, T. L. Grove, E. M. Stolper, S. Newman, and E. Hauri (2006), Mantle melting as a function of water content beneath back-arc basins, *Journal of J. Geophys. Res.*, B09208, doi: 10.129/2005JB003732.

Klein, E.M., and C. H. Langmuir (1987), Global correlations of ocean ridge basalt chemistry with axial depth and crustal thickness, *J. Geophys. Res.*, 92, 8089-8115, doi:10.1029/JB092iB08p08089.

Lagabrielle, Y., J. Goslin, H. Martin, J. L. Thirot, and J. M. Auzende (1997), Multiple active spreading centres in the hot north Fiji basin (southwest Pacific): A possible model for Archaean seafloor dynamics?, *Earth Planet. Sci. Lett.*, 149, 1–13, doi:10.1016/S0012-821X(97)00060-5.

Langmuir, C.H., E. M. Klein, and T. Plank (1992), Petrological systematics of mid-ocean ridge basalts: constraints on melt generation beneath ocean ridges, in: Morgan, J. P., D. K. Blackman, and J. M. Sinton (ed.) *Mantle flow and melt generation at mid-ocean ridges*, American Geophysical Union, Washington DC, 183-280.

Langmuir, C. H., A. Bézos, S. Escrig, and S. W. Parman (2006), Chemical systematics and hydrous melting of the mantle in back-arc basins, in: Christie, D. M., C. R. Fisher, S-M Lee, and S. Givens (ed.) *Back-arc spreading systems: geological, biological, chemical and physical interactions*, American Geophysical Union, Washington DC, 87-146.

Le Bas, M. J., R. W. Le Maitre, A. Streckeisen, B. Zanettin (1986), A chemical classification of volcanic rocks based on the total alkali-silica diagram, *J. Petrol.*, 27 (3), 745-750.

Loock, G., W. F. McDonough, S. L. Goldstein, and A. W. Hofmann (1990), Isotopic composition of volcanic glasses from the Lau Basin, *Marine Mining*, 9, 235-245.

Lupton, J. E., R. J. Arculus, R. R. Greene, L. J. Evans, and , C. I. Goddard (2009), Helium isotope variations in seafloor basalts from the Northwest Lau Backarc Basin: Mapping the influence of the Samoan hotspot, *Geophys. Res. Lett.*, 36, L17313, doi:10.1029/2009GL039468.

Melson, W. G., T. O’Hearn, and E. Jarosewich (2002), A data brief on the Smithsonian abyssal volcanic glass data file, *Geochem. Geophys. Geosyst.*, 3(4), 2001GC000249, doi:10.1029/2001GC000249.

Millen, D. W. and M. W. Hamburger (1998), Seismological evidence for tearing of the Pacific plate at the northern termination of the Tonga subduction zone, *Geology*, 26, 659-662, doi: 10.1130/0091-7613(1998)026<0659:SEFTOT>2.3.CO;2 .

Natland, J. (1980), The progression of volcanism in the Samoan linear volcanic chain, *Am. J. Sci.*, 280-A, 709–735.

Nilsson, K. (1993), Oxidation state, sulfur speciation, and sulfur concentration in basaltic mamgas: examples from Hess deep and the Lau Basin, Ph.D. Thesis, University of California, San Diego.

Niu, Y., and M. J. O'Hara (2008), Global Correlations of Ocean Ridge Basalt Chemistry with Axial Depth: a New Perspective, *J. Petrolog*, 49(4), 633-664, doi: 10.1093/petrology/egm051.

Nohara, M., K. Hirose, J. P. Eissen, T. Urabe, and M. Joshima (1994), North-Fiji Basin basalts and their magma sources. II: Sr-Nd isotopic and trace elements constraints, *Mar. Geol.*, 116, 179–196, doi:10.1016/0025-3227(94)90175-9.

Parson, L., J. Hawkins, and J. Allan (1992), Proceedings of the Ocean Drilling Program, Initial Results, 135, College Station, TX: Ocean Drilling Program, doi:10.2973/odp.proc.ir.135.1992.

Parson, L. M., and D. L. Tiffin (1993), Northern Lau Basin: Backarc extension at the leading edge of the Indo-Australian Plate, *Geo-Marine Letters*, 13(2), 107-115, doi: 10.1007/BF01204552.

Pearce, J. A., M. Ernewein, S. H. Bloomer, L. M. Parson, B. J. Murton, and L. E. Johnson (1995), Geochemistry of the Lau Basin volcanic rocks: influence of ridge segmentation and arc proximity, in: Smellie, J. L. (ed.) Volcanism Associated with Extension at Consuming Plate Margins, *Geological Society, London, Special Contributions* 81, 53-75.

Pearce, J. A, R. J. Stern, S. H. Bloomer, and P. Fryer (2005), Geochemical mapping of the Mariana arc-basin system: Implications for the nature and distribution of subduction components, *Geochem. Geophys. Geosyst.* 6, Q07006, doi:10.1029/2004GC000895.

Pearce, J.A. and R. J. Stern (2006), Origin of back-arc basin magmas: trace element and isotope perspectives, in: Christie, D. M., C. R. Fisher, S-M Lee, S. Givens (ed.) *Back-arc Spreading Systems—Geological, Biological, Chemical, and Physical Interactions*, 63–86, Washington, DC: Am. Geophys. Union.

Pearce, J. A., P. D. Kempton, and J. B. Gill (2007), Hf-Nd evidence for the origin and distribution of mantle domains in the SW Pacific, *Earth Planet. Sci. Lett.*, 260, 98–114, doi:10.1016/j.epsl.2007.05.023.

Peate, D. W., T. F. Kokfelt, C. J. Hawkesworth, P. W. V. van Calsteren, J. M. Hergt, and J. A. Pearce (2001), U-series isotope data on Lau Basin Glasses: the role of subduction-related fluids during melt generation in back-arc basins, *J. Petrolog.*, 42, 1449-1470, doi: 10.1093/petrology/42.8.1449.

Plank, T., and C. H. Langmuir (1998), The chemical composition of subducting sediment and its consequences for the crust and mantle, *Chem. Geol.*, 145, 325-394, doi:10.1016/S0009-2541(97)00150-2.

Poreda, R. J. (1985), Helium-3 and deuterium in back-arc basalts - Lau Basin and the Mariana Trough, *Earth Planet. Sci. Lett.*, 73, 244-254, doi:10.1016/0012-821X(85)90073-1.

Poreda, R. J., and H. Craig (1992), He and Sr isotopes in the Lau Basin mantle: depleted and primitive mantle components, *Earth Planet. Sci. Lett.*, 113, 487-493, doi:10.1016/0012-821X(92)90126-G.

Poreda, R. J., and K. A. Farley (1992), Rare gases in Samoan xenoliths, *Earth Planet. Sci. Lett.*, 113, 129–144, doi:10.1016/0012-821X(92)90215-H.

Reay, A., J. M. Rooke, R. C. Wallace, and P. Whelan (1974), Lavas from Niuafo’ou Island, Tonga, resemble ocean-floor basalts, *Geology*, 2, 605-606, doi:10.1130/0091-7613(1974)2<605:LFNITR>2.0.CO;2.

Regelous, M., S. Turner, T. J. Falloon, P. Taylor, J. Gamble, and T. Green (2008), Mantle dynamics and mantle melting benenath Niuafo’ou Island and the northern Lau back-arc region, *Contrib. Mineral Petrol.*, 156, 103-118, doi:10.1007/s00410-007-0276-7.

Salters, V. J. M., and A. Stracke (2004), Composition of the depleted mantle, *Geochem. Geophys. Geosyst.*, 5, Q05B07, doi:10.1029/2003GC000597.

Sinton, J. M., D. S. Wilson, D. M. Christie, R. N. Hey, and J. R. Delaney (1983), Petrologic consequences of rift propagation on oceanic spreading ridges, *Earth Planet. Sci. Lett.*, 62, 193-207, doi:10.1016/0012-821X(83)90083-3.

Sinton, J. M., R. C. Price, K. T. Johnson, H. Staudigel, and A. Zindler (1991), Petrology and geochemistry of submarine lavas from the Lau and North Fiji backarc basins, in: Kroenke, L. W. and J. V. Eades (ed.) *Basin Formation, Ridge Crest Processes and Metallogenesis in the North Fiji Basin (Circum-Pacific Council for Energy and Mineral Resources. Earth Science Series)*, vol.12, pp. 155–177, Am. Assoc. Pet. Geol., Tulsa, Okla.

Staudigel, H., G. R. Davies, S. R. Hart, K. M. Marchant, and B. M. Smith (1995), Large scale isotopic Sr, Nd and O isotopic anatomy of altered oceanic crust: DSDP/ODP sites 417/418, *Earth Planet. Sci. Lett.*, 130, 169-185, doi:10.1016/0012-821X(94)00263-X.

Stracke, A., M. Bizimis, and V. J. M. Salters (2003), Recycling oceanic crust: Quantitative constraints, *Geochem. Geophys. Geosyst.*, 4, 8003, doi:10.1029/2001GC000223.

Solidum, R. U. (2002), Geochemistry of volcanic arc lavas in central and southern Philippines: contribution from the subducted slab, Ph.D. Thesis, University of California, San Diego.

Stolper, E., and S. Newman (1994), The role of water in the petrogenesis of Mariana trough magmas, *Earth Planet. Sci. Lett.*, 121, 293-325, doi:10.1016/0012-821X(94)90074-4.

Sun, S.-S., and W. F. McDonough (1989), Chemical and isotopic systematics of oceanic basalts: Implications for mantle composition and processes, in: Saunders, A. D. and M. K. Norry (ed.) Magmatism in the Ocean Basins, *Geol. Soc. Spec. Publ.*, 42, 313–345.

Sunkel, G. (1990), Origin of petrological and geochemical variations of Lau Basin Lavas (SW Pacific), *Marine Mining*, 9, 205-234.

Taylor, B., and F. Martinez (2003), Back-arc basin basalt systematics, *Earth Planet. Sci. Lett.*, 210, 481-497, doi:10.1016/S0012-821X(03)00167-5.

Tian, L., P. R. Castillo, J. W. Hawkins, D. R. Hilton, B. B. Hannan, and A. J. Pietruszka (2008), Major and trace element and Sr-Nd isotope signatures of lavas from the Central Lau Basin: Implications for the nature and influence of subduction components in the back-arc mantle. *J. Volcanol. Geotherm. Res.*, 178, 657–670,,doi:10.1016/j.jvolgeores.2008.06.039.

Turner, S. and C. Hawkesworth (1997), Constraints on flux rates and mantle dynamics beneath island arcs from Tonga-Kermadec lava geochemistry, *Nature*, 389, 568-573, doi:10.1038/39257.

Turner, S. P., C. J. Hawkesworth, N. Rogers, J. Bartlett, T. Worthington, J. Hergt, J. A. Pearce, and I. Smith (1997), ^{238}U-^{230}Th disequilibria, magma petrogenesis, and flux rates beneath the depleted Tonga-Kermadec island arc, *Geochim. Cosmochim. Acta*, 61, 4855-4884, doi:10.1016/S0016-7037(97)00281-0.

Turner, S., and C. Hawkesworth (1998), Using geochemistry to map mantle flow beneath the Lau Basin, *Geology*, 26, 1019–1022, doi:10.1130/0091-7613(1998) 026<1019:UGTMMF>2.3.CO;2 .

Volpe, A. M., J. D. MacDougall, and J. W. Hawkins (1988), Lau Basin basalts (LBB): trace element and Sr-Nd isotopic evidence for heterogeneity in back arc basin mantle, *Earth Planet. Sci. Lett.*, 90, 174-186, doi:10.1016/0012-821X(88)90099-4.

Wendt, J. I., M. Regelous, K. D. Collerson, and A. Ewart (1997), Evidence for a contribution from two mantle plumes to island-arc lavas from northern Tonga, *Geology*, 25, 611–614, doi:10.1130/0091-7613(1997)025<0611:EFACFT>2.3.CO;2.

Workman, R. K., S. R. Hart, M. Jackson, M. Regelous, K. A. Farley, J. Blusztajn, M. Kurz, and H. Staudigel (2004), Recycled metasomatized lithosphere as the origin of the

Enriched Mantle II (EM2) end-member: Evidence from the Samoan Volcanic Chain, *Geochem. Geophys. Geosyst.*, 5, Q04008, doi:10.1029/2003GC000623.

White, W. M., and J. P. Morgan (2004), Two-stage melting of mantle plumes and the origin of rejuvenescent volcanism on oceanic islands, *Eos Trans. AGU*, Fall Meet. Suppl., abstract #V51B-0527.

Wright, E., and W. M. White (1986), The origin of Samoa: new evidence from Sr, Nd and Pb isotopes, *Earth Planet. Sci. Lett.*, 81, 151-1162, doi:10.1016/0012-821X(87)90152-X .

Zellmer, K. E., and B. Taylor (2001), A three-plate kinematic model for Lau Basin opening, *Geochem. Geophys. Geosyst.*, 8, Q09003, doi:2000GC000106.

This chapter, in full, was submitted to *Journal of Geophysical Research - Solid Earth* by L. Tian, P. R. Castillo, D. R. Hilton, J. W. Hawkins, B. B. Hanan, and A. J. Pietruszka (2011JB008475). The dissertation author was the primary investigator and author of this paper. The co-authors directed, supervised and contributed to the research.

CHAPTER 3

Petrology and Sr-Nd-Pb-He isotope geochemistry of post-spreading lavas on fossil spreading axes off Baja California Sur, Mexico

Abstract

Post-spreading volcanism has built large seamounts and volcanic ridges along the short axes of a highly segmented part of the East Pacific Rise crest that ceased spreading at the end of the Middle Miocene, offshore Baja California Sur, Mexico. Lava samples from Rosa Seamount, the largest volcano, are predominantly alkalic basalts, mugearites and benmoreites. This lavas series was generated through fractional crystallization and is compositionally similar to the moderately alkalic lava series in many oceanic islands. Samples from volcanic ridges at three adjacent failed spreading axes include mildly alkalic, transitional and tholeiitic basalts, and differentiated trachyandesites and andesite. The subtle but distinct petrologic and isotopic differences among the four sites may be due to differences in the degree of partial melting of a common, heterogeneous source. Post-spreading lavas from these four abandoned axes off Baja California Sur together with those from other fossil spreading axes and from seamount volcanoes that grew on the East Pacific Rise flanks define a compositional continuum ranging from normal-mid-ocean ridge basalt (N-MORB)-like to ocean island basalt (OIB)-like. We propose that the compositional spectrum of these intraplate volcanic lavas is due to different degrees of partial melting of the compositionally heterogeneous suboceanic mantle in the eastern Pacific.

A large degree of partial melting of this heterogeneous mantle during vigorous mantle upwelling at an active spreading center produces normal-MORB melts whereas a lesser degree of partial melting during weak mantle upwelling following cessation of spreading produces OIB-like melts. The latter melts have a low (<8 R_A) $^3He/^4He$ signature indicating their formation is different from that of OIBs from major "hotspot" volcanoes in the Pacific with high $^3He/^4He$ ratios, such as Hawaii and Galapagos.

Keywords: Sr-Nd-Pb-He isotopes; post-spreading lavas; fossil spreading axes; mantle heterogeneity; partial melting of the mantle

3.1. Introduction

The study of oceanic volcanism during the last four decades or so has primarily focused on the origin of lavas erupted along active spreading centers and linear volcanic island and seamount chains. Results of studies have led to the current popular views that the geochemically depleted, tholeiitic mid-ocean ridge basalts (MORB) are produced in response to plate separation and passive upwelling and adiabatic decompression melting of the mantle, and that the relatively enriched tholeiitic and alkalic ocean island basalts (OIB) that comprise the bulk of linear hotspot volcanoes are melts originating from either rising plumes of deep mantle materials [e.g., *Morgan*, 1971, 1972; *Hofmann*, 2003] or heterogeneities in the upper mantle sampled during fracturing of the lithosphere [e.g., *Meibom and Anderson*, 2004; *Natland and Winterer*, 2005; *Foulger*, 2007]. Dredge sampling of many of the thousands of large and small volcanoes not in linear chains and scattered across the ocean floor has proved that they commonly have at least a carapace of alkalic lava compositionally akin to alkalic OIB, as first reported by *Engel et al.* [1971]. These authors also recognized a pattern of tholeiitic central volcanoes transitioning to eruption of more alkalic lava, and while suggesting this evolution was mainly a result of fractionation of a tholeiitic melt they also considered decreasing extent of partial melting as a possible alternative. The latter explanation is more consistent with recent geochemical data, leading to a commonly accepted model in which a low degree of partial melting of a heterogeneous oceanic mantle, i.e., less than that responsible for tholeiitic MORB at and around active spreading axes, produces OIB-like alkalic magma at large and small volcanoes located on the flanks of the East Pacific Rise (EPR) [*Batiza and Vanko*, 1984; *Zindler et al.*, 1984].

Batiza and Vanko [1985] likewise proposed such an origin (low degree melting of a compositionally heterogeneous mantle) for the young alkalic lavas dredged from seamounts and volcanic ridges along the crest of Mathematician Ridge, where spreading ceased during the Pliocene when the Pacific plate captured the Mathematician microplate [*Mammerickx and Klitgord*, 1982]. Two former spreading segments on the northern part of Mathematician Ridge continue to erupt alkali basalt and more silicic differentiates, sometimes subaerially, at Isla San Benedicto [*Richards*, 1966] and Isla Socorro [*Seibe et al.*, 1995; *Bohrson and Reid*, 1995, 1997]. Long-continued post-spreading ridge-building eruption of alkalic lava has also occurred along several other failed spreading axes in the eastern Pacific. Examples include Davidson Seamount [*Clague et al.*, 2009; *Castillo et al.*, 2010] and Guide Seamount

[*Davis et al.*, 2002, 2010], which were both built along axes that had stopped spreading in the Early Miocene when the Pacific plate captured the Monterey microplate [*Lonsdale*, 1991], and narrow volcanic ridges that grew along extinct segments of the Galapagos Rise [*Batiza et al.*, 1982; *Haase and Stroncik*, 2002] following Late Miocene capture of the Bauer microplate by the Nazca plate [*Eakins and Lonsdale*, 2003].

This paper presents the petrology and geochemistry of post-spreading lavas on fossil spreading axes between 27°30′N and 25°20′N in the eastern Pacific off Baja California Sur, Mexico (Fig. 3.1) and evaluates the source of fossil spreading center volcanism. Major and trace element chemistry and Sr-Nd-Pb-He isotope geochemistry were obtained for whole-rock and a few glass samples from volcanic ridges built along four of the seven short EPR axes abandoned in the Middle Miocene (Fig. 3.1). Compared to the relatively uniform composition of MORB, post-spreading lavas from these ridges span a much larger range of composition, similar to lavas erupted along other fossil spreading axes [e.g., *Batiza et al.*, 1982; *Batiza and Vanko*, 1985; *Bohrson and Reid*, 1995; *Davis et al.*, 2002; *Castillo et al.*, 2010]. Like many riseflank central volcanoes [*Engel et al.*, 1971], there is evidence that lavas erupted along abandoned spreading axes evolve through time from tholeiitic to alkalic composition.

3.2. Geologic Setting and Sample Description

During the Early Miocene, the crest of the EPR, west of Baja California Sur, hosted a straight (almost unsegmented) Pacific-Cocos spreading axis, striking north-northwest (340°) for 900km between Clarion and Molokai transforms (Fig. 3.1;

Lonsdale [1991]). The westward-moving North American plate was converging on this spreading center, narrowing the northern part of the Cocos plate, which was being subducted at the Baja California and Middle American Trenches. Magnetic anomalies show [*Lonsdale*, 1991] that just before Chron C5Bn, i.e. ~15.5 Ma, the young lithosphere entering the Baja California Trench detached from the Cocos Plate to become the Magdalena microplate. Only two-thirds of the Cocos plate north of Clarion fracture zone was included in this microplate (the Pacific-Magdalena-Cocos triple junction, and a transform linking this junction to the North American plate, was 300km north of Clarion fracture zone); the southern third continued to be subducted as part of the Cocos plate at the Middle America Trench, then after ~5 myr [*DeMets and Traylen*, 2000] was detached as the still surviving Rivera microplate. Freed from the slab pull of old, dense Cocos lithosphere entering the Middle American Trench, the Magdalena plate stagnated, though overthrusting of North America persisted along its eastern margin. Along its western EPR margin, relative plate motion changed from rapid divergence between two subducting oceanic plates to separation of the Pacific plate from a stagnating microplate; i.e. the relative motion approached the absolute motion of the northwest-moving Pacific plate. As a result, the spreading rate almost halved, and the spreading direction rotated clockwise by 45-60°. The Pacific-Magdalena risecrest followed the usual response of the EPR crest to a change in spreading direction [*Nelson*, 1981; *Lonsdale*, 1985]: it segmented to form a chain of spreading axes, each of which rotated to stay orthogonal to the changing spreading direction while the overall strike of the chain remained ~340°. As the spreading direction grew ever closer to this azimuth, the spreading axes became shorter, and the links between them (northwest-striking shear zones forming transform and non-transform offsets) lengthened. Eventually, 60-100km-long shear zones linked the 7 short (10-60km-long) northeast-striking Pacific-Magdalena spreading axes named in Figure 3.1. A similar process earlier produced slow, northeast-striking spreading axes along the western margin of the Monterey microplate (e.g. Guide and Davidson axes, Fig. 1), and in the past 2.5 myr along the highly segmented, still active Pacific-Rivera EPR [*Lonsdale*, 1995].

Slow Pacific-Magdalena spreading built a segmented oceanic rise for just a few Myr after 15Ma, accreting igneous crust assumed to be of typical tholeiitic basalt composition. However, the only direct support for this assumption comes from the single locality where igneous basement of the rise flank has been sampled: Deep Sea Drilling Project (DSDP) Site 472, which recovered normal abyssal tholeiite [*Shibata et al.*, 1982]. Then the microplate was captured by the Pacific plate, so the intervening spreading axes became extinct, tectonically if not volcanically. The interactions of continental and oceanic plates that caused this event, and similar captures of, for example, the Monterey and Guadalupe microplates, are poorly understood and beyond the scope of this paper. The dynamics of most oceanic microplates that are bounded by two or more oceanic plates can be explained by a simple model [*Schouten et al.*, 1993] in which the microplate is propelled by drag forces imposed on it by the surrounding major plates, and is captured by one of the major plates once it has grown to a size and shape that resists these driving forces [e.g., *Eakins and Lonsdale*, 2003]. The dynamics of the Magdalena microplate were more complex, because as well as having a shearing boundary with the Cocos plate and a partly (but decreasingly) accreting boundary with the Pacific plate it had a long converging boundary where the North American continent was overthrusting its northeast margin, and at least initially the pull of a subducted slab provided another driving force on microplate motion. The microplate began to shrink rather than grow as most of its Pacific boundary became a shear zone rather than a zone of plate accretion, and any slab-pull force diminished as continued over-thrusting brought the North American margin closer to its short rotated spreading axes, but it is not clear why the microplate was captured by the Pacific plate before being completely overthrust by North America. Even the timing of Magdalena microplate capture is controversial [e.g., *Michaud et al.*, 2006], mainly because seafloor-spreading magnetic anomalies near most of the abandoned risecrest have been obscured by local anomalies from volcanic landforms built after spreading ceased. From analysis of profiles across those axes with the smallest amount of post-spreading additions, we estimate spreading ceased soon after Chron C5An, i.e. 12-11.5 Ma.

The rocks we describe here were obtained by dredging four of the volcanic ridges built along the abandoned risecrests off Baja California Sur, Mexico (Fig. 3.1) during Scripps Institution of Oceanography's (SIO) Phoenix 03 cruise in 1992 and Rosa 01 cruise in 1993. Our dredge sampling (Table 3.1) was preceded by magnetic profiling and multibeam bathymetry to identify the axes of spreading and to locate anomalous axial volcanic topography of likely post-spreading origin. Two of the extinct Pacific-Magdalena axes have been smothered by large seamounts: the (unsampled) 2700m-high Magdalena Seamount and the 3300-m high Rosa Seamount, named "Rosa Bank" by *Chase et al.* [1968], each covering almost the entire length of their respective axes (Fig. 3.1). Sara and Nithya axes have narrow 2 km-high fissural volcanic ridges along their entire lengths; Rosana and unsampled Teresa and Juanita (Fig. 3.1) each have a row of low (<1 km high) volcanic cones.

Most of the rocks recovered from these volcanic landforms are ferromanganese oxide-encrusted fragments of pillow lava and other types of lava flows, commonly with glassy rinds, and encrusted slabs of altered hyaloclastite. Most lava fragments have been affected by secondary alteration, but relatively fresh cores were found in many cases. Some of the samples from the summit of Rosa Seamount (dredges 9 and 10) have very fresh glass and lack a ferromanganese crust; we infer that they were erupted recently. The recovered lavas are lithologically variable, ranging from mafic basalt and basaltic andesite, to mugearite, benmoreite, trachyandesite, and andesite (Fig. 3.2). Many of the samples are highly vesicular with small, round or elongate vesicles that typically show a pronounced flow lineation. The majority of the moderately mafic volcanic rocks are dense, hypo- to holocrystalline and aphyric to phyric, the latter containing olivine, clinopyroxene and plagioclase phenocrysts. In general, the more mafic samples have higher phenocrysts contents. Dominant groundmass minerals are plagioclase, clinopyroxene, Fe-Ti oxides, and glass. The dredges also collected several round, unencrusted cobbles judged to be exotics, probably kelp-rafted from the nearby coast [*Emery and Tschudy*, 1941]; lithologies include metamorphic and granitic rocks.

3.3. Analytical Methods

The samples dredged from post-spreading volcanic ridges along Sara, Rosana, Rosa, and Nithya axes were analyzed for major and trace element chemistry and some were also analyzed for Sr-Nd-Pb-He isotopic compositions. For the chemical and Sr-Nd-Pb isotope analyses, fine powders were prepared from the fresh cores of individual samples using an alumina ceramic mill. Details of the sample preparation procedure are described in *Solidum* [2002].

Major element analyses were carried out on glass, fused from rock powders, by a fully automated, wavelength-dispersive ARL 840 X-ray fluorescence spectrometry (XRF) instrument using the procedure described in *Janney* [1996] and on solution prepared from sample powders by inductively coupled plasma optical emission spectrometry (ICP-OES) using the procedure described by *Murray et al.* [2000] with some modifications. An estimate of the volatile (e.g., H_2O and CO_2) contents in the rock samples was determined by weighing loss on ignition (LOI) following the procedure described in *Solidum* [2002]. Concentrations of trace elements Rb, Sr, Y, Ba, Pb, Th, U, Zr, Nb, Ta, and rare-earth elements (REEs) were determined by inductively coupled plasma mass spectrometry (ICP-MS) following the methods modified from *Janney and Castillo* [1996], whereas concentrations of compatible elements Cr and Ni were determined by ICP-OES. All the analyses were carried out at the SIO Analytical Facility.

Some of the whole rock samples were analyzed for Sr, Nd and Pb isotopes at SIO following the methods described by *Janney and Castillo* [1996, 1997] and *Solidum* [2002]. For Nd and Pb isotopic analysis, sample powders were digested with a double-distilled, 2:1 mixture of concentrated HF: HNO_3 acid, then Pb was first separated by re-dissolving the dried samples in 2N HBr and then passing the solutions through a small ion exchange column in a HBr medium. Residues from Pb extraction were collected and then passed through ion exchange columns using HCl as the eluent to collect REE. Finally, Nd was separated from the rest of the REE in an ion exchange column using alpha-hydroxyisobutyric (α-HIBA) acid as the eluent. To minimize alteration effects on bulk isotope analyses, leached sample powders were used for Sr isotopic analysis. The leaching procedure used was similar to that described by *Janney and Castillo* [1996, 1997]. The leached samples were also dissolved in a mixed HF: HNO_3 (2:1) acid as before and Sr was subsequently separated from the solution in an ion exchange resin using HCl as the eluent. The Sr, Nd and Pb isotopes were measured using a nine-collector, Micromass Sector 54 thermal ionization mass spectrometer (TIMS) at SIO. Strontium isotopes are reported relative to NBS 987 $^{87}Sr/^{86}Sr = 0.71025$, and Nd isotopes are reported relative to $^{143}Nd/^{144}Nd = 0.51185$ for the La Jolla Nd standard.

Helium (He) isotopes and concentrations were measured from the few available glass chips and one clinopyroxene separate. Helium gas trapped in vesicles and fluid inclusions in the glasses and mineral grain, respectively, was extracted using on-line vacuum crushing, and $^{3}He/^{4}He$ ratios and He concentrations were measured using a MAP 215E noble gas mass spectrometer at the SIO Fluids and Volatiles Laboratory. More details of the He isotope analytical procedure are given in *Shaw et al.* [2006]. Standard aliquots of air (1 R_A where $R_A = 1.4 \times 10^{-6}$) and Yellowstone Park He (16.45 R_A) were used to determine the abundance and isotopic composition of the samples. Typical crusher blanks were $\sim 6\times10^{-11} cm^3 STP$ ^{4}He.

Details of the analytical accuracy and precision of the major and trace elements and isotopic measurements are described in footnotes of Tables 3.2, 3.3, and 3.4, as appropriate.

3.4. Results

Major element, trace element and Sr, Nd, Pb, and He isotope data for samples from Sara, Rosana, Rosa, and Nithya are presented in Tables 3.2, 3.3 and 3.4.

The majority of volcanic rocks from Rosa Seamount, the largest of these four features, are alkalic basalts, mugearites and benmoreites. These samples define a broad, but coherent trend that plots slightly above the boundary between alkalic and tholeiitic fields in the silica versus total alkali diagram (Fig. 3.2), and hence they define a broad, moderately alkalic lava series. Our samples do not include hawaiite, suggesting a "Daly gap" or paucity of intermediate-composition lavas, as in many oceanic islands [*Chayes*, 1963, 1977; *Yoder*, 1973]. The remainder of Rosa samples includes basanites, a phonolitic tephrite and a trachyandesite. Lava samples from the high Sara volcanic ridge also include alkalic basalts in addition to transitional basalts, trachyandesites, and an andesite. The andesite and almost all of the trachyandesites (except sample ROSA D6-10) actually belong to the tholeiitic lava series although, as will be discussed below, they are not geochemically depleted like N-MORB, and thereby resemble tholeiitic lavas from intraplate eruptions at many volcanic chains. Fewer samples were dredged from the volcanic ridges along Rosana and Nithya axes. Of the four samples from Rosana, two are alkalic basalts and two are tholeiitic basalts. The three samples from Nithya are alkalic basalts to transitional basalts similar to enriched-MORB (E-MORB).

As a whole, the data display broad correlations between MgO and major elements (Fig. 3.3). For example, concentrations of SiO_2, Al_2O_3, Na_2O, and K_2O in Rosa lavas increase whereas Fe_2O_{3T} and to a lesser degree CaO decrease with decreasing MgO concentrations. Some of the major element oxides of Sara lavas behave similarly as those of Rosa lavas, but the former have lower Na_2O and K_2O and higher CaO for given MgO contents than the latter. Moreover, the correlation of Al_2O_3 with MgO of Sara lavas is opposite to that of Rosa lavas. The few samples from Rosana and Nithya do not define clear differentiation trends; nevertheless, they generally plot together with the basaltic lavas from Sara.

All samples are enriched in highly-incompatible relative to moderately incompatible trace elements (Fig. 3.4). Rosa has the most enriched pattern among the four axes, save for differentiated lavas from Sara that also have the most distinct negative Sr anomalies. Moreover, individual Rosa samples show sub-parallel trace element patterns, which collectively are more enriched in highly incompatible trace elements than an average alkalic OIB [*Sun and McDonough*, 1989]. They do, however, display slight positive spikes in high field strength elements (HFSEs) such as Nb and Zr, which is typical in OIB [*Hofmann*, 2003]. Basaltic lavas from Sara, Rosana and Nithya have lower highly incompatible but higher moderately incompatible trace element contents than Rosa lavas. In other words, the trace element patterns of the basaltic lavas from these three ridges cut across those of Rosa lavas.

The samples have moderate ranges in $^{87}Sr/^{86}Sr$ (0.7027 to 0.7035), but a constant $^{143}Nd/^{144}Nd$ ratio of ~0.51295 (total range = 0.51289 to 0.51300; Fig. 3.5). As a whole, the Sr and Nd isotope values of these four volcanoes fall within the range of other fossil spreading axes west of California [e.g., *Davis et al.*, 2002; *Castillo et al.*, 2010] and overlap with the values for basaltic rocks from Socorro and San Benedicto islands along the fossil Mathematician Ridge [e.g., *Bohrson and Reid*, 1995; 1997]. Furthermore, they overlap with the radiogenic, high $^{87}Sr/^{86}Sr$ and low $^{143}Nd/^{144}Nd$ end of the field for seamounts on the EPR flanks [e.g., *Zindler et al.*, 1984; *Graham et al.*, 1988; *Niu et al.*, 2002]. Interestingly, their $^{87}Sr/^{86}Sr$ and $^{143}Nd/^{144}Nd$ isotopic compositions also overlap with some of the OIB from the Galapagos archipelago and Iceland, save for one mugearite from Rosa Seamount, which overlaps with the OIB from the Hawaiian volcanic chain. The OIB from the large Galapagos, Iceland and Hawaiian hotspot volcanoes that overlap with the fossil spreading lavas in the Sr and Nd isotopic space have amongst the highest ($\geq$ 15 R_A) terrestrial $^3He/^4He$ ratios [e.g., *Stuart et al.*, 2003; *Class and Goldstein*, 2005].

The Pb isotopes of the samples are relatively radiogenic and span a wide range of values (e.g., $^{206}Pb/^{204}Pb = 18.86$ to 19.53). Consistent with Sr and Nd isotopes, their Pb isotopes overlap the available isotope data for other fossil spreading axes and the radiogenic end of riseflank seamounts (Fig. 3.5). Moreover, the Pb isotopic composition of the majority of lavas from these four axes overlaps with the OIB from the large Galapagos, Iceland and Hawaiian hotspot volcanoes, again those with high $^3He/^4He$ ratios.

Measured $^3He/^4He$ ratios and He concentrations are corrected for the effects of air contamination following procedures described in *Hilton* [1996]. The air-corrected $^3He/^4He$ ratios and ^4He concentrations in vesicles and fluid inclusions in fresh glasses and clinopyroxene from the axes of Rosa and Nithya, respectively, range from 1.25 to

7.18 R_A (where $R_A = {}^3He/{}^4He$ of air) and 0.26 to 23.4 × 10^{-9} cm^3 STP g^{-1} (Table 3.4 and Fig. 3.6). Thus, to a first order, none of the fossil spreading center OIB-like basalts has $^3He/^4He$ ratio higher than the canonical MORB value of 8±1 R_A [*Graham*, 2002]. It is important to note, however, that four out of seven analyses are dominated by air-derived He ($X < 3.5$) and their He concentrations are low ($[He]_c < 1.6 \times 10^{-9}$ cm^3STP/g). Under these circumstances, it is possible that either the correction procedure fails to completely resolve air from trapped He or any trapped He includes a radiogenic component produced within the sample after eruptive. Therefore, in the following discussion, we give greater weight to those three samples where $X > 10$, i.e., there is little air correction. Thus, two Rosa samples give air-corrected $^3He/^4He$ ratios of 7.18 R_A (ROSA D9-1rep.) and 5.67 R_A (ROSA D9-9) while the clinopyroxene sample from Nithya gives a $^3He/^4He$ value of 1.25 R_A (PX 127D-20).

The two Rosa samples are alkalic lavas that have relatively high concentrations of U and Th, so their $^3He/^4He$ ratios at the time of eruption may have been higher than present-day values. However, a substantial decrease in vesicle-sited $^3He/^4He$ values can only occur with almost complete diffusion of $^4He^*$ from the glass matrix (where it is produced) to the vesicle phase. For example, *Graham et al.* [1987] predicted that a maximum of 10% of the $^4He^*$ would diffuse from the glass matrix to the vesicles if the vesicularity was 1% and the vesicle radius was between 100 and 300 mm. The lavas in this study are highly vesicular so that the $^3He/^4He$ ratios of the larger vesicles, which are less affected by $^4He^*$ diffusion, would dominate the measured $^3He/^4He$ [*Graham et al.*, 1987]. Moreover, although the fossil spreading lavas of this study could be as old as 11.5Ma, based on the tectonic setting, we note earlier that the samples collected from the summit of Rosa Seamount, including ROSA D9-1 and ROSA D9-9, consist of pristine glass and appear to have been erupted recently. Thus, we believe that the $^3He/^4He$ ratios of samples ROSA D9-1 and ROSA D9-9 from Rosa Seamount can be considered representative of their mantle source at the time of eruption. Notably, volcanoes along axes of the fossil Mathematician Ridge [*Graham et al.*, 1988] and riseflank seamounts studied by *Hahm et al.* [2009] have similarly low ($\leq 8\ R_A$) $^3He/^4He$ ratios. In contrast, the clinopyroxene sample from Nithya has clearly incorporated post-eruptive radiogenic He, consistent with the antiquity of the volcano.

3.5. Discussion

3.5.1. Geochemical variations of post-spreading lavas on fossil spreading axes off Baja California Sur

The volcanic lavas erupted along the four fossil spreading axes display two types of compositional variation: (1) variations in the major and trace element contents of the alkali basalt to benmoreite lava series, e.g., from Rosa Seamount, that can be ascribed to fractional crystallization, and (2) intra- and inter-axis geochemical variations due to a compositionally heterogeneous mantle source.

The broad linear correlations between MgO and other major element oxides exhibited by the Rosa Seamount lava series (Figs. 3.2 and 3.3) are consistent with differentiation trends through fractional crystallization. The same can be said for the subparallel incompatible trace element concentration patterns of these Rosa Seamount lavas (Fig. 3.4). Specifically, the concentrations of incompatible elements such as Rb, Ba, Th, U, REEs, and HFSEs generally increase from primitive basalts to differentiated benmoreites (Fig. 3.7). The reverse is true for compatible trace elements such as Ni and Cr, which suggests that the differentiated lavas were derived from similar, parental primitive basalts through fractionation of minerals that included olivine and clinopyroxene. More importantly, basalts, mugearites and a benmoreite from the Rosa Seamount lava series have a limited range of Sr and Nd plus identical Pb isotope ratios (Fig. 3.5 and Table 3.3), clearly indicating that this lava series came from a single mantle source. In detail, however, the lava series defines bimodal groups in plots of Ba versus Zr (Ba/Zr = ~1.4. and 1.86) and Nb versus Zr (Nb/Zr = ~0.2 and 0.3) (Fig. 3.8), suggesting that the lava series was actually generated by a complex fractional crystallization process that likely occurred within the mantle at pressures that increased as the volcano grew, similar to the generation of the main lava series at Davidson Seamount [*Clague et al.*, 2009; *Castillo et al.*, 2010]. The presence of a few Rosa Seamount lavas that do not belong to this lava series (Figs. 3.3 and 3.7) and have different Sr, Nd and Pb isotopic ratios (Fig. 3.5 and Table 3.3) indicates that the mantle source of Rosa Seamount lavas was not compositionally homogeneous.

As noted earlier, the basaltic and andesitic lavas from Sara ridge range from alkalic to tholeiitic in composition (Fig. 3.2) and thus, unsurprisingly, their major element data do not form a single linear trend with MgO (Fig. 3.3). Moreover, their trace element concentration patterns appear to form two separate groups (Fig. 3.4) and their Sr, Nd and Pb isotopic compositions are variable and are, on average, different from those of Rosa Seamount (Fig. 3.5). Thus, unlike the bulk of Rosa Seamount lavas, Sara lavas cannot simply be related to one another through fractional crystallization of similar parental basalts. They originate from a compositionally heterogeneous mantle source, as do the basaltic samples from Rosana and Nithya ridges. As a whole, the trace element and isotopic signatures of Rosana and Nithya are overlapping with that of Sara; altogether, these are less geochemically enriched than those of Rosa Seamount (Figs. 3.4 and 3.5).

3.5.2. Comparison with post-spreading lavas on other fossil spreading axes in the eastern Pacific

As described earlier, there are many volcanic ridges or seamounts located along fossil spreading axes in the eastern Pacific, and alkalic volcanism is a common feature of these failed axes. Samples dredged from an axial ridge on fossil Galapagos Rise are alkalic basalts that have experienced variable degrees of crystal accumulation/fractionation and seawater alteration [*Batiza et al.*, 1982; *Haase and Stroncik*, 2002]. Although *Batiza et al*. [1982] reported sampling tholeiitic lava from the crest of the Galapagos Rise, they had mislocated the former spreading axis by ~35km; the geophysical mapping of *Eakins and Lonsdale* [2003] showed the axis to lie along the 3km-high "elongate seamount" from which *Batiza et al.* [1982] reported alkali-olivine basalt (their dredges 4 and 5). Samples from volcanic ridges along the Mathematician Ridge crest (Fig. 3.1) are vesicular alkalic basalts with large crystals of olivine and plagioclase [*Batiza and Vanko*, 1985], benmoreites [*Richards*, 1958] and trachyandesite [*Moore*, 1970]. Note that *Batiza and Vanko* [1985] originally described sampling their alkalic basalts from abandoned transform faults, but subsequent multibeam bathymetry (SIO, archival data) showed them to be from axial volcanoes on failed Mathematician spreading segments.

Socorro and San Benedicto Islands at the northern terminus of the Mathematician Ridge provide more evidence of post-abandonment alkaline magmatism that continues to the present, as indicated by recent eruption in Socorro Island in 1993 [*McClelland et al.*, 1993] and San Bendicto Island in 1952-53 [*Richards*, 1959]. The bulk of postcaldera volcanism in Socorro Island spans the fractional crystallization trend from alkalic basalt to hawaiite and mugearite [*Bohrson and Reid*, 1995]. The alkalic basalts have chemical characteristics (e.g., negative Ce anomaly and P_2O_5 enrichment) which are indicative of assimilation of hydrothermal sediments or apatite accumulated during previous episodes of magmatism. San Benedicto Island has an alkalic basalt to mugearite and trachyte lava series [*Richards*, 1966] which almost completely overlaps with the Socorro Island alkalic lava series in major and trace element composition [*Bohrson and Reid*, 1995]. Significant volumes of silicic peralkaline volcanic rocks (dominantly peralkaline trachytes and rhyolites) also occur on Socorro and San Benedicto Islands (Fig. 3.1), and these may have been formed by partial melting of basaltic basement [*Bohrson and Reid*, 1997, 1998].

Samples collected from Guide Seamount (Fig. 3.1) are mainly hawaiites, but also include alkalic basalts and mugearites [*Davis et al.*, 2002, 2010]. The broad spectrum of major element compositions of the lavas, especially among the hawaiites, reflects the chemical diversity of melts erupted at Guide Seamount. Samples from Davidson Seamount (Fig. 3.1) belong to an alkalic basalt to trachyte lava series generated through a complex fractional crystallization process [*Clague et al.*, 2009; *Castillo et al.*, 2010]. A diverse assemblage of small mafic and ultramafic xenoliths are present in the alkalic lavas from Davidson Seamount and these represent both trapped melts from the mantle and alkalic cumulates from the margins of magma chambers [*Davis et al.*, 2002, 2007]. Sampled Davidson Seamount lavas spanned five million years and the older, more differentiated and alkali-rich lavas occur near the summit of Davidson Seamount [*Clague et al.*, 2009].

Relatively smaller volumes of tholeiitic to transitional basalts have erupted at Socorro Island, the northern rift zone of San Benedicto Island [*Bohrson and Reid,* 1995], and at a small volcano near the fossil spreading axis-transform intersection south of Davidson Seamount [*Castillo et al.*, 2010]. Most of these tholeiitic basalts, however, are slightly more alkalic than N-MORB [*Bohrson and Reid,* 1995]. *Castillo et al.* [2010] propose that the few transitional basalts from south of Davidson Seamount were produced from the same source of the Davidson Seamount alkalic lava series, although at higher degree of partial melting.

Similar to Rosa Seamount, alkalic lavas from large volcanoes built along other fossil spreading axes in the eastern Pacific have trace element abundances and ratios resembling many alkalic ocean island lavas [e.g., *Castillo et al.* 2010]. The alkalic lavas from fossil spreading centers have higher abundances of incompatible elements and higher highly/moderately incompatible trace element ratios relative to tholeiitic basalts from riseflank seamounts (e.g., higher Ba/Zr, La/Sm and Nb/Zr ratios; Fig. 3.8). The highly incompatible trace element ratios of some of the transitional lavas are overlapping with those of the alkalic lavas [e.g., *Castillo et al.*, 2010]. There are also similarities or overlaps in the Sr, Nd and Pb isotopic compositions of all alkalic lavas on all fossil spreading axes (Fig. 3.5), and these compositions overlap the radiogenic end of Pacific MORB and trend toward to an enriched mantle component that contributes to the source of OIBs.

3.5.3. Petrogenesis of post-spreading lavas on fossil spreading axes

Rosa, Sara, Rosana, and Nithya lavas were erupted in identical tectonic settings, along short spreading axes that had failed simultaneously, but show significant compositional variation. From this variation and observations at better-dated counterparts along other fossil spreading axes, we infer temporal change in the composition of post-spreading eruptions.

The bulk of the lavas sampled from the largest volcanic ridge, Rosa Seamount (i.e., the one that probably has the longest history of volcanic eruption, with apparently recent flows on its summit) are alkalic in composition. As discussed above, most superficial lavas from prominent volcanic ridges and islands covering segments of fossil spreading axes in the eastern Pacific are also alkalic. In comparison, superficial lavas from the smaller volcanic features along Sara, Rosana and Nithya axes are less alkalic on average, with several samples having tholeiitic to transitional compositions, similar to E-MORB. Lavas from a small seamount located at the axis of a fossil spreading center in Drake Passage in the southern Pacific Ocean, erupted < 2 myr after the cessation of spreading, are also E-MORB [*Choe et al.,* 2007; *Choi et al.*, 2008]. The evidence suggests that the composition of risecrest lavas generally evolves from typical tholeiitic N-MORB while actively spreading to E-MORB and eventually to alkalic basalts, similar to OIB, and their differentiates, after spreading has stopped.

A better understanding of the mantle melting process beneath active spreading centers can provide clues as to why the composition of post-spreading erupted lavas evolve with time. The mantle rises beneath active risecrests in response to plate separation, decompresses adiabatically, begins to melt when it intersects the solidus, and continues melting to produce voluminous MORB. The whole process occurs in a melting column, which is defined by the mantle potential temperature that sets the depth of intersection between the solidus and the melting curve or by the melting interval between initial (deeper and hence higher pressure) and final (shallower and hence lower pressure) depth of melting, which in turn is defined by the balance between conductive cooling on the seafloor and adiabatic upwelling of hot mantle [e.g., *Langmuir et al.*, 1992; *Niu and Hékinian*, 1997; *Rubin and Sinton*, 2007; *Niu and O' Hara*, 2008]. Melting columns heights correlate with variations in axial topography, which are controlled by either mantle temperature [e.g., *Langmuir et al.*, 1992], mantle source mineralogy [e.g., *Niu and O'Hara*, 2008] or plate separation rate [e.g., *Niu and Hékinian*, 1997; *Rubin and Sinton*, 2007]. More relevant to the current discussion is variations in spreading rate. Compared to faster spreading centers, slower spreading ridges have shorter melting columns that produce less melt, which results from lower degrees and, to a limited extent, higher pressure of decompression partial melting of the mantle [*Langmuir et al.*, 1992; *Niu and O'Hara*, 2008]. By analogy, when spreading slows to a stop at dying risecrests, the amount of upwelling mantle also diminishes, resulting in even shorter melting columns and smaller degree of decompression partial melting. In general, basalts formed at lower degrees and greater pressures of melting are more alkalic, silica undersaturated and olivine normative compared to tholeiites that are formed at higher degree and lower pressure of melting [e.g., *Langmuir et al.*, 1992; *Dasgupta et al.*, 2007; *Pilet et al.*, 2008; and references therein]. Thus, lowering the degree of partial melting surely plays a major role in creating the general evolution of fossil spreading axes from N-MORB to alkalic OIB-like basalts [see also, *Choe et al.*, 2007; *Choi et al.*, 2008; *Castillo et al.*, 2010].

It is important to note, however, that Rosa Seamount alkalic lavas are generally more enriched (i.e., higher Ba/Zr, La/Sm, Nb/Zr, $^{87}Sr/^{86}Sr$, $^{206}Pb/^{204}Pb$, but lower $^{143}Nd/^{144}Nd$) than the less alkalic and tholeiitic lavas from Sara, Nithya and Rosana, which themselves still are geochemically more enriched than N-MORB (Figs. 3.4, 3.5, 3.8). Moreover, the apparently recent flows on Rosa Seamount indicate that it is still volcanically active ~11-12 myr after the cessation of spreading; Davidson Seamount remained volcanically active ~8 myr after spreading stopped there [*Clague et al.*, 2009]. Thus, decreasing degree of decompression melting alone cannot fully explain the observed compositional evolution and duration of magmatism along fossil spreading axes. Here we infer that a heterogeneous suboceanic mantle source is the other factor, along with a decreasing degree of partial melting, can explain the evolution of lava types in fossil spreading axes. The nature of such a heterogeneous mantle will be discussed in detail below.

3.5.4. Nature of the mantle source

Castillo et al. [2010] note that major and trace element concentration and radiogenic isotope data for fossil spreading axes and riseflank seamounts in the eastern Pacific define a coherent, broad compositional spectrum that is bounded by tholeiitic N-MORB-like and alkalic OIB-like lavas. They then adopt the generally accepted model for the origin of riseflank seamount lavas [e.g., *Batiza and Vanko*, 1984; *Zindler et al.*, 1984; *Graham et al.*, 1988] to explain this broad compositional spectrum. The model claims that the mantle source of MORB is heterogeneous, consisting of easily meltable, enriched components embedded in a depleted lherzolitic matrix. The OIB-like lavas originate from small degree of partial melting that preferentially fuses the enriched components in the heterogeneous source, producing a small amount of melt that by-passes the magma transport processes beneath the EPR that tend to homogenize MORB compositions. On the other hand, the N-MORB-like lavas most likely result from large degree of partial melting that fuses both the enriched and more dominant lherzolite components. The enriched signature in the resultant melt is buffered/diluted by the depleted signature during melt aggregation and mixing within crustal magma chambers. We adopt this model to explain post-spreading magmatism in the fossil spreading axes off Baja California Sur as well. As spreading slows down and/or even after it has ceased, mantle upwelling still occurs but at a diminishing rate; this scenario generally favors progressive sampling of the enriched, easily meltable components in the heterogeneous suboceanic mantle at the expense of the depleted lherzolitic matrix, producing a compositional continuum in the fossil spreading axis lava record.

We have also emphasized the tendency for temporal change from tholeiitic to alkalic eruptions at ridges built along abandoned risecrests and at central volcanoes that form riseflank seamounts. This temporal evolution combined with the aforementioned variable degrees of partial melting model for fossil spreading center magmatism defines an evolutionary scheme that is akin to the more recent alternative explanation for the origin of linear hotspot volcanoes that have traditionally been interpreted as products of deep mantle plumes [e.g., *Morgan*, 1971, 1972; *Hofmann*, 2003]. The alternative explanation invokes partial melting of upper mantle heterogeneities that happen to underlie lithospheric fractures [e.g., *Meibom and Anderson*, 2004; *Natland and Winterer*, 2005; *Foulger*, 2007]. Does this mean that magmas erupted along the healing lithospheric fractures along the axes of abandoned risecrests may have the same mantle source as the magmas that built, e.g., Galapagos and the Hawaiian volcanic chain? We conclude that their sources are different, from the absence in our samples of the high ^{3}He/^{4}He ratios (>8 +/- 1 R_A) that are distinctive features of these major volcanic systems [e.g., *Graham*, 2002]. One may argue that fossil spreading magmas may be coming from the HIMU mantle source, which produces some OIB with low ^{3}He/^{4}He ratios [e.g., *Eiler et al.*, 1997; *Hanyu et al.*, 1999]. However, the Sr and Nd isotopic signature of the bulk of fossil spreading lavas, and Rosa samples in particular, do not trend to the HIMU end-component (Fig. 3.5). Moreover, the “classic” HIMU islands are relatively rare [*Stracke et al.*, 2005] and some actually have high ^{3}He/^{4}He ratios (>8 +/- 1 R_A) [*Hilton et al.*, 2000]. Thus, if high ^{3}He/^{4}He ratio is considered diagnostic of the deep mantle plumes, we conclude that no such plumes were involved in building ridges along the abandoned EPR crest that we studied.

The production of the range of lava compositions along Sara, Rosa, Rosana, and Nithya axes by decreasing degree of partial melting of a heterogeneous upper mantle is illustrated in the Rb/Sr versus ^{87}Sr/^{86}Sr and La/Sm versus ^{143}Nd/^{144}Nd diagrams (Fig. 3.9). For simplicity, mixing of melts is assumed although actual mixing of sources prior to melting is also a possibility. In order to evaluate the model quantitatively, the depleted MORB mantle (DMM) and an enriched mantle component (EC) are chosen as the putative two end-member sources for the primary magmas of these volcanoes. The composition of DMM is obtained from that of the average depleted- (D-)MORB in *Salters and Stracke* [2004]. The composition of EC is not well defined except that it must be more enriched than our samples (e.g., $^{87}Sr/^{86}Sr > 0.703536$ and $^{143}Nd/^{144}Nd < 0.512894$; Fig. 3.5 and Table 3.3); here we back-calculated its composition from a geochemically enriched lava from the nearby Flint (off-axis) seamount [*Davis et al.* 1995; *Konter et al.*, 2009]. The lithology of the EC is assumed to be an amphibole-rich lherzolite [*Pilet et al.,* 2008]. To avoid any effect of fractional crystallization, only primitive basalts are used in the model calculations. Changes in Rb/Sr and La/Sm ratios (sub-horizontal solid curves) represent mixing lines between variable degrees of partial melt (0.05% to 2%) from DMM and 10% melt from EC. On the other hand, changes in $^{87}Sr/^{86}Sr$ and $^{143}Nd/^{144}Nd$ ratios (sub-vertical dash curves) represent changes in the proportions of the two sources for a given mixture. Although the exact amounts are different, the most enriched basalts (highest Rb/Sr and $^{87}Sr/^{86}Sr$ plus relatively higher La/Sm and lower $^{143}Nd/^{144}Nd$ ratios) from Rosa generally contain the lowest amount of low-degree partial melt from DMM. In contrast, the alkalic to tholeiitic basalts from Sara, Rosana and Nithya contain more of higher-degree partial melt from DMM. In other words, the geochemically enriched alkalic lavas from Rosa produced by smaller degree of partial melting contain lesser amount of DMM, but larger proportion of enriched component than the relatively less enriched alkalic to tholeiitic Sara, Rosana and Nithya. Rosa lavas also contain less of the lower-degree partial melt from DMM than most of the seamounts on the EPR flanks. Tholeiitic basalts sampled from the EPR axis have, of course, the highest content of the highest-degree partial melt from DMM.

3.6. Summary and conclusions

A highly segmented part of the EPR crest west of Baja California Sur, Mexico, ceased spreading at the end of the Middle Miocene, but continued eruptions built post-spreading volcanic ridges along the former spreading axes.

(1) The bulk of the lavas dredged from Rosa Seamount, the largest volcanic ridge and therefore the one most likely to have developed a long-lived magma chamber, belong to an alkalic rock series generated through fractional crystallization. Samples from the smaller Sara, Rosana and Nithya ridges mainly include mildly alkalic, transitional and tholeiitic basaltic and andesitic rocks.

(2) The petrologic and geochemical data from the four abandoned axes provide new evidence that post-abandonment alkalic volcanism is a common feature of large failed axes in the eastern Pacific. Their compositions overlap with those of lavas on other fossil spreading axes and riseflank seamounts, defining a compositional continuum ranging from MORB-like to OIB-like.

(3) Geochemical differences among lavas erupted along the four abandoned axes result from different degrees of partial melting of a compositionally heterogeneous suboceanic mantle and from different amounts of fractional crystallization. We infer that a large extent of partial melting may continue for a

geologically brief period after spreading ceases, initially producing tholeiitic MORB-like melts, then alkalic OIB-like melts as partial melting wanes. This temporal transition mirrors that inferred from the spatial pattern of riseflank seamounts, where near-axis volcanoes commonly erupt tholeiitic MORB-like lava, succeeded by alkalic OIB-like lava further down the riseflanks.

(4) Although the Sr, Nd and Pb isotopic signatures of the alkalic OIB-like lavas from fossil spreading axes in the eastern Pacific are similar to those of OIB from the Galapagos archipelago, Iceland and Hawaiian volcanic chain, they differ in lacking high ^{3}He/^{4}He ratios. This indicates that the origin of fossil spreading center magma is different from that of OIB magma comprising major "hotspot" volcanoes.

Acknowledgements

We are grateful to R. Solidum for analysis of some major elements data by XRF at SIO, C. MacIsaac, G. Lugmair and X. Liu for their assistance with the TIMS analysis, and J. Kluesner for help with Figure 3.1. We also thank two anonymous reviewers for their constructive comments and suggestions which significantly improved the manuscript and Joel Baker for thorough editorial handling. This work was funded by NSF OCE0550237 grant to PRC and DRH, NSF OCE9116493 to PFL, and the University of California Ship Fund.

Figure 3.1. Simplified map showing the study area. On the large scale map, the patterns of abandoned plate boundaries, fracture zones and the extents of post-spreading axial ridges are inferred from multibeam bathymetry; the pattern of crustal isochrons (updated from *Lonsdale* [1991]) is inferred from analysis of magnetic anomalies. The regional map also locates two other abandoned Pacific-Magdalena spreading axes (J=Juanita; M=Magdalena), and some other abandoned EPR axes with large post-spreading axial ridges: G=Guide; D=Davidson; Ne=Newton (sampled by *Batiza and Vanko* [1985]); Ga=Galileo (sampled by *Richards* [1958]). Labeled fracture zones are: Mu= Murray; Gu= Guadalupe; Mo=Molokai; Cl=Clarion.

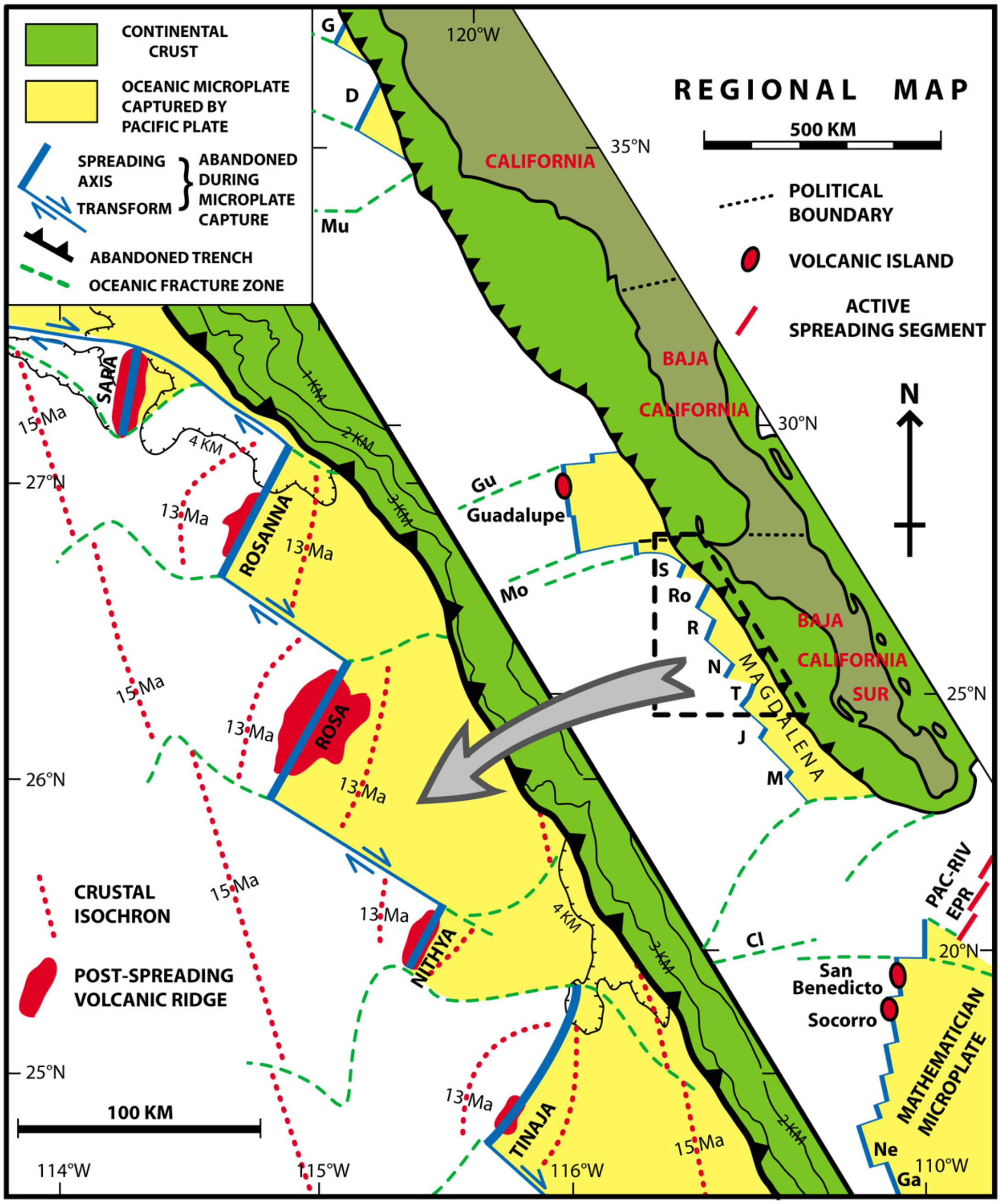
REGIONAL MAP
CONTINENTAL CRUST
OCEANIC MICROPLATE CAPTURED BY PACIFIC PLATE
SPREADING AXIS
TRANSFORM
ABANDONED DURING MICROPLATE CAPTURE
ABANDONED TRENCH
OCEANIC FRACTURE ZONE
500 KM
POLITICAL BOUNDARY
VOLCANIC ISLAND
ACTIVE SPREADING SEGMENT
N
120°W
35°N
30°N
25°N
20°N
110°W
CALIFORNIA
BAJA CALIFORNIA
BAJA CALIFORNIA SUR
MAGDALENA
G
D
Mu
Gu
Guadalupe
Mo
S
Ro
R
N
T
J
M
Cl
PAC-RIV
EPR
San Benedicto
Socorro
MATHEMATICIAN MICROPLATE
Ne
Ga
SARA
ROSANNA
ROSA
NITHYA
TINAJA
15 Ma
13 Ma
1 KM
2 KM
3 KM
4 KM
27°N
26°N
25°N
114°W
115°W
116°W
CRUSTAL ISOCHRON
POST-SPREADING VOLCANIC RIDGE
100 KM

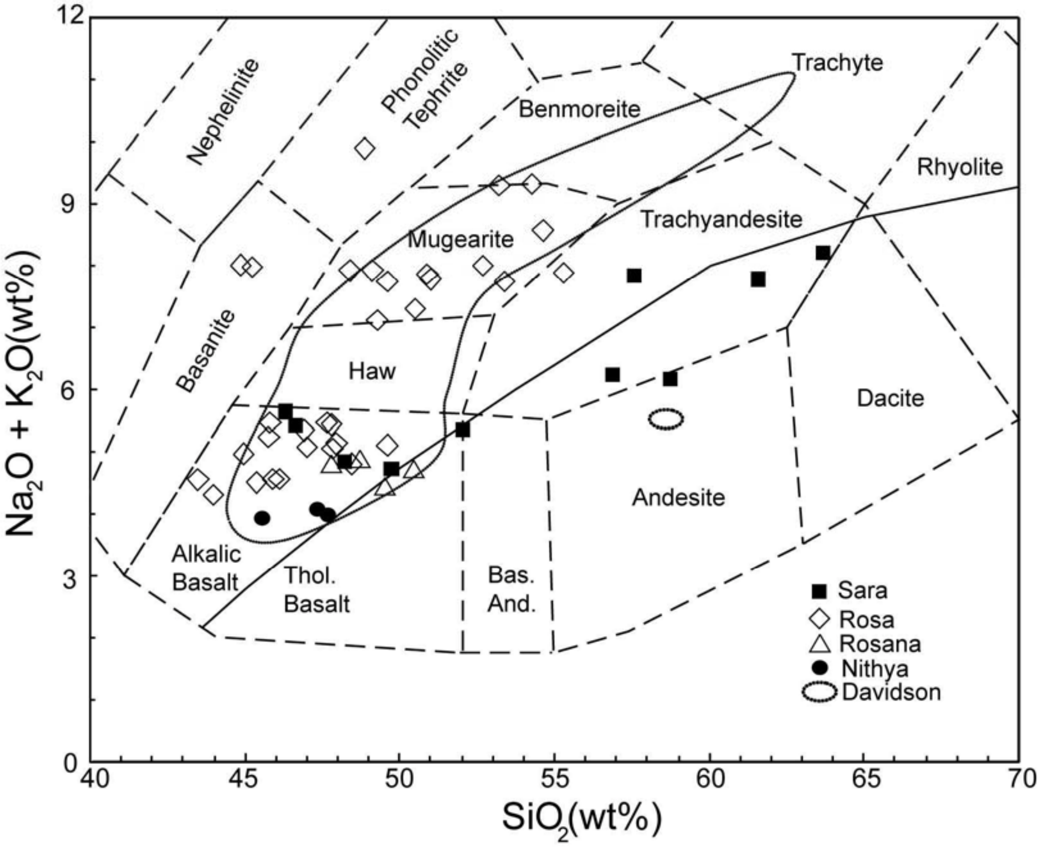

Figure 3.2. Silica (SiO_2) versus total alkalis ($Na_2O + K_2O$) diagram for samples from volcanic ridges along Sara, Rosa, Rosana, and Nithya axes. Field for lavas from Davidson Seamount [*Davis et al.*, 2002; *Castillo et al.*, 2010] is shown for reference.

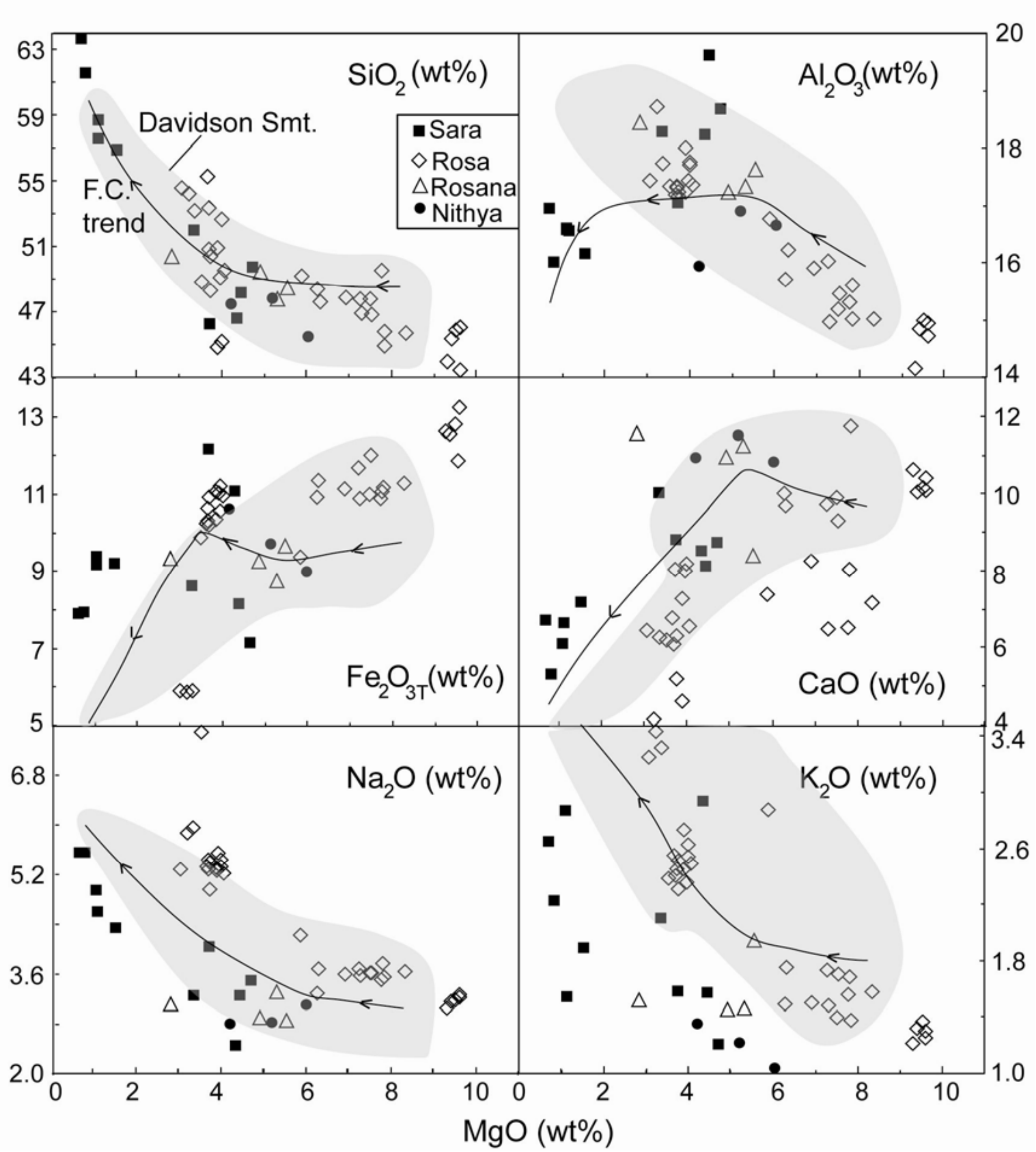

Figure 3.3. Wt% MgO versus major elements oxides SiO_2, Al_2O_3, Fe_2O_{3T}, CaO, Na_2O, and K_2O for samples from Sara, Rosa, Rosana, and Nithya. Field and fractional crystallization (F.C.) trend (solid curve with arrows) computed from a primitive basalt using the MELTS software package [*Ghiorso and Sack*, 1995; *Asimow and Ghiorso*, 1998] from Davidson Seamount [*Castillo et al.*, 2010] are shown for reference.

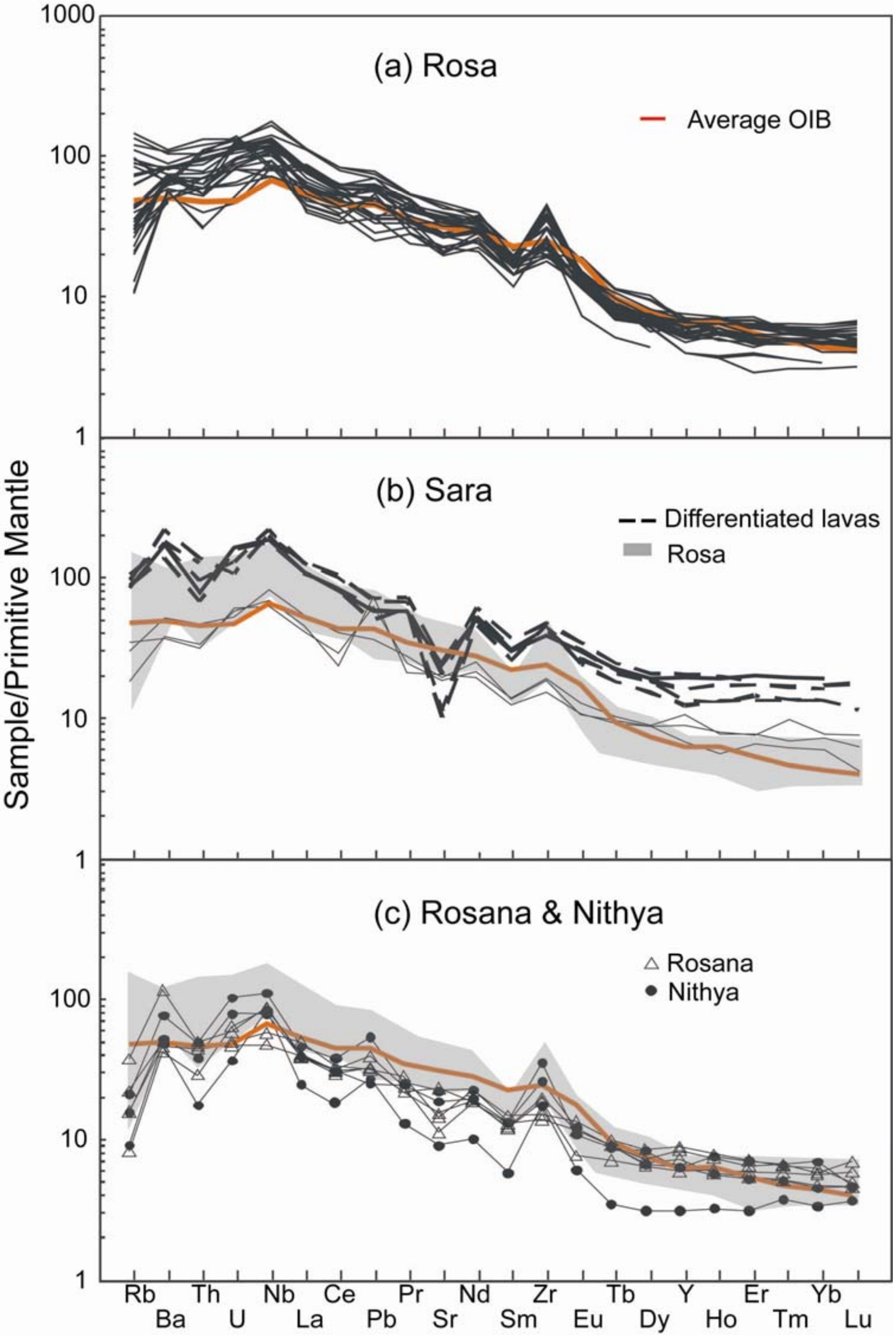

Figure 3.4. Incompatible trace element concentration diagrams for samples from Sara, Rosa, Rosana, and Nithya. The average OIB and normalizing values are from *Sun and McDonough* [1989].

Figure 3.5. (top) $^{87}Sr/^{86}Sr$ versus $^{143}Nd/^{144}Nd$ and (middle and bottom) $^{206}Pb/^{204}Pb$ versus $^{207}Pb/^{204}Pb$ and $^{208}Pb/^{204}Pb$ (lower two panels) for representative samples from Sara, Rosa, Rosana, and Nithya. Data for Davidson Seamount [*Davis et al.*, 2002; *Castillo et al.*, 2010], Guide Seamount [*Davis et al.*, 2002] and Socorro Island [*Bohrson and Reid*, 1995, 1997] are shown for reference. Also shown are fields for some seamounts on the EPR flanks [*Niu et al.*, 2002], EPR MORB, Galapagos Islands, Hawaii, and Iceland (GEOROC database: http://georoc.mpch-mainz.gwdg.de). HIMU, EM1 and EM2 are proposed mantle end-components, and NHRL is the northern hemisphere reference line from *Hart* [1984].

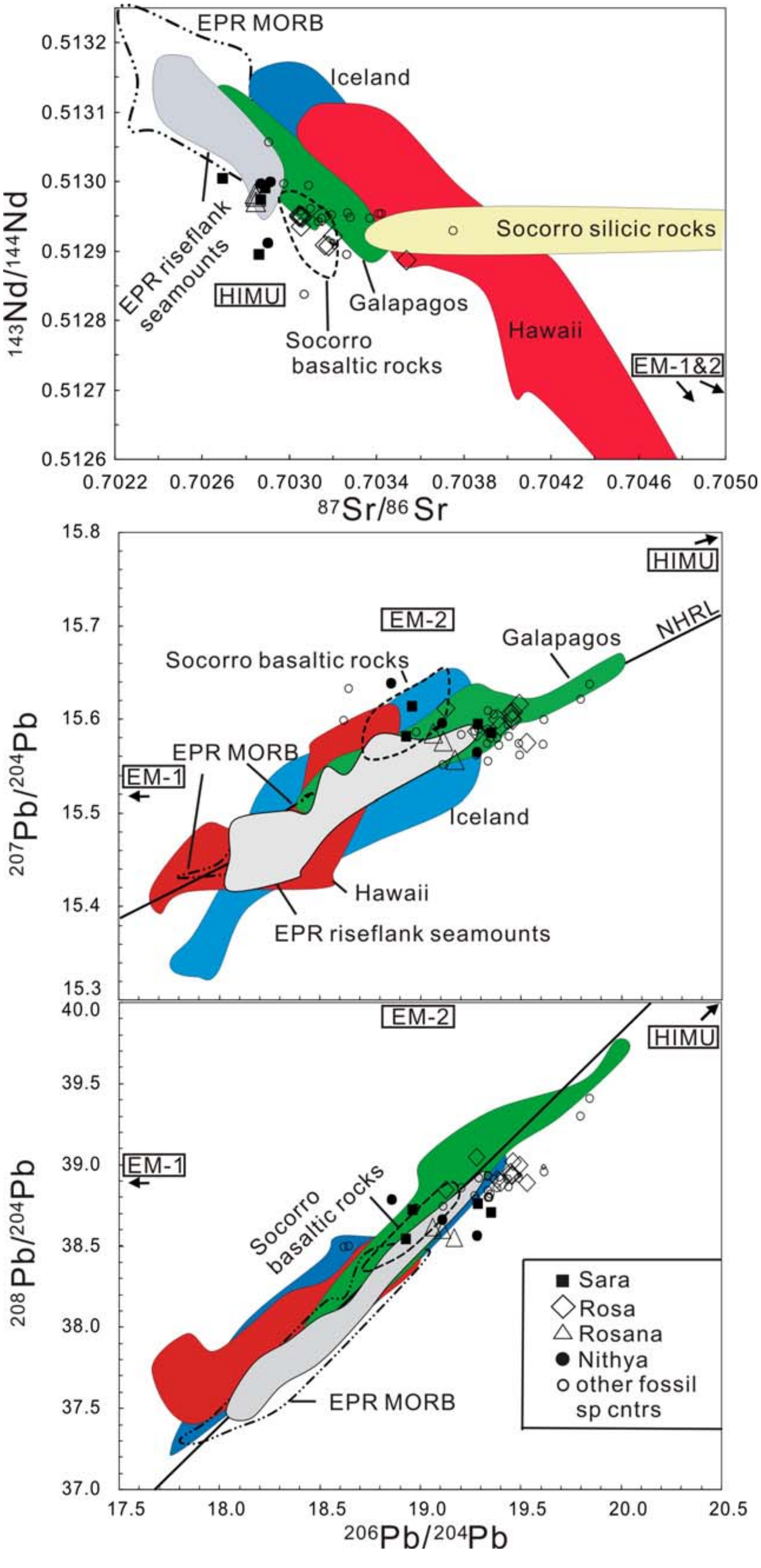

EPR MORB
Iceland
Socorro silicic rocks
EPR riseflank seamounts
HIMU
Galapagos
Hawaii
Socorro basaltic rocks
EM-1&2
^{143}Nd/^{144}Nd
0.5132
0.5131
0.5130
0.5129
0.5128
0.5127
0.5126
0.7022
0.7026
0.7030
0.7034
0.7038
0.7042
0.7046
0.7050
^{87}Sr/^{86}Sr
15.8
15.7
15.6
15.5
15.4
15.3
HIMU
EM-2
Galapagos
NHRL
Socorro basaltic rocks
EPR MORB
EM-1
Iceland
Hawaii
EPR riseflank seamounts
^{207}Pb/^{204}Pb
40.0
39.5
39.0
38.5
38.0
37.5
37.0
EM-2
HIMU
EM-1
Socorro basaltic rocks
EPR MORB
■ Sara
◇ Rosa
△ Rosana
● Nithya
○ other fossil sp cntrs
^{208}Pb/^{204}Pb
17.5
18.0
18.5
19.0
19.5
20.0
20.5
^{206}Pb/^{204}Pb

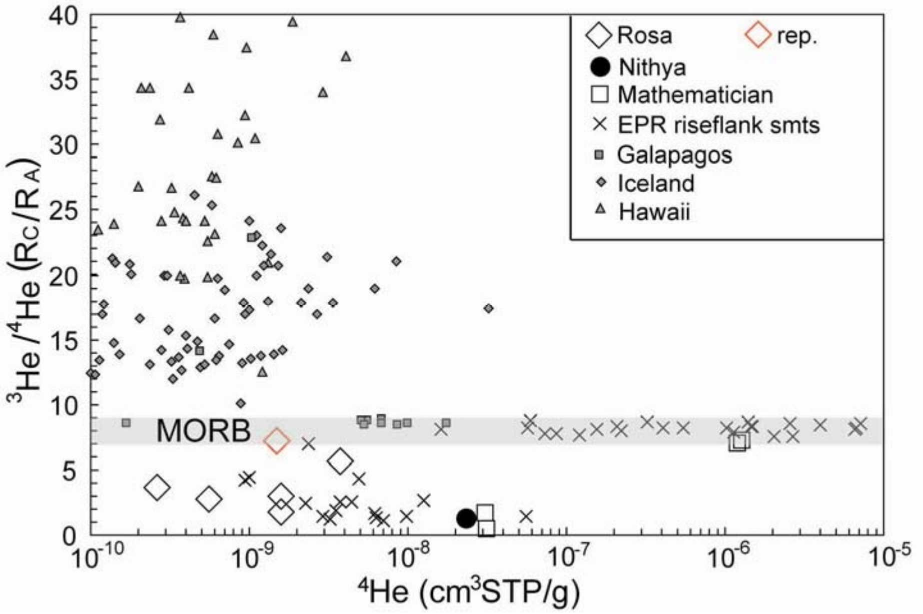

Figure 3.6. Relationships between ^{3}He/^{4}He ratios and ^{4}He abundances for representative samples from Rosa Seamount, Nithya ridge and Davidson Seamount. Shown for reference are data for axial ridges on Mathematician Ridge [*Graham et al.*, 1988], riseflank seamounts [*Graham et al.*, 1988; *Hahm et al.*, 2009], Galapagos archipelago, Hawaii, and Iceland [USGS-NoGaDat: http://pubs.usgs.gov/ds/2006/202; *Abedini et al.*, 2006].

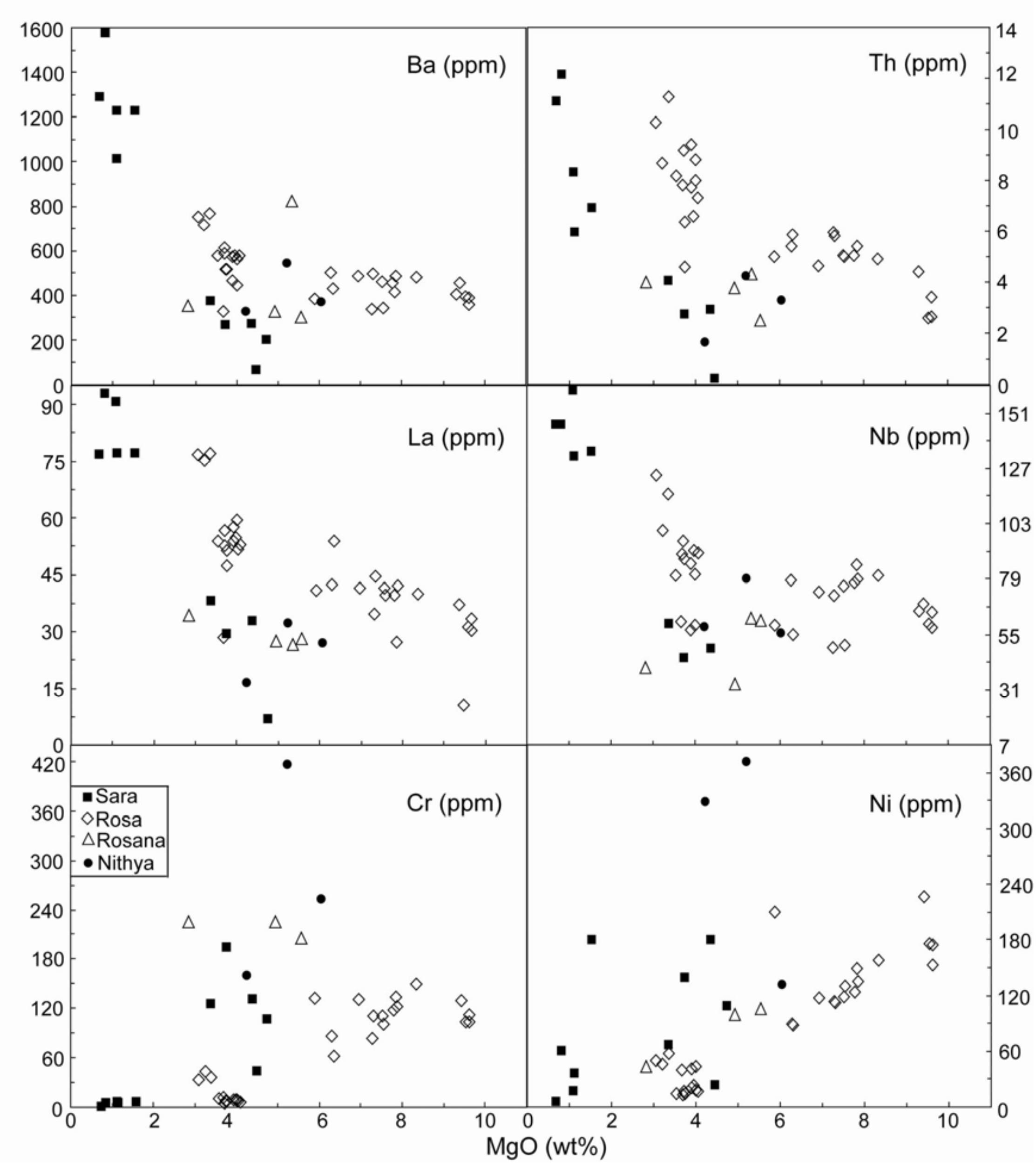

Figure 3.7. Wt% MgO versus ppm trace elements Ba, Th, La, Nb, Cr, and Ni for samples from Sara, Rosa, Rosana, and Nithya.

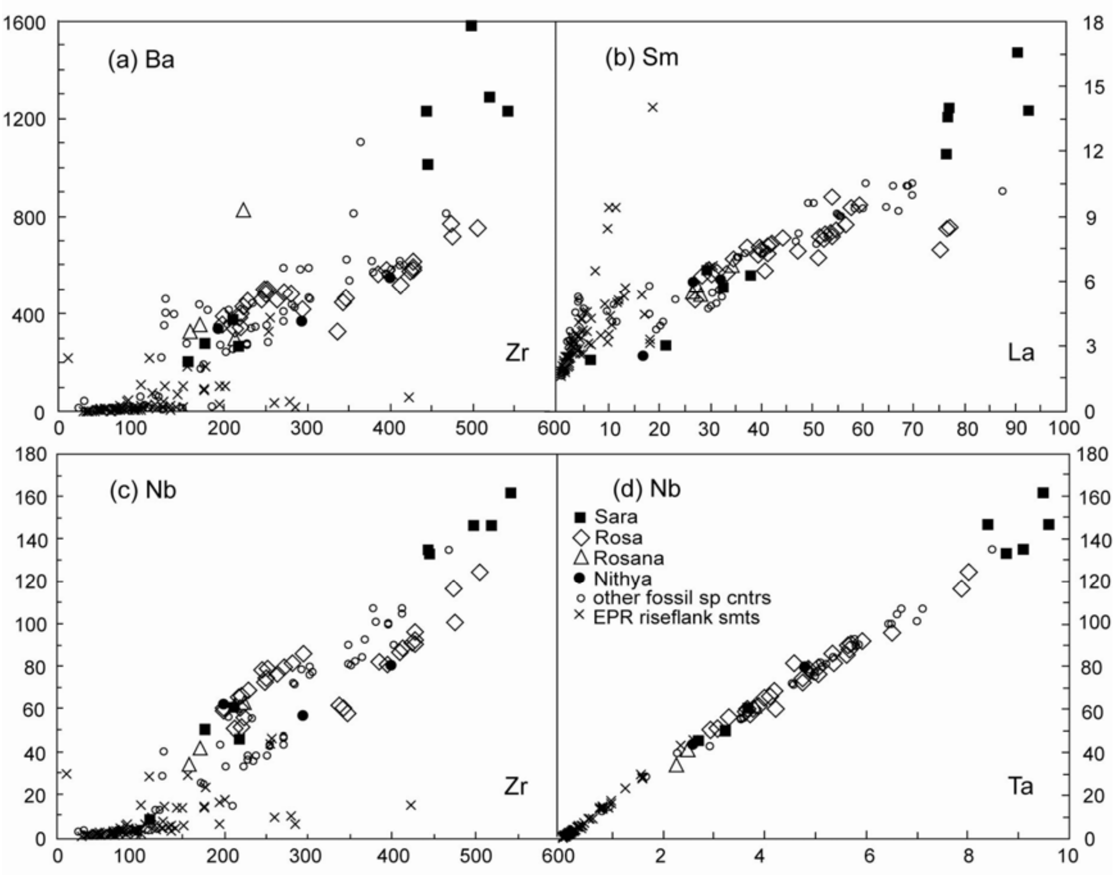

Figure 3.8. (A) Zr versus Ba, (B) La versus Sm, (C) Zr versus Nb, and (D) Ta versus Nb for samples from Sara, Rosa, Rosana, and Nithya. Shown for reference are data for other fossil spreading axes and riseflank seamounts. Sources of data as in Figure 3.5.

Figure 3.9. (a) Rb/Sr abundance ratio versus ^{87}Sr/^{86}Sr and (b) La/Sm abundance ratio versus ^{143}Nd/^{144}Nd for primitive basalts from Sara, Rosa, Rosana, and Nithya. The vertical line with numbers from depleted MORB mantle (DMM) indicates Rb/Sr and La/Sm abundance ratio at 0.05-2 % melting of a depleted MORB mantle source [Rb = 0.088 ppm, Sr = 9.80 ppm, ^{87}Sr/^{86}Sr = 0.7026; La = 0.234 ppm, Sm = 0.270 ppm, Nd = 0.713 ppm, ^{143}Nd/^{144}Nd = 0.51311; *Salters and Stracke*, 2004]. Here the initial mode of the depleted MORB mantle source was assumed to be olivine:orthopyroxene:clinopyroxene:garnet (60:25:10:5 mixture) lherzolite. An equilibrium batch partial melting model is used for calculation; bulk D (partition coefficient) for Rb is 0.0003, for Sr 0.0093, for La 0.0015, for Sm 0.0406, and for Nd 0.0153 in the lherzolite. The sub-horizontal linear solid curves are mixing lines between the various DMM melts (F%: degree of partial melting) and 10% melt of an enriched mantle component (EC; Rb = 6.45 ppm, Sr = 127.5 ppm, ^{87}Sr/^{86}Sr = 0.704162; La = 4.61 ppm, Sm = 3.85 ppm, Nd = 10.64 ppm, ^{143}Nd/^{144}Nd = 0.512869). The trace element abundances of EC are back-calculated by assuming that a primitive basalt from Flint seamount [*Davis et al.*, 1995] was produced by 20% partial melting of this source; its Sr and Nd isotopic values are from *Konter et al.* [2009], normalized relative to NBS 987 ^{87}Sr/^{86}Sr = 0.71025, and ^{143}Nd/^{144}Nd = 0.51185 for the La Jolla Nd standard. The EC source is assumed to be an amphibole:olivine:orthopyroxene:clinopyroxene:garnet (55:20:05:15:05) lherzolite. Bulk D for Rb is 0.1981, for Sr 0.1990, for La 0.089, for Sm 0.579, and for Nd 0.282 in the amphibole lherzolite. Vertical dash curves represent various DMM:EC melt mixtures. Detailed predictions of this model depend on the initial mineralogy of two end-members, source composition, style of melting, and the chosen D values, but the applicability of the model results is not affected by these parameters. Fields for basalts from Davidson Seamount, Socorro Island, selected riseflank seamounts, and adjacent EPR axis are shown for reference. Data sources are as in Figure 3.5.

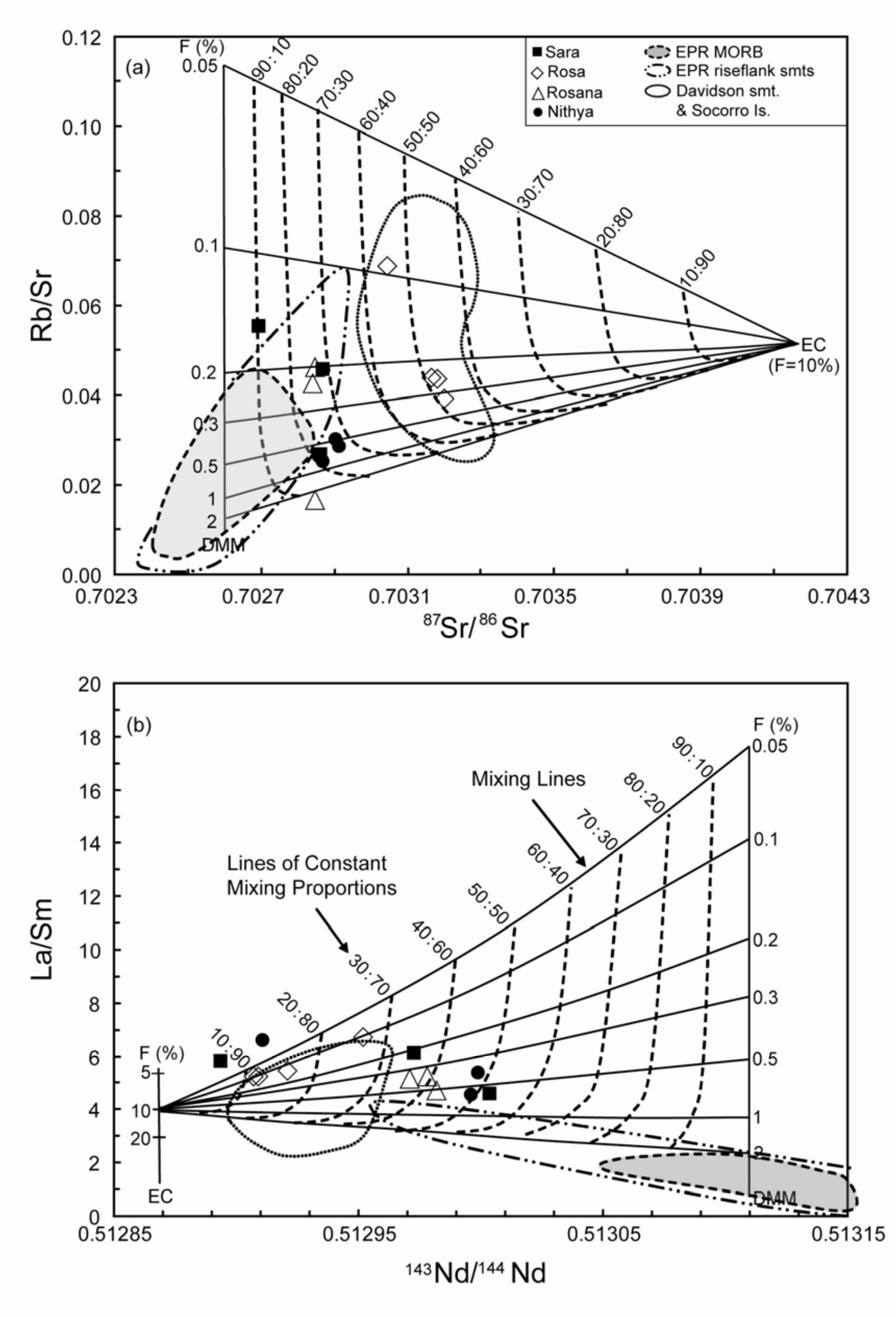
(a)
F (%)
0.05
0.1
0.2
0.3
0.5
1
2
DMM
90:10
80:20
70:30
60:40
50:50
40:60
30:70
20:80
10:90
EC
(F=10%)
■ Sara
◇ Rosa
△ Rosana
● Nithya
EPR MORB
EPR riseflank smts
Davidson smt.
& Socorro Is.
Rb/Sr
0.00
0.02
0.04
0.06
0.08
0.10
0.12
0.7023
0.7027
0.7031
0.7035
0.7039
0.7043
$^{87}Sr/^{86}Sr$
(b)
Mixing Lines
Lines of Constant
Mixing Proportions
F (%)
0.05
0.1
0.2
0.3
0.5
1
2
DMM
90:10
80:20
70:30
60:40
50:50
40:60
30:70
20:80
10:90
F (%)
5
10
20
EC
La/Sm
0
2
4
6
8
10
12
14
16
18
20
0.51285
0.51295
0.51305
0.51315
$^{143}Nd/^{144}Nd$

Table 3.1. Dredge locations for post-spreading lavas on fossil spreading axes off Baja California Sur, Mexico

Location	Voyage	Dredge Station	Lat. (N)	Long.(W)	Depth (m)
Sara	ROSA	5	27°19.82'	115°42.42'	2092-1810
	ROSA	6	27°18.49'	115°41.94'	1758-1541
	ROSA	7	27°17.10'	115°43.02'	2112-2006
	ROSA	8	27°12.66'	115°43.89'	2840-2335
Rosana	ROSA	11	26°50.94'	115°16.44'	2800-2325
Rosa	ROSA	9	26°12.65'	115°1.56'	1000-625
	ROSA	10	26°12.94'	114°59.11'	1090-820
	PHOENIX	128	26°10.36'	115°01.46'	870-520
Nithya	PHOENIX	127	25°26.99'	114°33.90'	1730-1540

Table 3.2. Major and trace element compositions of post-spreading lavas on fossil spreading axes off Baja California Sur, Mexico

Location	Sara	Sara	Sara	Sara	Sara	Sara	Sara
Voyage	ROSA	ROSA	ROSA	ROSA	ROSA	ROSA	ROSA
Sample	5-1	5-5	6-1	6-2	6-5A	6-7	6-9
Rock type[a]	AB	TrB	An	TrAn	TrAn	AB	TrAn
SiO_2[b]	46.58	49.68	58.72	56.86	63.66	48.15	61.55
TiO_2	2.44	1.34	1.70	1.66	0.58	0.28	0.54
Al_2O_3	18.23	18.68	16.56	16.15	16.94	19.61	16.01
Fe_2O_{3T}	11.06	7.13	9.14	9.20	7.88	8.15	7.91
MnO	0.34	0.13	0.30	1.02	0.22	0.13	1.09
MgO	4.37	4.73	1.12	1.54	0.70	4.47	0.82
CaO	8.49	8.72	6.62	7.18	6.72	8.09	5.31
Na_2O	2.46	3.50	4.60	4.34	5.55	3.26	5.54
K_2O	2.95	1.22	1.56	1.90	2.66	1.58	2.24
P_2O_5							
LOI	3.30	1.26	3.53	3.63	1.01	1.45	1.47
Cr[c]	133	108	7	8	3	46	7
Ni	181.1	111.0	37.7	181.4	7.6	25.0	62.5
Rb	11.9		58.5	55.4	64.3	4.4	62.6
Sr	447.9	287.7	447.8	519.4	216.9	198.7	245.1
Y	42.1	11.1	75.4	90.7	57.2		62.2
Zr	178	157	446	444	520		498
Nb	49.7		132.5	134.6	146.1		146.0
Ba	273	198	1011	1225	1286	69	1574
La	32.8	6.7	77.1	76.9	76.7		92.7
Ce	43.1	17.1	151.9	148.7	153.5		191.7
Pr	5.9	1.9	17.2	16.5	16.2		19.1
Nd	27.4	10.2	73.4	70.7	64.2		78.7
Sm	5.7	2.3	14.0	13.5	11.8		13.9
Eu	1.8	0.8	5.2	5.2	4.2		4.5
Tb	1.0	0.4	2.5	2.5	2.0		2.3
Dy	6.7	2.9	14.0	14.5	11.5		13.8
Ho	1.3	0.6	2.9	3.2	2.2		2.2
Er	3.8	1.5	8.6	9.9	6.6		7.1
Tm	0.7	0.2	1.3	1.5	1.0		1.0
Yb	3.9	1.6	8.2	9.6	6.8		6.8
Lu	0.6						0.9
Ta	3.23		8.78	9.10	9.60		8.42
Pb	5.3		3.6	4.3	4.3	1.4	5.0
Th	2.91		5.96	6.92	11.11	0.23	12.16
U	1.25	0.14	3.41	3.54		0.14	2.33

Table 3.2. Major and trace element compositions (continued)

Location	Sara	Sara	Sara	Rosa	Rosa	Rosa	Rosa
Voyage	ROSA	ROSA	ROSA	ROSA	ROSA	ROSA	ROSA
Sample	6-10	7-1*	8-1	9-1*	9-2	9-3	9-4
Rock type[a]	TrAn	AB	TrB	P-T	Mug	Mug	Mug
SiO_2[b]	57.55	46.25	51.99	48.80	49.54	50.84	49.06
TiO_2	1.69	2.57	2.26	2.31	2.25	2.23	2.30
Al_2O_3	16.60	17.04	18.28	17.34	17.35	17.33	17.44
Fe_2O_{3T}	9.39	12.16	8.63	9.89	10.95	10.65	11.04
MnO	0.25	0.36	0.16	0.20	0.19	0.18	0.20
MgO	1.10	3.74	3.37	3.54	4.06	3.70	3.96
CaO	6.08	8.77	10.02	6.19	6.55	6.08	8.01
Na_2O	4.95	4.04	3.24	7.49	5.23	5.44	5.55
K_2O	2.89	1.60	2.11	2.41	2.51	2.42	2.37
P_2O_5		0.66		0.59			
LOI	2.60	2.14	1.82	0.74	0.46	0.82	0.42
Cr[c]	8	196	127	13	9	8	12
Ni	19.5	141.0	68.1	16	18.5	14.8	25.1
Rb	69.1	22.5	19.5	55.6	40.2	46.5	38.6
Sr	545.7	406.7	427.6	809.4	698.1	728.7	735.4
Y	95.7	49.1	31.1	31.0	26.7	28.2	26.5
Zr	542	219	212	395	424	428	428
Nb	161.1	45.6	60.5	81.0	90.8	90.2	92.1
Ba	1228	265	374	577	575	590	579
La	90.5	29.5	38.1	54.0	52.8	52.5	54.8
Ce	181.9	52.7	74.3	105.3	106.0	104.0	110.0
Pr	20.7	7.0	7.9	12.4	11.6	11.5	12.0
Nd	84.4	29.6	35.0	44.9	45.9	43.6	47.0
Sm	16.5	6.5	6.2	8.0	8.2	8.0	8.4
Eu	5.9	2.2	1.8	2.5	2.3	2.3	2.3
Tb	2.7	1.1	1.1	1.1	0.9	0.9	0.9
Dy	15.8	6.7	6.7	5.5	5.4	5.2	5.4
Ho	3.4	1.3	0.9	1.0	1.0	1.0	1.0
Er	9.0	3.8	3.3	2.8	2.5	2.9	2.5
Tm	0.0	0.5	0.5	0.4	0.4	0.4	0.4
Yb	8.6	3.6	3.0	2.6	2.6	2.7	2.6
Lu	1.4	0.5	0.3	0.4	0.4	0.4	0.4
Ta	9.51	2.70	3.70		5.69	5.64	5.92
Pb	5.2	4.6	2.6	4.1	4.0	3.2	4.9
Th	8.33	2.74	4.06	8.19	7.30	7.80	6.60
U	2.80	1.33	1.15	2.36	2.47	2.35	2.37

Table 3.2. Major and trace element compositions (continued)

Location	Rosa	Rosa	Rosa	Rosa	Rosa	Rosa	Rosa
Voyage	ROSA	ROSA	ROSA	ROSA	ROSA	ROSA	ROSA
Sample	9-5	9-6	9-7	9-8	9-9	9-10*	9-11
Rock type[a]	Bas	Bas	Mug	TrAn	Mug	Mug	Mug
SiO_2[b]	45.18	44.80	48.33	55.27	50.94	50.45	52.64
TiO_2	2.34	2.29	2.31	2.27	2.33	2.42	2.40
Al_2O_3	17.75	17.99	17.16	17.18	17.24	17.24	17.69
Fe_2O_{3T}	11.21	11.09	10.20	10.23	10.34	10.92	10.55
MnO	0.19	0.18	0.18	0.18	0.18	0.20	0.19
MgO	4.00	3.90	3.75	3.67	3.90	3.74	4.00
CaO	8.16	4.60	5.18	6.78	7.27	6.29	8.18
Na_2O	5.34	5.26	5.39	5.33	5.31	4.97	5.44
K_2O	2.64	2.75	2.53	2.56	2.47	2.33	2.56
P_2O_5						0.59	
LOI	0.40	0.49	0.74	0.73	0.40	0.67	0.63
Cr[c]	10	12	11	15	11		11
Ni	20.5	22.6	16.4	42.4	43.8		45.6
Rb	60.0	45.4	27.3	18.0	53.4	57.5	60.4
Sr	758.3	772.7	600.0	412.4	683.1	728.3	657.6
Y	30.5	29.3	21.4		30.5	30.3	32.1
Zr	385	409	413	336	347		343
Nb	81.7	86.4	88.3	61.4	57.6		59.9
Ba	564	575	516	325	464	518	445
La	51.6	53.8	47.3	28.4	57.7	51.2	59.4
Ce	102.2	106.5	94.9	60.9	109.6	98.0	109.0
Pr	11.3	11.6	10.5	7.9	13.3	11.1	13.6
Nd	43.9	45.6	41.5	30.1	50.4	40.5	51.2
Sm	8.1	8.3	7.4	6.2	9.4	7.1	9.5
Eu	2.2	2.3	2.0	2.2	3.1	2.3	3.1
Tb	0.9	0.9	0.7	1.0	1.2	1.0	1.2
Dy	5.4	5.4	4.6	4.5	6.9	5.0	7.0
Ho	1.1	1.1	0.9	0.9	1.1	0.9	1.1
Er	3.0	2.9	2.5	2.4	3.2	2.5	3.3
Tm	0.4	0.4	0.4	0.4	0.4	0.4	0.4
Yb	2.8	2.8	2.3	2.3	2.7	2.3	2.7
Lu	0.4	0.4	0.4	0.3	0.4	0.3	0.4
Ta	4.59	5.35	5.68	3.88	3.71		3.76
Pb	4.0	3.9	2.7	3.8	4.3	3.4	4.4
Th	7.98	7.73	4.60		9.41	6.35	8.80
U	2.22	2.29	2.56		2.67	1.83	2.88

Table 3.2. Major and trace element compositions (continued)

Location	Rosa	Rosa	Rosa	Rosa	Rosa	Rosa	Rosa
Voyage	ROSA	ROSA	ROSA	ROSA	ROSA	ROSA	ROSA
Sample	9-12	10-1	10-2	10-3	10-4	10-5*	10-6
Rock type[a]	Mug	AB	AB	AB	Ben	Ben	AB
SiO_2[b]	53.34	45.70	47.90	45.75	53.17	54.24	48.39
TiO_2	2.33	2.73	2.91	2.70	1.20	1.25	2.89
Al_2O_3	17.30	15.01	15.91	15.59	17.72	18.72	15.71
Fe_2O_{3T}	10.30	11.28	11.13	11.08	5.91	5.88	10.91
MnO	0.18	0.20	0.15	0.17	0.15	0.18	0.15
MgO	3.71	8.34	6.93	7.82	3.36	3.21	6.27
CaO	8.02	7.16	8.24	8.04	6.27	4.15	10.00
Na_2O	5.28	3.64	3.61	3.76	5.96	5.87	3.29
K_2O	2.47	1.59	1.52	1.70	3.34	3.45	1.51
P_2O_5						0.64	
LOI	0.57	0.51	1.28	0.49	1.77	1.93	2.73
Cr[c]	9	151	133	136	39	46	89
Ni	19.4	159.6	119.4	151.6	59.7	48.0	91.1
Rb	69.8	16.4	22.7	6.6	91.0	85.3	14.4
Sr	831.8	561.0	676.8	467.7	976.0	925.6	663.3
Y	33.9	23.8	25.1		32.0	30.0	25.7
Zr	427	281	249	294	474	476	252
Nb	96.1	81.4	74.2	85.6	116.4	100.3	79.1
Ba	615	482	483	416	767	717	501
La	56.7	40.0	41.4	27.2	77.1	75.2	42.3
Ce	112.3	84.7	85.7	58.3	144.4	139.0	87.8
Pr	12.2	9.4	9.7	6.5	15.0	14.7	10.0
Nd	47.9	38.9	40.6	27.7	53.8	49.4	40.9
Sm	8.6	7.4	7.6	5.1	8.5	7.4	7.7
Eu	2.5	2.0	2.1	1.2	2.4	2.3	2.1
Tb	1.0	0.8	0.8	0.6	0.9	0.9	0.8
Dy	6.0	5.0	5.2	3.2	5.3	4.8	5.2
Ho	1.2		1.0	0.6	1.1	0.9	1.0
Er	2.9		2.3	1.4	3.1	2.4	2.4
Tm	0.5		0.4	0.2	0.5	0.4	0.4
Yb	3.1	2.3	2.3	1.5	3.1	2.5	2.4
Lu	0.5	0.3	0.4	0.2	0.5	0.3	0.4
Ta	6.50	5.37	4.74	5.62	7.86		4.87
Pb	4.4		2.5	2.6	5.5	4.9	2.5
Th	9.18	4.89	4.62		11.27	8.68	5.40
U	2.42		1.76	2.01	2.74	2.54	2.71

Table 3.2. Major and trace element compositions (continued)

Location	Rosa	Rosa	Rosa	Rosa	Rosa	Rosa	Rosa
Voyage	ROSA	ROSA	ROSA	ROSA	ROSA	ROSA	ROSA
Sample	10-7	10-8	10-9	10-10	10-11	10-12*	10-13*
Rock type[a]	AB	AB	AB	AB	Mug	AB	AB
SiO_2[b]	49.54	46.94	47.77	44.90	54.58	46.84	47.58
TiO_2	2.73	2.75	2.64	2.69	1.21	2.75	3.01
Al_2O_3	15.31	14.97	15.18	15.00	17.42	15.46	16.23
Fe_2O_{3T}	10.91	10.89	10.99	11.17	5.90	12.01	11.36
MnO	0.16	0.17	0.24	0.20	0.13	0.25	0.19
MgO	7.77	7.30	7.52	7.85	3.06	7.54	6.32
CaO	6.51	6.50	9.91	11.73	6.47	9.28	9.68
Na_2O	3.52	3.57	3.62	3.56	5.30	3.62	3.69
K_2O	1.58	1.50	1.42	1.40	3.27	1.72	1.77
P_2O_5						0.67	0.72
LOI	2.02	0.58	0.52	0.21	1.95	0.57	1.40
Cr[c]	121	113	113	125	36	102	65
Ni	126.1	114.0	120.6	137.1	52.7	132.0	90.0
Rb	21.7	26.9	19.1	20.2	76.2	19.0	26.6
Sr	550.3	664.8	582.4	562.9	899.0	434.6	678.1
Y	22.7	28.0	23.3	24.0	29.6	30.6	29.8
Zr	246	248	263	272	505	220	224
Nb	78.1	72.5	76.5	79.7	124.2	51.0	56.0
Ba	457	497	460	485	753	344	429
La	39.6	44.4	41.4	41.9	76.6	39.8	53.9
Ce	82.1	91.7	84.6	88.2	144.8	76.1	98.3
Pr	9.2	10.2	9.5	9.8	14.9	9.7	12.9
Nd	38.2	42.3	38.8	40.6	53.4	38.5	50.7
Sm	7.2	8.0	7.2	7.7	8.4	7.6	9.9
Eu	1.9	2.2	2.0	2.1	2.4	2.5	3.2
Tb	0.8	0.9	0.8	0.8	0.9	1.1	1.2
Dy	4.8	5.5	4.8	5.1	5.2	5.5	7.4
Ho	0.9	1.0	0.9	1.0	1.0	0.9	1.2
Er	2.2	2.6	2.2	2.3	3.0	2.5	3.4
Tm	0.3	0.4	0.3	0.4	0.4	0.4	0.4
Yb	2.2	2.6	2.2	2.4	2.9	2.4	2.7
Lu	0.3	0.4	0.3	0.4	0.5	0.3	0.4
Ta	4.89	4.76	5.05	5.07	8.03	3.08	3.29
Pb	2.3	4.0	3.2	4.4	5.3		2.6
Th	5.03	5.83	5.07	5.42	10.26	5.00	5.88
U	1.98	2.01	1.86	1.98	2.71	1.30	1.68

Table 3.2. Major and trace element compositions (continued)

Location	Rosa	Rosa	Rosa	Rosa	Rosa	Rosa	Rosa
Voyage	ROSA	PHOENIX	PHOENIX	PHEONIX	PHOENIX	PHEONIX	PHOENIX
Sample	10-14*	128-15*	128-16*	128-17*	128-18*	128-19*	128-20*
Rock type[a]	AB	AB	Mug	AB	AB	AB	AB
SiO_2[b]	47.75	45.32	49.21	43.92	46.04	45.84	43.41
TiO_2	2.94	3.08	3.11	2.99	3.15	3.11	3.12
Al_2O_3	16.02	14.85	16.77	14.15	14.94	14.98	14.72
Fe_2O_{3T}	11.67	12.56	9.37	12.62	13.23	12.80	11.85
MnO	0.20	0.20	0.16	0.19	0.20	0.21	0.20
MgO	7.27	9.41	5.88	9.31	9.62	9.53	9.61
CaO	9.74	10.05	7.37	10.62	10.41	10.15	10.07
Na_2O	3.68	3.16	4.23	3.07	3.24	3.18	3.28
K_2O	1.75	1.34	2.89	1.23	1.32	1.38	1.27
P_2O_5	0.73	0.54	0.81	0.56	0.61	0.56	0.53
LOI	1.14	0.32	1.56	2.37	0.97	0.31	0.57
Cr[c]	85	132	134		114	106	105.9
Ni	115.0	229.0	212.4		177.1	177.5	154.7
Rb	13.2	3.5	12.6	28.5	8.1	6.8	25.2
Sr	424.9	419.4	590.1	709.9	441.4	482.3	572.6
Y	30.0		22.6	31.3	17.9	17.9	26.6
Zr	212	228	218	221	217	199	198
Nb	50.4	68.8	60.1	65.9	65.6	60.4	58.7
Ba	338	453	385	402	387	392	357
La	34.6	10.6	41.0	37.2	30.4	31.4	33.3
Ce	67.7	23.1	92.2	76.4	65.8	66.9	75.3
Pr	8.8		9.3	9.1	7.7	7.8	8.5
Nd	34.8		38.6	40.3	33.4	33.8	31.9
Sm	7.0		6.5	7.6	6.3	6.4	6.3
Eu	2.3		1.9	2.3	2.0	2.0	2.1
Tb	1.0		0.9	1.1	0.8	0.8	0.9
Dy	4.9		4.6	6.0	4.4	4.5	4.2
Ho	0.9		0.8	1.1	0.6	0.6	0.8
Er	2.5		2.1	2.9	1.9	1.9	2.3
Tm	0.4		0.4	0.4	0.3	0.3	0.3
Yb	2.3		2.0	2.6	1.6	1.6	2.2
Lu	0.3		0.3	0.4			0.3
Ta	2.95	4.20	4.22	4.11	3.98	3.66	3.63
Pb	3.3		3.6	3.5	1.8		2.0
Th	5.93		4.99	4.39	2.66	2.57	3.39
U	1.68		1.36	1.72	1.10		0.97

Table 3.2. Major and trace element compositions (continued)

Location	Rosana	Rosana	Rosana	Rosana	Nithya	Nithya	Rosana
Voyage	ROSA	ROSA	ROSA	ROSA	PHOENIX	PHOENIX	ROSA
Sample	11-1*	11-4	11-5*	11-6*	127-18*	127-19*	11-6*
Rock type[a]	AB	AB	ThB	ThB	TrB	TrB	ThB
SiO_2[b]	47.78	48.48	49.46	50.41	47.81	47.45	50.41
TiO_2	2.12	2.11	2.06	2.22	2.44	2.32	2.22
Al_2O_3	17.33	17.64	17.23	18.44	16.88	15.92	18.44
Fe_2O_{3T}	8.74	9.68	9.27	9.34	9.70	10.60	9.34
MnO	0.16	0.16	0.23	0.21	0.19	1.07	0.21
MgO	5.32	5.54	4.93	2.83	5.21	4.23	2.83
CaO	11.22	8.38	10.97	11.58	11.48	10.93	11.58
Na_2O	3.31	2.87	2.92	3.14	2.83	2.81	3.14
K_2O	1.48	1.97	1.47	1.54	1.23	1.37	1.54
P_2O_5	0.63		0.66	0.61	1.50	1.48	0.61
LOI	1.49	1.64	1.45	1.60	2.70	3.36	1.60
Cr[c]		207	227	227	419	162	227
Ni		107.6	101.5	45.4	374.1	330.4	45.4
Rb	24.2	5.3	10.2	14.3	13.5	5.9	14.3
Sr	493.8	329.6	240.2	308.9	474.2	195.2	308.9
Y	38.8	27.5	33.5	41.0	29.1	14.3	41.0
Zr	224	212	159	171	400	199	171
Nb	62.9	61.8	34.2	41.7	79.8	42.5	41.7
Ba	824	300	326	354	543	343	354
La	26.7	28.1	27.4	34.4	32.3	17.1	34.4
Ce	52.7	56.0	56.9	59.9	68.5	31.7	59.9
Pr	6.1	6.2	6.7	7.9	7.1	3.7	7.9
Nd	25.4	26.2	25.3	30.4	31.1	13.9	30.4
Sm	5.5	5.4	5.8	6.7	6.0	2.6	6.7
Eu	2.0	1.3	2.0	2.3	1.8	1.0	2.3
Tb	1.0	0.8	1.0	1.1	1.0	0.4	1.1
Dy	5.4	4.9	5.1	6.4	6.2	2.3	6.4
Ho	1.2	1.0	1.0	1.3	1.3	0.5	1.3
Er	3.1	2.9	2.6	3.5	3.4	1.5	3.5
Tm	0.5	0.4	0.4	0.5	0.5	0.3	0.5
Yb	2.9	2.8	2.4	3.1	3.5	1.7	3.1
Lu	0.5	0.4	0.3	0.4	0.4	0.3	0.4
Ta		3.79	2.26	2.48	4.80	3.69	2.48
Pb	2.3	2.3	2.8	2.3	3.9	2.0	2.3
Th	4.31	2.50	3.79	4.02	4.22	1.50	4.02
U	1.25	1.36	1.00	1.05	2.19	0.80	1.05

Table 3.2. Major and trace element compositions (continued)

Location				
Cruise	Analysis of international rock standard			
Sample	AGV-1		BHVO-1	
Rock type[a]				
	recommended	measured	recommended	measured
SiO_2[b]	58.79	59.79	49.94	49.65
TiO_2	1.05	0.99	2.71	2.84
Al_2O_3	17.14	16.83	13.8	13.84
Fe_2O_{3T}	6.76	6.71	12.23	12.48
MnO	0.092	0.10	0.168	0.16
MgO	1.53	1.47	7.23	7.30
CaO	4.94	4.62	11.4	10.15
Na_2O	4.26	4.20	2.26	2.41
K_2O	2.91	2.94	0.52	0.50
P_2O_5	0.49		0.273	
LOI				
Cr[c]	10.1		289	293
Ni	16		121	121
Rb	67.3	68.3	11	10.7
Sr	662	672	403	396
Y	20	21.7	27.6	27.0
Zr	227	230	179	175
Nb	15	14.3	19	19.2
Ba	1226	1225	139	130
La	38	37.4	15.8	15.4
Ce	67	69.6	39	39.7
Pr	7.6	8.0	5.7	5.45
Nd	33	32.8	25.2	25.5
Sm	5.9	5.7	6.2	6.0
Eu	1.64	1.77	2.06	1.96
Tb	0.7	0.72	0.96	0.95
Dy	3.6	3.48	5.2	5.24
Ho	0.67	0.65	0.99	1.00
Er	1.7	1.75	2.4	2.38
Tm	0.34	0.32	0.33	0.33
Yb	1.72	1.72	2.02	2.02
Lu	0.27	0.268	0.291	0.292
Ta	0.9	0.83	1.23	1.17
Pb	36	35.2	2.6	2.47
Th	6.5	6.48	1.08	1.13
U	1.92	1.91	0.42	0.44

Table 3.2. Major and trace element compositions (continued)

* Major elements oxides were measured by XRF.

a. AB = Alkalic Basalt; TrB = Transitional Basalt; ThB = Tholeiitic Basalt; An = Andesite; Da = Dacite; TrAn = Trachy-Andesite; Mug = Mugearite; Ben = Benmoreite; Bas = Basanite; P-T = Phonolitic Tephrite.

b. Major elements oxides in wt%. Fe_2O_{3T} is total Fe expressed as Fe^{3+}. Each sample was analyzed in duplicates and reproducibility was better than 5% based on repeated analyses of known rock standards analyzed as unknowns. The accuracy of the standard is within 5% of the suggested values (AGV-1, n = 33; BHVO-1, n =16; *Govindaraju*, 1994), except for TiO_2, MnO, CaO and Na_2O, which are $\leq$10%. Several samples were analyzed through both XRF and ICP-OES to evaluate the major element analytical methods, and the discrepancy is within 4% (CaO < 1%; TiO_2, < 2%; SiO_2, Al_2O_3 and MgO < 3%; Fe_2O_{3T}, MnO, Na_2O, K_2O < 4%).

c. Trace elements in ppm. Each sample was analyzed in duplicates and reproducibility was better than 5% based on repeated analyses of known rock standards analyzed as unknowns. The accuracy of the standard is within 10% of the suggested values (AGV-1, n = 42; BHVO-1, n = 33; *Govindaraju*, 1994), but generally better than ±5% for rare earth elements (REEs).

Table 3.3. Strontium, Nd and Pb isotopic compositions of representative samples on fossil spreading axes off Baja California Sur, Mexico

Location	Sample Name	$^{87}Sr/^{86}Sr$	2σ	$^{143}Nd/^{144}Nd$	2σ
Sara	ROSAD5-1	0.702863	9	0.512894	11
	ROSAD6-10	0.702891	7	0.512990	7
	ROSAD7-1	0.702695	10	0.513004	9
	ROSAD8-1	0.702869	12	0.512973	8
Rosa	ROSAD9-1	0.703045	10	0.512952	10
	ROSAD9-8	0.703059	10	0.512948	7
	ROSAD9-9	0.703059	6	0.512950	9
	ROSAD9-10	0.703046	9	0.512949	6
	ROSAD9-11	0.703053	10	0.512935	14
	ROSAD10-5	0.703150	11	0.512950	9
	ROSAD10-12	0.703180	9	0.512907	8
	ROSAD10-13	0.703199	11	0.512921	7
	PX128-16	0.703536	10	0.512887	5
	PX128-20	0.703164	8	0.512909	8
Rosana	ROSAD11-4	0.702846	10	0.512978	7
	ROSAD11-5	0.702842	10	0.512982	8
	ROSAD11-6	0.702846	10	0.512971	7
Nithya	PX127-18	0.702914	10	0.512999	8
	PX127-19	0.702903	12	0.512911	15
	PX127-20	0.702871	11	0.512996	8

Table 3.3. Strontium, Nd and Pb isotopic compositions (continued)

Location	Sample Name	$^{206}Pb/^{204}Pb$	2σ	$^{207}Pb/^{204}Pb$	2σ	$^{208}Pb/^{204}Pb$	2σ
Sara	ROSAD5-1	18.961	1	15.613	1	38.722	3
	ROSAD6-10	19.354	2	15.585	2	38.702	5
	ROSAD7-1	18.930	2	15.581	1	38.539	3
	ROSAD8-1	19.290	2	15.594	2	38.758	5
Rosa	ROSAD9-1	19.451	1	15.607	1	38.955	2
	ROSAD9-8	19.462	1	15.608	1	39.020	1
	ROSAD9-9	19.453	1	15.602	1	38.939	2
	ROSAD9-10	19.458	1	15.599	1	38.935	2
	ROSAD9-11	19.398	1	15.592	1	38.887	2
	ROSAD10-5	19.531	6	15.575	5	38.890	12
	ROSAD10-12	19.126	3	15.612	2	38.843	6
	ROSAD10-13	19.493	3	15.616	2	38.996	2
	PX128-16	19.279	1	15.587	1	39.048	3
	PX128-20	19.382	2	15.6	1	38.911	6
Rosana	ROSAD11-4	19.171	1	15.557	1	38.551	2
	ROSAD11-5	19.063	1	15.585	1	38.619	1
	ROSAD11-6	19.113	2	15.577	1	38.600	3
Nithya	PX127-18	19.110	1	15.595	1	38.644	2
	PX127-19	18.858	1	15.638	1	38.788	1
	PX127-20	19.285	2	15.564	2	38.560	6

Strontium isotopic ratios were measured through dynamic multi-collection and fractionation corrected to $^{86}Sr/^{88}Sr = 0.1194$. Repeated measurements of NBS 987 yielded $^{87}Sr/^{86}Sr = 0.710256 \pm 0.000017$ (n = 18); 2σ indicates in-run precisions. Neodymium isotopic ratios were measured in oxide form through dynamic multi-collection and fractionation corrected to $^{146}NdO/^{144}NdO = 0.72225$ ($^{146}Nd/^{144}Nd = 0.7219$). Repeated measurements of the La Jolla Nd standard yielded $^{143}Nd/^{144}Nd = 0.511856 \pm 0.000010$ (n = 17). Lead isotopic ratios were measured through static multi-collection and were fractionation corrected using the repeated measurements of NBS SRM 981,(n=22; $^{206}Pb/^{204}Pb = 16.899 \pm 0.007$, $^{207}Pb/^{204}Pb = 15.445 \pm 0.010$, and $^{208}Pb/^{204}Pb = 36.550 \pm 0.026$) relative to those of *Todt et al.* [1996]. Total procedural blanks are negligible: < 10 picograms (pg) for Nd, < 35 pg for Sr, and <74 pg for Pb.

Table 3.4. Helium isotope composition of representative samples on fossil spreading axes off Baja California Sur, Mexico

Location	Sample Name	Weight (g)	^{3}He/^{4}He (R/R$_A$)[a]	X	^{3}He/^{4}He (R$_C$/R$_A$)[a]	[He]$_C$ (10^{-9} cm^3 STP g^{-1})
Rosa	ROSA D9-1	1.1278	1.15	1.06	3.65±0.95	0.26
	ROSA D9-1rep.[b]	0.8310	7.04	43.06	7.18±0.21	1.5
	ROSA D9-8	1.4283	1.54	3.44	1.76±0.16	1.6
	ROSA D9-9	0.7549	5.56	43.42	5.67±0.18	3.7
	ROSA D9-10	1.4548	1.39	1.28	2.78±0.30	0.56
	ROSA D9-11	0.6569	2.32	2.99	2.98±0.20	1.6
Nithya	PX 127D-20[c]	0.9658	1.23	11.94	1.25±0.04	23.4

[a] Measured ^{3}He/^{4}He (R) ratios are corrected for the addition of atmospheric helium to air-corrected values (R$_C$), and are reported normalized to R$_A$ which is the air ^{3}He/^{4}He value (1.4×10^{-6}): X (column 5) is the measured air-normalized He/Ne ratio. Measured helium concentrations are also corrected for the effects of atmospheric He to air-corrected values [He]$_C$, (column 7). The correction details are reported by *Hilton* (1996).

[b] Repeat analysis.

[c] Clinopyoxene separate. All other samples are glasses.

References

Abedini, A. A., S. Hurwitz, and W.C. Evans (2006), USGS-NoGaDat - A global dataset of noble gas concentrations and their isotopic ratios in volcanic systems, *USGS Digital Data Ser., 202*, http://pubs.usgs.gov/ds/2006/202/, U.S. Geol. Surv., Reston, Va.

Asimow, P. D., and M. S. Ghiorso (1998), Algorithmic modifications extending MELTS to calculate subsolidus phase relations, *Am. Mineral.*, *83*, 127-121.

Batiza, R., and D. Vanko (1984), Petrology of Young Pacific Seamounts, *J. Geophys. Res.*, *89*(B13), 11235-11260, doi:10.1029/JB089iB13p11235.

Batiza, R., and D. Vanko (1985), Petrologic evolution of large failed rifts in the eastern Pacific: petrology of volcanic and plutonic rocks from the Mathematician Ridge area and the Guadalupe Trough, *J. Petrol.*, *26*, 564-602.

Batiza, R., R. Oestrike, and K. Futa (1982), Chemical and isotopic diversity in basalts dredged from the East Pacific Rise at 10°S, the fossil Galapagos Rise and the Nazca plate, *Mar. Geol.*,*49*, 115-132, doi:10.1016/0025-3227(82)90032-9.

Bohrson, W. A., and M. R. Reid (1995), Petrogenesis of alkaline basalts from Socorro Island, Mexico; trace element evidence for contamination of ocean island basalt in the shallow ocean crust, *J. Geophys. Res.*, *100*(B12), 24,555-24,576, doi:10.1029/95JB01483.

Bohrson, W. A., and M. R. Reid (1997), Genesis of silicic peralkaline volcanic rocks in an ocean island setting by crustal melting and open-system processes: Socorro Island, Mexico, *J. Petrol.*, *38*, 1137-1166, doi:10.1093/petrology/38.9.1137.

Bohrson, W. A., and M. R. Reid (1998), Genesis of evolved ocean island magmas by deep- and shallow-level basement recycling, Socorro Island, Mexico: constraints from Th and other isotope signatures, *J. Petrol.*, *39*, 995-1008, doi:10.1093/petrology/39.5.995.

Castillo, P. R., D. A. Clague, A. S. Davis, and P. F. Lonsdale (2010), Petrogenesis of Davidson Seamount lavas and its implications for fossil spreading center and intraplate magmatism in the eastern Pacific, *Geochem. Geophys. Geosyst.*, *11*, Q02005, doi:10.1029/2009GC002992.

Chase, T. E., S. M. Smith, and P. Wilde (1968), Western extensions of the Clarion and Molokai fracture zones of the Pacific Ocean, *Spec. Pap. Geol. Soc. Am., 101,* 38.

Chayes, F. (1963), Relative abundance of intermediate members of the oceanic basalt–trachyte association, *J. Geophys. Res., 68*, 519–1534, doi:10.1029/JZ068i005p01519.

Chayes, F. (1977), The oceanic basalt–trachyte relation in general and in the Canary Island, *American Mineralogist*, *62*, 666–671.

Choe, W. H., J. I. Lee, M. J. Lee, S. D. Hur, and Y. K. Jin (2007), Origin of E-MORB in a fossil spreading center: the Antarctic-Phoenix Ridge, Drake Passage, Antarctica, *Geosci. J., 11*, 185-199,doi:10.1007/BF02913932.

Choi, S. H., W. H. Choe, and J. I. Lee (2008), Mantle heterogeneity beneath the Antarctic-Phoenix Ridge off Antarctic Peninsula, *Isl. Arc*, *17*, 172-782, doi:10.1111/j.1440-1738.2007.00609.x.

Clague, D. A., J. B. Paduan, R. A. Duncan, J. J. Huard, A. S. Davis, P. R. Castillo, P. Lonsdale, and A. DeVogelaere (2009), Five million years of compositionally diverse, episodic volcanism: Construction of Davidson Seamount atop an abandoned spreading center, *Geochem. Geophys. Geosyst.*, *10*, Q12009, doi:10.1029/2009GC002665.

Class, C., and S. Goldstein (2005), Evolution of helium isotopes in the Earth's mantle, *Nature*, *436*, 1107–1112, doi:10.1038/nature03930.

Dasgupta, R., M. M. Hirschmann, and N. D. Smith (2007), Partial melting experiments of peridotite + CO_2 at 3 GPa and genesis of alkalic ocean island basalts, *J. Petrol.*, 48, 2093–2124, doi:10.1093/petrology/egm053.

Davis, A. S., S. H. Gunn, W. A. Bohrson, L.-B. Gray, and J. R. Hei (1995), Chemically diverse, sporadic volcanism at seamounts offshore southern and Baja California, *Geol. Soc. Am. Bull.*, *107*, 554–570, doi:10.1130/0016-7606(1995)107<0554:CDSVAS>2.3.CO;2.

Davis, A. S., D. A. Clague, W. A. Bohrson, G. B. Dalrymple, and H. G. Greene (2002), Seamounts at the continental margin of California: A different kind of oceanic intraplate volcanism, *Geol. Soc. Am. Bull.*, *114*, 316-333, doi:10.1130/00167606(2002)1 14<0316:SAT-CMO>2.0.CO;2.

Davis, A. S., D. A. Clague, and J, B. Paduan (2007), Diverse origins of xenoliths from seamounts at the continental margin, offshore central California, *J. Petrol.*, *48*, 829-852, doi:10.1093/petrology/egm003.

Davis, A. S., D. A. Clague, J. B. Paduan, B. L. Cousens, and J. Huard (2010), Origin of volcanic seamounts at the continental margin of California related to changes in plate margins, *Geochem. Geophys. Geosyst.*, *11(5)*, Q05006, doi:10.1029/2010GC003064.

DeMets, C., and S. Traylen (2000), Motion of the Rivera plate since 10 Ma relative to the Pacific and North American plates and the mantle, *Tectonophysics*, 318, 119-159, doi:10.1016/S0040-1951(99)00309-1.

Eakins, B. W., and P. F. Lonsdale (2003), Structural patterns and tectonic history of the Bauer microplate, Eastern Tropical Pacific, *Mar. Geophys. Res.*, *24*, 171-205, doi: 10.1007/s11001-004-5882-4.

Eiler, J. M., K. A. Farley, J. W. Valley, E. Hauri, H. Craig, S. R. Hart and E. M. Stolper (1997), Oxygen isotope variations in ocean island basalt phenocrysts, *Geochim. Cosmochim. Acta*, 61, 2281-2293, doi:10.1016/S0016-7037(97)00075-6.

Emery, K. O., and R. H. Tschudy (1941), Transportation of rock by kelp, *Geol. Soc. Am. Bull.*, *52*, 855-862.

Engel, A. E. J., C. G. Engel and R. G. Havens (1971), Mafic and ultramafic rocks, in *The Sea*, vol. 4, part 1, edited by A. E. Maxwell, pp. 465-420, Wiley-Interscience, New York.

Foulger, G. R. (2007), The "plate" model for the genesis of melting anomalies, *Spec. Pap. Geol. Soc. Am.*, *430*, 1-28, doi:10.1130/2007.2430(01).

Ghiorso, M. S., and R. O. Sack (1995), Chemical mass transfer in magmatic processes. IV. A revised and internally consistent thermodynamic model for the interpolation and extrapolation of liquid-solid equilibria in magmatic systems at elevated temperatures and pressures, *Contri. Mineral. Petrol.*, *119*, 197-212, doi: 10.1007/BF00307281.

Graham, D. W. (2002), Noble gas isotope geochemistry of mid-ocean ridge and ocean island basalts: Characterization of mantle source reservoirs, *Rev. Mineral. Geochem.*, *47*, 247–315, doi:10.2138/rmg.2002.47.8.

Graham, D. W., W. J. Jenkins, M. D. Kurz, and R. Batiza (1987), Helium isotope disequilibrium and geochronology of glassy submarine basalts, *Nature*, 326, 384–386, doi:10.1038/326384a0.

Graham, D. W., A. Zindler, M. D. Kurz, W. J. Jenkins, and R. Batiza (1988), He, Pb, Sr and Nd isotope constraints on magma genesis and mantle heterogeneity beneath young Pacific seamounts, *Contrib. Mineral. Petrol.*, *99*(4), 446–463, doi:10.1007/BF00371936.

Govindaraju, K. (1994), 1994 compilation of working values and descriptions for 383 geostandards, *Geostand. Newsl.*, *18*, 1–158.

Haase, K. M., and N. A. Stroncik (2002), Volcanism on the fossil Galapagos Rise spreading center, SE Pacific, *Eos Trans. AGU*, *83*(47) Fall Meeting Suppl., Abstract V52A-1278.

Hahm, D., P. R. Castillo and D. R. Hilton (2009), A deep mantle source for high ^{3}He/^{4}He ocean island basalts (OIB) inferred from Pacific near-ridge seamount lavas, *Geophys. Res. Lett.*, *36*, L20316, doi:10.1029/2009GL040560.

Hanyu , T., I. Kaneoka, and K. Nagao (1999), Noble gas study of HIMU and EM ocean island basalts in the Polynesian region, *Geochim. Cosmochim. Acta*, 63, 1181-1201, doi:10.1016/S0016-7037(99)00044-7.

Hart, S. R. (1984), A large-scale isotope anomaly in the Southern Hemisphere mantle, *Nature*, *309*, 753–757, doi:10.1038/309753a0.

Hilton, D. R. (1996), The helium and carbon isotope systematics of a continental geothermal system: results from monitoring studies at Long Valley caldera (California, USA), *Chem. Geol.*, *127*, 269-295, doi:10.1016/0009-2541(95)00134-4.

Hilton, D. R., C. G. Macpherson, and T. R. Elliott (2000), Helium isotope ratios in mafic phenocrysts and geothermal fluids from La Palma, the Canary Islands (Spain): implications for HIMU mantle sources, *Geochim. Cosmochim. Acta*, *64*, 2119-2332, doi:10.1016/S0016-7037(00)00358-6.

Hofmann, A. W. (2003), Sampling mantle heterogeneity through oceanic basalts: isotopes and trace elements, *Treatise Geochem.*, *2*, 1-44, doi:10.1016/B0-08-043751-6/02123-X.

Janney, P. E. (1996), Geochemistry of basalts from the Western Pacific Ocean: Local and regional effects of the widespread Cretaceous volcanic vent, Ph.D. dissertation, Univ. of Calif., San Diego.

Janney, P. E., and P. R. Castillo (1996), Basalts from the Central Pacific Basin: evidence for the origin of Cretaceous igneous complexes in the Jurassic Western Pacific, *J. Geophys. Res.*, *101*, 2875-2893, doi:10.1029/95JB03119.

Janney, P. E., and P. R. Castillo (1997), Geochemistry of Mesozoic Pacific mid-ocean ridge basalt: Constraints on melt generation and the evolution of the Pacific upper mantle, *J. Geophys. Res.*, *102*(B3), 5207-5229, doi:10.1029/96JB03810.

Konter, J., H. Staudigel, J. Blichert-Toft, B. B. Hanan, M. Polve, G. R. Davies, N. Shimizu, and P. Schiffman (2009), Geochemical stages at Jasper Seamount and the origin of intraplate volcanoes, *Geochem. Geophys. Geosyst.*, *10*, Q02001, doi:10.1029/2008GC002236.

Langmuir, C. H., E. M. Klein, and T. Plank (1992), Petrological systematics of mid-ocean ridge basalts: Constraints on melt generation beneath ocean ridges, in *Mantle Flow and Melt Generation at Mid-Ocean Ridges, Geophys. Monogr. Ser.*, *71*, edited by J. P. Morgan, D. K. Blackman, and J. M. Sinton, 183–280, AGU, Washington, D. C.

Lonsdale, P. (1985), Nontransform offsets of the Pacific-Cocos plate boundary and their traces on the rise flank, *Geo. Soc. Am. Bull.*, *96*, 313-327, doi: 10.1130/0016-7606(1985)96<313:NOOTPP>2.0.CO;2.

Lonsdale, P. (1991), Structural patterns of the Pacific floor offshore of peninsular California, in *The Gulf and Peninsular Province of the Californias*, edited by J. P. Dauphin and B. R. Simoneit, *AAPG Mem.*, *47*, 87–125.

Lonsdale, P. (1995), Segmentation and disruption of the East Pacific Rise in the mouth of the Gulf of California, *Mar. Geophys. Res.*, *17*, 323-359, doi:10.1007/BF012 27039.

Mammerickx, J., and K. D. Klitgord (1982), Northern East Pacific Rise: Evolution from 25 m.y. to the present, *J. Geophys. Res.*, *87*, 6751-6759, doi:10.1029/JB087iB08 p06751.

McClelland, L., E, Venzke and J. Goldberg (1993), Socorro (Mexico) vesicular lava eruption from underwater vent 3 km W of the island, *Smithson. Inst. Bull. Global Volcan. Network*, *18*, 9-11.

Meibom, A., and D. L. Anderson (2004), The statistical upper mantle assemblage, *Earth Planet. Sci. Lett.*, *217*, 123–139, doi:10.1016/S0012-821X(03)00573-9.

Michaud, F., J. Y. Royer, J. Bourgois, J. Dyment, T. Calmus, W. Bandy, M. Sosson, C. Mortera-Gutiérrez, B. Sichler, M. Rebolledo-Viera, and B. Pontoise (2006), Ocean-ridge subduction vs. slab break off: Plate tectonic evolution along the Baja California Sur continental margin since 15 Ma, *Geology*, *34*, 13-16, doi:10.1130/g22050.1.

Moore, J. G. (1970), Submarine basalt from the Revillagigedo Island region, Mexico, *Mar. Geol.*, *9*, 331-345, doi:10.1016/0025-3227(70)90022-8.

Morgan, W. J. (1971), Convection plumes in the lower mantle, *Nature*, *230*(5288), 42-43, doi:10.1038/230042a0.

Morgan, W. J. (1972), Deep Mantle Convection Plumes and Plate Motions, *Am. Assoc. Pet. Geol. Bull.*, *56*(2), 203-213, doi: 10.1306/819A3E50-16C5-11D7-8645000102C1

865D.

Murray, R. W., D. J. Miller and K. A. Kryc (2000), Analysis of major and trace elements in rocks, sediments, and interstitial waters by Inductively Coupled Plasma-Atomic Emission Spectrometry (ICP-AES) (online), *Tech. Note 29*, Ocean Drill. Program, College Station, Tex. (Available at http://www-odp.tamu.edu /publications /tnotes/tn29/INDEX.HTM).

Natland, J. H, and E. L. Winterer (2005), Fissure control on volcanic action in the Pacific, in *Plates, plumes, and paradigms, Geol. Soc. Spec. Pub.*, vol. 388, edited by G. R. Foulger et al., pp. 687-710, GSA, Boulder, Colorado, doi:10.1130/2005.2388(39).

Nelson, K. D. (1981), A simple thermal-mechanical model for mid-ocean ridge topographic variation, *Geophys. J. Roy. Astron. Soc.,65*, 19-30, doi: 10.1111/j.1365-246X.1981.tb02698.x.

Niu Y., and R. Hékinian (1997), Spreading-rate dependence of the extent of mantle melting beneath ocean ridges, *Nature*, *385*, 326–329, doi:10.1038/385326a0.

Niu, Y., M. Regelous, I. J. Wendt, R. Batiza, and M. J. O’Hara (2002), Geochemistry of near-EPR seamounts: importance of source vs. process and the origin of enriched mantle component, *Earth Planet. Sci. Lett.*, *199*(3-4), 327-345, doi:10.1016/S0012-821X(02)00591-5.

Niu, Y. L., and M. J. O’Hara (2008), Global correlations of ocean ridge basalt chemistry with axial depth: A new perspective, *J. Petrol.*, *49*, 633–664, doi:10.1093/ petrology/egm051.

Pilet, S., M. B. Baker, and E. M. Stolper (2008), Metasomatized lithosphere and the origin of alkaline lavas, *Science*, *320*, 916–919, doi:10.1126/science.1156563.

Richards, A. F. (1958), Petrographic notes on two Eastern Pacific Ocean islands, *Geol. Soc. Am. Bull.*, *62*, 1634.

Richards, A. F. (1959), Geology of the Islas Revillagigedo, Mexico, 1. Birth and development of Volcan Barcena, Isla San Benedicto, *Bull. Volcan.*, *22*, 75-123.

Richards, A. F. (1966), Geology of the Islas Revillagigedo, Mexico, 2. Geology and petrography of Isla San Benedicto, *Proc. Cal. Aca. Sci.*, *33*, 361-414.

Rubin, K. H., and J. M. Sinton (2007), Inferences on mid-ocean ridge thermal and magmatic structure from MORB compositions, *Earth Planet. Sci. Lett.*, *260*(1-2), 257-276, doi:10.1016/j.epsl.2007.05.035.

Salters, V. J. M., and A. Stracke (2004), Composition of the depleted mantle, *Geochem. Geophys. Geosyst.*, *5*, Q05004, doi:10.1029/2003GC000597.

Schouten, H., K. D. Klitgord, and D. G. Gallo (1993), Edge-driven microplate kinematics, *J. Geophys. Res.*, *98*(B4), 6689-6701, doi:10.1029/92JB02749.

Shaw, A. M., D. R. Hilton, T. P. Fischer, J. A. Walker, and G. A. M. de Leeuw (2006), Helium isotope variations in mineral separates from Costa Rica and Nicaragua: assessing crustal contributions, timescale variations and diffusion-related mechanisms, *Chem. Geol.*, *230*, 124-139, doi:10.1016/j.chemgeo.2005.12.003.

Shibata,T., S. E. DeLong, and P. Lyman (1982), Petrographic and Chemical Characteristics of Abyssal Tholeiites from Deep Sea Drilling Project Leg 63 off Baja California, *Initial Rep. Deep Sea Drill. Proj.*, *63*, 687-699, doi:10.2973/dsdp.proc.63. 125.1981.

Siebe, C., J.-C. Komorowski, C. Navarro, J. McHone, H. Delgado and A. Cortes (1995), Submarine eruption near Socorro Island, Mexico: Geochemistry and scanning electron microscopy studies of floating scoria and reticulite, *J. Volcanol. Geotherm. Res.*, 68, 239–271, doi:10.1016/0377-0273(95)00029-1.

Solidum, R. U. (2002), Geochemistry of volcanic arc lavas in central and southern Philippines: contributions from the subducted slab, Ph.D. dissertation, Univ. of Calif., San Diego.

Stracke, A., A. W. Hofmann, and S. R. Hart (2005), FOZO, HIMU, and the rest of the mantle zoo, *Geochem. Geophys. Geosyst.*, *6*, Q05007, doi: 10.1029/2004GC000824.

Stuart, F. M., S. Lass-Evans, J. G. Fitton and M. E. Robert (2003), High ^{3}He/^{4}He ratios in picritic basalts from Baffin Island and the role of a mixed reservoir in mantle plumes**,** *Nature*, *424*, 57-59, doi:10.1038/nature01711**.**

Sun, S.-S., and W. F. McDonough (1989), Chemical and isotopic systematics of oceanic basalts: Implications for mantle composition and processes, in *Magmatism in the Ocean Basins*, edited by A. D. Saunders and M. K. Norry, *Geol. Soc. Spec. Publ.*, *42*, 313–345.

Todt, W., R. A. Cliff, A. Hanser, and A. W. Hoffman (1996), Evaluation of a ^{202}Pb-^{205}Pb double spike for high-precision lead isotope analysis, in *Earth Processes: Reading the Isotopic Code, Geophys. Monogr. Ser.*, vol. 95, edited by A. Basu and S. Hart, pp. 429–437, AGU, Washington, D. C.

Yoder, H. S. (1973), Contemporaneous basaltic and rhyolitic magmas, *American Mineralogist* , *58*, 153–171.

Zindler, A., H. Staudigel, and R. Batiza (1984), Isotope and trace element geochemistry of young Pacific seamounts: implications for the scale of upper mantle heterogeneity, *Earth Planet. Sci. Lett.*, *70*(2), 175-195, doi:10.1016/0012-821X(84)90004-9.

This chapter, in full, is a reprint of the material as it appears in *Geochemistry, Geophysics, Geosystems*, 2011, by L. Tian, P. R. Castillo, P. F. Lonsdale, D. Hahm, and D. R. Hilton (doi: 10.1029/2010GC003319). The dissertation author was the primary investigator and author of this paper. The co-authors directed, supervised and contributed to the research.

CHAPTER 4

Geochemistry of post-spreading lavas from fossil Mathematician and Galapagos spreading axes, revisited

Abstract

The Mathematician Ridge, located west of the northern end of the East Pacific Rise (EPR) at about 10-20°N, 110°W, was abandoned during the Pliocene when the Pacific plate captured the Mathematician microplate. The Galapagos Rise, located east of the southern segment of the EPR at about 10-18°S, 95°W, stopped spreading after the Late Miocene capture of the Bauer microplate by the Nazca plate. New major and trace element and Sr, Nd and Pb isotope data have been collected from lavas dredged from volcanoes along the crest of Mathematician Ridge and volcanic ridges built along segments of the Galapagos Rise. These lavas consist predominantly of alkalic basalts, similar to the post-spreading alkalic basalts from other fossil spreading axes and riseflank seamounts in the eastern Pacific. Collectively, the alkalic basalts have higher incompatible trace element contents and highly/moderately incompatible trace element ratios (e.g., La/Sm and Nb/Zr) than EPR basalts, similar to average alkalic ocean island basalts (OIB). They also have similar Sr, Nd and Pb isotopic compositions which overlap with geochemically enriched mid-ocean ridge basalts (MORB) and relatively ~depleted OIB from major oceanic volcanic chains such as Galapagos and Hawaii. The new data support the proposal that the geochemically enriched, alkalic lavas from fossil spreading axes in the eastern Pacific are produced by low degree of partial melting of a heterogeneous suboceanic mantle consisting of geochemically enriched components that are embedded in a depleted lherzolite matrix.

Keywords: geochemistry; post-spreading lavas; fossil spreading axes; mantle heterogeneity

4.1. Introduction

It is generally accepted that in response to plate separation at active spreading centers geochemically depleted, tholeiitic mid-ocean ridge basalts (MORB) are produced from passively upwelling and adiabatically decompressing mantle. However, mid-ocean ridge segments could be abandoned due to changes in spreading geometry or reorganization of lithospheric plates [*Batiza*, 1989; *Lonsdale*, 1991]. Studies have shown that after the cessation of spreading, fossil ocean ridges continue to produce lavas which are geochemically enriched and more alkaline than normal-MORB. For example, the volcanically-active Socorro and San Benedicto islands at the northern part of Mathematician Ridge, which became extinct at ~3.5 Ma, consist of an alkaline basalt-trachyte series [*Richards*, 1966; *Bohrson and Reid*, 1995]. Alkalic lava eruption also occurred along several other failed spreading axes in the eastern Pacific, such as in Davidson, Guide, and Rosa seamounts [*Clague et al.*, 2009; *Castillo et al.*, 2010; *Davis et al.*, 2010; *Tian et al.*, 2011]. *Clague et al.* [2009] suggest that Davidson Seamount remained volcanically active for at least ~8 Myr after spreading stopped; the apparently recent flows on Rosa Seamount indicate that it is still volcanically active ~11-12 Myr after the cessation of spreading [*Tian et al.*, 2011]. Alkalic lavas from fossil spreading centers have higher abundances of incompatible elements, higher highly/moderately incompatible trace element ratios and more radiogenic Sr, Nd and Pb isotopic compositions relative to normal-MORB. Lavas from a small seamount located at the axis of a fossil spreading center in Drake Passage in the southern Pacific Ocean, erupted up to 2 Myr after the cessation of spreading, are enriched-MORB [*Choe et al.,* 2007; *Choi et al.*, 2008; *Haase et al.*, 2011]. Samples from several volcanoes along fossil spreading axes off Baja California Sur are tholeiitic to transitional lavas in composition, similar to enriched-MORB [*Tian et al.*, 2011].

The more alkaline and enriched magmas erupted along abandoned spreading axes were proposed to be from low degree melting of a compositionally heterogeneous mantle [*Choe et al.,* 2007; *Choi et al.*, 2008; *Castillo et al.*, 2010; *Haase et al.*, 2010; *Tian et al.* 2011], and melting underneath a dying spreading centre may be due to either buoyancy driven upwelling of the underlying hot and/or enriched mantle or rapid motion of the spreading axis with respect to the underlying asthenosphere [*Castillo et al.*, 2010]. Moreover, the erupted lavas also evolve through time, becoming more alkaline and geochemically enriched with the waning of volcanism [*Castillo et al.*, 2010; *Haase et al.*, 2011; *Tian et al.* 2011].

This chapter presents new and additional major and trace element and Sr, Nd and Pb isotope data for lavas dredged from volcanic outcrops near and along the axes of Mathematician Ridge [*Batiza and Vanko*, 1985] and Galapagos Rise [*Batiza et al.*, 1982]. The main objective of this study is to combine the new data with those for post-spreading lavas from other abandoned spreading axes elsewhere in order to add further constraints on the true nature of the suboceanic mantle in the eastern Pacific and verify whether relatively lower degree of partial melting of such a source can generate the geochemically enriched composition of the melts produced after the cessation of spreading along ocean ridges.

4.2. Geologic setting and previous work

The Mathematician Ridge (Fig. 4.1), located west of the northern end of the East Pacific Rise (EPR) at about 10-20°N, 110°W, was abandoned during the Pliocene when the Pacific plate captured the Mathematician microplate. Bathymetric and magnetic evidences suggest that the abandonment occurred first at ~6.5 Ma at the southern end of the Mathematician Ridge between the Orozco and Clipperton fracture zones and at ~3.5 Ma in the segment north of 15^{o} N [e.g., *Mammerickx and Klitgord*, 1982; *Mammerickx et al.*, 1988]. Four alkaline volcanic islands - Socorro, San Benedicto, Clarion, and Roca Partida are located at the northern terminus of the Mathematician Ridge [e.g., *Richards*, 1959; *McClelland et al.*, 1993; *Bohrson and Reid*, 1995]. This island group, also known as Revillagigedo Archipelago, and the numerous seamounts on the Mathematician Ridge, are proposed to have been formed by post-abandonment volcanic activity [*Batiza and Vanko*, 1985]. Socorro Island, at the intersection of the ridge with the Clarion fracture zone, is the largest in the archipelago and was built by intense activity continuing to the present [e.g., *Siebe et al.*, 1995; *Bohrson and Reid*, 1995, 1997]. Postcaldera mafic volcanism on Socorro Island consists predominantly of alkalic basalt, hawaiite and mugearite and a lesser amount of mildly alkalic-transitional basalt [*Bohrson and Reid*, 1995]. Lavas erupted on San Benedicto Island constitute an alkalic basalt to mugearite and trachyte series [*Richards*, 1966]. Significant volumes of silicic peralkaline volcanic rocks (dominantly peralkaline trachytes and rhyolites) also occur on Socorro and San Benedicto Islands [*Bohrson and Reid*, 1997, 1998].

Samples collected from volcanic ridges along the Mathematician Ridge crest (Fig. 4.1) include vesicular alkalic basalts with large crystals of olivine and plagioclase [*Batiza and Vanko*, 1985], benmoreites [*Richards*, 1958] and trachyandesite [*Moore*, 1970]. Although *Batiza and Vanko* [1985] originally described their sampling of alkalic basalts from abandoned transform faults, subsequent multibeam bathymetry showed them to be from axial volcanoes on failed Mathematician spreading segments [*Tian et al.*, 2011].

The Galapagos Rise (Fig. 4.1) was first identified as inactive by *Menard et al.* [1964]. It is parallel to and older than the EPR between 10-18°S. Bathymetry together with magnetic and satellite altimetry data suggest that the Galapagos Rise axis became extinct at ~6 Ma after the Late Miocene capture of the Bauer microplate by the Nazca plate. *Batiza et al*. [1982] reported sampling tholeiitic lava from the crest of the Galapagos Rise, but they had mislocated the former spreading axis by ~35 km. Geophysical mapping of *Eakins and Lonsdale* [2003] shows the axis of the Galapagos Rise to lie along the 3km-high “elongate seamount” from which *Batiza et al.* [1982] reported alkali-olivine basalt (their dredges 4 and 5). Alkalic basalts from two southern segments of the Galapagos Rise at 10°S, 95°W were also reported by *Haase and Stroncik* [2002].

4.3. Samples and analytical Methods

The samples from the fossil Mathematician Ridge area analyzed in this study were obtained from the volcanoes along the axis of Mathematician Ridge (Dredge 1 and 2), inner rift valley wall (Dredge 7) and two seamounts near the Revillagigedo Archipelago (Dredge 10 and 11) [*Batiza and Vanko*, 1985]. Those from the fossil Galapagos Rise area are from the EPR segment at ~10°S (Dredge 1 and 2), narrow volcanic ridges along the Galapagos Rise (Dredge 4 and 5) and a seamount adjacent to the rise (Dredge 3) [*Batiza et al.*, 1982]. Sample locations are given in Table 4.1.

Major and trace elements and Sr-Nd-Pb isotopes were measured from glass chips from few quenched margins and on rock powders prepared from the fresh cores of individual samples. An estimate of the volatile (e.g., H_2O and CO_2) contents in the rock samples was determined by weighing loss on ignition (LOI) following the procedure described in *Solidum* [2002]. Concentrations of major elements and compatible elements Cr and Ni were determined by inductively-coupled - plasma optical emission spectrometry (ICP-OES); concentrations of trace elements Rb, Sr, Y, Ba, Pb, Th, U, Zr, Nb, and rare-earth elements (REEs) were determined by inductively-coupled - plasma mass spectrometry (ICP-MS). All the analyses were carried out at the Scripps Institution of Oceanography (SIO) Analytical Facility. Some of the whole rock and glass samples were also analyzed for Sr, Nd and Pb isotopes at SIO. To minimize alteration effects on bulk isotope analyses, glasses and leached sample powders were used for Sr isotopic analysis. Analytical procedures used are described in *Tian et al.* [2011].

Details of the analytical accuracy and precision of the isotopic measurements are described in footnotes of the appropriate data tables.

4.4. Results

Table 4.2 presents the major and trace element abundances of samples from the fossil Mathematician Ridge and Galapagos Rise areas, and Table 4.3 presents the Sr, Nd and Pb isotopic values of some of the samples.

4.4.1. Mathematician Ridge area

All lavas sampled from the volcanoes along the axis of Mathematician Ridge are basaltic in composition and include both tholeiitic and alkalic basalts; samples from the inner rift valley wall are tholeiitic basalts; samples from the seamounts near Revillagigedo Archipelago include alkalic basalts and two trachytes (Fig. 4.2). The values of Al_2O_3 and CaO increase whereas that of FeO_T decreases with decreasing MgO in the tholeiitic and alkalic basalts from the axial volcanoes; TiO_2 remains constant but Na_2O and K_2O do not show clear correlations with MgO (Fig. 4.3). The values of TiO_2 and FeO_t increase with decreasing MgO whereas Al_2O_3 and CaO remain ~constant with changing MgO in the alkalic basalts from the seamounts near the archipelago. The tholeiitic basalts from the inner rift valley wall are relatively primitive (MgO = 9.42 to 10.88). Their Al_2O_3 and Na_2O increase and CaO decreases with decreasing MgO; TiO_2 and FeO_t remain constant but CaO and K_2O do not correlate with MgO. In general, the major element characteristics of the alkalic basaltic lavas from the Mathematicians Ridge area generally form continuous major element trends that overlap with those defined by Socorro Island alkalic lava series except for the K_2O contents in the former are higher for given MgO than in the latter.

All samples from the axial volcanoes and two seamounts near the Revillagigedo Archipelago are enriched in highly incompatible relative to moderately incompatible elements (Fig. 4.4), similar to the alkalic lavas from Socorro Island. However, the basaltic samples from the axial volcanoes are more enriched in highly incompatible elements than the alkalic basalt from one of the two seamounts (AMD 11-3). Sample AMD 10-3, a trachyte from the other seamount, has a negative Eu anomaly. All samples display positive spikes in high field strength elements (HFSE), such as Nb and Zr, which is typical in the majority of ocean island basalt (OIB) [*Hofmann*, 2003]. On the other hand, the primitive tholeiitic basalts from the inner rift valley wall are depleted in highly incompatible elements relative to moderately incompatible elements, similar to normal-MORB.

Samples from the axial volcanoes have a limited range of $^{87}Sr/^{86}Sr$ (0.70280 to 0.70293) and $^{143}Nd/^{144}Nd$ ratios (0.51296 to 0.51302; Fig. 4.5). These Sr and Nd isotope values fall within the range of other fossil spreading axes in the eastern Pacific [e.g., *Davis et al.*, 2002; *Castillo et al.*, 2010; *Tian et al.*, 2011] and overlap with the radiogenic, high $^{87}Sr/^{86}Sr$ and low $^{143}Nd/^{144}Nd$ end of the fields for EPR MORB and Pacific riseflank seamounts [e.g., *Zindler et al.*, 1984; *Graham et al.*, 1988; *Niu et al.*, 2002]. The two samples from the seamounts near the archipelago have higher $^{87}Sr/^{86}Sr$ but lower $^{143}Nd/^{144}Nd$ ratios than the axial volcanoes, with sample AMD 11-3 plotting within the field of basaltic rocks from Socorro Island [e.g., *Bohrson and Reid*, 1995; 1997]. Only one of the three samples from the inner rift valley wall overlaps with depleted EPR MORB or riseflank seamounts. The other two have high $^{87}Sr/^{86}Sr$ for given $^{143}Nd/^{144}Nd$ ratios; it appears that the Sr isotopic ratios of these two samples still bear the effect of seawater alteration despite acid-leaching their powders prior to dissolution.

The Pb isotopes of the samples from the axial volcanoes are relatively radiogenic and span a moderate range of values (e.g., $^{206}Pb/^{204}Pb$ = 19.253 to 19.796). Consistent with their Sr and Nd isotopes, their Pb isotopes overlap with available isotope data for other fossil spreading axes. However they are generally more radiogenic than riseflank seamounts and basaltic rocks from Socorro Island (Fig. 4.5). Moreover, their Pb isotopic composition also overlaps with OIB from the Galapagos linear volcanoes, but is more radiogenic than those from Hawaii. Samples from the two seamounts near the archipelago have higher $^{207}Pb/^{204}Pb$ and $^{208}Pb/^{204}Pb$ values than those from axial volcanoes at comparable $^{206}Pb/^{204}Pb$. Consistent with their Sr and Nd isotopes, only one of the tholeiitic samples from the inner rift valley wall plot within the field for depleted EPR MORB. The other two samples have higher $^{207}Pb/^{204}Pb$ and $^{208}Pb/^{204}Pb$ for given $^{206}Pb/^{204}Pb$ values relative to depleted EPR MORB, again possibly due to seawater alteration.

4.4.2. Galapagos Rise area

Samples from the volcanic ridges along the Galapagos Rise are mainly alkalic basalts and a lesser amount of tholeiitic to transitional basalts; samples from the adjacent seamount are tholeiitic basalts; samples from the EPR segments are tholeiitic to transitional basalts and one alkalic basalt (Fig. 4.2). Basaltic lavas from the

Galapagos Rise display large variation in MgO (4.2 to 18.4 wt %). However, the group with high MgO contents contains a few olivine megacrysts and, thus, may have suffered olivine accumulation. In general, their values of TiO_2, Al_2O_3, CaO, Na_2O, and K_2O increase whereas that of FeO_t decreases with decreasing MgO (Fig. 4.3). They have higher TiO_2, Al_2O_3, Na_2O, and K_2O values at comparable MgO than samples from the adjacent seamount and EPR segments.

Lavas from the volcanic ridges are enriched in highly incompatible relative to moderately incompatible elements and have positive spikes in Nb and Zr (Fig. 4.4). They show similar trace element distribution patterns as average OIB. Samples from the adjacent seamount, however, are depleted in highly incompatible relative to moderately incompatible elements, similar to normal-MORB. The basaltic samples from the EPR segments also display small positive spikes in Nb and Zr, but are only slightly enriched in highly incompatible relative to moderately incompatible elements, similar to enriched-MORB.

The Sr and Nd isotope values of samples from the volcanic ridges overlap with those of lavas from other fossil spreading axes in the eastern Pacific [e.g., *Davis et al.*, 2002; *Castillo et al.*, 2010; *Tian et al.*, 2011] and OIB from the Galapagos linear volcanoes (Fig. 4.5). Their Pb isotopic compositions overlap with the depleted end of other fossil spreading axes, which collectively overlap with enriched EPR MORB and riseflank seamounts as well as with OIBs from Hawaii and Galapagos linear volcanoes. The Sr, Nd and Pb isotopes of two of the three samples from the adjacent seamount plot within the depleted EPR MORB field, consistent with their depleted incompatible element compositions. The other sample, similar to the altered samples from the inner rift valley wall in the Mathematician Ridge area, has high $^{87}Sr/^{86}Sr$ for a given $^{143}Nd/^{144}Nd$ ratio than EPR MORB and, thus, is also most probably altered. However, the Pb isotopes of the adjacent seamount samples all plot within the fields of depleted EPR MORB and riseflank seamounts. The lone sample from the EPR segment analyzed for isotopes plots within the fields for enriched EPR MORB and riseflank seamounts, similar to the volcanic ridge samples.

4.5. Discussion

4.5.1. Formation of magmas at the fossil spreading axes

The majority of basaltic lavas from the Mathematician Ridge and Galapagos Rise are alkalic in composition, having higher abundances of incompatible trace elements and highly/moderately incompatible trace element ratios relative to tholeiitic MORB (Fig. 4.6). They resemble alkalic lavas from other fossil spreading axes in the eastern Pacific. Moreover, these alkalic lavas have similar Sr, Nd and Pb isotopic compositions (Fig. 4.5) that overlap with the radiogenic end of EPR MORB and riseflank seamounts and invariably with the depleted isotopic signature of OIB from Hawaii and Galapagos linear volcanoes.

Normal-MORB-like tholeiitic basalts are present only in the inner rift valley wall of the Mathematician Ridge and in the seamount adjacent to the Galapagos Rise. Relatively smaller volumes of transitional and tholeiitic basalts are also found in Socorro Island, the northern rift zone of San Benedicto Island [*Bohrson and Reid,* 1995], a small volcano near the fossil spreading axis-transform intersection south of Davidson Seamount [*Castillo et al.*, 2010], and several volcanic ridges built along fossil spreading axes off Baja California Sur [*Tian et al.*, 2011]. Collectively, the new geochemical data, similar to those for post-spreading lavas from other fossil spreading axes, define a compositional continuum ranging from normal-MORB-like to OIB-like, which in turn is similar to the composition of lavas from riseflank seamounts in the eastern Pacific [*Castillo et al.*, 2010; *Tian et al.*, 2011].

Tian et al. [2011 - Chapter 3] and *Castillo et al.* [2010] proposed that the composition of risecrest lavas generally evolves from tholeiitic normal-MORB while the seafloor is actively spreading to enriched-MORB and, eventually, to alkalic basalts similar to OIB and their differentiates after spreading has stopped. The observed compositional evolution requires a compositionally heterogeneous suboceanic mantle in the eastern Pacific, consisting of enriched mantle components embedded in a depleted lherzolitic matrix. At active spreading centers, the compositionally heterogeneous mantle rises in response to plate separation, decompresses adiabatically, and begins melting to produce voluminous tholeiitic MORB. When spreading slows to a stop at dying risecrests, the amount of upwelling mantle also diminishes, resulting in a smaller degree of decompression partial melting. The lower degree of partial melting of the heterogeneous mantle forms relatively incompatible element-enriched melts. The proposal that lower degree of partial melting of a heterogeneous mantle creates temporal evolution of fossil spreading axes from normal-MORB to alkalic OIB-like basalts is highly consistent with the observed positive correlation between geochemical enrichment (e.g., increasing La/Sm values) and decreasing age of lavas erupted on the fossil Phoenix Ridge in the southern Pacific Ocean [*Haase et al.*, 2011].

The driving mechanism for continued magma generation at increasingly smaller degrees of partial melting at extinct spreading ridges, however, is not certain. *Castillo et al.* [2010] propose two such mechanisms. Melting underneath a dying spreading centre may result from buoyancy-driven upwelling of hot lithospheric and asthenospheric mantle material. Specifically, easily fusible and incompatible element-enriched portions will begin to melt relatively deep and the melt produced causes active upwelling due to mantle depletion and/or melt buoyancy [e.g., *Sotin and Parmentier,* 1989; *Jha et al.*, 1994; *Raddick et al.*, 2002]. Alternatively, continued magmatism at fossil spreading centers may result from rapid motion of the abandoned spreading axes thickening over a fertile mantle relative to the underlying asthenosphere. Interestingly, *Haase et al.* [2011] observed a correlation between height of post-spreading volcanoes and final spreading rate of the spreading center. To explain such a correlation, they suggest that faster spreading rates immediately prior to cessation of spreading generate more residual upwelling, which led to higher degrees of partial melting, and hence, more voluminous magmatism. Post-spreading magmatism will terminate either when the melting of the enriched components and resultant residual upwelling stop, or when the increase in lithospheric thickness due to cooling prevents further melting [*Castillo et al.*, 2010].

4.5.2. Nature of the mantle source

As noted above, intraplate fossil spreading center lavas in the eastern Pacific come from a heterogeneous mantle source. The enriched components in such a source lithologically could be pyroxenites [e.g., *Hirschmann et al.*, 2003] or amphibole-rich or carbonatite-metasomatized peridotites [*Keshav et al.*, 2004] that have lower solidi than and are randomly distributed in the form of veins, plums, and layers in the enclosing lherzolite matrix. The origin of these components is uncertain, but one of the proposed sources is subducted crustal material stored in the upper mantle [e.g., *Meibom and Anderson*, 2004]. Alternatively, *Castillo et al.* [2010] propose that the most likely process to generate these enriched components is through metasomatic infiltration of carbonatitic fluids [*Hirose*, 1997] or low-degree melts generated at low degrees of partial melting of mantle rocks [*Niu et al.*, 2002; *Niu and O'Hara*, 2008] at the base of the lithosphere.

The compositional spectrum of intraplate lavas including those from fossil spreading centers and riseflank seamounts is represented by their roughly linear arrays in the plots between incompatible trace element ratio versus incompatible trace element and radiogenic isotope ratios (Fig. 4.7). To a first order, the spectrum of data is bounded by two components: one component is geochemically depleted (high ^{143}Nd/^{144}Nd but low ^{87}Sr/^{86}Sr, ^{206}Pb/^{204}Pb, Nb/Zr, and La/Sm ratios) whereas the other is geochemically enriched (low ^{143}Nd/^{144}Nd but high ^{87}Sr/^{86}Sr, ^{206}Pb/^{204}Pb, Nb/Zr, and La/Sm ratios). The compositional range from normal-MORB-like to OIB-like of intraplate lavas in the eastern Pacific results from mixing of sources or melts from these two end-components through varying degrees of partial melting [*Castillo et al.*, 2010; *Tian et al.*, 2011]. During large degree of partial melting beneath active spreading centers or near-axis seamount volcanoes, both components are fused, but the enriched signature in the resultant melt is buffered/diluted by the depleted signature during melt aggregation and mixing within crustal magma chambers and hence, depleted, normal-MORB-like tholeiitic melts are produced. When spreading slows down and/or even after it has ceased but mantle upwelling still occurs at a diminishing rate, or beneath seamounts far from the axial mantle upwelling zone, progressive sampling of the enriched, easily meltable components in the heterogeneous suboceanic mantle is favored at the expense of the depleted lherzolitic matrix, producing enriched-MORB-like and even OIB-like alkalic lavas.

As in *Tian et al.* [2011], the range of compositions of lavas from the Mathematician Ridge and Galapagos Rise, along with those from other fossil spreading axes and riseflank seamounts in the eastern Pacific, by decreasing degree of partial melting of a heterogeneous upper mantle is modeled using Rb/Sr versus $^{87}Sr/^{86}Sr$ and La/Sm versus $^{143}Nd/^{144}Nd$ diagrams (Fig. 4.8). For simplicity, mixing of melts is assumed in the model although actual mixing of sources prior to melting is also a possibility. The depleted MORB mantle (DMM) and an enriched mantle component (EC) are chosen as the putative two end-member sources for the primary magmas of these volcanoes. The composition of DMM is obtained from that of the average depleted- (D-)MORB in *Salters and Stracke* [2004]. The composition of EC is not well defined except that it must be more enriched than our basaltic samples (e.g., $^{87}Sr/^{86}Sr > 0.703093$ and $^{143}Nd/^{144}Nd < 0.513024$; Fig. 4.5 and Table 4.3); here its composition is back-calculated from a geochemically enriched lava from the nearby Flint (off-axis) seamount [*Davis et al.* 1995; *Konter et al.*, 2009]. The lithology of the EC is assumed to be an amphibole-rich lherzolite [*Pilet et al.*, 2008]. To avoid significant effects of fractional crystallization, only primitive basalts are used in the model calculations.

Changes in Rb/Sr and La/Sm ratios (sub-horizontal solid curves) represent mixing lines between variable degrees of partial melt (0.05% to 2%) from DMM and 10% melt from EC. On the other hand, changes in $^{87}Sr/^{86}Sr$ and $^{143}Nd/^{144}Nd$ ratios (sub-vertical dash curves) represent changes in the proportions of the two sources for a given mixture. The alkalic basalts from Mathematician Ridge and fossil Galapagos Rise are generally overlapping with those from Davidson Seamount and volcanic ridges built on the fossil spreading axes off Baja California Sur, and contain a low amount of low-degree partial melt from DMM. In contrast, the tholeiitic basalts from the inner rift valley wall of Mathematician Ridge are overlapping with the field of EPR MORB, and contain more higher-degree partial melt from DMM. In other words, the geochemically enriched, alkalic, post-spreading lavas from Mathematician Ridge and Galapagos Rise produced by smaller degree of partial melting contain lesser amount of DMM melt, but larger proportion of enriched component melt, than the geochemically depleted, tholeiitic lavas produced when spreading was still active. It should be also noted that the alkalic basalts from Mathematician Ridge and Galapagos Rise lavas are less enriched compared to those from Davidson Seamount and volcanic ridges built along fossil spreading axes off Baja California Sur, and in fact generally overlapping with those tholeiitic and transitional lavas. Moreover, a few alkalic basalts from Socorro Island do not lie within the modeled mixing fields. These indicate that the entire compositional spectrum of intraplate lavas cannot be simply produced by mixing a depleted end-component with a single or homogenous enriched end-component in the upper mantle beneath the eastern Pacific. The enriched components are also quite heterogeneous.

4.6. Conclusions

New major and trace element and Sr, Nd and Pb isotope data have been collected from lavas dredged from fossil Mathematician Ridge and Galapagos Rise areas.

Lavas from volcanoes along the crest of Mathematician Ridge and volcanic ridges along the Galapagos Rise consist predominantly of alkalic basalts that are similar to the post-spreading alkalic basalts from other fossil spreading axes and riseflank seamounts in the eastern Pacific. Samples from the Mathematician Ridge area also include tholeiites from the inner rift valley wall and alkalic basalts and trachytes from a seamount near Revillagigedo Archipelago whereas those from the Galapagos Rise area also include tholeiitic basalts from an adjacent seamount and tholeiitic to transitional basalts from the nearby EPR segment.

Similar to alkalic lavas from other fossil spreading axes in the eastern Pacific, the alkalic basalts from Mathematician Ridge and Galapagos Rise have higher incompatible trace element contents and highly/moderately incompatible trace element ratios than EPR basalts, similar to alkalic riseflank seamount lavas and average alkalic OIB. They also have similar Sr, Nd and Pb isotopic compositions that overlap with enriched-MORB, riseflank seamount lavas, and depleted OIB from major linear volcanic chains such as Galapagos and Hawaii. Collectively, lavas from fossil spreading axes, similar to those from Pacific riseflank seamounts, constitute a compositional continuum ranging from MORB-like to OIB-like.

The new data from Mathematician Ridge and Galapagos Rise further illustrate that the geochemically enriched, alkalic lavas from fossil spreading axes in the eastern Pacific are produced by low degree of partial melting of a heterogeneous suboceanic mantle, which consists of enriched components embedded in a lherzolite matrix.

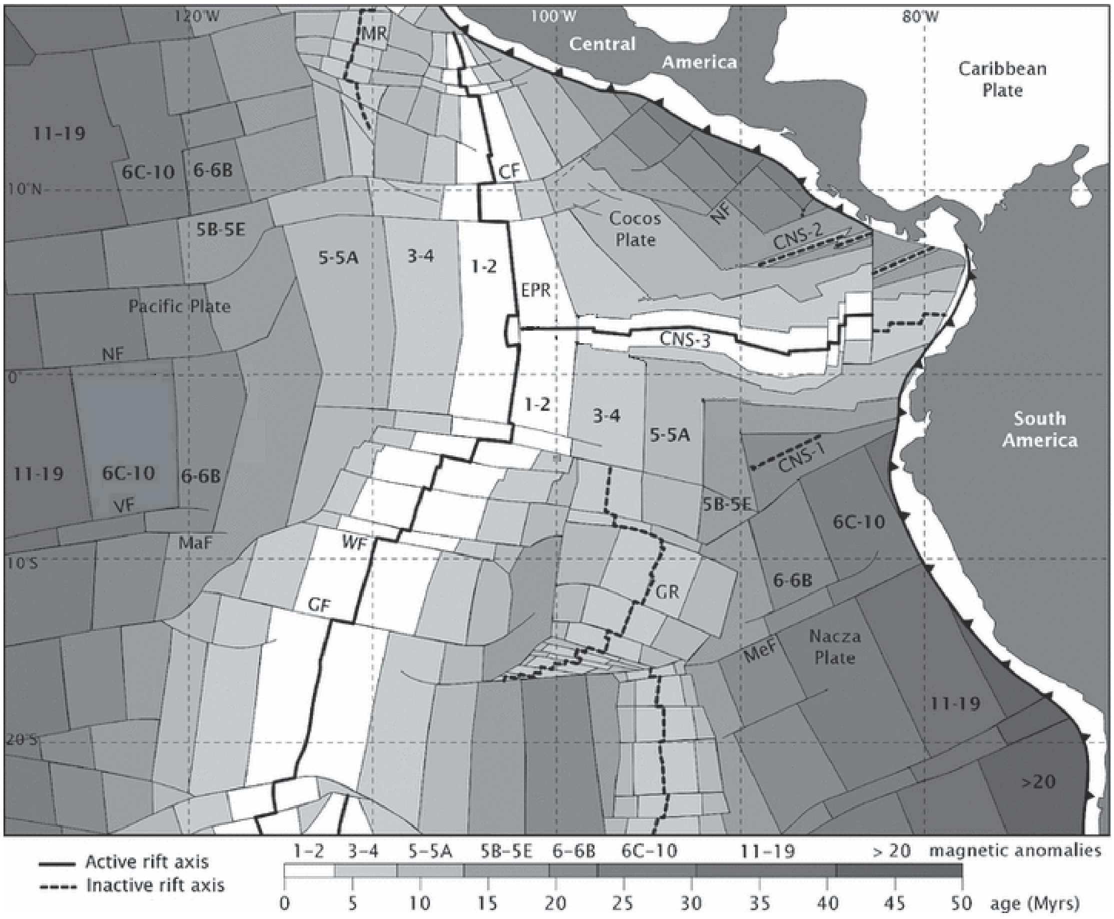
120°W
100°W
80°W
MR
Central America
Caribbean Plate
11-19
6C-10
6-6B
10°N
CF
5B-5E
Cocos Plate
NF
CNS-2
5-5A
3-4
1-2
EPR
Pacific Plate
NF
CNS-3
0°
1-2
3-4
5-5A
South America
CNS-1
11-19
6C-10
6-6B
VF
5B-5E
6C-10
MaF
WF
10°S
GR
6-6B
GF
MeF
Nacza Plate
11-19
20°S
>20
Active rift axis
Inactive rift axis
1-2
3-4
5-5A
5B-5E
6-6B
6C-10
11-19
> 20
magnetic anomalies
0
5
10
15
20
25
30
35
40
45
50
age (Myrs)

Figure 4.1. Simplified map showing the location of fossil Mathematician Ridge and Galapagos Rise and age of the surrounding oceanic crust (modified from *Meschede et al.*, 2008). CF, Clipperton Fault Zone; CNS, Cocos-Nazca Spreading Center; EPR, East Pacific Rise; GF, Garrett Fault Zone; GR, Galapagos Rise; MR, Mathematician Ridge; MaF, Marquesas Fault Zone; MeF, Mendana Fault Zone; NF, Nicaragua Fault Zone; VF, Viru Fault Zone; WF, Wilkes Fault Zone.

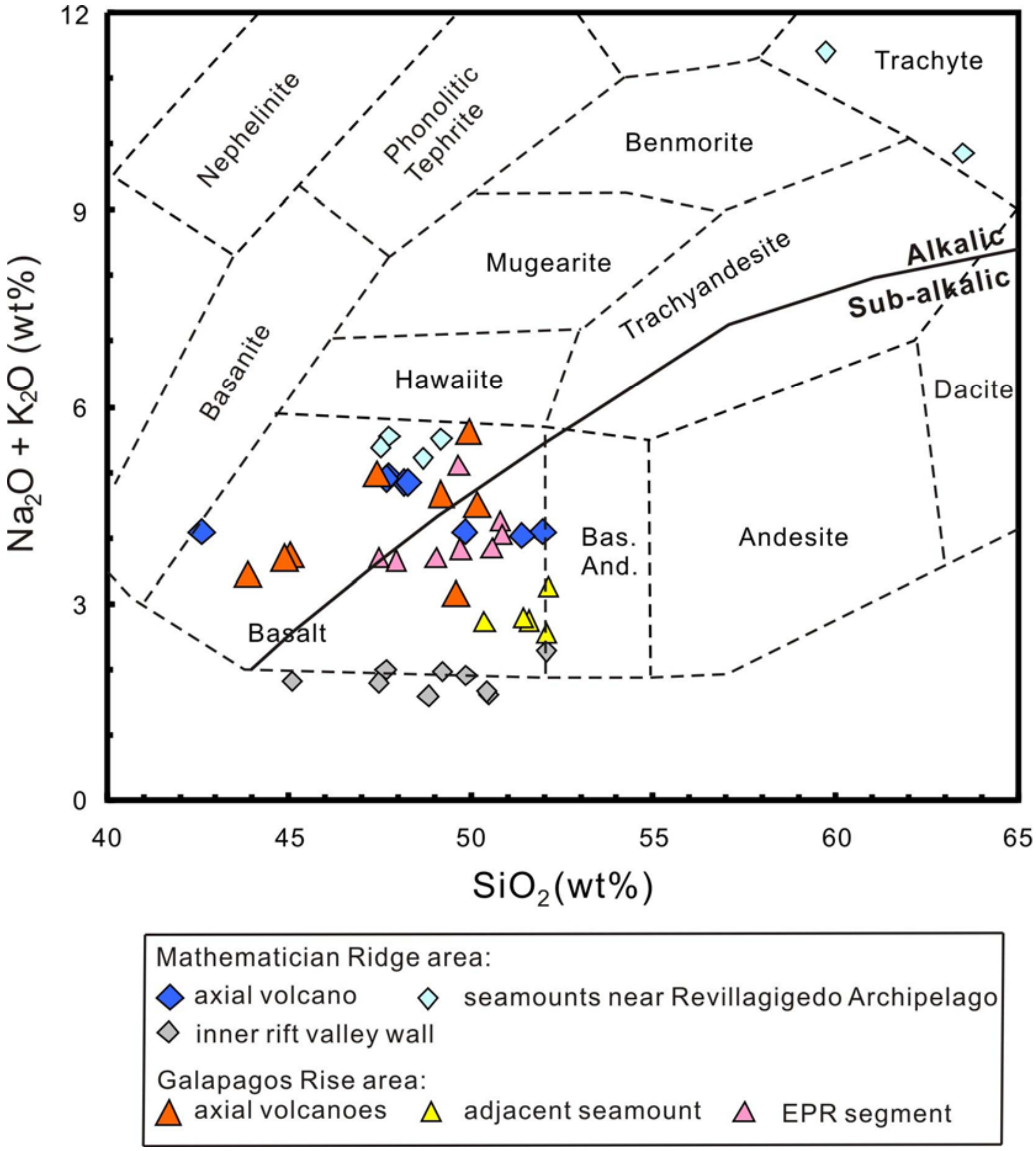

Figure 4.2. Silica (SiO_2) versus total alkalis ($Na_2O + K_2O$) diagram (after *Cox et al.*, 1979) for samples from the fossil Mathematician Ridge and Galapagos Rise areas. Bas. And. = Basaltic Andesite.

Figure 4.3. Weight % MgO versus TiO_2, Al_2O_3, FeO_t, CaO, Na_2O, and K_2O for samples from the fossil Mathematician Ridge and Galapagos Rise areas. Alkalic lavas from Socorro Island are shown for comparison [*Bohrson and Reid*, 1995].

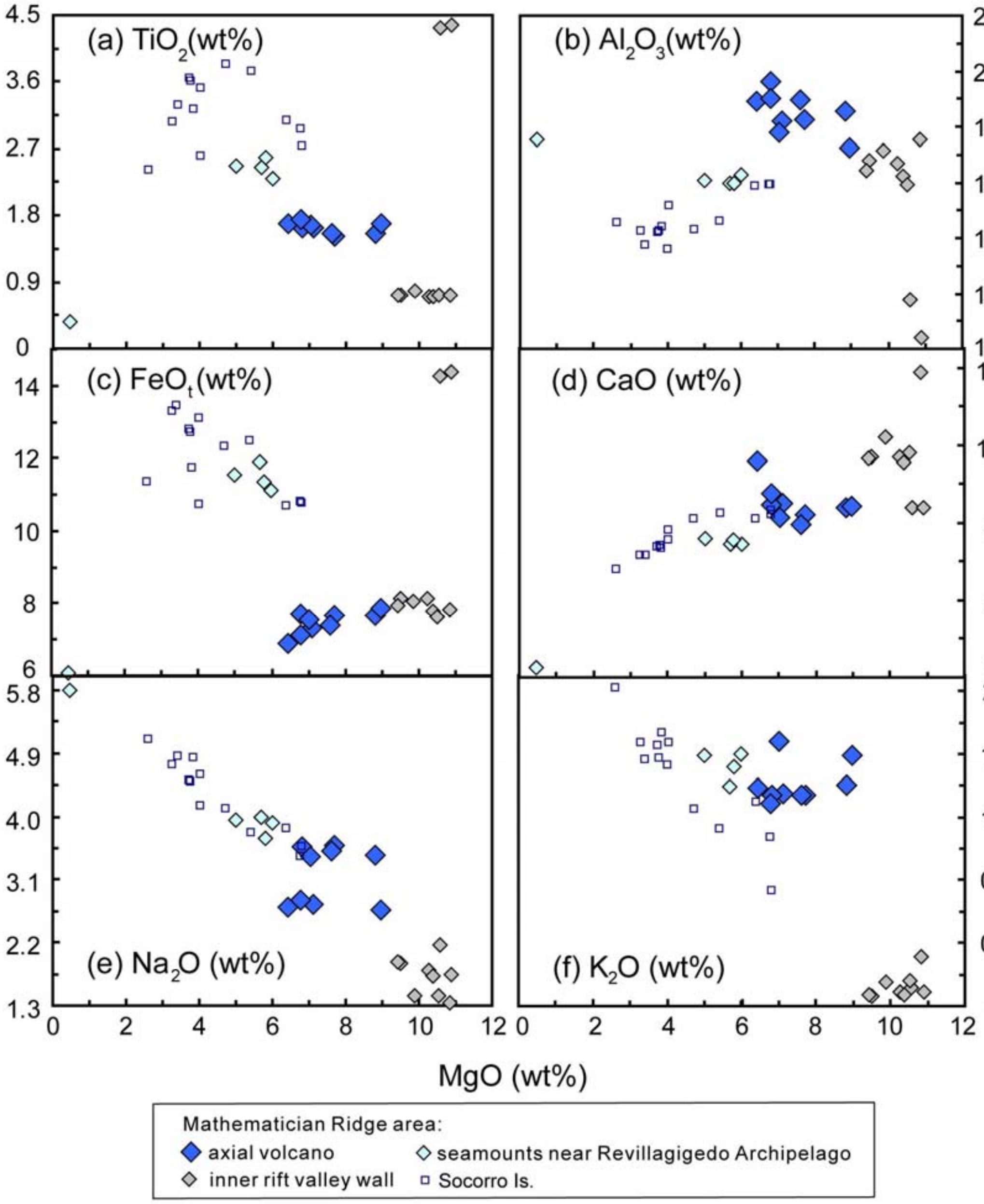
(a) TiO_2(wt%)
(b) Al_2O_3(wt%)
(c) FeO_t(wt%)
(d) CaO (wt%)
(e) Na_2O (wt%)
(f) K_2O (wt%)
4.5
3.6
2.7
1.8
0.9
0
22
20
18
16
14
12
10
14
12
10
8
6
17
13
9
5
1
5.8
4.9
4.0
3.1
2.2
1.3
2.0
1.6
1.2
0.8
0.4
0
0
2
4
6
8
10
12
MgO (wt%)
Mathematician Ridge area:
◆ axial volcano
◇ seamounts near Revillagigedo Archipelago
◆ inner rift valley wall
□ Socorro Is.

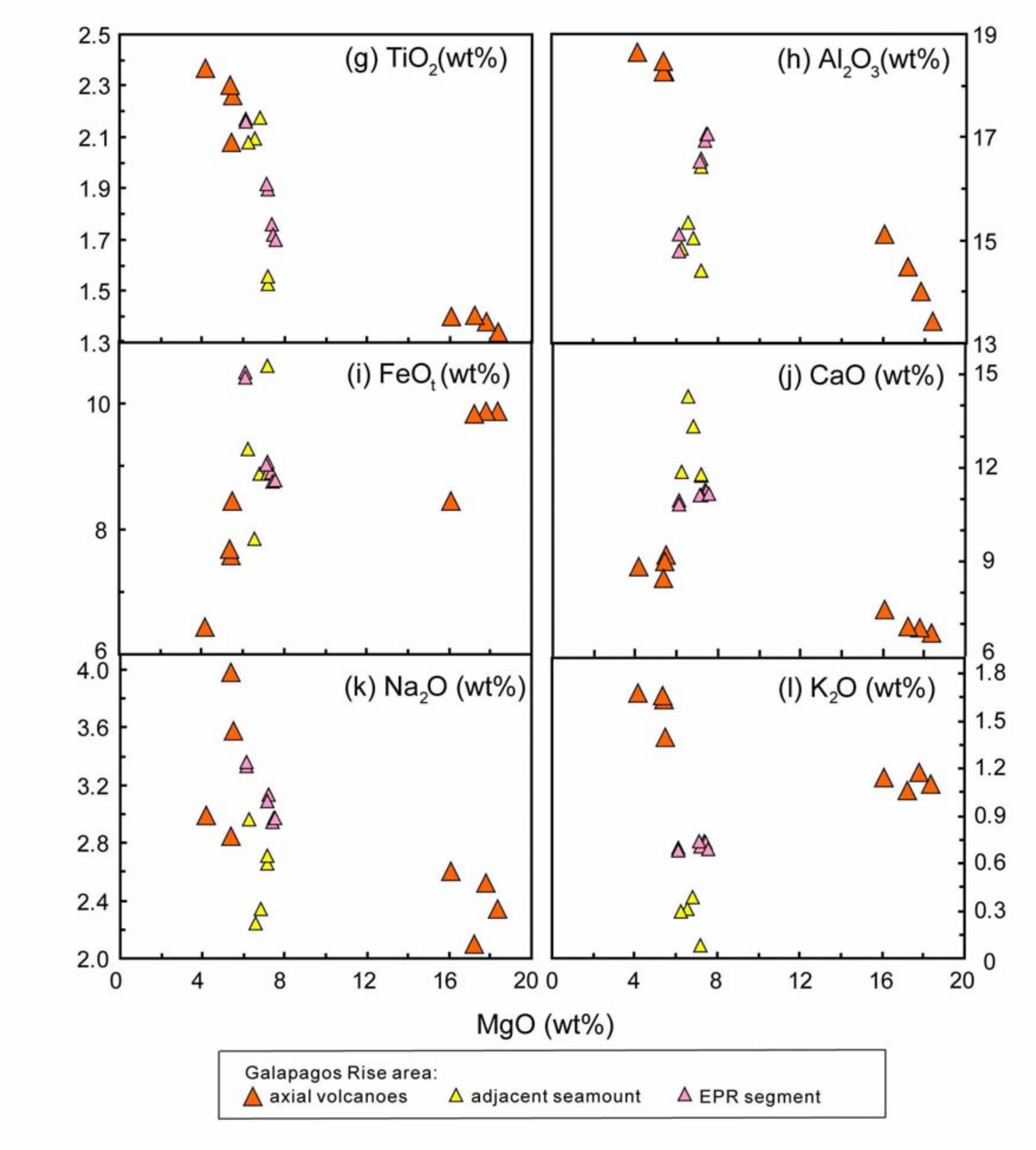

Figure 4.3. MgO versus major elements oxides (continued)

Figure 4.4. Primitive-mantle normalized incompatible trace element concentration diagrams for samples from (a) Mathematician Ridge and (b) Galapagos Rise areas. Average normal-MORB, enriched-MORB and OIB and primitive mantle normalizing values are from *Sun and McDonough* [1989]. Alkalic lavas from Socorro Island are shown for comparison [*Bohrson and Reid*, 1995].

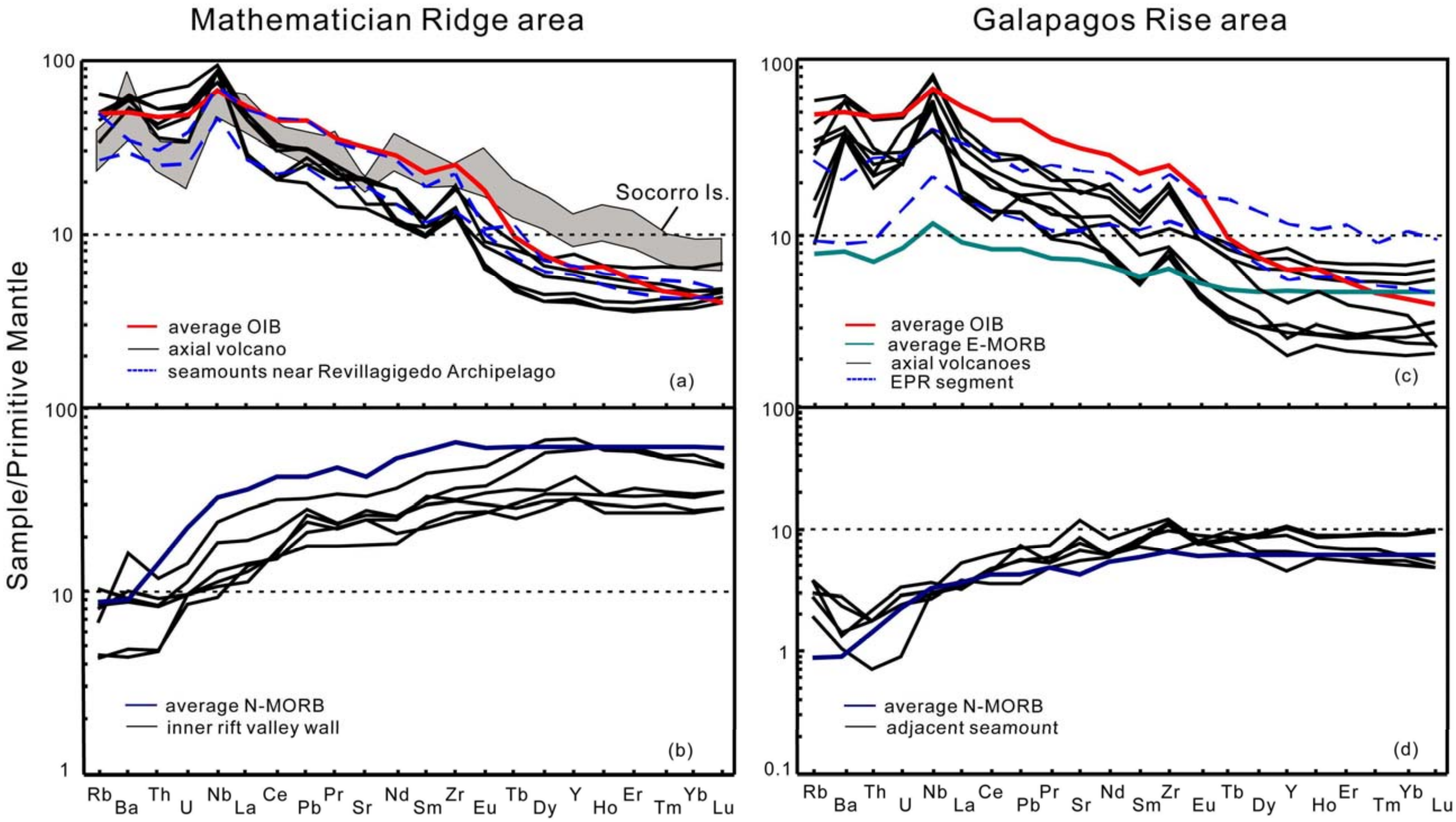
Mathematician Ridge area
Galapagos Rise area
Sample/Primitive Mantle
100
10
1
0.1
Socorro Is.
average OIB
axial volcano
seamounts near Revillagigedo Archipelago
(a)
average N-MORB
inner rift valley wall
(b)
average OIB
average E-MORB
axial volcanoes
EPR segment
(c)
average N-MORB
adjacent seamount
(d)
Rb Ba Th U Nb La Ce Pb Pr Sr Nd Sm Zr Eu Tb Dy Y Ho Er Tm Yb Lu

Figure 4.5. (left panel) $^{87}Sr/^{86}Sr$ versus $^{143}Nd/^{144}Nd$ and (right two panels) $^{206}Pb/^{204}Pb$ versus $^{207}Pb/^{204}Pb$ and $^{208}Pb/^{204}Pb$ for representative samples from Mathematician Ridge and Galapagos Rise areas. Data for Davidson Seamount [*Davis et al.*, 2002; *Castillo et al.*, 2010], Guide Seamount [*Davis et al.*, 2002], fossil spreading axes off Baja California Sur [*Tian et al.*, 2011], Socorro Island [*Bohrson and Reid*, 1995], and EPR riseflank seamounts [*Niu et al.*, 2002] are shown for reference. Also shown are fields for EPR MORB, Galapagos Islands, and Hawaii (GEOROC database: http://georoc.mpch-mainz.gwdg.de). HIMU, EM1 and EM2 are proposed mantle end-components, and NHRL is the northern hemisphere reference line from *Hart* [1984].

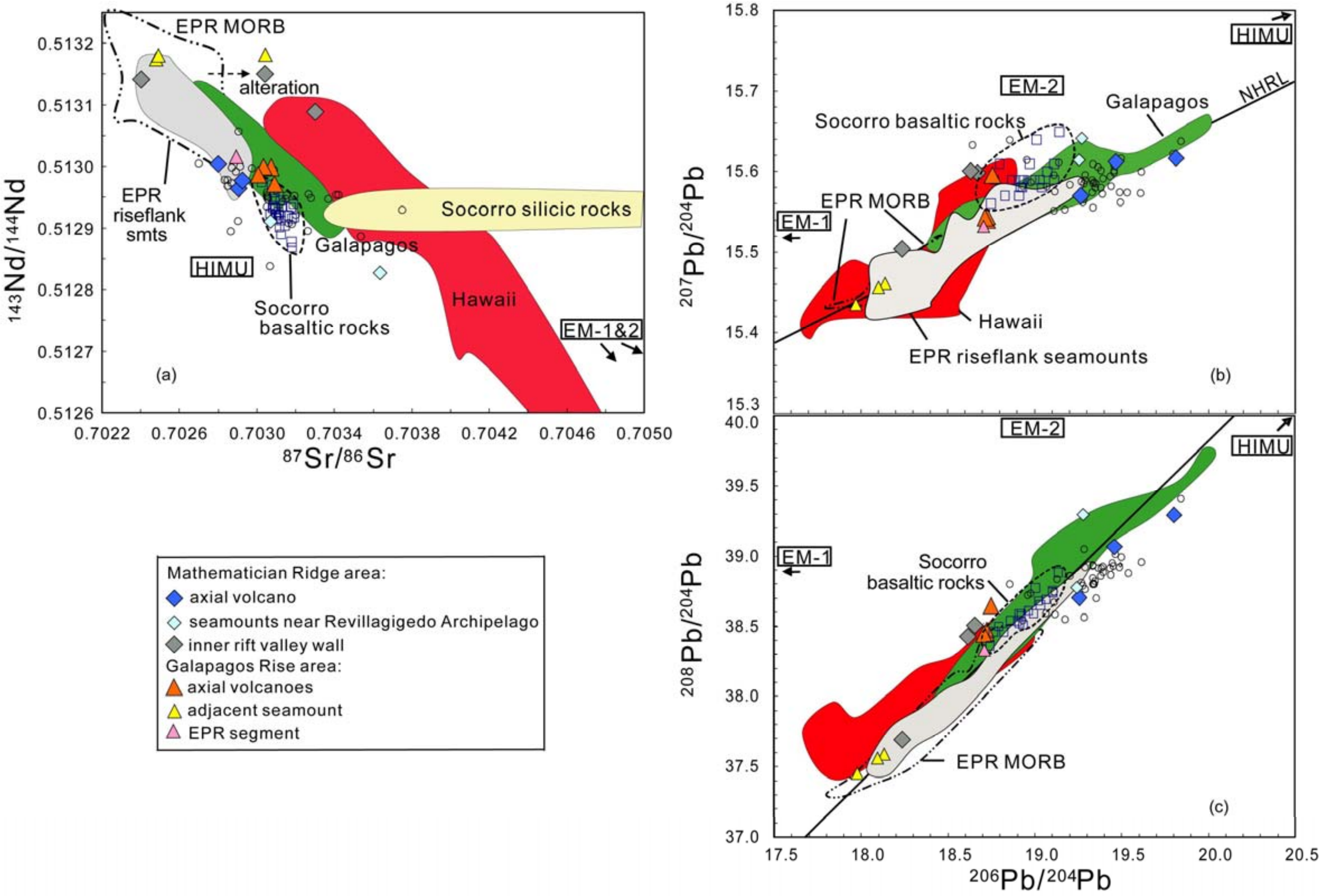
EPR MORB
alteration
EPR riseflank smts
HIMU
Galapagos
Socorro silicic rocks
Socorro basaltic rocks
Hawaii
EM-1&2
(a)
0.5132
0.5131
0.5130
0.5129
0.5128
0.5127
0.5126
0.7022
0.7026
0.7030
0.7034
0.7038
0.7042
0.7046
0.7050
$^{87}Sr/^{86}Sr$
$^{143}Nd/^{144}Nd$
Mathematician Ridge area:
axial volcano
seamounts near Revillagigedo Archipelago
inner rift valley wall
Galapagos Rise area:
axial volcanoes
adjacent seamount
EPR segment
15.8
15.7
15.6
15.5
15.4
15.3
HIMU
EM-2
Galapagos
NHRL
Socorro basaltic rocks
EPR MORB
EM-1
Hawaii
EPR riseflank seamounts
(b)
$^{207}Pb/^{204}Pb$
40.0
39.5
39.0
38.5
38.0
37.5
37.0
EM-2
HIMU
EM-1
Socorro basaltic rocks
EPR MORB
(c)
17.5
18.0
18.5
19.0
19.5
20.0
20.5
$^{206}Pb/^{204}Pb$
$^{208}Pb/^{204}Pb$

Figure 4.6. (a) La versus Sm and (b) Nb versus Zr for samples from Mathematician Ridge and Galapagos Rise areas. Note that tholeiitic lavas from the inner rift wall of Mathematician Ridge largely overlap with the depleted end of EPR riseflank seamounts, having lower Nb/Zr and La/Sm ratios compared to alkalic lavas from fossil spreading centers. Data sources are as in Figure 4.5.

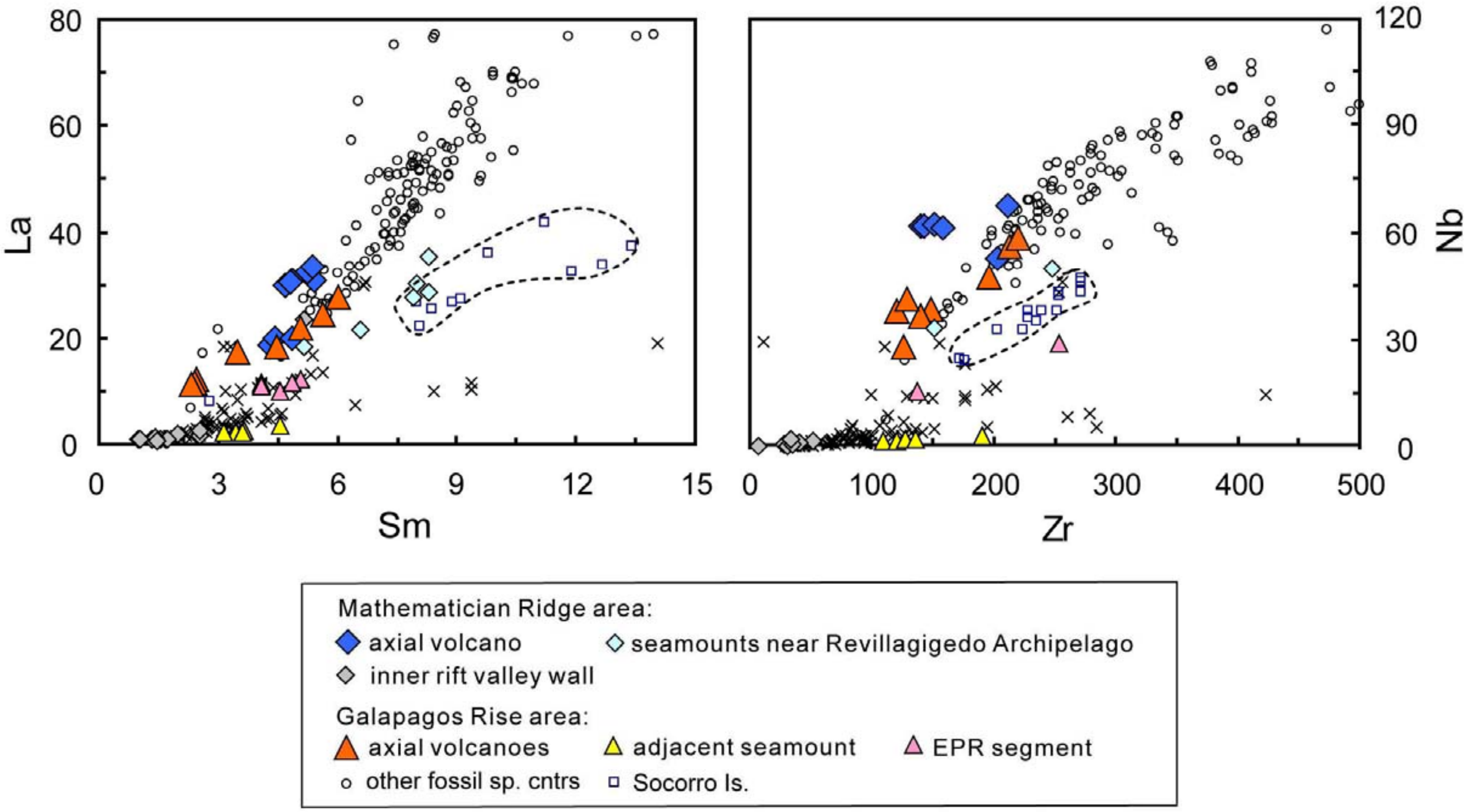

80
60
40
20
0
La
0
3
6
9
12
15
Sm
0
100
200
300
400
500
Zr
120
90
60
30
0
Nb
Mathematician Ridge area:
axial volcano
seamounts near Revillagigedo Archipelago
inner rift valley wall
Galapagos Rise area:
axial volcanoes
adjacent seamount
EPR segment
other fossil sp. cntrs
Socorro Is.

Figure 4.7. Variations of (a) Nb/Zr, (b) $^{87}Sr/^{86}Sr$, (c) $^{143}Nd/^{144}Nd$, (d) $^{206}Pb/^{204}Pb$ versus La/Sm for samples from Mathematician Ridge and Galapagos Rise areas. Note the correlations between incompatible trace element ratios and incompatible trace element and radiogenic isotope ratios. Data sources are as in Figure 4.5.

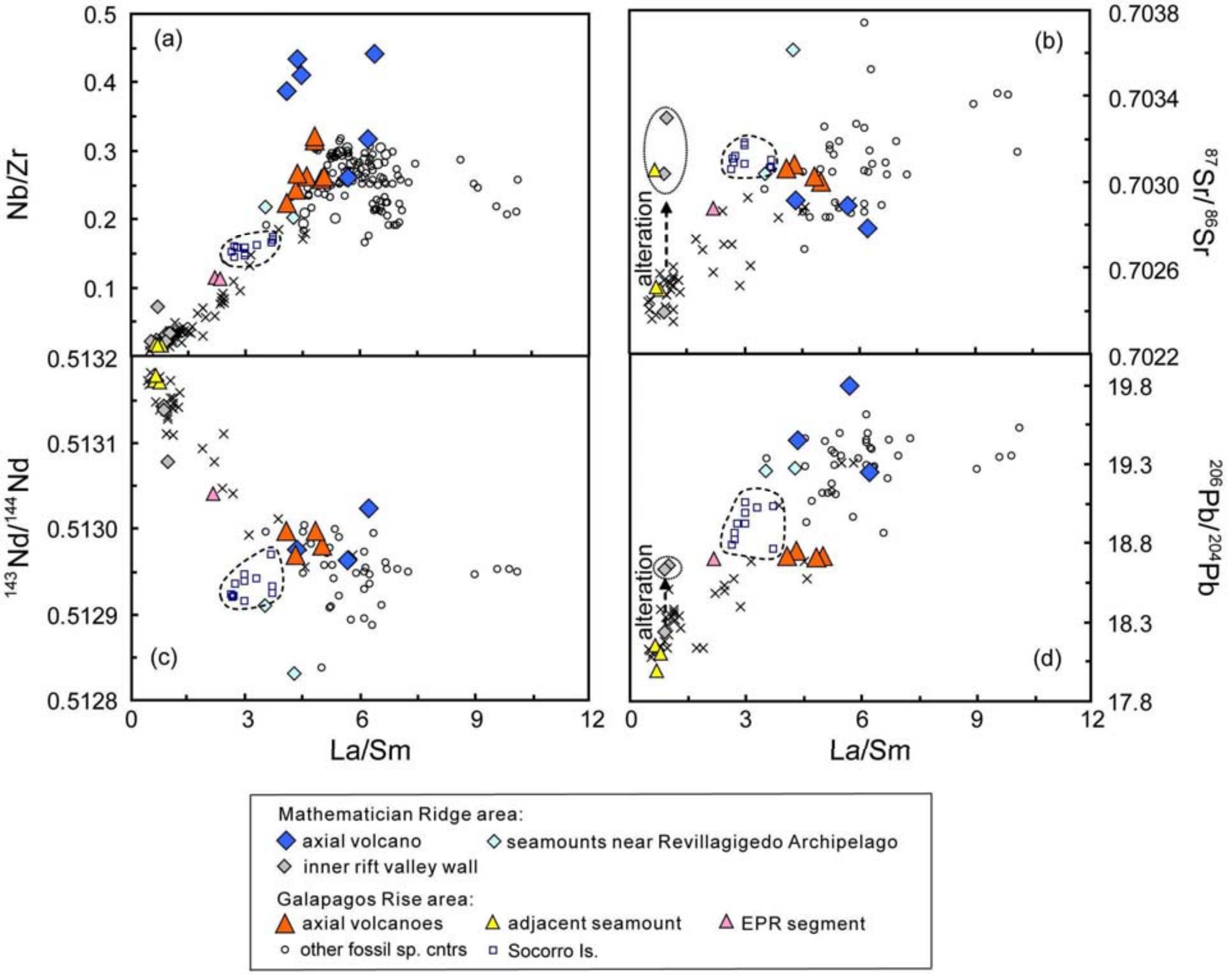
(a)
(b)
(c)
(d)
Nb/Zr
0.5
0.4
0.3
0.2
0.1
^{87}Sr/^{86}Sr
0.7038
0.7034
0.7030
0.7026
0.7022
^{143}Nd/^{144}Nd
0.5132
0.5131
0.5130
0.5129
0.5128
^{206}Pb/^{204}Pb
19.8
19.3
18.8
18.3
17.8
alteration
alteration
0
3
6
9
12
La/Sm
La/Sm
Mathematician Ridge area:
◆ axial volcano
◇ seamounts near Revillagigedo Archipelago
◆ inner rift valley wall
Galapagos Rise area:
▲ axial volcanoes
▲ adjacent seamount
▲ EPR segment
○ other fossil sp. cntrs
□ Socorro Is.

Figure 4.8. (a) Rb/Sr abundance ratio versus ^{87}Sr/^{86}Sr and (b) La/Sm abundance ratio versus ^{143}Nd/^{144}Nd for primitive basalts from Sara, Rosa, Rosana, and Nithya. The vertical line with numbers from depleted MORB mantle (DMM) indicates Rb/Sr and La/Sm abundance ratio at 0.05-2 % melting of a depleted MORB mantle source [Rb = 0.088 ppm, Sr = 9.80 ppm, ^{87}Sr/^{86}Sr = 0.7026; La = 0.234 ppm, Sm = 0.270 ppm, Nd = 0.713 ppm, ^{143}Nd/^{144}Nd = 0.51311; *Salters and Stracke*, 2004]. Here the initial mode of the depleted MORB mantle source was assumed to be olivine:orthopyroxene:clinopyroxene:garnet (60:25:10:5 mixture) lherzolite. An equilibrium batch partial melting model is used for calculation; bulk D (partition coefficient) for Rb is 0.0003, for Sr 0.0093, for La 0.0015, for Sm 0.0406, and for Nd 0.0153 in the lherzolite. The sub-horizontal linear solid curves are mixing lines between the various DMM melts (F%: degree of partial melting) and 10% melt of an enriched mantle component (EC; Rb = 6.45 ppm, Sr = 127.5 ppm, ^{87}Sr/^{86}Sr = 0.704162; La = 4.61 ppm, Sm = 3.85 ppm, Nd = 10.64 ppm, ^{143}Nd/^{144}Nd = 0.512869). The trace element abundances of EC are back-calculated by assuming that a primitive basalt from Flint seamount [*Davis et al.*, 1995] was produced by 20% partial melting of this source; its Sr and Nd isotopic values are from *Konter et al.* [2009], normalized relative to NBS 987 ^{87}Sr/^{86}Sr = 0.71025, and ^{143}Nd/^{144}Nd = 0.51185 for the La Jolla Nd standard. The EC source is assumed to be an amphibole:olivine:orthopyroxene: clinopyroxene:garnet (55:20:05:15:05) lherzolite. Bulk D for Rb is 0.1981, for Sr 0.1990, for La 0.089, for Sm 0.579, and for Nd 0.282 in the amphibole lherzolite. Vertical dash curves represent various DMM:EC melt mixtures. Detailed predictions of this model depend on the initial mineralogy of two end-members, source composition, style of melting, and the chosen D values, but the applicability of the model results is not affected by these parameters. Fields for basalts from Socorro Island, other fossil spreading centers in the eastern Pacific (grouped as tholeiitic/transitional basalts and alkalic basalts), selected riseflank seamounts, and adjacent EPR axis are shown for reference. Data sources are as in Figure 4.5.

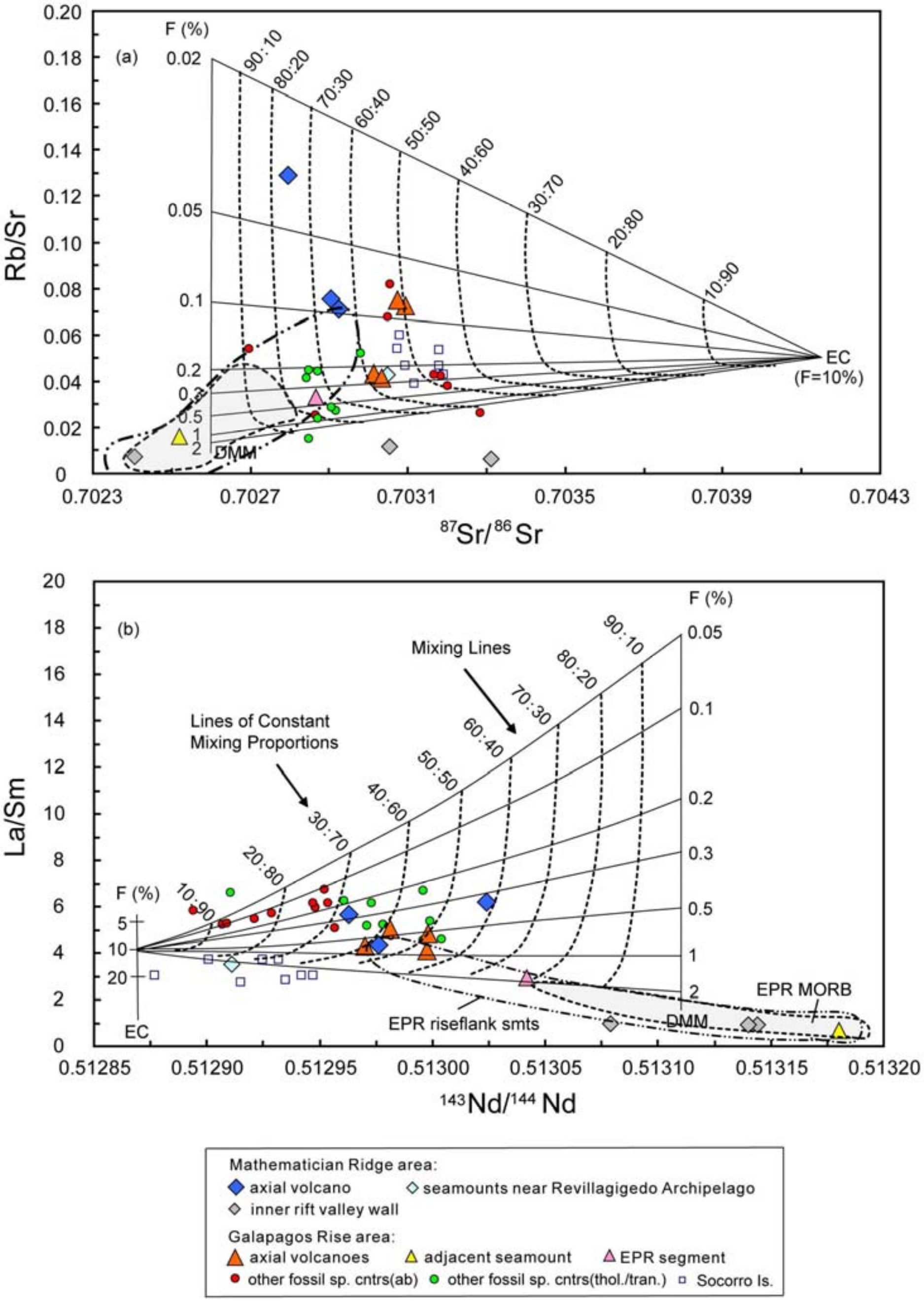
(a)
Rb/Sr
0.20
0.18
0.16
0.14
0.12
0.10
0.08
0.06
0.04
0.02
0
0.7023
0.7027
0.7031
0.7035
0.7039
0.7043
$^{87}Sr/^{86}Sr$
F (%)
0.02
0.05
0.1
0.2
0.3
0.5
1
2
DMM
90:10
80:20
70:30
60:40
50:50
40:60
30:70
20:80
10:90
EC
(F=10%)
(b)
La/Sm
20
18
16
14
12
10
8
6
4
2
0
0.51285
0.51290
0.51295
0.51300
0.51305
0.51310
0.51315
0.51320
$^{143}Nd/^{144}Nd$
F (%)
0.05
0.1
0.2
0.3
0.5
1
2
F (%)
5
10
20
EC
Mixing Lines
Lines of Constant
Mixing Proportions
90:10
80:20
70:30
60:40
50:50
40:60
30:70
20:80
10:90
EPR MORB
DMM
EPR riseflank smts
Mathematician Ridge area:
axial volcano
seamounts near Revillagigedo Archipelago
inner rift valley wall
Galapagos Rise area:
axial volcanoes
adjacent seamount
EPR segment
other fossil sp. cntrs(ab)
other fossil sp. cntrs(thol./tran.)
Socorro Is.

Table 4.1. Dredge locations for lavas from the fossil Mathematician Ridge and Galapagos Rise areas

Dredge number	Start position	End position	Depth (m)	Feature
Mathematician Ridge area				
AMD1	16°05.3´N, 111°32.5´W	16°05.3´N, 111°32.5´W	1901-1096	Axial volcano
AMD2	16°07´N, 111°32.8´W	16°05´N, 111°33.0´W	2166-1795	Axial volcano
AMD7	16°51.1´N, 111°14.9´W	16°51.2´N, 111°13.7´W	3466-3018	Inner rift valley
AMD10	18°10.8´N, 113°55.0´W	18°13.0´N, 113°48.6´W	1462-1252	Seamount near Revillagigedo Archipelago
AMD11	18°18.3´N, 114°39.6´W	18°25.2´N, 114°46.5´W	1349-987	Seamount near Revillagigedo Archipelago
Galapagos Rise area				
WD1	9°49.1´S, 110°9.1´W	9°50.1´S, 110°8.9´W	2900	East Pacific Rise
WD2	10°8.0´S, 110°12.1´W	10°8.8´S, 110°11.3´W	2800	East Pacific Rise
WD3	10°16.6´S, 93°45.7´W	10°16.0´S, 93°44.4´W	3780-3420	Adjacent seamount
WD4	10°22.1´S, 94°35.6´W	10°23.1´S, 94°34.8´W	1350-540	Axial volcano
WD5	10°37.4´S, 94°49.2´W	10°37.6´S, 94°48.9´W	3780-3510	Axial volcano

Table 4.2. Major and trace element compositions of samples from the fossil Mathematician Ridge and Galapagos Rise areas

	Mathematician Ridge area						
Location[a]	axial	axial	axial	axial	axial	axial	axial
Sample no.	AMD1-1	AMD1-2	AMD1-3	AMD1-6	AMD1-7	AMD1-8	AMD1-10
SiO_2[b]	*47.73*	*48.18*	42.61	49.84	*48.28*	51.97	*47.66*
TiO_2	*1.52*	*1.55*	1.63	1.70	*1.55*	1.74	*1.64*
Al_2O_3	*18.23*	*18.56*	18.19	18.90	*18.96*	19.04	*19.64*
FeO_t	*7.67*	*7.67*	7.30	6.91	*7.40*	7.11	*7.72*
MnO	*0.13*	*0.14*	0.13	0.14	*0.14*	0.15	*0.14*
MgO	*7.71*	*8.82*	7.11	6.42	*7.6*	6.78	*6.8*
CaO	*9.4*	*9.78*	10.00	12.22	*8.92*	10.52	*9.9*
Na_2O	*3.59*	*3.44*	2.74	2.70	*3.50*	2.80	*3.56*
K_2O	*1.34*	*1.40*	1.35	1.38	*1.34*	1.28	*1.34*
P_2O_5	*0.41*	*0.44*			*0.44*		*0.45*
LOI	*0.69*	*0.73*	0.77	0.59	*0.78*	0.60	*0.43*
Rb[c]	30.8		31.6	30.6		28.5	
Sr	440		420	431		432	
Y	24.80		27.80	19.23		18.30	
Zr	140		203	142		152	
Nb	61.83		52.80	61.80		62.15	
Ba	435		424	425		416	
La	30.90	*29.80*	30.71	18.66	*30.50*	19.78	*32.50*
Ce	56.41	*55.10*	53.62	36.34	*56.20*	36.86	*63.30*
Pr	6.11		6.83	5.65		5.73	
Nd	24.05		24.46	15.57		16.56	
Sm	4.85	*4.69*	5.41	4.29	*4.81*	4.44	*5.25*
Eu	1.43	*1.50*	1.98	1.10	*1.51*	1.12	*1.65*
Tb	0.75	*0.78*	0.97	0.51	*0.81*	0.52	*0.83*
Dy	4.22		4.81	3.03		3.02	
Ho	0.84		0.93	0.61		0.61	
Er	2.33		2.54	1.76		1.72	
Tm	0.35		0.38	0.28		0.27	
Yb	2.30	*2.37*	2.31	1.94	*2.34*	1.84	*2.79*
Lu	0.36	*0.35*	0.35	0.32	*0.36*	0.30	*0.42*
Pb	2.19		2.20	1.79		1.95	
Th	4.43		4.42	3.04		3.44	
U	1.16		1.12	0.71		0.99	

Table 4.2. Major and trace element compositions (continued)

	Mathematician Ridge area						
Location[a]	axial	axial	rift valley	rift valley	rift valley	rift valley	rift valley
Sample no.	AMD2-1	AMD2-2	AMD7-3	AMD7-36	AMD7-39	AMD7-40	AMD7-41
SiO_2[b]	*49.66*	50.81	*49.87*	*47.48*	52.08	55.48	*49.22*
TiO_2	*1.67*	1.69	*0.71*	*0.71*	4.33	0.72	*0.72*
Al_2O_3	*17.80*	17.25	*16.68*	*16.24*	11.79	15.93	*16.79*
FeO_t	*7.55*	7.87	*8.14*	*7.78*	14.25	7.64	*8.14*
MnO	*0.14*	0.17	*0.14*	*0.14*	0.47	0.16	*0.12*
MgO	*7.02*	8.96	*10.25*	*10.38*	10.58	10.52	*9.49*
CaO	*9.31*	9.89	*12.42*	*12.08*	9.79	12.61	*12.4*
Na_2O	*3.43*	2.66	*1.81*	*1.73*	2.16	1.44	*1.90*
K_2O	*1.68*	1.59	*0.09*	*0.07*	0.12	0.17	*0.06*
P_2O_5	*0.50*		*0.02*	*0.05*			*0.06*
LOI	*1.00*	0.59	*1.38*	*1.15*	2.08	1.21	*1.77*
Rb[c]	40.5	21.2			0.4	0.5	
Sr	314	294			70	58	
Y	34.64	20.59			31.11	14.39	
Zr	212	*158*			52	35	
Nb	67.16	61.21			1.72	0.80	
Ba	404	372			11	7	
La	33.39	19.78	*1.04*	*0.96*	1.93	0.88	*1.07*
Ce	58.67	36.24	*4.39*	*3.92*	5.60	2.83	*3.86*
Pr	6.41	3.99			0.93	0.64	
Nd	20.26	15.60			4.96	3.52	
Sm	5.37	4.84	*1.69*	*1.56*	1.96	1.32	*1.70*
Eu	1.52	1.06	*0.65*	*0.64*	0.82	0.51	*0.68*
Tb	0.88	0.55	*0.48*	*0.50*	0.63	0.31	*0.56*
Dy	5.26	3.30			5.01	2.29	
Ho	1.07	0.67			0.98	0.49	
Er	3.06	1.94			2.81	1.39	
Tm	0.48	0.31			0.39	0.22	
Yb	3.14	2.10	*1.95*	*1.90*	2.53	1.37	*2.02*
Lu	0.50	0.34	*0.30*	*0.27*	0.35	0.21	*0.29*
Pb	2.13	1.38			0.23	0.19	
Th	5.58	3.66			0.10	0.08	
U	1.49	1.12			0.03	0.02	

Table 4.2. Major and trace element compositions (continued)

	Mathematician Ridge area						
Location[a]	rift valley	rift valley	rift valley	rift valley	smt.	smt.	smt.
Sample no.	AMD7-43	AMD7-46	AMD7-47	AMD7-49	AMD10-1	AMD10-3	AMD11-2
SiO_2[b]	45.09	48.83	*47.67*	50.43	*59.73*	63.51	*49.18*
TiO_2	4.36	0.77	*0.72*	0.73	*0.36*	0.33	*2.30*
Al_2O_3	10.38	17.13	*16.44*	17.54	*17.55*	17.63	*16.28*
FeO_t	14.38	8.05	*7.93*	7.82	*6.07*	5.86	*11.13*
MnO	0.24	0.14	*0.13*	0.14	*0.24*	0.17	*0.17*
MgO	10.88	9.87	*9.42*	10.84	*0.46*		*5.99*
CaO	9.78	13.46	*12.34*	16.76	*1.53*	1.58	*7.93*
Na_2O	1.73	1.44	*1.92*	1.35	*5.8*	4.40	*3.91*
K_2O	0.09	0.15	*0.07*	0.32	*5.61*	5.46	*1.60*
P_2O_5			*0.05*		*0.08*		*0.57*
LOI	1.07	1.66	*1.75*	1.52	*3.47*	1.22	*0.74*
Rb[c]	0.7	0.3	0.3	0.5		31.3	
Sr	55	52	38	52		633	
Y	26.87	15.47	14.81	19.32		29.81	
Zr	41	28	30	35		248	
Nb	1.31	0.91	0.66	0.75		50.00	
Ba	6	3	3	6		242	
La	1.31	0.98	0.95	0.77	*90.30*	35.38	*30.30*
Ce	3.85	2.67	2.73	2.98	*180.90*	81.93	*63.60*
Pr	0.65	0.62	0.49	0.61		9.24	
Nd	3.49	2.80	2.47	3.36		36.26	
Sm	1.43	0.99	1.05	1.46	*14.89*	8.28	*7.98*
Eu	0.63	0.45	0.46	0.58	*2.78*	1.79	*2.48*
Tb	0.50	0.33	0.27	0.39	*2.29*	1.21	*1.24*
Dy	4.25	2.53	2.07	2.61		5.16	
Ho	1.02	0.55	0.44	0.55		0.97	
Er	2.92	1.59	1.29	1.76		2.73	
Tm	0.41	0.25	0.20	0.26		0.40	
Yb	2.74	1.62	1.33	1.68	*5.92*	2.60	*2.80*
Lu	0.36	0.26	0.21	0.26	*0.88*	0.35	*0.44*
Pb	0.20	0.15	0.12	0.17		3.20	
Th	0.07	0.04	0.04	0.07		2.58	
U	0.02	0.02	0.02	0.02		0.81	

Table 4.2. Major and trace element compositions (continued)

	Mathematician Ridge area			Galapagos Rise area			
Location[a]	smt.	smt.	smt.	EPR seg.	EPR seg.	EPR seg.	EPR seg.
Sample no.	AMD11-3	AMD11-4	AMD11-6	WD1-1	WD2B	WD2-2	WD2-3
SiO$_2$[b]	*47.76*	*47.52*	*48.68*	51.41	50.86	*49.04*	*47.48*
TiO$_2$	*2.46*	*2.45*	*2.58*	2.17	2.16	*1.76*	*1.72*
Al$_2$O$_3$	*16.06*	*15.97*	*15.95*	15.11	14.78	*16.94*	*17.06*
FeO$_t$	*11.53*	*11.90*	*11.37*	10.50	10.42	*8.90*	*8.75*
MnO	*0.15*	*0.17*	*0.18*			*0.16*	*0.16*
MgO	*5.00*	*5.68*	*5.79*	6.13	6.12	*7.41*	*7.44*
CaO	*8.19*	*7.88*	*8.13*	10.96	10.82	*11.3*	*11.24*
Na$_2$O	*3.96*	*3.99*	*3.69*	3.33	3.36	*2.95*	*2.97*
K$_2$O	*1.59*	*1.39*	*1.52*	0.70	0.68	*0.74*	*0.73*
P$_2$O$_5$	*0.61*	*0.61*	*0.62*	0.29	0.3	*0.34*	*0.22*
LOI	*0.76*	*0.60*	*0.61*		*0.98*	*0.97*	*1.07*
Rb[c]	16.9						
Sr	396						
Y	26.52						
Zr	151						
Nb	33.00						
Ba	205						
La	18.24	*28.60*	*27.60*		*12.30*	*11.70*	*11.10*
Ce	39.39	*61.20*	*57.60*		*29.10*	*26.20*	*25.90*
Pr	5.09						
Nd	20.01						
Sm	5.17	*8.30*	*7.92*		*5.07*	*4.08*	*4.09*
Eu	1.71	*2.58*	*2.43*		*1.75*	*1.44*	*1.41*
Tb	0.79	*1.36*	*1.27*		*1.27*	*1.06*	*1.08*
Dy	4.47						
Ho	0.83						
Er	2.20						
Tm	0.32						
Yb	2.10	*2.81*	*2.71*		*4.06*	*2.95*	*2.92*
Lu	0.32	*0.46*	*0.42*		*0.60*	*0.44*	*0.43*
Pb	1.69						
Th	2.10						
U	0.53						

Table 4.2. Major and trace element compositions (continued)

	Galapagos Rise area						
Location[a]	EPR seg.	EPR seg.	EPR seg.	smt.	smt.	smt.	smt.
Sample no.	WD2-6*	WD2-7*	WD2-8	WD3-1	WD3-2	WD3-3	WD3-4*
SiO_2[b]	*50.57*	*49.72*	*47.95*	51.58	51.98	*52.12*	50.36
TiO_2	*1.90*	*1.92*	*1.70*	1.53	2.10	*2.08*	2.18
Al_2O_3	*16.59*	*16.54*	*17.06*	16.43	15.34	*14.84*	15.03
FeO_t	*9.08*	*9.03*	*8.78*	10.60	7.85	*9.28*	8.89
MnO			*0.15*		0.19	*0.20*	0.19
MgO	*7.21*	*7.15*	*7.54*	7.18	6.59	*6.26*	6.83
CaO	*11.14*	*11.11*	*11.15*	11.76	14.30	*11.86*	13.35
Na_2O	*3.14*	*3.09*	*2.97*	2.66	2.24	*2.96*	2.35
K_2O	*0.71*	*0.74*	*0.69*	0.08	0.32	*0.30*	0.39
P_2O_5	*0.26*	*0.27*	*0.22*	0.14		*0.14*	
LOI	*1.08*	*1.18*	*0.98*		0.46	0.55	0.36
Rb[c]	17.2	6.1		1.8	2.4	1.2	1.9
Sr	498	231		115	180	161	248
Y	54.07	26.29		29.96	46.31	48.38	40.47
Zr	253	137		109	120	127	135
Nb	28.88	15.60		1.92	2.10	2.14	2.21
Ba	146	65		10	16	7	19
La	23.26	11.41	*11.00*	2.63	2.28	2.33	3.65
Ce	52.89	24.53	*25.40*	6.25	7.90	8.43	10.91
Pr	7.03	3.02		1.34	1.49	1.61	2.04
Nd	31.06	15.96		7.99	8.08	8.57	11.26
Sm	7.96	4.87	*4.07*	3.66	3.42	3.63	4.54
Eu	2.86	1.80	*1.43*	1.48	1.26	1.27	1.35
Tb	1.76	0.98	*1.07*	0.92	0.87	0.90	1.04
Dy	10.26	5.13		4.89	6.46	6.72	6.29
Ho	1.82	0.99		1.00	1.39	1.45	1.18
Er	5.62	2.84		2.96	4.17	4.30	3.31
Tm	0.69	0.40		0.41	0.66	0.69	0.51
Yb	5.34	2.55	*2.91*	2.68	4.41	4.52	2.93
Lu	0.72	0.35	*0.42*	0.36	0.71	0.73	0.39
Pb	1.67	0.89		0.25	0.52	0.39	0.50
Th	2.37	0.81		0.15	0.15	0.06	0.15
U	0.60	0.30		0.05	0.05	0.02	0.06

Table 4.2. Major and trace element compositions (continued)

	Galapagos Rise area						
Location[a]	smt.	axial	axial	axial	axial	axial	axial
Sample no.	WD3-5*	WD4-2	WD4-3	WD4-4	WD5-1	WD5-2	WD5-3*
SiO_2[b]	51.43	49.17	50.18	*47.42*	*45.04*	*43.87*	*49.94*
TiO_2	1.56	2.37	2.30	*2.26*	*1.40*	*1.34*	*2.08*
Al_2O_3	14.42	18.64	18.48	*18.28*	*15.12*	*13.44*	*18.27*
FeO_t	8.89	6.43	7.68	*8.44*	*8.44*	*9.87*	*7.57*
MnO		0.15	0.09	*0.12*	*0.16*	*0.18*	
MgO	7.18	4.15	5.39	*5.48*	*16.06*	*18.38*	*5.40*
CaO	11.8	8.84	8.47	*9.22*	*7.44*	*6.72*	*8.99*
Na_2O	2.71	3.00	2.85	*3.58*	*2.60*	*2.34*	*3.98*
K_2O	0.08	1.67	1.66	*1.40*	*1.14*	*1.10*	*1.64*
P_2O_5	0.14			*0.62*	*0.32*	*0.32*	*0.44*
LOI		2.13	2.85	2.53	*1.62*	*1.33*	
Rb[c]	2.4	27.1	37.1	18.1	10.1	5.7	20.3
Sr	140	375	368	432	231	227	272
Y	20.41	29.02	38.61	33.81	11.89	12.86	19.41
Zr	74	196	213	219	97	86	126
Nb	2.59	47.55	55.75	58.35	38.49	38.41	28.19
Ba	9	403	432	407	265	247	267
La	2.18	21.95	27.70	24.47	17.32	12.35	18.29
Ce	8.05	41.69	52.42	47.04	36.27	24.45	34.08
Pr	1.46	5.06	6.17	5.61	3.92	2.73	4.94
Nd	8.28	21.93	26.35	24.12	15.97	10.88	17.86
Sm	3.15	5.09	6.03	5.63	3.46	2.45	4.48
Eu	1.32	1.62	1.77	1.76	0.97	0.77	1.65
Tb	0.72	0.81	0.97	0.91	0.49	0.38	0.83
Dy	4.28	4.77	5.84	5.39	2.71	2.25	3.76
Ho	0.94	0.95	1.17	1.07	0.51	0.45	0.81
Er	2.66	2.64	3.29	2.98	1.35	1.25	1.99
Tm	0.39	0.40	0.51	0.45	0.20	0.20	0.29
Yb	2.51	2.64	3.36	2.95	1.22	1.31	1.79
Lu	0.35	0.42	0.53	0.47	0.18	0.21	0.18
Pb	0.40	1.40	2.00	1.93	1.13	0.97	1.23
Th	0.18	2.67	3.95	3.80	1.91	1.86	2.51
U	0.07	0.53	1.04	0.98	0.84	0.54	0.63

Table 4.2. Major and trace element compositions (continued)

	Galapagos Rise area		International standard[b]			
Location[a]	axial	axial	AGV-1		BHVO-1	
Sample no.	WD5-5	WD5-7	measured	recommended	measured	recommended
SiO_2[b]	*44.87*	49.58	60.09	58.79	52.62	49.94
TiO_2	*1.38*	1.41	1.02	1.05	2.78	2.71
Al_2O_3	*14.02*	14.48	16.94	17.14	13.51	13.8
FeO_t	*9.87*	9.84	6.00	6.08	11.01	11.00
MnO	*0.18*	0.15	0.093	0.092	0.164	0.168
MgO	*17.8*	17.20	1.49	1.53	7.43	7.23
CaO	*6.89*	6.94	4.89	4.94	11.39	11.4
Na_2O	*2.52*	2.09	4.30	4.26	2.30	2.26
K_2O	*1.18*	1.06	2.84	2.91	0.53	0.52
P_2O_5	*0.30*			0.49		0.273
LOI	*1.67*	0.24				
Rb[c]	8.0	21.6	67.9	68.3	11.0	10.7
Sr	192	266	678	672	405	396
Y	9.50	14.23	19.95	21.7	26.02	27
Zr	85	93	232	230	184	175
Nb	38.01	41.25	14.48	14.3	19.47	19.2
Ba	251	286	1231	1225	140	130
La	11.54	11.24	37.27	37.4	15.72	15.4
Ce	24.00	21.83	68.27	69.6	39.37	39.7
Pr	2.67	3.65	8.00	8	5.49	5.45
Nd	10.70	10.04	32.34	32.8	26.08	25.5
Sm	2.39	2.33	5.76	5.7	6.16	6
Eu	0.74	0.79	1.68	1.77	2.10	1.96
Tb	0.35	0.37	0.70	0.72	0.96	0.95
Dy	2.03	2.25	3.60	3.48	5.22	5.24
Ho	0.39	0.46	0.67	0.65	0.94	1
Er	1.06	1.30	1.70	1.75	2.40	2.38
Tm	0.16	0.21	0.33	0.32	0.34	0.33
Yb	1.03	1.47	1.69	1.72	2.02	2.02
Lu	0.16	0.24	0.26	0.268	0.31	0.292
Pb	0.95	1.20	36.29	35.2	2.44	2.47
Th	1.59	2.15	6.49	6.48	1.11	1.13
U	0.54	0.58	1.92	1.91	0.43	0.44

Table 4.2. Major and trace element compositions (continued)

	Galapagos Rise area		International standard[b]			
Location[a]	axial	axial	AGV-1		BHVO-1	
Sample no.	WD5-5	WD5-7	measured	recommended	measured	recommended
SiO_2[b]	*44.87*	49.58	60.09	58.79	52.62	49.94
TiO_2	*1.38*	1.41	1.02	1.05	2.78	2.71
Al_2O_3	*14.02*	14.48	16.94	17.14	13.51	13.8
FeO_t	*9.87*	9.84	6.00	6.08	11.01	11.00
MnO	*0.18*	0.15	0.093	0.092	0.164	0.168
MgO	*17.8*	17.20	1.49	1.53	7.43	7.23
CaO	*6.89*	6.94	4.89	4.94	11.39	11.4
Na_2O	*2.52*	2.09	4.30	4.26	2.30	2.26
K_2O	*1.18*	1.06	2.84	2.91	0.53	0.52
P_2O_5	*0.30*			0.49		0.273
LOI	*1.67*	0.24				
Rb[c]	8.0	21.6	67.9	68.3	11.0	10.7
Sr	192	266	678	672	405	396
Y	9.50	14.23	19.95	21.7	26.02	27
Zr	85	93	232	230	184	175
Nb	38.01	41.25	14.48	14.3	19.47	19.2
Ba	251	286	1231	1225	140	130
La	11.54	11.24	37.27	37.4	15.72	15.4
Ce	24.00	21.83	68.27	69.6	39.37	39.7
Pr	2.67	3.65	8.00	8	5.49	5.45
Nd	10.70	10.04	32.34	32.8	26.08	25.5
Sm	2.39	2.33	5.76	5.7	6.16	6
Eu	0.74	0.79	1.68	1.77	2.10	1.96
Tb	0.35	0.37	0.70	0.72	0.96	0.95
Dy	2.03	2.25	3.60	3.48	5.22	5.24
Ho	0.39	0.46	0.67	0.65	0.94	1
Er	1.06	1.30	1.70	1.75	2.40	2.38
Tm	0.16	0.21	0.33	0.32	0.34	0.33
Yb	1.03	1.47	1.69	1.72	2.02	2.02
Lu	0.16	0.24	0.26	0.268	0.31	0.292
Pb	0.95	1.20	36.29	35.2	2.44	2.47
Th	1.59	2.15	6.49	6.48	1.11	1.13
U	0.54	0.58	1.92	1.91	0.43	0.44

Table 4.2. Major and trace element compositions (continued)

[a] Axial = volcanoes or narrow volcanic ridges along the axes of the fossil Mathematician Ridge and Galapagos Rise; rift valley = inner rift valley wall along the Mathematician Ridge; smt. = seamount near Revillagigedo Archipelago in the Mathematician Ridge area or seamount adjacent to the fossil Galapagos spreading axis; EPR seg. = segment of the East Pacific Rise near the Galapagos Rise.

[b] Major elements oxides in wt%. Italics are published data from *Batiza and Vanko* [1985] and *Batiza et al*. [1982]. FeO_t is total Fe expressed as Fe^{2+}. Each sample was analyzed in duplicate and reproducibility was better than 5% based on repeated analyses of standards AGV-1 and BHVO-1 analyzed as unknowns. The accuracy of the standards is within 5% of the suggested values (AGV-1, n = 36; BHVO-1, n =21; *Govindaraju*, 1994).

c. Trace elements in ppm. Italics are published data from *Batiza and Vanko* [1985] and *Batiza et al*. [1982]. Each sample was analyzed in duplicate and reproducibility was better than 5% based on repeated analyses of standards AGV-1 and BHVO-1 analyzed as unknowns. The accuracy of the standard is within 10% of the suggested values (AGV-1, n = 49; BHVO-1, n = 40; *Govindaraju*, 1994), but generally better than ±5% for rare earth elements (REEs).

* Glasses. All others were measured from whole rock powders.

Table 4.3. Sr-Nd-Pb isotope compositions of representative samples from the fossil Mathematician Ridge and Galapagos Rise areas [a]

Sample	**$^{87}Sr/^{86}Sr$**	**2σ**	**$^{143}Nd/^{144}Nd$**	**2σ**
Mathematician Ridge area				
AMD1-3	0.702904	9	0.512963	7
AMD1-6	0.702925	10	0.512976	8
AMD2-1	0.702796	10	0.513024	8
AMD7-39	0.703311	12	0.513079	4
AMD7-43	0.703052	10	0.513144	13
AMD7-47	0.702407	10	0.513140	16
AMD10-3	0.703625	11	0.512831	9
AMD11-3	0.703049	9	0.512911	4
Galapagos Rise area				
WD2-6*	0.702887	7	0.513042	8
WD3-2	0.703071	9	0.513174	8
WD3-4*	0.702508	10	0.513172	6
WD3-5*	0.702522	10	0.513180	8
WD4-2	0.703093	11	0.512970	8
WD5-1	0.703013	10	0.512981	10
WD5-3*	0.703074	10	0.512997	7
WD5-5	0.703035	9	0.512998	8

Table 4.3. Sr-Nd-Pb isotope compositions (continued)

Sample	**$^{206}Pb/^{204}Pb$**	**2σ**	**$^{207}Pb/^{204}Pb$**	**2σ**	**$^{208}Pb/^{204}Pb$**	**2σ**
Mathematician Ridge area						
AMD1-3	19.796	2	15.616	1	39.287	4
AMD1-6	19.454	3	15.612	2	39.062	6
AMD2-1	19.253	3	15.570	3	38.699	7
AMD7-39	18.662	2	15.598	2	38.491	5
AMD7-43	18.633	8	15.600	6	38.420	16
AMD7-47	18.238	4	15.503	3	37.684	8
AMD10-3	19.279	3	15.639	3	39.079	7
AMD11-3	19.256	7	15.613	2	38.842	6
Galapagos Rise area						
WD2-6*	18.700	2	15.522	2	38.302	4
WD3-2	18.155	3	15.461	3	37.596	6
WD3-4*	18.104	4	15.456	4	37.576	9
WD3-5*	17.991	5	15.430	4	37.432	5
WD4-2	18.750	3	15.595	2	38.642	6
WD5-1	18.722	6	15.539	5	38.452	12
WD5-3*	18.722	5	15.544	5	38.472	11
WD5-5	18.708	4	15.542	3	38.443	8

[a] Strontium isotopic ratios were measured through dynamic multi-collection and fractionation corrected to $^{86}Sr/^{88}Sr = 0.1194$. Repeated measurements of NBS 987 yielded $^{87}Sr/^{86}Sr = 0.710256 \pm 0.000017$ (n = 18); 2σ indicates in-run precisions. Neodymium isotopic ratios were measured in oxide form through dynamic multi-collection and fractionation corrected to $^{146}NdO/^{144}NdO = 0.72225$ ($^{146}Nd/^{144}Nd = 0.7219$). Repeated measurements of the La Jolla Nd standard yielded $^{143}Nd/^{144}Nd = 0.511856 \pm 0.000010$ (n = 17). Lead isotopic ratios were measured through static multi-collection and were fractionation corrected using the repeated measurements of NBS SRM 981,(n=22; $^{206}Pb/^{204}Pb = 16.899 \pm 0.007$, $^{207}Pb/^{204}Pb = 15.445 \pm 0.010$, and $^{208}Pb/^{204}Pb = 36.550 \pm 0.026$) relative to those of *Todt et al.* [1996]. Total procedural blanks are negligible: < 35 picograms (pg) for Sr, < 10 pg for Nd,and <74 pg for Pb.

* Glasses. All others are measured from whole rock powder.

References

Batiza, R., R. Oestrike, and K. Futa (1982), Chemical and isotopic diversity in basalts dredged from the East Pacific Rise at 10°S, the fossil Galapagos Rise and the Nazca plate, *Mar. Geol.*, *49*, 115-132.

Batiza, R., and D. Vanko (1985), Petrologic evolution of large failed rifts in the eastern Pacific: petrology of volcanic and plutonic rocks from the Mathematician Ridge area and the Guadalupe Trough, *J. Petrol.*, *26*, 564-602.

Batiza, R. (1989), Failed rifts, in: Winterer, E. L., D. M. Hussong, and R. W. Decker (ed.), *The eastern Pacific ocean and Hawaii*, *Geol. Soc. Am.*, Boulder, Colorado.

Bohrson, W. A., and M. R. Reid (1995), Petrogenesis of alkaline basalts from Socorro Island, Mexico; trace element evidence for contamination of ocean island basalt in the shallow ocean crust, *J. Geophys. Res.*, *100*(B12), 24,555-24,576.

Bohrson, W. A., and M. R. Reid (1997), Genesis of silicic peralkaline volcanic rocks in an ocean island setting by crustal melting and open-system processes: Socorro Island, Mexico, *J. Petrol.*, *38*, 1137-1166.

Bohrson, W. A., and M. R. Reid (1998), Genesis of evolved ocean island magmas by deep- and shallow-level basement recycling, Socorro Island, Mexico: constraints from Th and other isotope signatures, *J. Petrol.*, *39*, 995-1008.

Castillo, P. R., D. A. Clague, A. S. Davis, and P. F. Lonsdale (2010), Petrogenesis of Davidson Seamount lavas and its implications for fossil spreading center and intraplate magmatism in the eastern Pacific, *Geochem. Geophys. Geosyst.*, *11*, Q02005.

Choe, W. H., J. I. Lee, M. J. Lee, S. D. Hur, and Y. K. Jin (2007), Origin of E-MORB in a fossil spreading center: the Antarctic-Phoenix Ridge, Drake Passage, Antarctica, *Geosci. J.*, *11*, 185-199.

Choi, S. H., W. H. Choe, and J. I. Lee (2008), Mantle heterogeneity beneath the Antarctic-Phoenix Ridge off Antarctic Peninsula, *Isl. Arc*, *17*, 172-782.

Clague, D. A., J. B. Paduan, R. A. Duncan, J. J. Huard, A. S. Davis, P. R. Castillo, P. Lonsdale, and A. DeVogelaere (2009), Five million years of compositionally diverse, episodic volcanism: Construction of Davidson Seamount atop an abandoned spreading center, *Geochem. Geophys. Geosyst.*, *10*, Q12009.

Cox, K. G., J. D. Bell, and R. J. Pankhurst (1979), The interpretation of igneous rocks, London: Allen and Unwin.

Davis, A. S., S. H. Gunn, W. A. Bohrson, L.-B. Gray, and J. R. Hei (1995), Chemically diverse, sporadic volcanism at seamounts offshore southern and Baja California, *Geol. Soc. Am. Bull.*, *107*, 554–570.

Davis, A. S., D. A. Clague, W. A. Bohrson, G. B. Dalrymple, and H. G. Greene (2002), Seamounts at the continental margin of California: A different kind of oceanic intraplate volcanism, *Geol. Soc. Am. Bull.*, *114*, 316-333.

Davis, A. S., D. A. Clague, J. B. Paduan, B. L. Cousens, and J. Huard (2010), Origin of volcanic seamounts at the continental margin of California related to changes in plate margins, *Geochem. Geophys. Geosyst.*, *11(5)*, Q05006.

Eakins, B. W., and P. F. Lonsdale (2003), Structural patterns and tectonic history of the Bauer microplate, Eastern Tropical Pacific, *Mar. Geophys. Res.*, *24*, 171-205.

Graham, D. W., A. Zindler, M. D. Kurz, W. J. Jenkins, and R. Batiza (1988), He, Pb, Sr and Nd isotope constraints on magma genesis and mantle heterogeneity beneath young Pacific seamounts, *Contrib. Mineral. Petrol.*, *99*(4), 446–463.

Govindaraju, K. (1994), 1994 compilation of working values and descriptions for 383 geostandards, *Geostand. Newsl.*, *18*, 1–158.

Hart, S. R. (1984), A large-scale isotope anomaly in the Southern Hemisphere mantle, *Nature*, *309*, 753–757.

Haase, K. M., and N. A. Stroncik (2002), Volcanism on the fossil Galapagos Rise spreading center, SE Pacific, *Eos Trans. AGU*, *83*(47), Fall Meeting Suppl., Abstract V52A-1278.

Haase, K. M., C. Beier, S. Fretzdorff, P. T. Leat, R. A. Livermore, T. L. Barry, J. A. Pearce, and F. Hauff (2011), Magmatic evolution of a dying spreading axis: evidence for the interaction of tectonics and mantle heterogeneity from the fossil Phoenix Ridge, Drake Passage, *Chem. Geol.*, *280*, 115-125.

Hirose, K. (1997) Partial melt compositions of carbonated peridotite at 3 GPa and genesis of alkali basalt magmas, *Geophys. Res. Lett.*, *24*, 2837– 2840.

Hirschmann, M.M., T. Kogiso, M. B. Baker, and E. M. Stolper (2003), Alkalic magmas generated by partial melting of garnet pyroxenite, *Geology*, *31*, 481-484.

Hofmann, A. W. (2003), Sampling mantle heterogeneity through oceanic basalts: isotopes and trace elements, *Treatise Geochem.*, *2*, 1-44.

Jha, K., E. M. Parmentier, and J. Phipps Morgan (1994), The role of mantle depletion and met retention buoyancy in spreading-center segmentation, *Earth Planet. Sci. Lett.*, *125*, 221-234.

Keshav, S., G. H. Gudfinnsson, G. Sen, and Y. Fei (2004), High-pressure melting experiments on garnet clinopyroxenite and the alkalic to tholeiitic transition in ocean-island basalts, *Earth Planet. Sci. Lett.*, *223*, 365-379.

Konter, J., H. Staudigel, J. Blichert-Toft, B. B. Hanan, M. Polve, G. R. Davies, N. Shimizu, and P. Schiffman (2009), Geochemical stages at Jasper Seamount and the origin of intraplate volcanoes, *Geochem. Geophys. Geosyst.*, *10*, Q02001.

Lonsdale, P. (1991), Structural patterns of the Pacific floor offshore of peninsular California, in: Dauphin, J. P. and B. R. Simoneit (ed.) *The Gulf and Peninsular Province of the Californias*, *AAPG Mem.*, *47*, 87–125.

Mammerickx, J., and K. D. Klitgord (1982), Northern East Pacific Rise: Evolution from 25 m.y. to the present, *J. Geophys. Res.*, *87*, 6751-6759.

Mammerickx, J., D. F. Naar, and R. L. Tyce (1988), The Mathematician paleoplate, *J. Geophys. Res.*, *93*, 3025-3040.

McClelland, L., E, Venzke and J. Goldberg (1993), Socorro (Mexico) vesicular lava eruption from underwater vent 3 km W of the island, *Smithson. Inst. Bull. Global Volcan. Network*, *18*, 9-11.

Menard, H. W., T. E. Chase, and S. M. Smith (1964), Galapagos Rise in the southeaster Pacific, *Deep-Sea Res.*, *11*, 233-242.

Mescheded, M., U. Barckhausen, M. Engels, and W. Weinrebe (2008), The trace of the Pacific-Cocos-Nazca triple junction of an overlapping spreading center, *Terra Nova*, *20*, 246-251.

Meibom, A., and D. L. Anderson (2004), The statistical upper mantle assemblage, *Earth Planet. Sci. Lett.*, *217*, 123–139.

Moore, J. G. (1970), Submarine basalt from the Revillagigedo Island region, Mexico, *Mar. Geol.*, *9*, 331-345.

Niu, Y., M. Regelous, I. J. Wendt, R. Batiza, and M. J. O’Hara (2002), Geochemistry of near-EPR seamounts: importance of source vs. process and the origin of enriched mantle component, *Earth Planet. Sci. Lett.*, *199*(3-4), 327-345.

Niu, Y. L., and M. J. O’Hara (2008), Global correlations of ocean ridge basalt chemistry with axial depth: A new perspective, *J. Petrol.*, *49*, 633–664.

Pilet, S., M. B. Baker, and E. M. Stolper (2008), Metasomatized lithosphere and the origin of alkaline lavas, *Science*, *320*, 916–919.

Raddick, M. J., E. M. Parmentier, and D. S. Scheirer (2002), Buoyant decompression melting: a possible mechanism for intraplate volcanism, *J. Geophys. Res.*, *107*(B10), 2228-2241.

Richards, A. F. (1958), Petrographic notes on two Eastern Pacific Ocean islands, *Geol. Soc. Am. Bull.*, *62*, 1634.

Richards, A. F. (1959), Geology of the Islas Revillagigedo, Mexico, 1. Birth and development of Volcan Barcena, Isla San Benedicto, *Bull. Volcan.*, *22*, 75-123.

Richards, A. F. (1966), Geology of the Islas Revillagigedo, Mexico, 2. Geology and petrography of Isla San Benedicto, *Proc. Cal. Aca. Sci.*, *33*, 361-414.

Salters, V. J. M., and A. Stracke (2004), Composition of the depleted mantle, *Geochem. Geophys. Geosyst.*, *5*, Q05004.

Siebe, C., J.-C. Komorowski, C. Navarro, J. McHone, H. Delgado and A. Cortes (1995), Submarine eruption near Socorro Island, Mexico: Geochemistry and scanning electron microscopy studies of floating scoria and reticulite, *J. Volcanol. Geotherm. Res.*, *68*, 239–271.

Solidum, R. U. (2002), Geochemistry of volcanic arc lavas in central and southern Philippines: contributions from the subducted slab, Ph.D. dissertation, Univ. of Calif., San Diego.

Sotin, C., and E. M. Parmentier (1989), Dynamical consequences of compositional and thermal density stratification beneath spreading centers, *Geophys. Res. Lett.*, *16*, 835-838.

Sun, S.-S., and W. F. McDonough (1989), Chemical and isotopic systematics of oceanic basalts: Implications for mantle composition and processes, in: Saunders, A. D., and M. K. Norry (ed.) *Magmatism in the Ocean Basins*, *Geol. Soc. Spec. Publ.*, *42*, 313-345.

Tian, L., P. R. Castillo, P. F. Lonsdale, D. Hahm, and D. R. Hilton (2011), Petrology and Sr-Nd-Pb-He isotope geochemistry of postspreading lavas on fossil spreading axes off Baja California Sur, Mexico, *Geochem. Geophys. Geosyst.*, *12*, Q0AC10.

Todt, W., R. A. Cliff, A. Hanser, and A. W. Hoffman (1996), Evaluation of a ^{202}Pb-^{205}Pb double spike for high-precision lead isotope analysis, in: Basu, A. and S.

Hart (ed.) *Earth Processes: Reading the Isotopic Code, Geophys. Monogr. Ser.*, *95*, 429–437, AGU, Washington, D. C.

Zindler, A., H. Staudigel, and R. Batiza (1984), Isotope and trace element geochemistry of young Pacific seamounts: implications for the scale of upper mantle heterogeneity, *Earth Planet. Sci. Lett.*, *70*(2), 175-195.

CHAPTER 5

A geochemical comparison of alkalic lavas in the Trans-Mexican volcanic belt, Baja California and intraplate volcanoes in the eastern Pacific

Abstract

The Trans-Mexican Volcanic Belt (TMVB) is a continental volcanic arc built along the southern edge of the North American plate. The volcanic rocks along TMVB are compositionally diverse and the origin of its alkalic lavas with ocean island basalt (OIB)-like composition is highly controversial. Alkalic lavas from four regions in the western, central and eastern TMVB are compared with similar OIB-like alkalic lavas from peninsular Baja California and intraplate volcanoes in the eastern Pacific in order to ascertain their geochemical similarities and differences and to constrain the compositions of their respective magma sources. A few of the alkalic lavas from TMVB have similar trace element and isotopic compositions as the OIB-like alkalic lavas from Baja California and eastern Pacific, suggesting that they might have come from a similar source, the compositionally heterogeneous Pacific asthenosphere. Majority of the TMVB alkalic lavas, however, are compositionally more heterogeneous, more so than the less-alkalic Nb-enriched basalts in Baja California that represent OIB-like alkalic lavas that had been contaminated by other mantle components and/or crustal materials. More detailed studies are needed in order

to understand the true mechanism(s) for the formation of all OIB-like alkalic lavas along TMVB.

5.1. Introduction

The Trans-Mexican Volcanic Belt (TMVB) is located between 18° and 21° N, and extends in an east-west direction from Puerto Vallarta in the Pacific Coast to Veracruz in the Gulf of Mexico (Fig. 5.1). It is a late Miocene-Quaternary volcanic arc, which traditionally has been related to the subduction of Cocos and Rivera oceanic plates under the North American plate along the Middle America trench [e.g., *Nixon*, 1982; *Luhr et al.*, 1985; *DeMets and Stein*, 1990]. Volcanism in TMVB is diverse, and in particular alkaline lavas with a chemical signature similar to ocean island basalts (OIB) had been emplaced in close spatial and temporal association with the more abundant cal-alkaline lavas since late Miocene [e.g., *Verma and Nelson*, 1989; *Moore et al.*, 1994; *Luhr*, 1997; *Wallace and Carmichael*, 1999; *Verma*, 2000; *Petrone et al.*, 2003, 2006; *Orozco-Esquivel et al.*, 2007; *Verma and Luhr*, 2010]. These alkalic lavas are reported to be usually Na rich, and have, e.g., high high field strength element (HFSE)/large ion lithophile element (LILE) and high /HFSE/light rare earth element (REE) ratios, similar to OIB. The presence of such oceanic-type alkalic lavas in TMVB is controversial and has been linked to a variety of mechanisms such as mantle plume activity beneath the TMVB since late Miocene [*Moore et al.*, 1994; *Márquez et al.*, 1999], partial melting of a veined heterogeneous mantle as a result of continental rifting [e.g., *Sheth et al.*, 2000; *Verma*, 2000, 2002; *Verma and Hasenaka*, 2004], melting of subarc mantle metasomatized by slab-derived melts [e.g., *Cai et al.*, 2007; *Gómez-Tuena et al.*, 2007; *Straub et al.*, 2009], and melting of asthenospheric material recently introduced into the mantle wedge [e.g., *Luhr*, 1997; *Wallace and Carmichael*, 1999; *Ferrari et al.*, 2001; *Petrone et al.*, 2003; *Ferrari*, 2004].

More recently, *Castillo* [2008] proposed that similar OIB-like alkalic lavas, also termed high-Nb basalts, in the nearby peninsular Baja California, Mexico are products of relatively small degrees of partial melting of the heterogeneous sub-Pacific asthenosphere that was overridden by the North American plate as it moves west-northwest. The proposed mechanism is similar to the one proposed for the formation of OIB-like intraplate lavas that form riseflank seamounts and fossil spreading ridges in the eastern Pacific; the OIB-like lavas were formed by small degrees of partial melting of the compositionally heterogeneous Pacific asthenosphere, which consists of geochemically enriched components enclosed in a depleted peridotite matrix [*Batiza and Vanko*, 1984; *Zindler et al.*, 1984; *Clague et al.*, 2009; *Castillo et al.*, 2010; *Tian et al.*, 2011/Chapter 3; Chapter 4]. However, *Castillo* [2008] based his arguments on limited data for intraplate lavas in the eastern Pacific that was available in the literature at that time.

In this chapter, the geochemistry of alkalic lavas from four regions along TMVB and similar alkalic lavas from the nearby peninsular Baja California [*Storey et al.*, 1989; *Luhr et al.*, 1995; *Castillo*, 2008] are compared with new geochemical data for alkalic lavas from fossil spreading centers off Baja California Sur, representing alkalic lavas from intraplate volcanoes in the eastern Pacific [*Tian et al.*, 2011/Chapter 3] (Fig. 5.1). The main objectives of this short chapter are to ascertain geochemical similarities among these alkalic lavas in order to explore the possibility that they all indeed share a common, heterogeneous mantle source. These information are a necessary first step in order to better understand the true mechanism(s) for generating OIB-like alkalic lavas along TMVB.

5.2. Geological background and samples investigated

The TMVB is 1000 km long and 20-200 km wide and contains more than 8000 individual volcanic structures. Most studies relate magmatism along TMVB to the northeastward subduction of the Cocos and Rivera plates beneath the North American plate. The western part of TMVB is thought to be formed by subduction of the oceanic Rivera Plate beneath the continental North American plate [*Pardo and Suarez*, 1993; 1995]. This part of the volcanic arc is dominated by a structural triple junction that meets ~60 km SSW of Guadalajara. The well-developed rift system consists of three major rifts: northwest-trending Tepic-Zacoalco rift, north-south-trending Colima rift, and east-west-trending Chapala rift [e.g., *Luhr et al.*, 1985]. Subduction of the Cocos plate between ~105° W and ~95° W is thought to feed the main part of the TMVB, which extends from Volcán de Colima in the west to Pico de Orizaba in the east. Several large fields of basaltic and andesitic cinder and lava cones exist, e.g., the Michoacán-Guanajuato volcanic field (MGVF) in the west and the Sierra del Chichinautzin volcanic field (SCN) south of Mexico City. Further to the east, this belt also includes the huge Cerro Grande volcanic complex and the intrusive and sub-volcanic bodies of e.g., Chiconquiaco-Palma Sola.

Published geochemical data for alkalic and transitional between alkalic and tholeiitic lavas, henceforth simply transitional, from the following four regions in TMVB (Fig. 5.2) are used in this study: (1) the San Pedro - Ceboruco graben (SPC; part of the Tepic-Zacoalco rift) in the western TMVB [*Petrone et al.*, 2003; 2006], (2) the MGVF located in the west-central TMVB [*Verma and Hasenaka*, 2004], (3) the SCN at the volcanic front of central TMVB [*Wallace and Carmichael*, 1999; *Verma*, 2000], (4) the volcanic fields of Tlanchino, Álamo, Sierra de Tantima, Chiconquiaco-Palma Sola, Poza Rica, Los Atlixcos, and Naolinco in the eastern TMVB [*Orozco-Esquivel et al.*, 2007].

5.3. Chemical and Sr and Nd isotopic compositions of alkalic lavas from TMVB

Samples from SPC include both alkalic and transitional lavas [*Petrone et al.*, 2003; 2006] as defined by their total alkali and silica contents (Fig. 5.2). They have 44.1 - 54.7 wt% SiO_2, 3.9 - 7.4 wt% MgO, and 51-85 Mg# ($100Mg/(Mg+Fe^{2+})$). These samples are generally enriched in highly incompatible elements relative to moderately incompatible elements (Fig. 5.3) and their REE patterns are characterized by $(La/Sm)_N > 1.86$. In detail, alkalic lavas from the northern volcanic chain in SPC have positive spikes in HFSE (Nb, Zr and Ti), which are similar to the typical pattern of average OIB [*Sun and McDonough*, 1989]. Furthermore, their trace element patterns are similar to those of alkalic lavas from peninsular Baja California, particularly those from San Quintin - the archetypal OIB-like alkalic lavas in the region [*Storey et al.*, 1989; *Luhr et al.*, 1995; *Castillo*, 2008] (henceforth simply San Quintin) and fossil spreading centers offshore Baja California Sur [*Tian et al.*, 2011/Chapter 3]. The transitional lavas from the Amado Nervo shield volcano display slightly different patterns with negative trough in Nb, though they still have higher Nb contents (14 - 25 ppm) than typical TMVB arc lavas (e.g., < 11 ppm; Valle de Bravo-Zitácuaro volcanic field, *Gómez-Tuena et al.*, 2007). The trace element characteristics of the latter group is similar to those of the Nb-enriched basalts variety of the OIB-like alkalic lavas from peninsular Baja California [*Aguillón-Robles et al.*, 2001; *Benoit et al.*, 2002], with relatively lower HFSE abundances and less alkalic (to tholeiitic) composition than the alkalic lavas from San Quintin. Alkalic lavas from the northern volcanic chain have $^{87}Sr/^{86}Sr$ and $^{143}Nd/^{144}Nd$ ratios overlapping with those of all alkalic lavas from peninsular Baja California and intraplate volcanoes in the eastern Pacific. However, the transitional lavas from the Amado Nervo shield volcano have higher $^{87}Sr/^{86}Sr$ and lower $^{143}Nd/^{144}Nd$ values (Fig. 5.4).

Alkalic lavas from MGVF [*Verma and Hasenaka*, 2004] have 47.2 - 54.9 wt% SiO_2, 3.0 - 8.7 wt% MgO, and 49 - 73 Mg#. All samples show light-REE enrichment and one sample is highly enriched with $(La/Sm)_N$ up to 8.7. Most samples show Nb depletion relative to LILE and REE except for two samples, and have patterns similar to those of the Nb-enriched basalts from peninsular Baja California (Fig. 5.3). In terms of isotopic composition (Fig. 5.4), the alkalic lavas from MGVF range from the field for all alkalic lavas from peninsular Baja California and intraplate volcanoes in the eastern Pacific to higher $^{87}Sr/^{86}Sr$ and lower $^{143}Nd/^{144}Nd$ values.

Alkalic and transitional lavas from SCN [*Wallace and Carmichael*, 1999; *Verma*, 2000] have 49.3 - 55.8 wt% SiO_2, 6.0 - 10.1 wt% MgO, and 61 - 74 Mg#. They are enriched in highly incompatible elements relative to moderately incompatible elements and the majority has variable degrees of Nb depletion (Fig. 5.3). Their overall trace element patterns are similar to those of Nb-enriched basalts in peninsular Baja California. In terms of isotopic compositions (Fig. 5.4), the alkalic and transitional lavas from SCN partly overlap with all alkalic lavas from peninsular Baja California and intraplate volcanoes in the eastern Pacific, but also extend to higher $^{87}Sr/^{86}Sr$ and lower $^{143}Nd/^{144}Nd$ compositions.

Alkalic samples from ETMVB [*Orozco-Esquivel et al.,* 2007] span a range with 42.1 - 53.7 wt% SiO_2, 2.5 - 13.3 wt% MgO, and 31 - 69 Mg#. The samples are generally enriched in highly incompatible elements relative to moderately incompatible elements (Fig. 5.3), and have enriched REE patterns characterized by $(La/Sm)_N > 1.76$. These alkalic lavas can be divided into two groups based on their trace element patterns (Fig. 5.3). One group is enriched in Nb, Zr and Ti, similar to the alkalic lavas from San Quintin and fossil spreading centers, although they have remarkable depletion in K. The other group is also OIB-like, but has varying degrees of Nb depletion, similar to the Nb-enriched basalts. The groups display two different, almost parallel trends in the $^{87}Sr/^{86}Sr$ and $^{143}Nd/^{144}Nd$ diagram (Fig. 5.4). The Sr and Nd isotopic compositions of the Nb-enriched basalt group overlap with all alkalic lavas from peninsular Baja California and intraplate volcanoes in the eastern Pacific, but the variable Nb group has lower $^{143}Nd/^{144}Nd$ values at similar $^{87}Sr/^{86}Sr$ relative to the former.

In summary, alkalic lavas from the four regions along TMVB are generally enriched in highly incompatible elements relative to moderately incompatible elements, with light-REE-enriched patterns. A few samples are compositionally similar to the true OIB-like (i.e., San Quintin variety) alkalic lavas from peninsular Baja California and fossil spreading centers in the eastern Pacific. However, most of the TMVB alkalic lavas have varying degrees of Nb depletion. These latter alkalic lavas still have relatively high absolute abundances of Nb (> 14 ppm), similar to the Nb-enriched basalts variety of alkalic basalts from peninsular Baja California. The Sr and Nd isotopic compositions of alkalic lavas from TMVB overlap with those for all alkalic lavas from peninsular Baja California and intraplate volcanoes in the eastern Pacific, but also trend toward higher $^{87}Sr/^{86}Sr$ and $^{143}Nd/^{144}Nd$ values.

5.4. Discussion

5.4.1. Hypotheses to explain the alkaline magmatism in the TMVB

During the last several decades, a number of hypotheses had been proposed to account for the existence of OIB-like alkalic magmas along TMVB. *Moore et al.* [1994] first suggested the presence of a mantle plume beneath Guadalajara and this is responsible for the occurrence of OIB-like alkalic lavas in this region. This model was later expanded by *Márquez et al.* [1999] for the entire TMVB, who proposed that the OIB-like alkalic magmatism is the expression of an active mantle plume that impacted western Mexico in the late Miocene. However, the plume model was criticized by *Ferrari and Rosas-Elguera* [1999] who showed that 1) there is no evidence for a propagating rift and/or age progression of volcanism as required by the plume model 2) there is also no evidence for a regional uplift caused by a plume head that impacted western Mexico, 3) only a small fraction of the subduction-related volcanism has an intraplate compositional affinity, and 4) the total volume of intraplate volcanism of the purported plume is much lower than typical flood basalts associated with a mantle plume in a continental environment.

Sheth et al. [2000], *Verma* [2000, 2002] and *Verma and Hasenaka* [2004] proposed a variably veined mantle source for magmas throughout the TMVB, consisting of kilometer scale domains of peridotite with veins of amphibole and or/phlogopite, and vein-free periodotite. They argued that upwelling along rifts of the veined peridotite would generate alkalic magmas whereas upwelling of the vein-free or poorly veined peridotite would produce subalkalic magmas. Their model argues against any role of subduction in the genesis of lavas along TMVB, a claim that was strongly criticized by many other workers [e.g., *Blatter and Carmichael*, 2001; *Ferrari et al.*, 2002; *Ferrari*, 2003; *Siebe et al.*, 2004; *Schaaf et al.*, 2005].

Other workers consider the co-existence of adakitic and OIB-type alkalic lavas as an indication of slab melting [e.g., *Cai et al.*, 2007; *Gómez-Tuena et al.*, 2007; *Straub et al.*, 2009], as adakites are suggested to be products of direct melting of subducted oceanic basalt [*Defant and Drummond*, 1990]. These workers propose that the OIB-type arc magmas were products of a pre-existing MORB-type subarc mantle that had been fertilized by silicic slab melts with high LILE/REE and LILE/HFSE ratios. However, the strong similarity of OIB-type alkalic lavas from both intraplate volcanoes from the eastern Pacific and Baja California and possible absence of true "adakites" in TMVB [*Petrone and Ferrari*, 2008] are inconsistent with this model.

Another popular idea is that the OIB-like magmas along TMVB originate from the advection of subduction-unmodified asthenospheric material beneath the region. The asthenospheric material could have been brought into the mantle wedge from behind the arc as a result of subduction-induced corner flow and/or slab rollback [e.g., *Luhr*, 1997; *Wallace and Carmichael*, 1999; *Blatter and Carmichael*, 2001; *Righter and Rosas-Elguera*, 2001], by lateral infiltration from the actively rifting area in the Gulf of California, from the stretched boundary between the subducted Rivera and Cocos plates via corner flow [e.g., *Ferrari et al.*, 2001; *Petrone et al.*, 2003], or through a slab window formed after detachment of the lower part of the subducted Rivera and Cocos plate [*Ferrari*, 2004]. This model is actually similar to the one proposed later by *Castillo* [2008] for the formation of OIB-like alkalic lavas in peninsular Baja California and this proposal will be described in more detail below.

Alkalic lavas were erupted together with subduction related lavas in peninsular Baja California after subduction has stopped at ~12.5 Ma along the western margin of Mexico [e.g., *Klitgord and Mammerickx*, 1982]. *Castillo* [2008] proposes that the OIB-like alkalic lavas in the peninsula originate from easily fusible, but variably distributed enriched components in the asthenosphere through relatively small degree of partial melting, similar to the mechanism for the production of post-spreading lavas erupted along fossil spreading centers in the eastern Pacific described in detail by *Tian et al.* (2011/Chapter 3) and in Chapter 4 of this thesis. However, these so-called “intraplate” alkalic lavas in peninsular Baja California actually range from OIB-like lavas, best represented by lavas from San Quintin, Baja California [*Storey et al.*, 1989; *Luhr et al.*, 1995] and compositionally similar to the OIB-like intraplate lavas in the eastern Pacific, to Nb-enriched basalts that are only slightly alkalic to tholeiitic in composition and have variable Nb concentrations [*Aguillón-Robles et al.*, 2001; *Benoit et al.*, 2002]. *Castillo* [2008] proposes that the parental magmas of Nb-enriched basalts originate from the same enriched mantle source as the OIB-like intraplate lavas that has been contaminated by other mantle components, or are melts from such an enriched mantle source that have been contaminated by other melts or crustal materials. Niobium-enriched basalts are also generally more fractionated than the OIB-like alkalic lavas [*Castillo*, 2008].

5.4.2. Are the alkalic lavas from TMVB the same lavas as those in peninsular Baja California and eastern Pacific?

As described earlier, there are chemical and isotopic similarities and differences between alkalic lavas from TMVB and those from peninsular Baja California and fossil spreading centers in the eastern Pacific (Figs. 5.3 and 5.4). These geochemical similarities and differences are further illustrated in Figure 5.5. A few TMVB alkalic lavas share highly incompatible trace element ratios, including those that are highly resistant to alteration and are fluid-immobile in subduction zones (e.g., Nb/Zr), with alkalic lavas from San Quintin and fossil spreading centers, but the majority does not. The isotopic compositions of the alkalic lavas from TMVB also overlap with all alkalic lavas from peninsular Baja California and fossil spreading centers in the eastern Pacific, but also extend toward higher $^{87}Sr/^{86}Sr$ and lower $^{143}Nd/^{144}Nd$ ratios. Ratios of highly incompatible trace element ratios, similar to radiogenic isotopic ratios, are not fractionated during normal magmatic differentiation process and, thus, both reflect the composition of the magma source. Consequently, data indicate that the mantle source of the OIB-like alkalic lavas from TMVB and those from peninsular Baja California and intraplate volcanoes in the eastern Pacific overlap in composition to a certain degree, but the mantle source of the former is much more heterogeneous than that of the latter. Thus, to a first order, results of the comparative investigation indicate that although there are overlaps, the magma source of the OIB-like alkalic lavas along TMVB is different from that in peninsular Baja California and eastern Pacific. Thus, the true mechanism(s) for generating OIB-like alkalic basalts along TMVB are different from that generating OIB-like, intraplate lavas in peninsular Baja California and eastern Pacific.

It is important to reiterate, however, that the OIB-like alkalic basalts in peninsular Baja California have a wider compositional range than the OIB-like intraplate lavas from the eastern Pacific. Specifically, unlike the oceanic intraplate lavas, the former have a compositionally variable Nb-enriched basalts variety that may have been formed through mixing of their enriched mantle source with other mantle components including the pre-existing, subduction-metasomatized mantle beneath the peninsula and/or through assimilation of continental or arc lithospheric materials by primary alkalic magmas during their transit toward the surface. Thus, it is possible that the alkalic lavas from TMVB are compositionally more variable because the underlying mantle and/or lithospheric lid along TMVB are even more heterogeneous than those in peninsular Baja California. Moreover, as discussed in Chapters 3 and 4, new data for several fossil spreading centers in the eastern Pacific clearly indicate that the more fusible, enriched mantle components comprising the source of the oceanic intraplate lavas are actually inherently heterogeneous, and this can also contribute to the heterogeneity of all OIB-like intraplate lavas, whether they are erupted in the oceanic or continental environment. Investigating in detail the effects of these various factors are needed in order to constrain the true mechanism(s) for generating the OIB-like alkalic lavas along TMVB.

5.5. Conclusions

The compositions of OIB-like alkalic lavas from the SPC, MGVF, SCN, and ETMVB regions along TMVB are compared with those of OIB-like alkalic lavas from peninsular Baja California and fossil spreading centers offshore Baja California Sur, representing OIB-like intraplate lavas in the eastern Pacific. The trace element and isotopic compositions of a few TMVB lavas are similar to those of the San Quintin variety of OIB-like alkalic lavas in the peninsular Baja California and those from intraplate lavas from fossil spreading ridges, suggesting that they may indeed share a common, initial mantle source, the heterogeneous Pacific asthenosphere. Majority of TMVB lavas, similar to the Nb-enriched basalts variety in the peninsular Baja California, however, are compositionally more heterogeneous than the OIB-like alkalic lavas, indicating that the magma source of alkalic lavas along TMVB is much more heterogeneous than those of OIB-like alkalic lavas from both peninsular Baja California and intraplate volcanoes in the eastern Pacific. More detailed investigations are needed in order to constrain the true mechanism(s) to produce the OIB-like alkalic lavas along TMVB.

Figure 5.1. Simplified map of the Trans-Mexican Volcanic Belt (TMVB), modified from *Ferrari* [2004]. SPC: San Pedro - Ceboruco graben; MGVF: Michoacán - Guanjuato volcanic field; SCN: Sierra Chichinautzin; THT: Tlanchinol-Huejutla-Tantima basaltic flows; CPS: Chiconquiaco - Palma Sola mafic plateau; ETMVB: eastern TMVB. The inset shows the relative tectonic setting of TMVB.

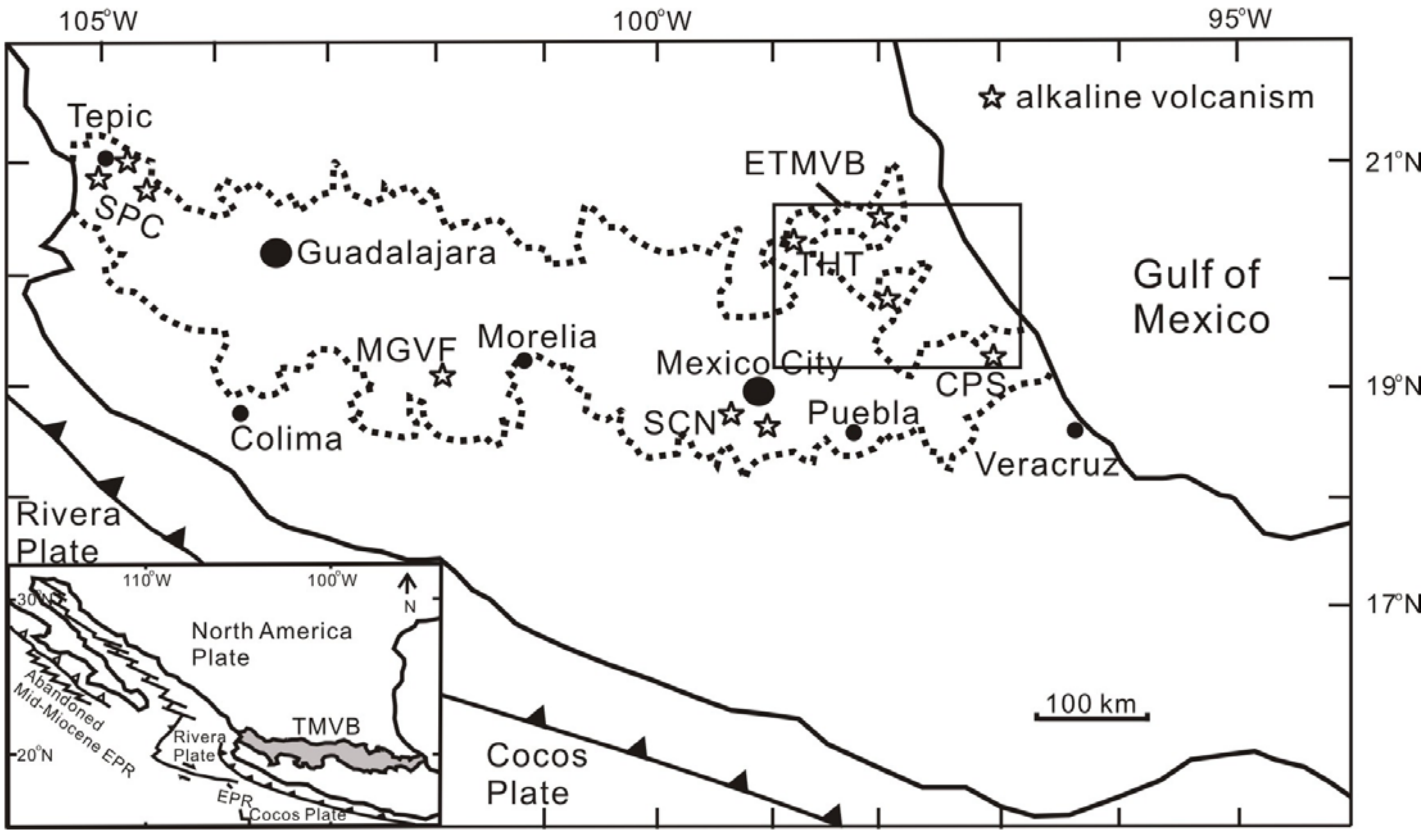
105°W
100°W
95°W
21°N
19°N
17°N
☆ alkaline volcanism
Tepic
SPC
Guadalajara
ETMVB
THT
Gulf of
Mexico
MGVF
Morelia
Mexico City
CPS
Colima
SCN
Puebla
Veracruz
Rivera
Plate
Cocos
Plate
100 km
110°W
100°W
N
30°N
North America
Plate
Abandoned
Mid-Miocene EPR
Rivera
Plate
TMVB
20°N
EPR
Cocos Plate

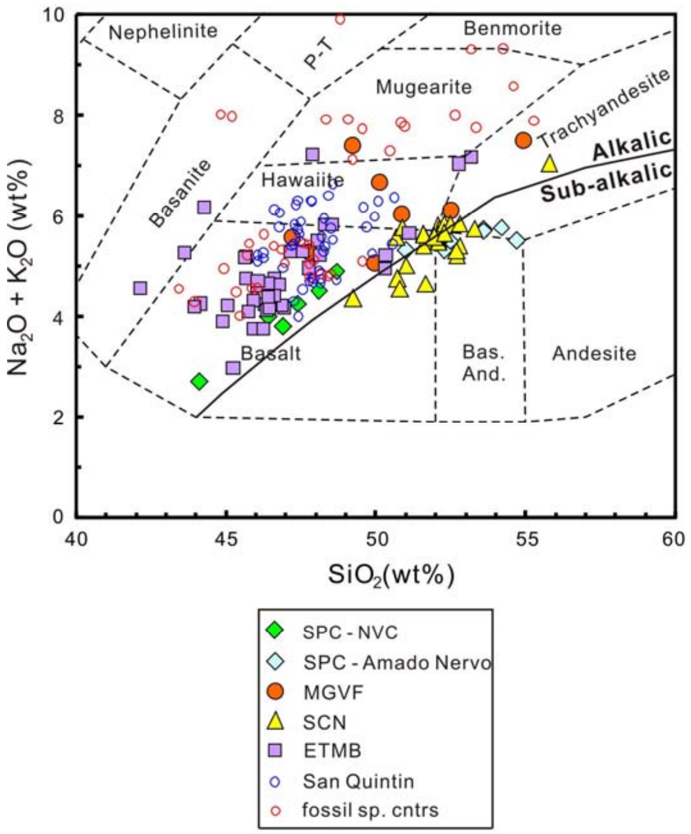

Figure 5.2. Silica (SiO_2) versus total alkalis ($Na_2O + K_2O$) diagram [*Cox et al.*, 1979] of samples from TMVB that were investigated [SPC: *Petrone et al.*, 2003; 2006; MGVF: *Verma and Hasenaka*, 2004; SCN: *Wallace and Carmichael*, 1999; *Verma*, 2000; ETMVB: *Orozco-Esquivel et al.*, 2007]. Samples from SPC are divided into alkalic (Northern Volcanic Chain - NVC) and transitional lavas (Amado Nervo). Reference data are for OIB-like alkalic lavas from San Quintin, Baja California [*Storey et al.*, 1989; *Luhr et al.*, 1995] and fossil spreading centers off Baja California Sur, representing intraplate volcanoes in the eastern Pacific [*Tian et al.*, 2011/Chapter 3].

Figure 5.3. Primitive mantle-normalized incompatible trace element plots for samples from TMVB. Normalizing values are from *Sun and MacDonough* [1989]. Alkalic lavas from San Quintin, Baja California and fossil spreading centers off Baja California Sur, and Nb-enriched basalts (NEB) from peninsular Baja California [*Aguillón-Robles et al.*, 2001; *Benoit et al.*, 2002] are plotted for comparison. Alkalic lavas from the ETMVB are divided into two groups: group A is enriched in HFSE, similar to OIB-like alkalic lavas from San Quintin and fossil spreading centers; group B has varying degrees of Nb depletion, more like the peninsular Baja California NEB. Other data sources are as in Figure 5.2.

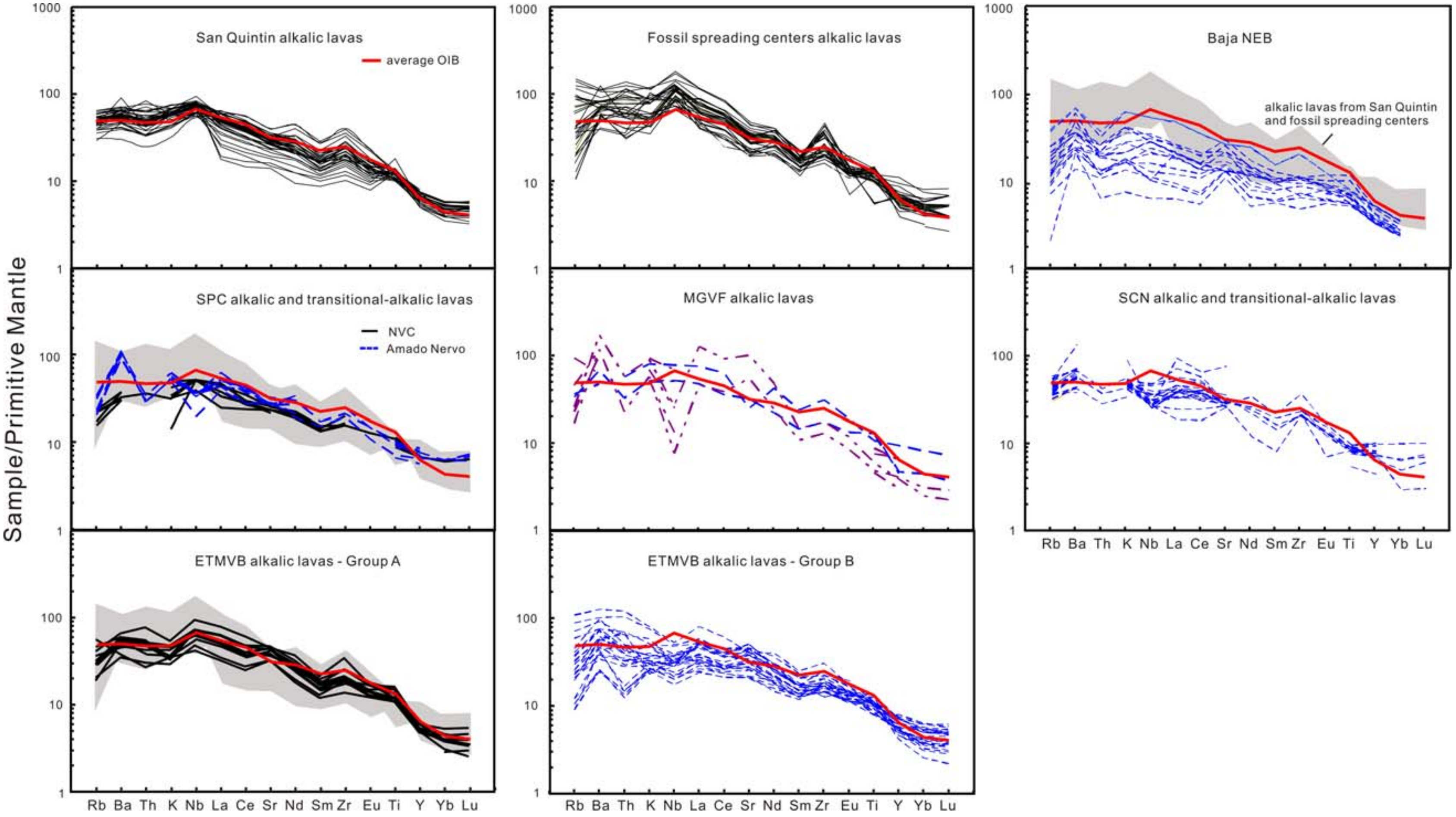
Sample/Primitive Mantle
1000
100
10
1
San Quintin alkalic lavas
average OIB
Fossil spreading centers alkalic lavas
Baja NEB
alkalic lavas from San Quintin and fossil spreading centers
SPC alkalic and transitional-alkalic lavas
NVC
Amado Nervo
MGVF alkalic lavas
SCN alkalic and transitional-alkalic lavas
ETMVB alkalic lavas - Group A
ETMVB alkalic lavas - Group B
Rb Ba Th K Nb La Ce Sr Nd Sm Zr Eu Ti Y Yb Lu

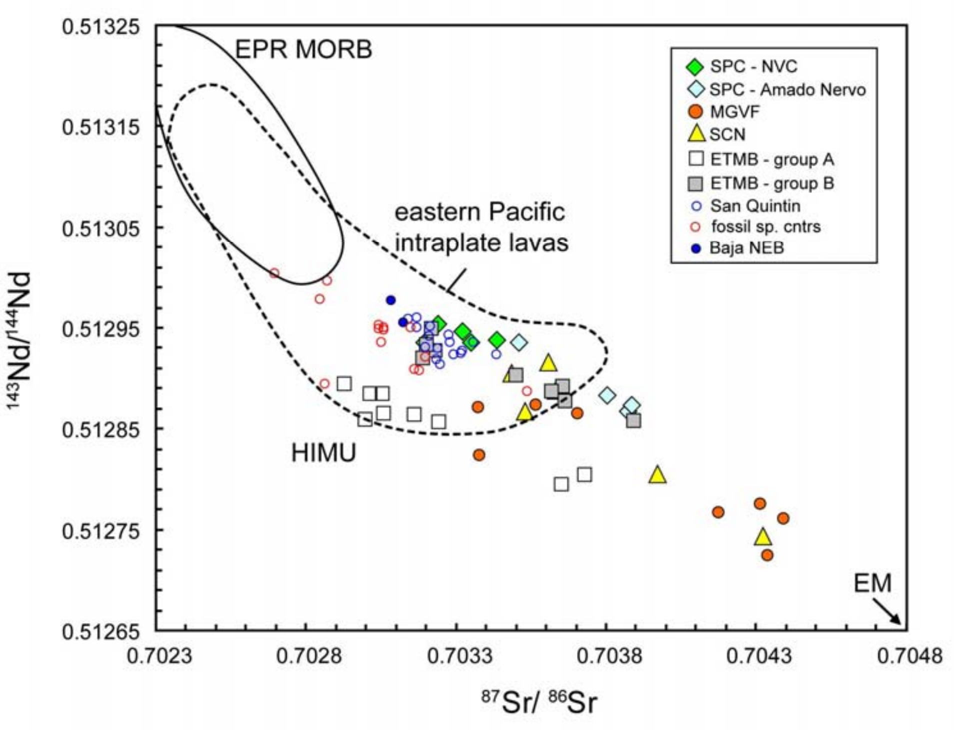

Figure 5.4. Plot of ^{87}Sr/^{86}Sr versus ^{143}Nd/^{144}Nd for samples from TMVB. Alkalic lavas from San Quintin, Baja California and fossil spreading centers off Baja California Sur, and NEB from peninsular Baja California are plotted for comparison. Also plotted are fields for East Pacific Rise (EPR) MORB (GEOROC database: http://georoc.mpch-mainz.gwdg.de) and eastern Pacific intraplate lavas [*Niu et al.*, 2002; *Davis et al.*, 2002; *Castillo et al.*, 2010; *Tian et al.*, 2011/Chapter 3; *Bohrson and Reid*, 1995; Chapter 4]. HIMU and EM are proposed mantle end-components from *Hart* [1984]. Other data symbols and sources are as in Figures 5.2 and 5.3.

Figure 5.5. Plots of (a) La versus Sm and (b) Zr versus Nb for samples from TMVB. Alkalic lavas from San Quintin, Baja California and fossil spreading centers off Baja California Sur, and NEB from peninsular Baja California are plotted for comparison. Data symbols and sources are as in Figures 5.2 and 5.3.

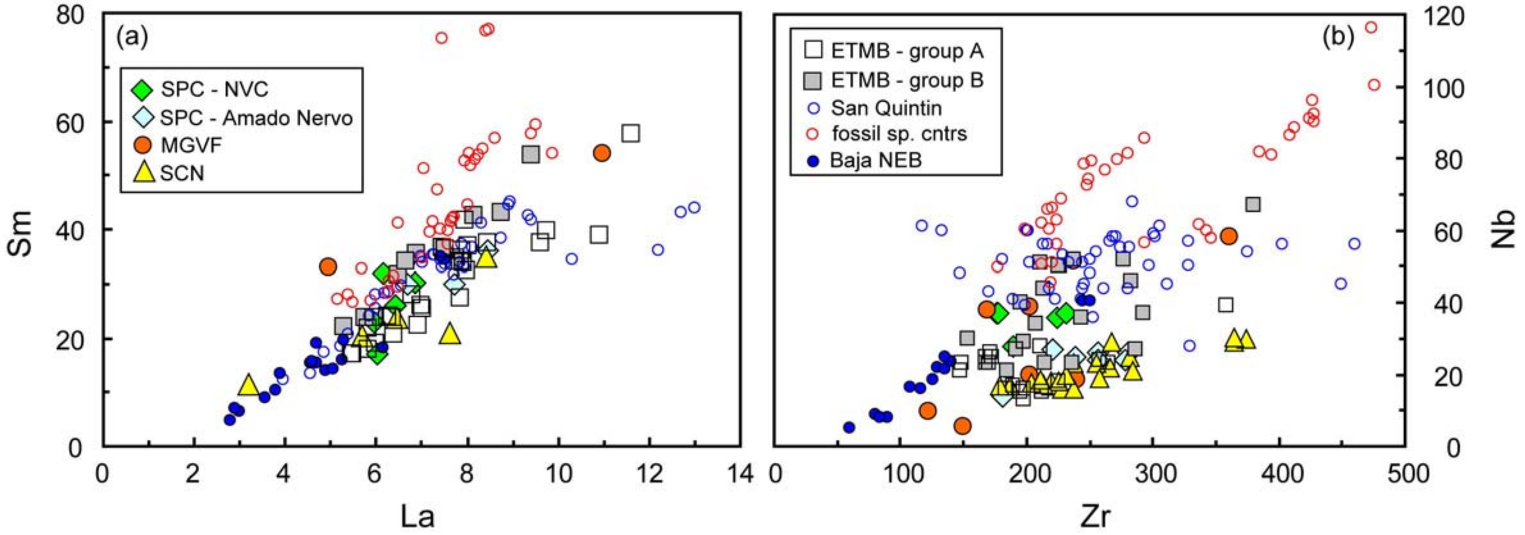
(a)
SPC - NVC
SPC - Amado Nervo
MGVF
SCN
Sm
La
0
20
40
60
80
0
2
4
6
8
10
12
14
(b)
ETMB - group A
ETMB - group B
San Quintin
fossil sp. cntrs
Baja NEB
Nb
Zr
0
100
200
300
400
500
0
20
40
60
80
100
120

References

Aguillón-Robles, A., T. Calmus, H. Bellon, R. C. Maury, J. Cotten, J. Bourgois, and F. Michaud (2001), Late Miocene adakite and Nb-enriched basalts from Vizcaino Peninsula, Mexico: indicators of East Pacific Rise subduction below southern Baja California, *Geology*, *29*, 531-534.

Batiza, R., and D. Vanko (1984), Petrology of Young Pacific Seamounts, *J. Geophys. Res.*, *89*(B13), 11235-11260.

Benoit, M, Aguillón-Robles, A., T. Calmus, R. Maury, H. Bellon, J. Cotton, J. Bourgois, and and F. Michaud (2002), Geochemical diversity of Late Miocene volcanism in southern Baja California, Mexico: implications of mantle and crustal sources during the opening of an asthenospheric window, *J. Geol.*, *110*, 627-648.

Blatter, D. and I. Carmichael (2001), Hydrous phase equilibria of a Mexican high-silica andesite: a candidate for mantle origin?, *Geochim. Cosmochim. Acta*, *65*, 4043–4065.

Bohrson, W. A., and M. R. Reid (1995), Petrogenesis of alkaline basalts from Socorro Island, Mexico; trace element evidence for contamination of ocean island basalt in the shallow ocean crust, *J. Geophys. Res.*, *100*(B12), 24,555-524,576.

Cai, Y., S. L. Goldstein, C. H. Langmuir, A. Gómez-Tuena, A. Lagatta, S. M. Straub, and A. Martín Del Pozzo (2007), Subduction contributions in the Trans-Mexican Volcanic Belt: implications from lava chemistry and Hf-Nd-Pb isotopes, *Eos Trans. AGU*, Fall Meet. Suppl., Abstract V52A-03.

Castillo, P. R. (2008), Origin of the adakite-high-Nb basalt association and its implications for postsubduction magmatism in Baja California, Mexico, *Geol. Soc. Am. Bull.*, *120*, 451-462.

Castillo, P. R., D. A. Clague, A. S. Davis, and P. F. Lonsdale (2010), Petrogenesis of Davidson Seamount lavas and its implications for fossil spreading center and intraplate magmatism in the eastern Pacific, *Geochem. Geophys. Geosyst.*, *11*, Q02005.

Clague, D. A., J. B. Paduan, R. A. Duncan, J. J. Huard, A. S. Davis, P. R. Castillo, P. Lonsdale, and A. DeVogelaere (2009), Five million years of compositionally diverse, episodic volcanism: Construction of Davidson Seamount atop an abandoned spreading center, *Geochem. Geophys. Geosyst.*, *10*, Q12009.

Cox, K. G., J. D. Bell, and R. J. Pankhurst (1979), The interpretation of igneous rocks, London: Allen and Unwin.

Davis, A. S., D. A. Clague, W. A. Bohrson, G. B. Dalrymple, and H. G. Greene (2002), Seamounts at the continental margin of California: A different kind of oceanic intraplate volcanism, *Geol. Soc. Am. Bull.*, *114*, 316-333.

DeMets, C and S. Stein (1990), Present-day kinematics of the Rivera plate and implications for tectonics in southwestern Mexico, *J. Geophys. Res.*, *95*(B13), 21931–21948.

Defant, M. J. and M. S. Drummond (1990), Derivation of some modern arc magmas by melting young subducted lithosphere, *Nature*, *347*, 662-665.

Ferrari, L. (2003), The geochemical puzzle of the Trans-Mexican Volcanic Belt: mantle plume, continental rifting, or mantle perturbation induced by subduction?, http://www.mantleplumes.org/Mexico2.html.

Ferrari, L. (2004), Slab detachment control on mafic volcanic pulse and mantle heterogeneity in central Mexico, *Geology*, *32*(1), 77–80.

Ferrari, L. and J. Rosas-Elguera (1999), Alkalic (OIB type) and calc-alkalic volcanism in the Mexican Volcanic Belt: a case for plume-related magmatism and propagating rifting at an active margin?, Comment to the article by Márquez, A., R. Oyarzun, M. Doblas, and S. P. Verma, *Geology*, *27*, 1055–1056.

Ferrari, L., C. M. Petrone, and L. Francalanci (2001), Generation of OIB-type volcanism in the western Trans-Mexican Volcanic Belt by slab rollback, astenosphere infiltration and variable flux-melting, *Geology*, *29*, 507–510.

Ferrari, L., C. M. Petrone, and L. Francalanci (2002), Generation of OIB-type volcanism in the western Trans-Mexican Volcanic Belt by slab rollback, astenosphere infiltration and variable flux-melting, Reply to a comment by Torres-Alvarado, I. S., S. P. Verma, and F. Velasco-Tapia, *Geology, 30,* 858–859.

Gómez-Tuena, A., A. B. LaGatta, C. H. Langmuir, S. L. Goldstein, F. Ortega-Gutiérrez, and G. Carrasco-Núñez (2003), Temporal control of subduction magmatism in the eastern Trans-Mexican Volcanic Belt; mantle sources, slab contributions and crustal contamination, *Geochem. Geophys. Geosyst.*, *4*(8), 8912-8944.

Gómez-Tuena, A. C. H. Langmuir, S. L. Goldstein, S. M. Straub, and F. Ortega-Gutiérrez (2007), Geochemical evidence for slab melting in the Trans-Mexican Volcanic Belt, *J. Petrolog.*, *48,* 537-562.

Hart, S. R. (1984), A large-scale isotope anomaly in the Southern Hemisphere mantle, *Nature, 309,* 753–757.

Klitgord, K. D. and J. Mammerickx (1982), North East Pacific Rise: magnetic anomaly and bathymetric framework, *J. Geophys. Res., 87,* 6725-6750.

Luhr, J. F. (1997), Extensional tectonics and the diverse primitive volcanic rocks in the western Mexican Volcanic Belt, *Can. Mineral., 35,* 473–500.

Luhr, J., S. Nelson, J. Allan, and I. Carmichael (1985), Active rifting in southwestern Mexico: manifestations of an incipient eastward spreading-ridge jump, *Geology, 13,* 54–57.

Luhr, J. F., J. J. Aranda-Gomez, and T. B. Housh (1995), San Quintin volcanic field, Baja California Norte, Mexico: geology, petrology and geochemistry, *J. Geophys. Res.*, *100*, 10353-10380.

Márquez, A., R. Oyarzun, M. Doblas, and S. P. Verma (1999), Alkalic (ocean-island basalt type) and calc-alkalic volcanism in the Mexican volcanic belt: a case for plume-related magmatism and propagating rifting at an active margin?, *Geology, 27,* 51–54.

Moore, G., C. Marone, I. S. E. Carmichael, and P. Renne (1994), Basaltic volcanism and extension near the intersection of the Sierra Madre volcanic province and the Mexican volcanic belt, *Geol. Soc. Amer. Bull.*, *106*, 383–394.

Niu, Y., M. Regelous, I. J. Wendt, R. Batiza, and M. J. O’Hara (2002), Geochemistry of near-EPR seamounts: importance of source vs. process and the origin of enriched mantle component, *Earth Planet. Sci. Lett.*, *199*(3-4), 327-345.

Nixon, G. T. (1982), The relationship between Quaternary volcanism in central Mexico and the seismicity and structure of subducted ocean lithosphere, *Geol. Soc. Amer. Bull.*, *93*, 514–523.

Orozco-Esquivel, T., C. M. Petrone, L. Ferrari, T. Tagami, and P. Manetti (2007), Geochemical and isotopic variability in lavas from the eastern Trans-Mexican Volcanic Belt: slab detachment in a subduction zone with varying dip, *Lithos*, *93*, 149-174.

Pardo, M and G. Suarez (1993), Steep subduction geometry of the Rivera Plate beneath the Jalisco Block in western Mexico, *Geophys. Res. Lett.*, *20*, 2391-2394.

Pardo, M and G. Suarez (1995), Shape of the subducted Rivera and Cocos plates in southern Mexico: seismic and tectonic implications, *J. Geophys. Res.*, *100*, 12357-12373.

Petrone, C. M., L. Francalanci, R. W. Carlson, L. Ferrari, and S. Conticelli (2003), Unusual coexistence of subduction-related and intraplate-type magmatism: Sr, Nd and Pb isotope and trace element data from the magmatism of the San Pedro-Ceboruco graben (Nayarit, Mexico), *Chem. Geol.*, *193*, 1–24.

Petrone, C. M., L. Francalanci, L. Ferrari, P. Schaaf, and S. Conticelli (2006), The San Pedro-Cerro Grande Volcanic Complex (Nayarit, Mexico): inferences on volcanology and magma evolution, in: C. Siebe, G. Aguirre-Dìaz, and J. L. Macìas (ed.) *Neogene-Quaternary continental margin volcanism: a perspective in Mexico, Geol. Soc. Am. Sp. Paper*, *402*(03), 65-98.

Petrone, C. M. and L. Ferrari (2008), Quaternary adakite-Nb-enriched basalt association in the western Trans-Mexican Volcanic Belt: is there any slab melt evidence, *Contrib. Mineral. Petrol.*, *156*, 73-86.

Righter, K. and J. Rosas-Elguera (2001), Alkaline lavas in the volcanic front of the western Mexican volcanic belt; geology and petrology of Ayutla and Tapalpa volcanic fields, *J. Petrolog.*, *42*, 2333-2361.

Schaaf, P., J. Stimac, C. Siebe, and J. L. Macías (2005), Geochemical evidence for mantle origin and crustal processes in volcanic rocks from Popocatépetl and surrounding monogenetic volcanoes, central Mexico, *J. Petrolog.*, *46*, 1243-1282.

Sheth, H., I. Torres-Alvarado, and S. Verma (2000), Beyond subduction and plumes: a unified tectonic-petrogenetic model for the Mexican volcanic belt, *Int. Geol. Rev.*, *42*(12), 1116–1132.

Siebe, C., V. Rodríguez-Lara, P. Schaaf, and M. Abrams (2004), Geochemistry, Sr–Nd isotope composition, and tectonic setting of Holocene Pelado, Guespalapa and Chichinautzin scoria cones, south of Mexico City, *J. Volcanol. Geotherm. Res.*, *130*, 197-226.

Storey, M., G. Rogers, A. D. Sauders, and D. J. Terrell (1989), San Quintin volcanic field, Baja California, Mexico: “witin-plate” magmatism following ridge subduction, *Terra Nova*, *1*, 195-202.

Straub, S. M., A. Gomez-Tuena, G. F. Zellmer, Y. Cai, F. M. Stuart, R. Espinasa-Perena, C. H. Langmuir, and S. L. Goldstein (2009), The origin of “OIB-type” magmas in the central Mexican Volcanic Belt, *Eos Trans. AGU*, Fall Meet. Suppl., Abstract V31B-1966.

Sun, S.-S. and W. F. McDonough (1989), Chemical and isotopic systematics of oceanic basalts: Implications for mantle composition and processes, in: A. D. Saunders and M. K. Norry (ed.) *Magmatism in the Ocean Basins, Geol. Soc. Spec. Publ.*, *42*, 313–345.

Tian, L., P. R. Castillo, P. F. Lonsdale, D. Hahm, and D. R. Hilton (2011), Petrology and Sr-Nd-Pb-He isotope geochemistry of postspreading lavas on fossil spreading axes off Baja California Sur, Mexico, *Geochem. Geophys. Geosyst.*, *12*, Q0AC10.

Verma, S. P. (2000), Geochemistry of the subducting Cocos plate and the origin of subduction-unrelated mafic volcanism at the volcanic front of the central Mexican Volcanic Belt. in:, G. Aguirre-Dìaz, H. Delgado-Granados, and J. M. Stock (ed.), *Cenozoic Tectonics and Volcanism of Mexico, Geol. Soc. Am. Sp. Paper, 334*, 195–222.

Verma, S. P. (2002), Absence of Cocos Plate subduction-related basic volcanism in southern Mexico; a unique case on Earth?, *Geology*, *30*(12), 1095–1098.

Verma, S. P. and S. A. Nelson (1989), Isotopic and trace element constraints on the origin of evolution of alkaline and cal-alkaline magmas in the northwestern Mexico Volcanic Belt, *J. Geophys. Res.*, *94*, 4531-4544.

Verma, S. P. and T. Hasenaka (2004), Sr, Nd, and Pb isotopic and trace element geochemical constraints for a veined-mantle source of magmas in the Michoacάn-Guanajuato Volcanic Field, western-central Mexican Volcanic Belt, *Geochem. J.*, *58*, 43-65.

Verma, S. P. and J. F. Luhr (2010), Sr, Nd and Pb isotopic evidence for the origin and evolution of the Cάntaro-Colima volcanic chain, Western Mexican Volcanic Belt, *J. Volcanol. Geotherm. Res.*, *197*, 33-51.

Wallace, M. E. and D. H. Green (1991), The effect of bulk rock composition on the stability of amphibole in the upper mantle: implications for solidus positions and mantle metasomatism, *Miner. Petrol.*, *44*, 1–19.

Wallace, P. J., and I. S. E. Carmichael (1999), Quaternary volcanism near the valley of Mexico: implications for subduction zone magmatism and the effects of crustal thickness variations on primitive magma compositions, *Contrib. Minearl Petrol.*, *135*, 291-314.

Zindler, A., H. Staudigel, and R. Batiza (1984), Isotope and trace element geochemistry of young Pacific seamounts: implications for the scale of upper mantle heterogeneity, *Earth Planet. Sci. Lett.*, *70*(2), 175-195.